NATIONAL TRANSPORTATION SAFETY BOARD

Office of Research and Engineering
Materials Laboratory Division
Washington, D.C. 20594

January 15, 2016

MATERIALS LABORATORY FACTUAL REPORT Report No. 15-131

A. ACCIDENT INFORMATION

Place : Las Vegas, Nevada
Date : September 8, 2015
Vehicle : Boeing 777-200, G-VIIO
NTSB No. : DCA15FA185
Investigator : Lorenda Ward, AS-10

B. COMPONENTS EXAMINED

Multiple fragments from a GE90-85B-G11 high pressure compressor stage 8-10 spool (P/N: 1694M80G04, S/N: GWNHA236).
Engine Serial Number: 900-294;
Engine Time Since New: 66,801.22 hours;
Engine Cycles Since New: 9,992;
8-10 Spool Time Since New: 74,170 hours;
8-10 Spool Cycles Since New: 11,459;
8-10 Spool Time Since Last Piece-Part Inspection: 26,671 hours;
8-10 Spool Cycles Since Last Piece-Part Inspection: 3,943;
Engine Time Since Last Shop Visit: 3,645 hours;
Engine Cycles Since Last Shop Visit: 503.

C. DETAILS OF THE EXAMINATION

On September 8, 2015, at about 1613 Pacific daylight time (PDT), British Airways flight 2276, a Boeing 777-236ER, registration number G-VIIO, powered by two General Electric GE90-85BG11 turbofan engines experienced a No. 1 engine (left) uncontained failure and subsequent fire during the takeoff ground roll on runway 07L at McCarran International Airport (LAS), Las Vegas, Nevada.

On-scene examination of the engine indicated that a breach in the engine case had occurred in the vicinity of the high-pressure compressor (HPC) 8th stage disk, part of the HPC stage 8-10 spool, shown in figure 1. The spool is manufactured by welding a stage 8 disk, made from alloy DA718, to a stage 9-10 spool, made from alloy R88DT. The weld pad, where the two components are joined, is aft of the stage 8 disk rim, as indicated in figure 1. Aft of the weld pad is a set of seal teeth (middle seal teeth), followed by the stage 9 disk. Forward of the stage 8 disk rim is a set of seal teeth (forward seal teeth) and the forward rabbeted flange.

Portions of the stage 8-10 spool from the forward rabbeted flange to the middle seal teeth were separated from the spool and multiple fragments had been liberated from the engine. The liberated engine fragments were gathered from the runway and additional fragments were removed from the engine. The fragments were sent to the NTSB Materials Laboratory for examination and are shown in figure 2. A laboratory examination was held on September 14 and 15, 2015 with the following individuals in attendance:

Donald Kramer, Ph.D. – NTSB – Materials Engineer
Harald Reichel – NTSB – Powerplants Engineer
William Rossey – General Electric – Materials Engineer
Richard Yhap – FAA – Air Safety Investigator

The fragments were examined to determine, as much as possible, their origin. Pieces from the same part of the spool (for example, stage 8 disk rim pieces), were then grouped together. As shown in figure 2, the majority of the fragments originated from the forward seal teeth, the stage 8 disk rim, or the inertia weld/middle seal teeth. Approximately 4 ft of the disk rim was accounted for out of a total rim length of approximately 7 ft. There were some additional engine pieces from the forward flange as well as some pieces that were not identified.

The fracture surfaces of the fragments were examined to determine where the failure initiated. A feature of interest was located in the web of one of the stage 8 disk rim pieces, indicated by a white rectangle in figure 2 and shown in figures 3a through 3c. The feature was located approximately 0.9 inch inboard of the blade slot bottom at the thinnest part of the web (approximately 0.118 inch), as nominally indicated by the red pen mark on the cross section in figure 3c (not an exact marking). Examination of the fractured web revealed the presence of a tinted/discolored hemi-elliptical shaped flat-fracture region, as shown in figures 4a and 4b, that was approximately 0.63 inch in width and extended from the aft face of the web to within 0.004 inch of the forward face of the web. The orientation of the hemi-elliptical region was consistent with the fracture initiating on the aft face of the web and the tinted appearance was consistent with high temperature oxidation of the fracture surface. The flat fracture region transitioned smoothly to a 45°-inclined tinted/discolored region that was consistent with cyclic tensile loading. The cyclic tensile loading region extended circumferentially from both sides of the flat fracture region over a total length of approximately 1.7 inch after which point the appearance of the fracture surface was consistent with tensile overstress.

The fracture surface was cleaned and examined with a scanning electron microscope (SEM), primarily in the flat-fracture region. The examination indicated that the flat fracture region exhibited an intergranular appearance near the initiation site, a transition zone of variable size starting at approximately 0.007 inch from the aft face of the web, and a transgranular appearance further away from the origin, as indicated in

figure 5.[1] Representative higher magnification views of the intergranular and transgranular regions are shown in figures 6a and 6b, respectively. At this magnification the transgranular regions exhibited fatigue striations consistent with high alternating stress low-cycle fatigue crack growth. Detailed characterization and determination of crack propagation mode of the intergranular region was carried out at a later date.[2]

The fracture surface was deformed where it met the aft face pushing material out of the original plane of fracture (see figure 5). To examine this in greater detail the aft face of the web was examined in the SEM where it met the fracture, as shown in figure 7a. Smeared material, which was also visually apparent, was observed on the aft face in the vicinity of the fracture. The composition of the smeared material was examined using energy dispersive X-ray spectroscopy (EDS), as shown in figure 7b, and consisted primarily of aluminum (Al).

A series of SEM images was taken from the origin (aft wall) to the forward wall of the web to measure striation spacing as the crack progressed in low cycle fatigue. The series of SEM images that were taken are shown in Appendix A along with their coordinates relative to the deformed origin. The striation spacing measurements are shown in Table 1. An analysis of the striation spacing can be found in an accompanying study report.[3]

Donald Kramer, Ph.D.
Sr. Materials Engineer

[1] The aft face of the web was damaged and was deformed inward approximately 0.003 inch along the aft face of the fracture, placing the transition from intergranular to transgranular at approximately 0.010 inch from the aft face in the undamaged condition.
[2] See GE Aviation Metallurgical Investigation Report FAL2015-17359, included as Appendix B in this report.
[3] See NTSB Materials Laboratory Study Report 15-131S.

Table 1: Striation density measurements on the HPC stage 8 disk web. The X, Y coordinates are relative to the (deformed) origin. Increases in Y are associated with moving from the aft face of the web toward the forward face of the web. X is along the circumferential direction of the disk.

X, mm	Y, mm	Number of striations	Distance, µm	Number of Striations / mm
0.159	0.413	7	2.507	2792
0.159	0.413	4	1.542	2594
0.079	0.549	6	1.534	3911
0.079	0.549	6	1.126	5329
0.076	0.604	6	1.880	3191
0.076	0.604	4	1.040	3846
-0.038	0.835	7	2.560	2734
-0.038	0.871	6	2.310	2597
-0.038	0.871	5	1.530	3268
-0.163	1.183	8	3.690	2168
-0.163	1.183	9	4.690	1919
-0.163	1.183	4	2.760	1449
0.014	1.446	8	5.080	1575
0.014	1.446	5	2.650	1887
0.085	1.556	5	2.600	1923
0.085	1.556	10	4.200	2381
0.005	2.076	7	4.411	1587
0.038	2.106	6	4.050	1481
0.000	2.597	9	9.770	921
0.000	2.597	4	5.090	786

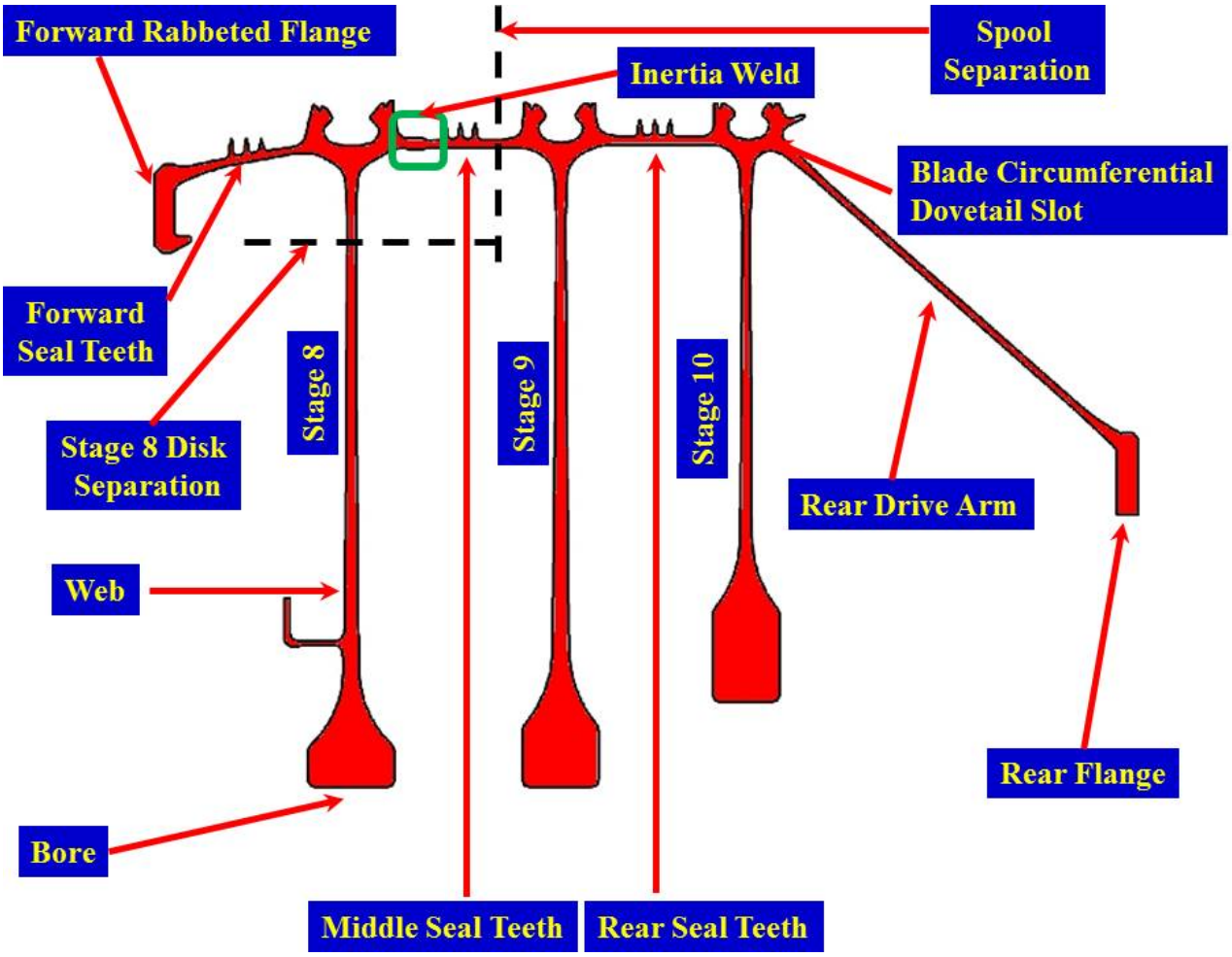

Figure 1: Cross section schematic of the high pressure compressor stage 8-10 spool.[4]

[4] For more engine schematics and information on the HPC stage 8-10 spool, see the Powerplants Group Chairman Factual Report.

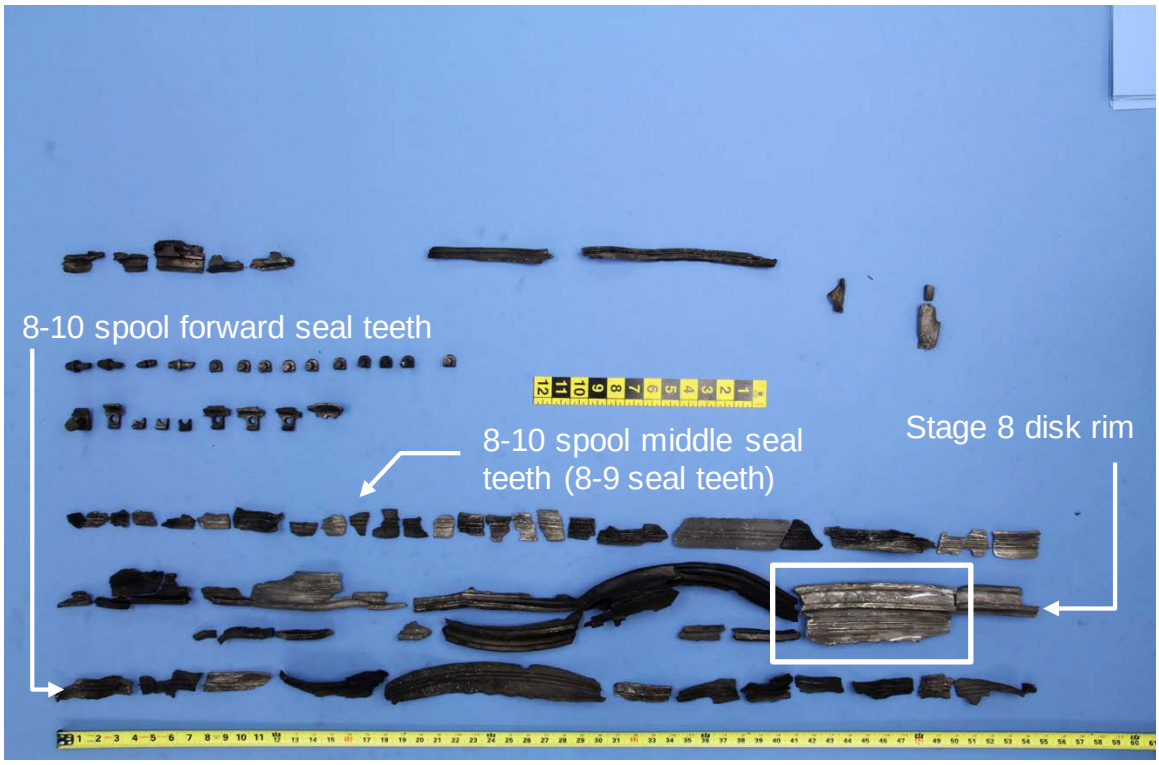

Figure 2: Image of the engine pieces brought to the NTSB Materials Laboratory. Pieces that could be identified as belonging to either the forward seal teeth, stage 8 disk rim, or 8-10 spool middle seal teeth have been lined up from left to right. Approximately 4 ft of the disk rim was recovered.

a)

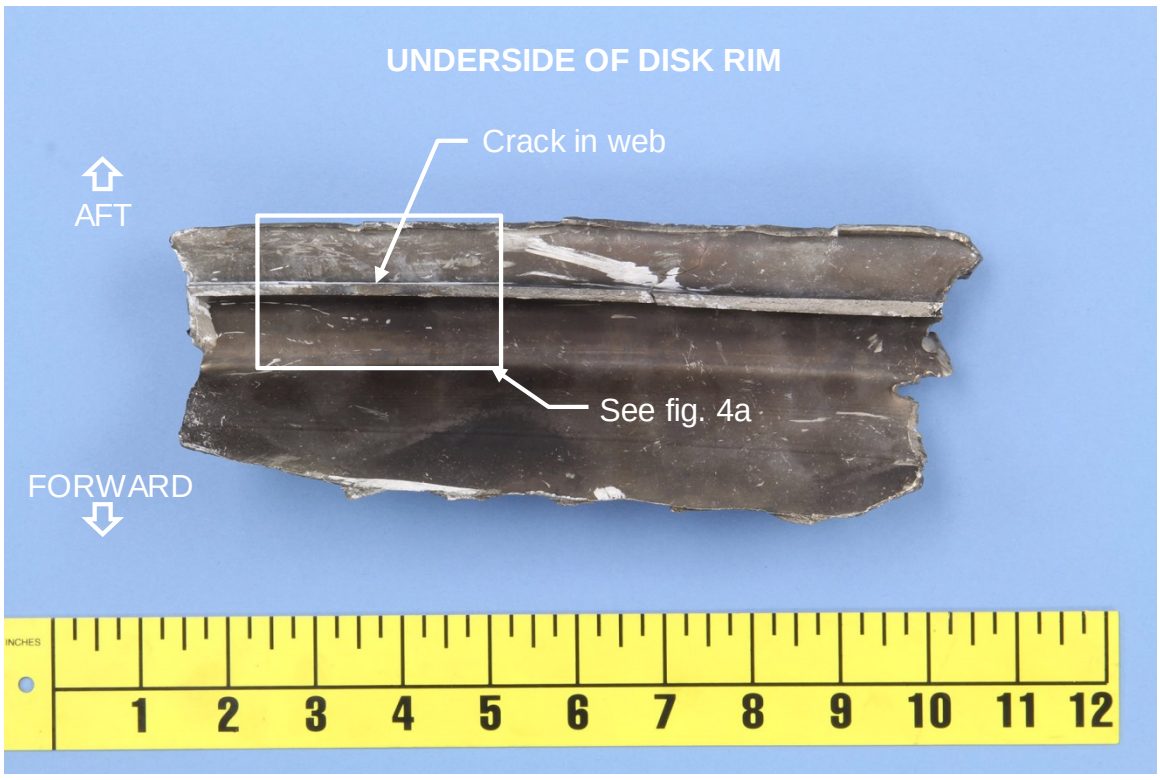

b)

Figure 3: Images of the piece of disk rim where the feature of interest was observed in the disk web, a) top view showing the disk rim; b) view of the underside showing the fracture web;

c) 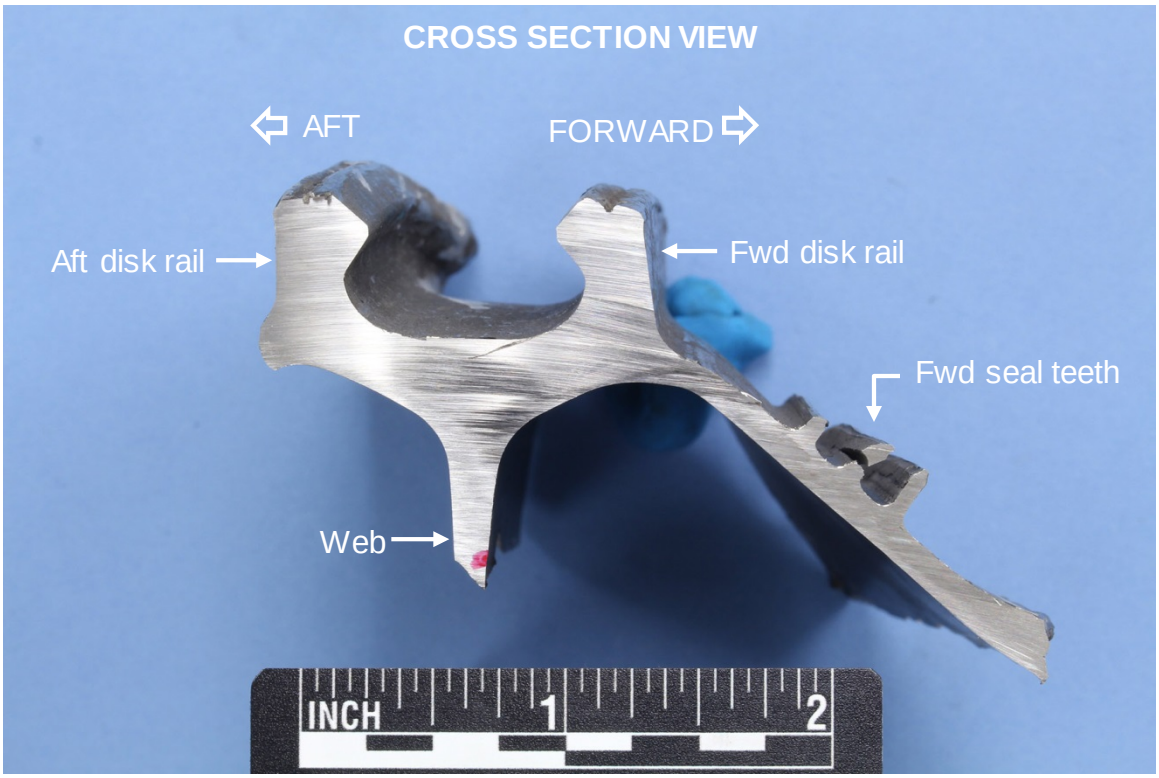

Figure 3 (cont.): c) cross section view showing the web and the approximate location of the crack relative to the slot bottom (red pen mark).

a)

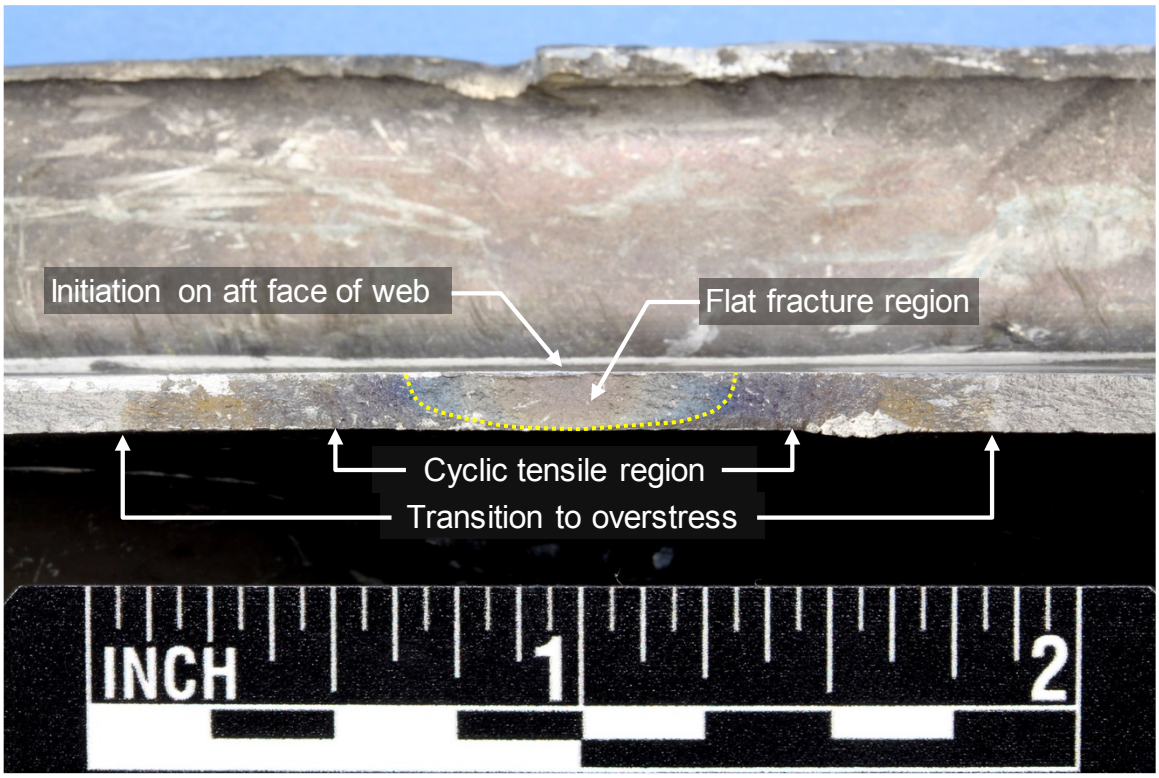

b)

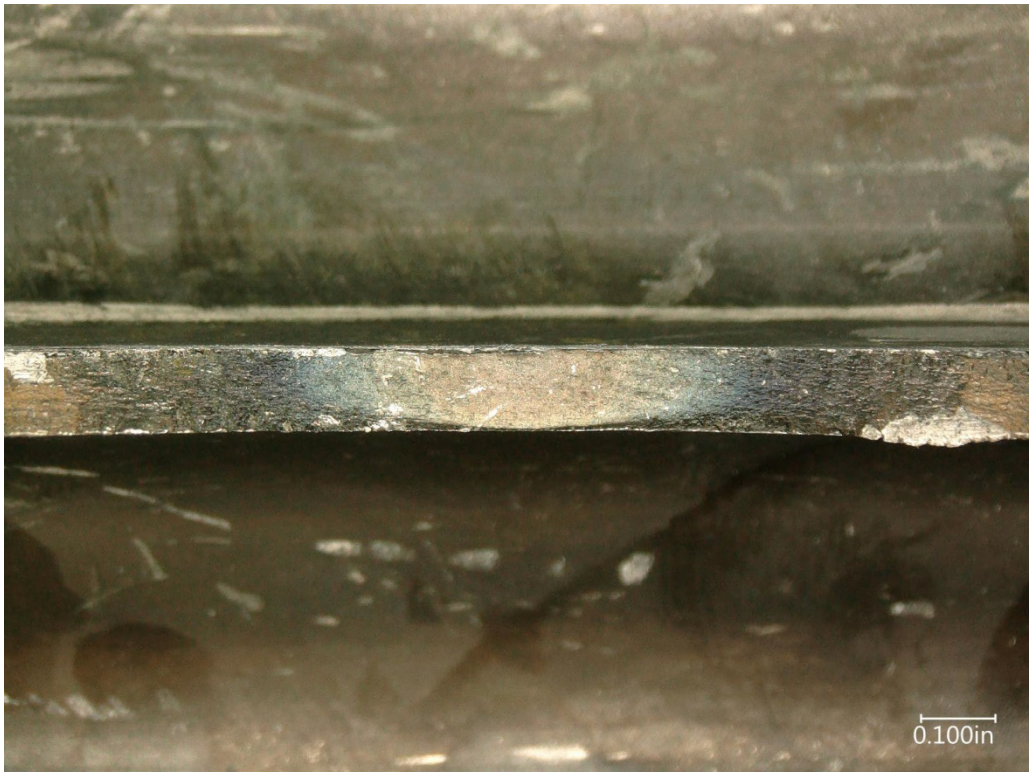

Figure 4: a) and b) Higher magnification images of the underside of the HPC stage 8 disk rim piece at the location indicated in figure 3b. Metallurgical examination indicated that a crack initiated at the aft face of the web at this location and progressed in the longitudinal direction and the circumferential direction.

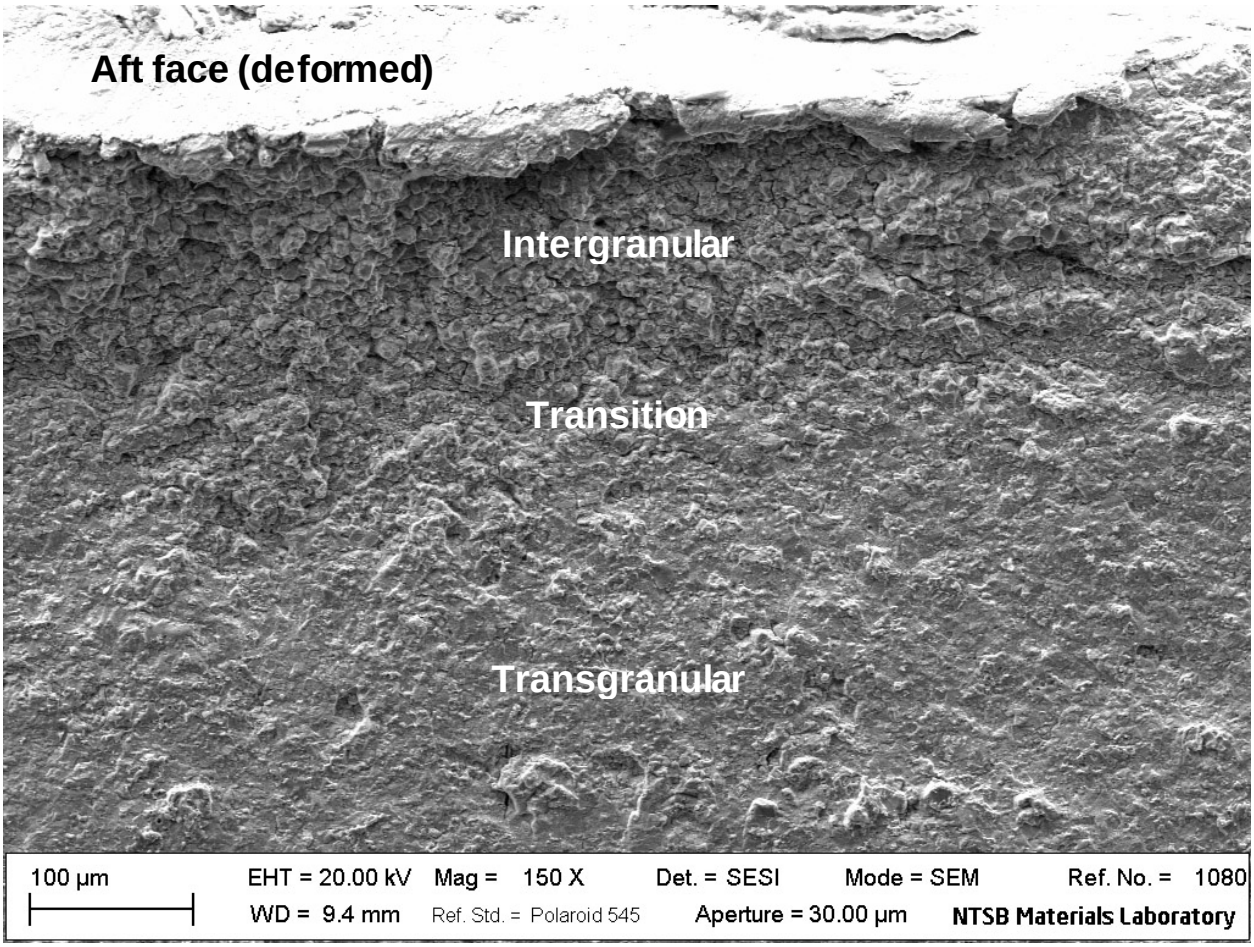

Figure 5: SEM image of the fracture surface at the aft face of the web where the crack initiated. The fracture surface exhibited an intergranular morphology near the aft face which transitioned to transgranular at approximately 0.007 inch.

a)

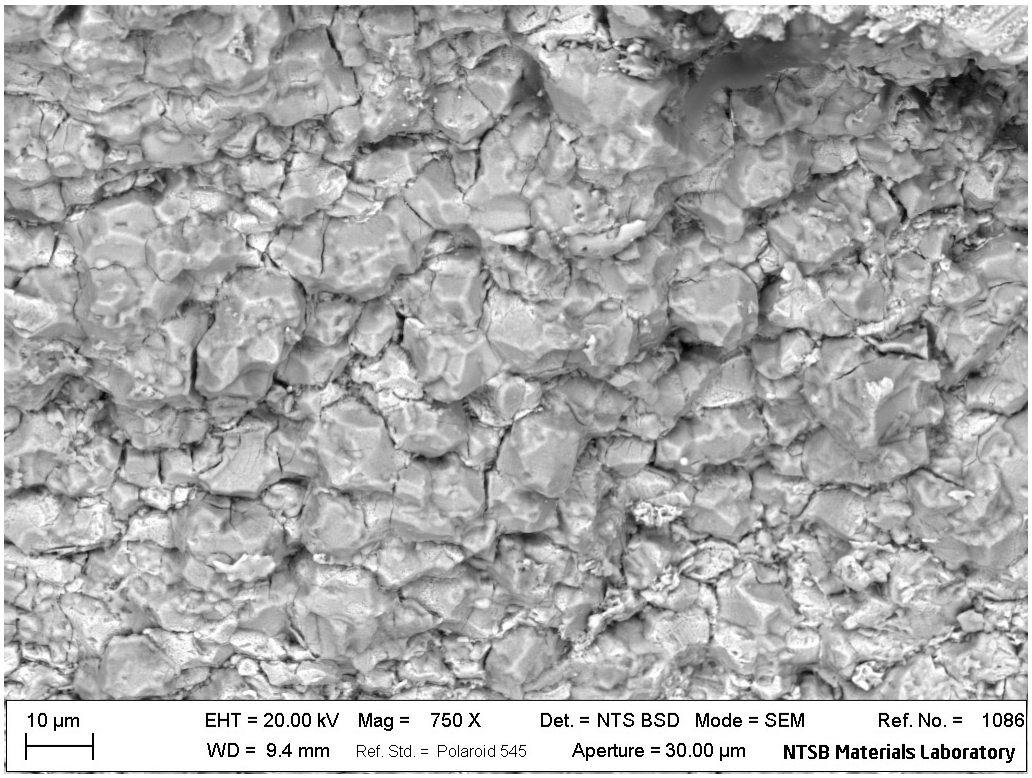

b)

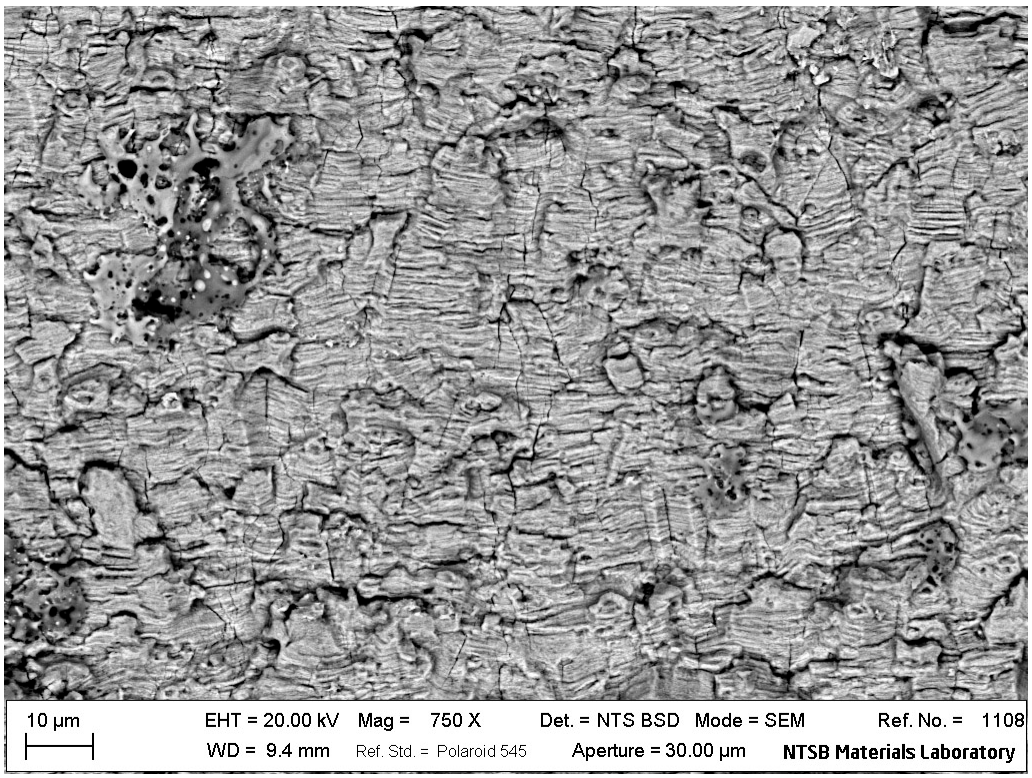

Figure 6: Higher magnification SEM images showing the fracture morphology in the a) intergranular region and b) transgranular region.

a)

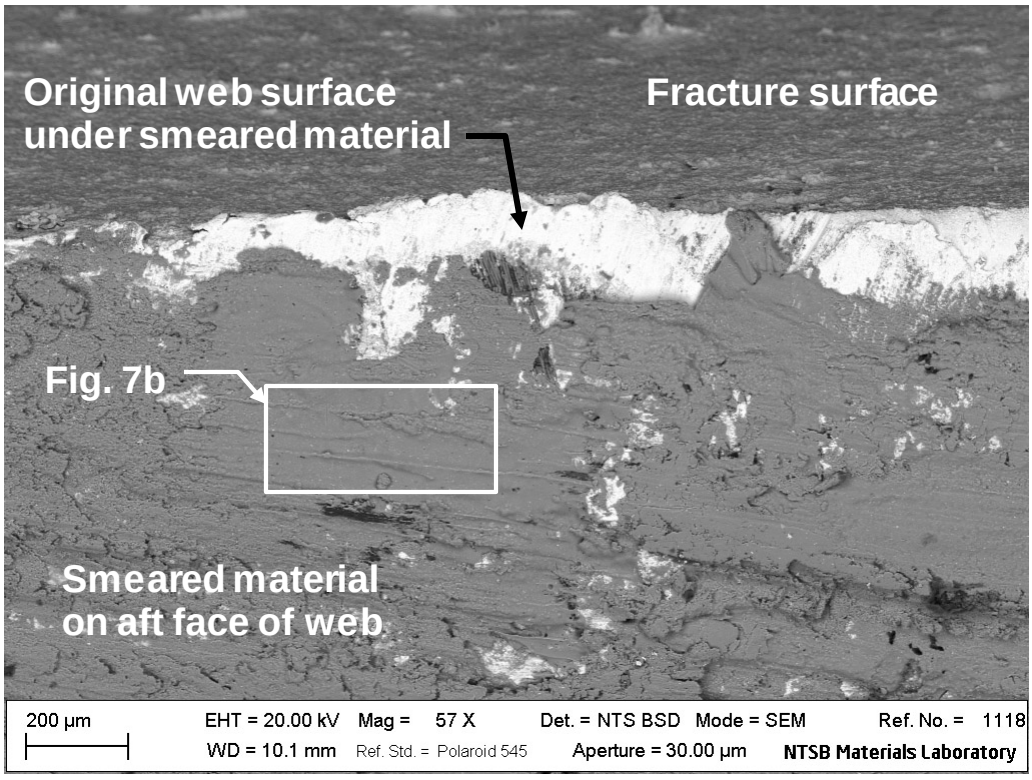

b)

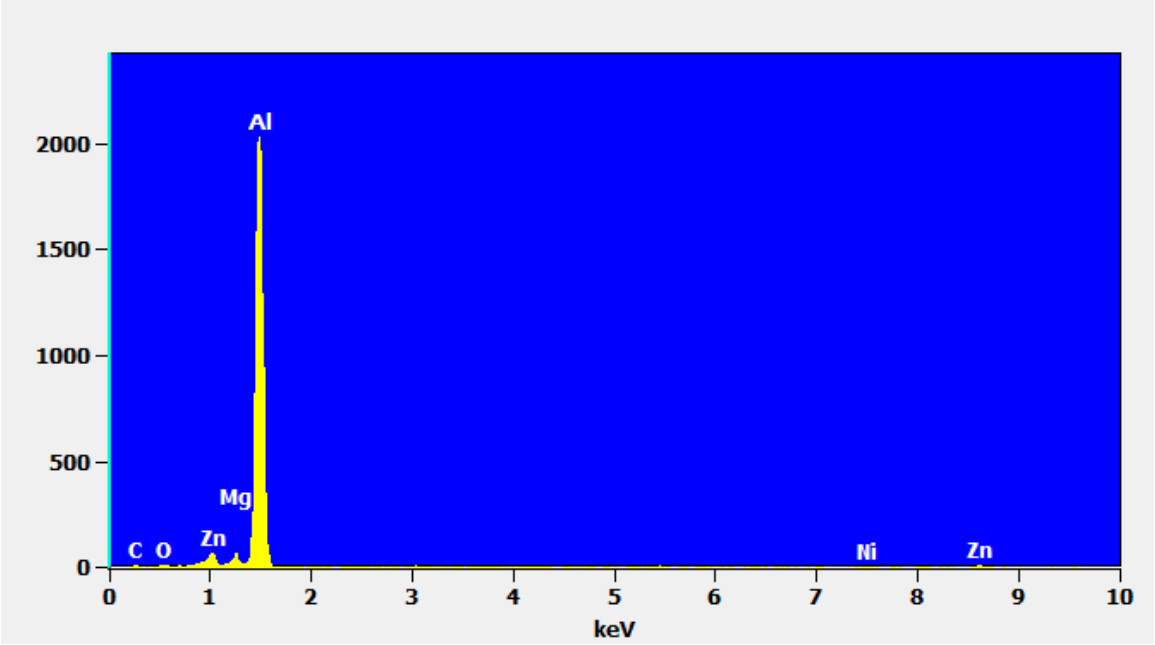

Figure 7: a) SEM image of the aft face of the web where it met the fracture surface. Smeared material was observed on the aft face; b) EDS of the smeared material exhibiting primarily aluminum (Al).

APPENDIX A: SEM Images for Striation Counting

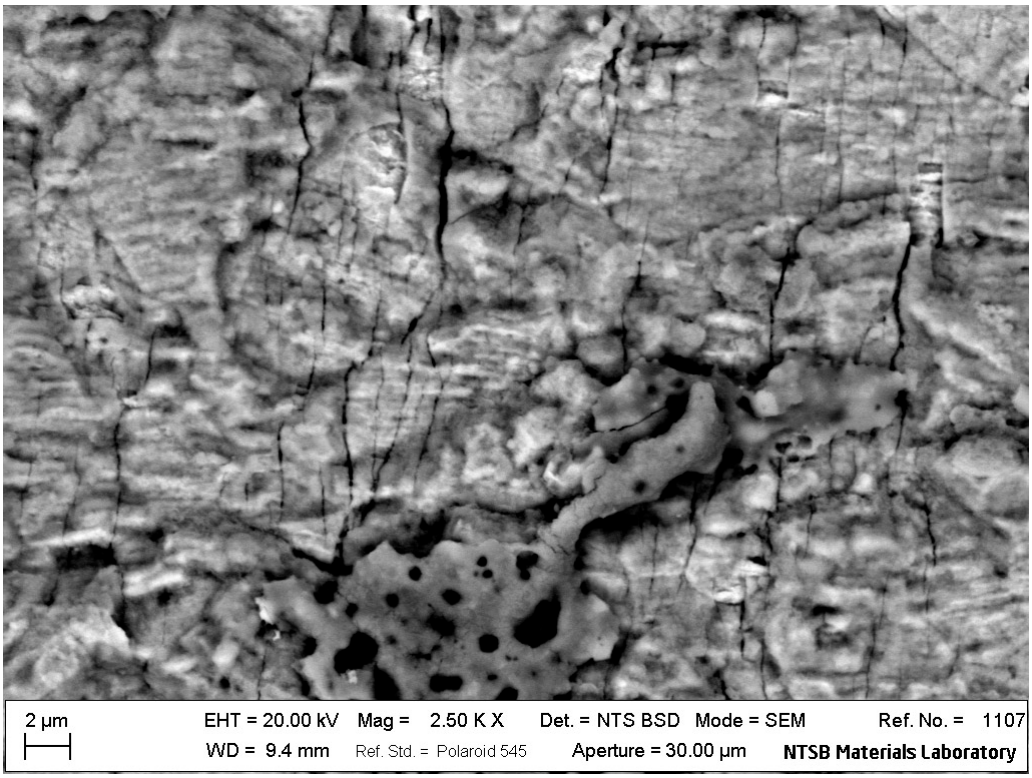

X = 0.159 mm, Y = 0.413 mm

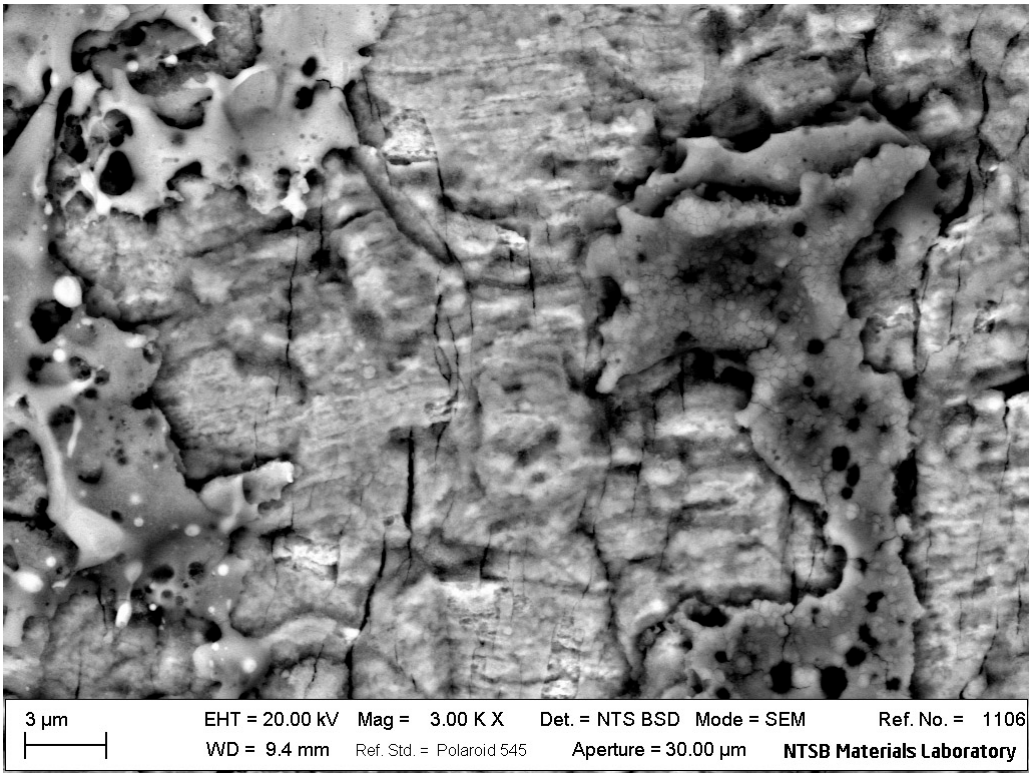

X = 0.079 mm, Y = 0.549 mm

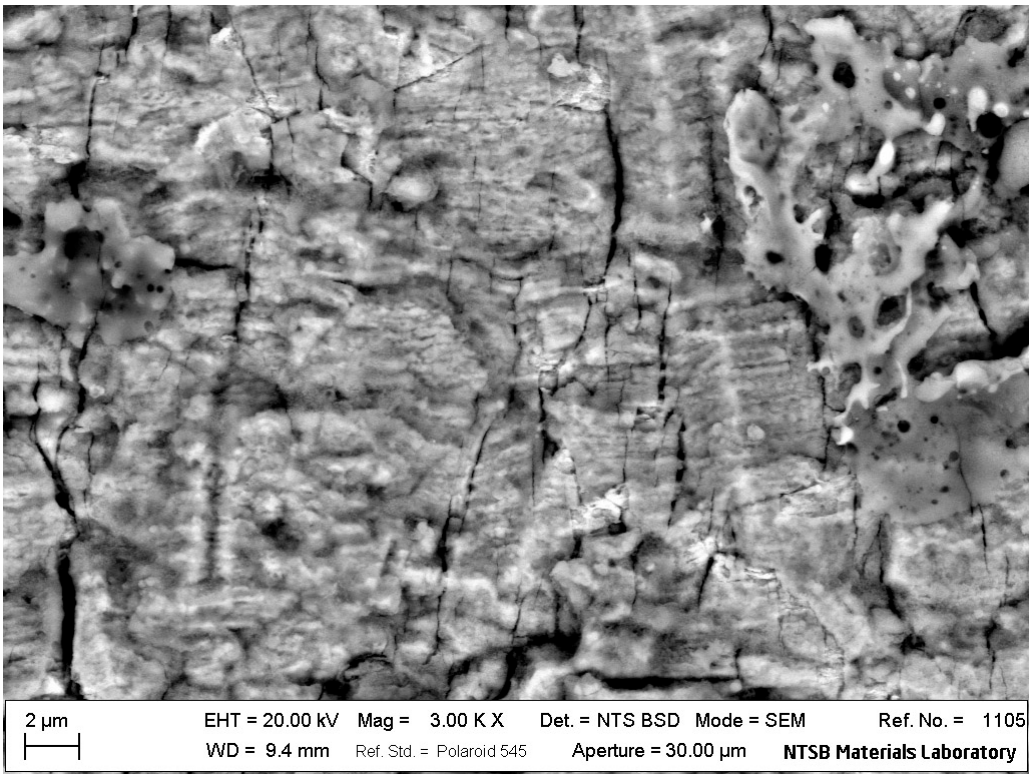

X = 0.076 mm, Y = 0.604 mm

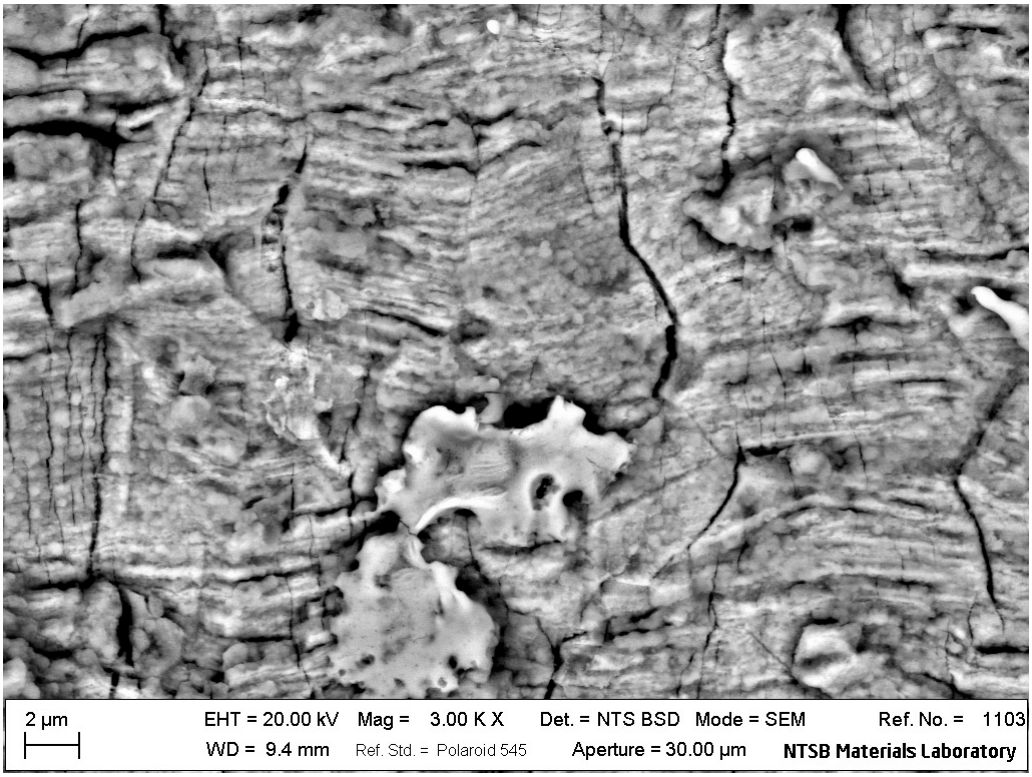

X = -0.038 mm, Y = 0.835 mm

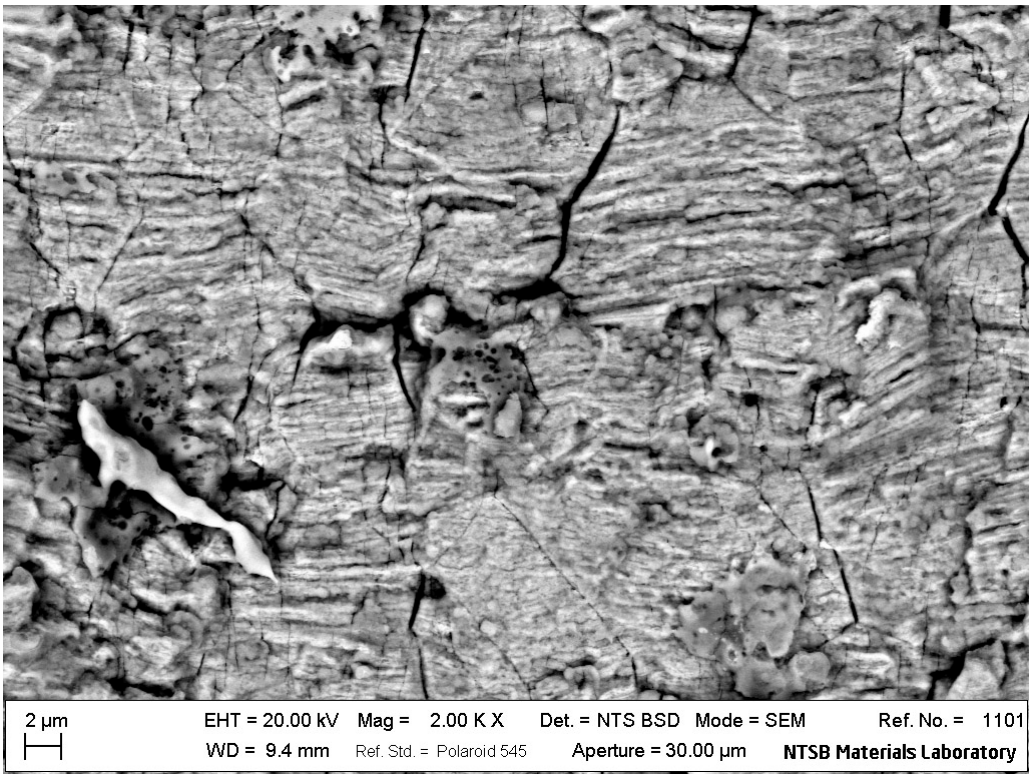

X = -0.038 mm, Y = 0.871 mm

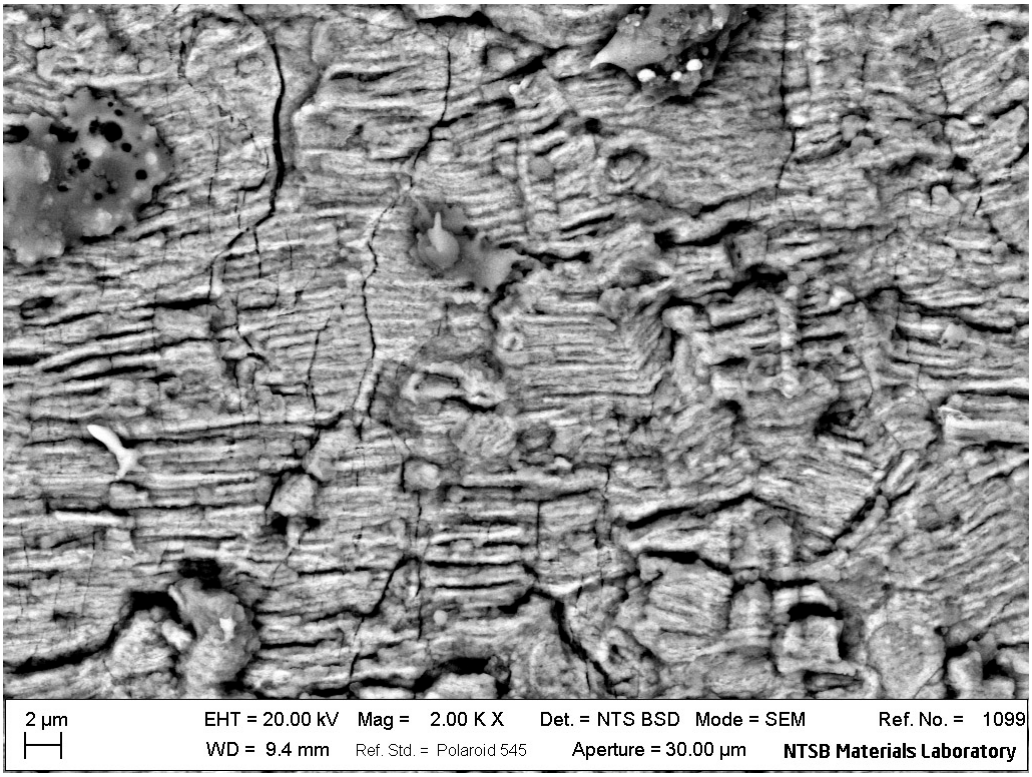

X = -0.163 mm, Y = 1.183 mm

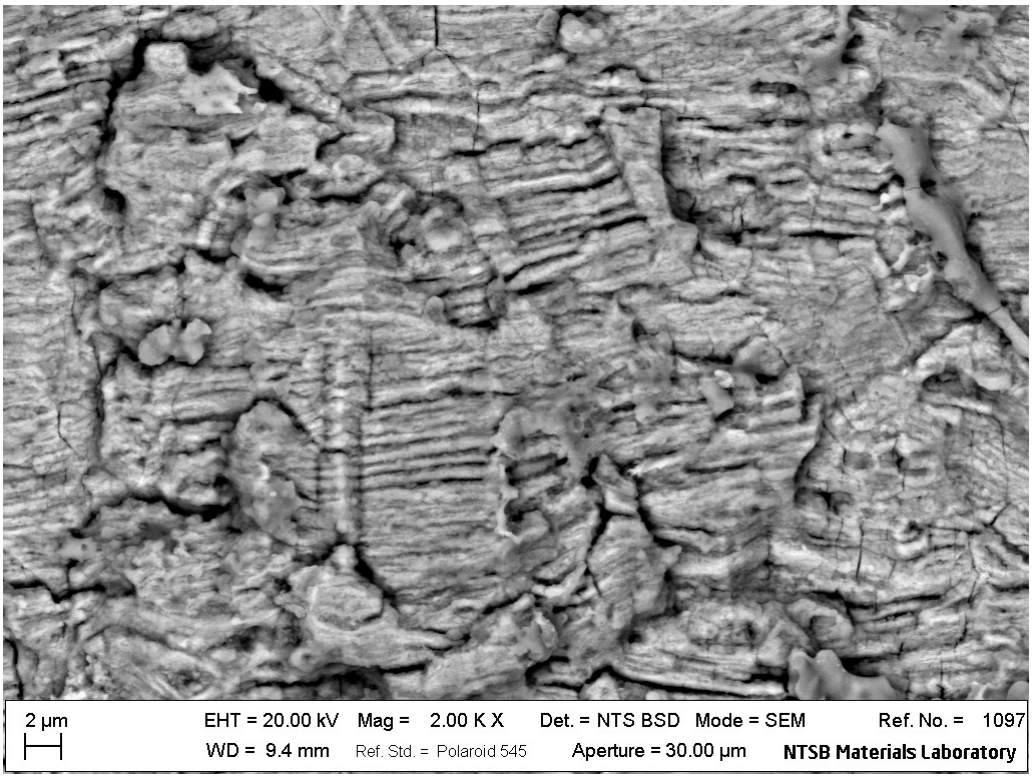

X = 0.014 mm, Y = 1.446 mm

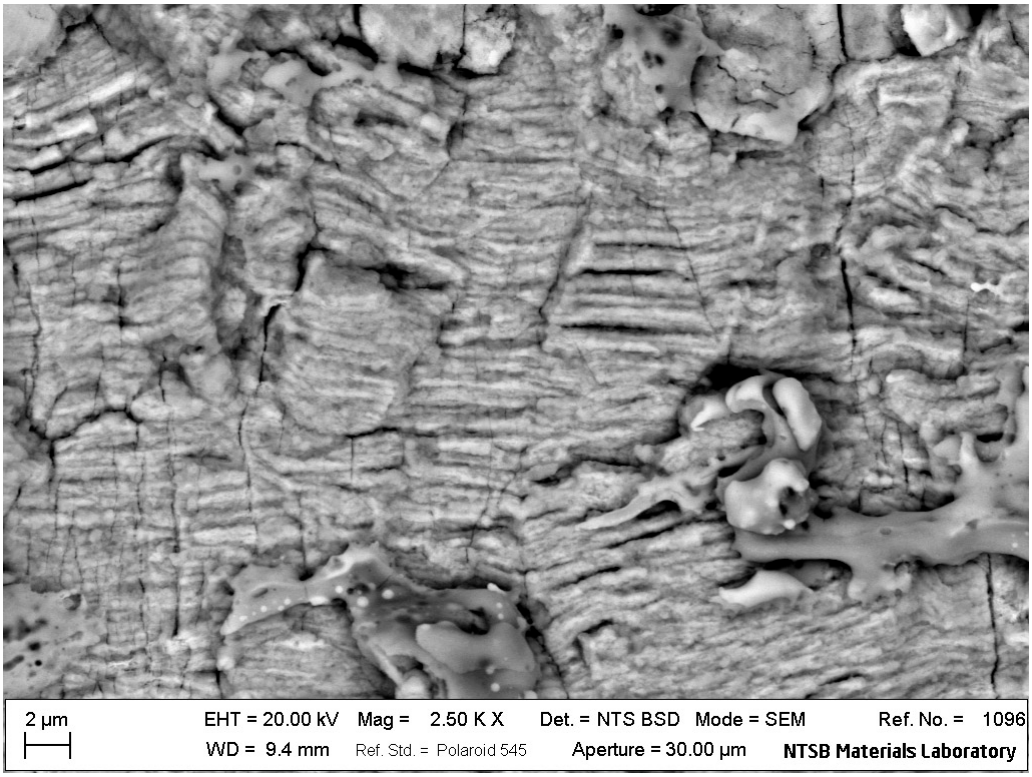

X = 0.085 mm, Y = 1.556 mm

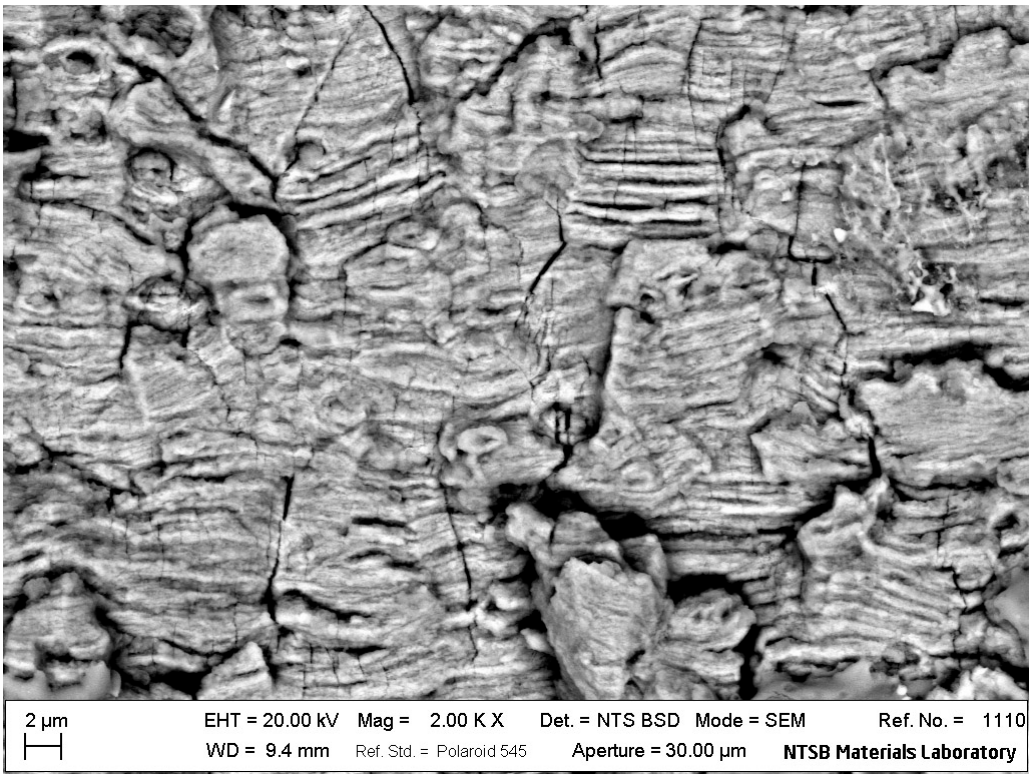

X = 0.005 mm, Y = 2.076 mm

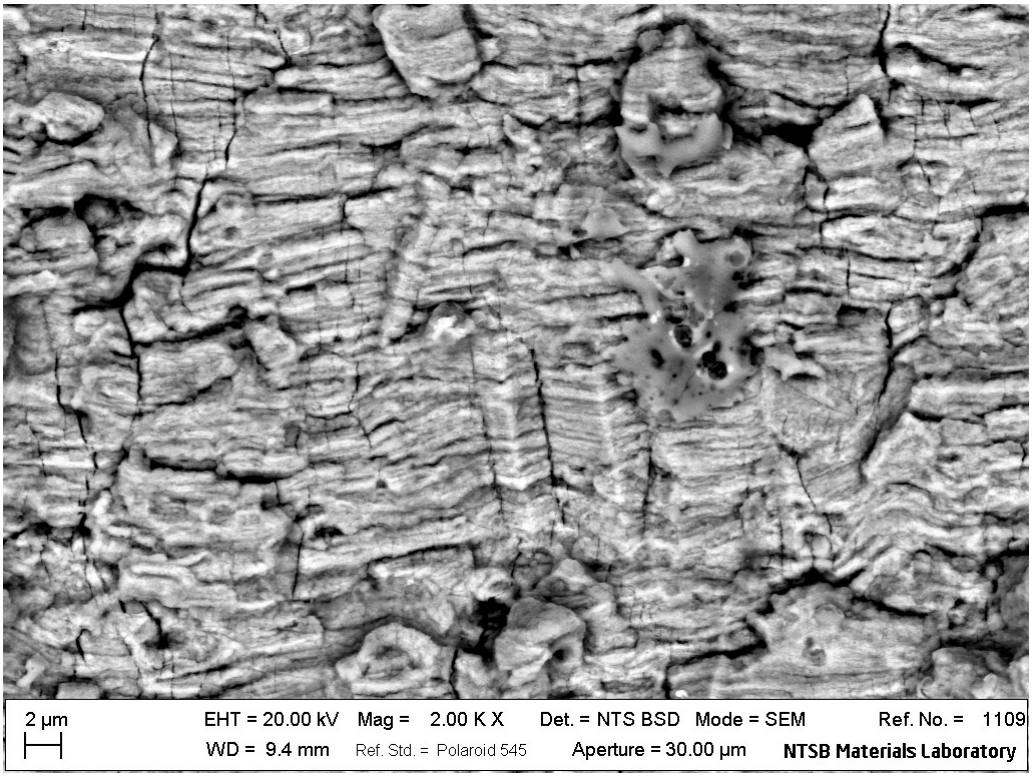

X = 0.038 mm, Y = 2.106 mm

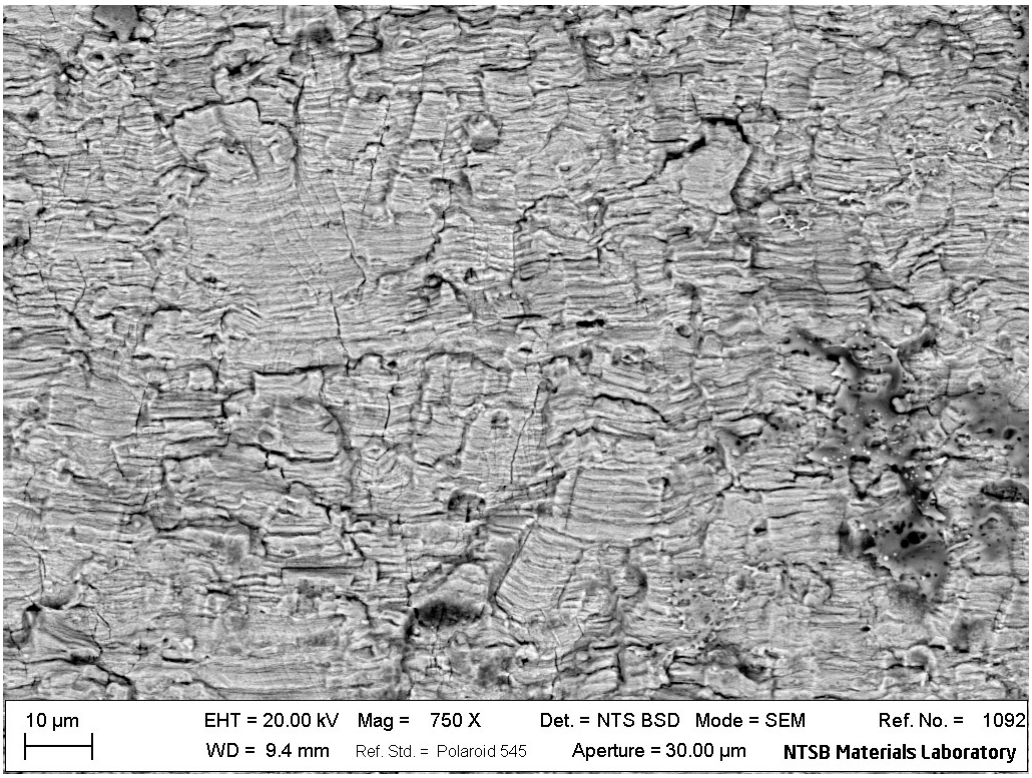

X = 0.000 mm, Y = 2.597 mm

APPENDIX B: GE Aviation Metallurgical Investigation Report FAL2015-17359

Metallurgical Investigation Report
Log No. FAL2015-17359- Final_Rev B

METALLURGICAL EVALUATION OF A GE90-85B UNCONTAINED EVENT HPC 8-10 SPOOL FROM ESN 900-294 OPERATED BY BRITISH AIRWAYS IN LAS VEGAS, FLIGHT 2276

HPC 8-10 Spool
P/N 1694M80G04
S/N GWNHA236
TSN/CSN 74,170 / 11,459

William R. Rossey Jr.
MPED-Metallurgical Investigations
Date: May 17, 2016

Export Classification: NLR, 9E991

imagination at work

Background

- A GE90-85B high pressure compressor (HPC) 8-10 spool (P/N 1694M80G04, S/N GWNHA236) from ESN 900-294 operated by British Airways was submitted for metallurgical evaluation after an uncontained event occurred in Las Vegas on September 8, 2015. Reportedly, the event occurred while the plane was taking-off after it reached a top speed of approximately 80 knots. Following the event, the take-off was aborted and the plane was taxied to a safe location for disembarkment. All passengers were deplaned successfully with minor injuries reported, but an ensuing fire occurred that consumed part of the adjacent wing/fuselage.

- The engine accumulated a total of 66,801 hours since new (TSN) and 9,992 cycles since (CSN), while the part accumulated **74,170 TSN** / **11,459 CSN**. The part was inspected at piece-part level at the last overhaul **26,671 hours / 3,943 cycles** prior, which included alkaline cleaning, stripping and re-coating of the seal teeth, fluorescent penetrant inspection (FPI), and eddy current inspection of the inertia weld. Prior to the overhaul the part was installed on ESN 900-121 with the same operator. A graphical depiction of the part history timeline can be seen in Figure 1.

- The investigation is headed by the National Transportation Safety Board (NTSB). The “party members” to the investigation are GE, Boeing, and the Federal Aviation Administration (FAA). The Air Accidents Investigation Branch (AAIB) is an accredited representative to the investigation and British Airways is a technical advisor to the AAIB. As part of the metallurgical investigation, the initial sections of the liberated rim portions of the stage 8 disk were examined in the NTSB materials laboratory in Washington, DC on September 14 and 15, 2015. The remainder of the spool that was still contained in the engine was examined in the GE Aviation material lab in Evendale, OH from September 23rd onward. GE Aviation also enlisted the analytical capabilities of GE Global Research Center (GRC) for specific follow-on testing.

8-10 Spool S/N GWNHA236 History

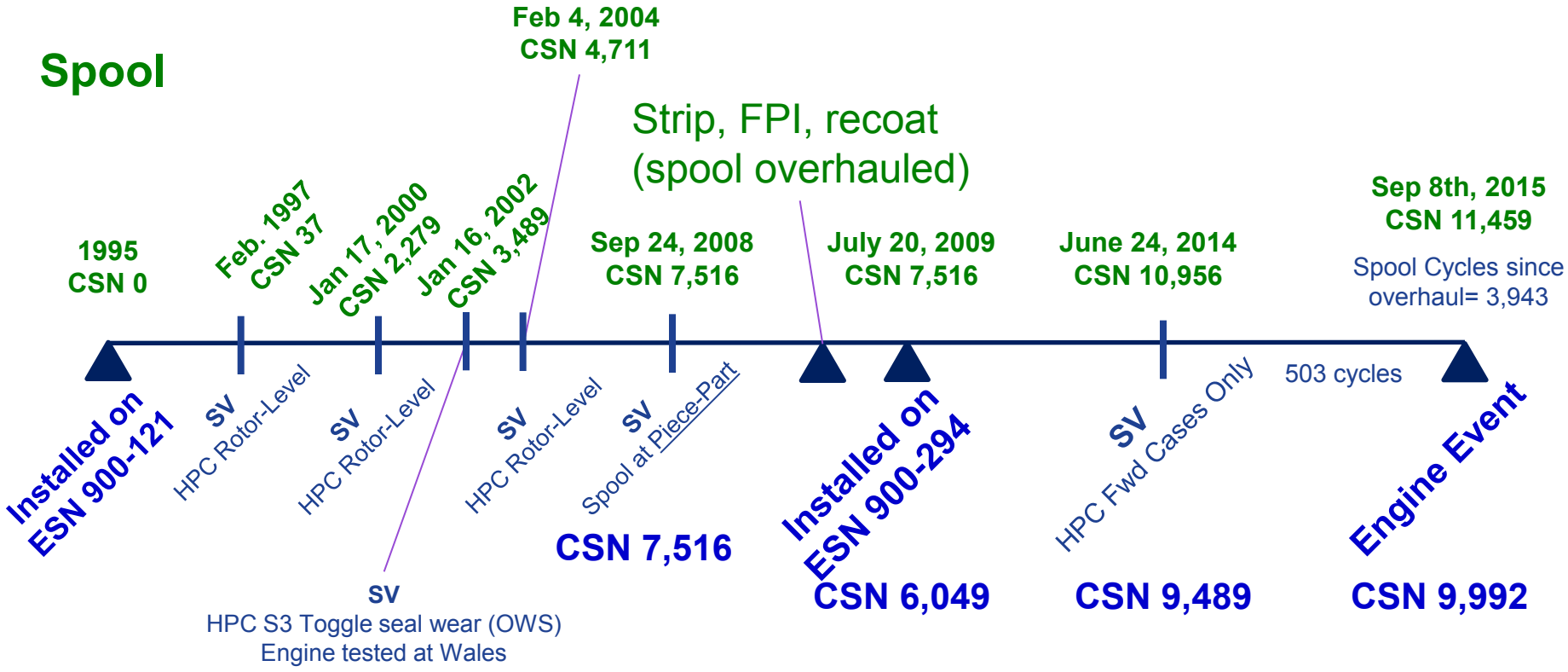

Notes:

- HPC Rotor level= 8-10 spool not at Piecepart level per definition below (inspect per 72-00-31)
- Piecepart level = 8-10 spool removed from the rotor assembly and de-bladed (inspect per 72-31-08)

Figure 1: Description of the significant timeline events on the 8-10 spool being investigated. It had 11,459 cycles since new and was inspected at piece-part level 3,943 cycles prior.

Summary

• The metallurgical investigation of the 8-10 spool revealed a single, planar, heat-tinted, thumbnail-shaped fracture consistent with fatigue that extended in the web of the stage 8 disk at the rim transition area, approximately **0.950 inch** inboard of the slot bottom. The crack extended in a circumferential orientation and initiated from the aft face at the web thinnest location (approximately **0.118 inch** thick). The fatigue region was planar for **0.62 inch,** then transitioned to slanted cyclic tensile fracture for a total length of approximately **1.72 inch**, prior to overstress fracture. Scanning electron microscope (SEM) examination of both mating fracture surfaces showed that it **initially propagated** with **intergranular** features for **7-10 mils** (0.007-0.010 inch)- with local variation, consistent with hold-time, high-alternating stress, low-cycle fatigue **(hold-time LCF / sustained-peak, low-cycle fatigue- SPLCF)**. The crack then transitioned to transgranular, striated areas that decreased in density progressing through the web thickness, consistent with more cyclic-driven **LCF**. It should be noted that both fracture halves at the aft surface/origin area had **1-3 mils** of impact **damage**, consistent with post-fracture, event-related damage. Based on the striated areas **over 5,000 cycles** of growth were obtained by multiple estimates (not including the initial intergranular region of growth).

• Metallographic mounts adjacent to the origin area (excluding the post-fracture surface damage) showed **no microstructural anomalies.** The grain structure conformed to the requirements of properly processed DA718. The part hardness, composition, and geometry conformed to the requirements. Further characterization of the intergranular region by microprobe, Auger, high-resolution SEM, and TEM, did not reveal any detrimental species at the grain boundaries, only base metal oxides.

• Though the origin area was damaged, **multiple secondary cracks** were found within 16 mils radially of the fatigue region. These secondary cracks, up to approximately **3 mils** long and **0.5 mil deep**, initiated in a combination of intergranular/transgranular modes at the base of oxidized/etched carbides with **no surface/microstructural anomalies**. Two of these cracks were analyzed and found to be oxidized, meandering/branching, generally progressing normal to the surface, and were blunted, consistent with pre-existing fatigue cracks that slowed/stopped. Secondary cracks were not found on the diametrically opposed side in the same radial plane, nor on the forward faces (with one exception at/near the slant fracture).

• Other findings included visual differences in shot peening appearance between the forward and aft sides of the stage 8 web. On the forward face the peening was more pronounced, whereas on the aft face it was pronounced in the bore region, but decreased radially moving towards the rim. **Residual stress** measurements were taken on both sides of the event disk and 2 comparison disks of similar vintage. The data showed that on the forward web of the comparison disks the residual stress profiles conformed to expectations for a well peened surface, whereas the event disk profile was different/less compressive near the fracture, though it approached the profiles of the other disks further inboard radially. All disk aft web faces near the outer radius had profiles consistent with GE experience for as-turned surfaces (with little/no peening).

• In summary, the fracture of the spool was the result of a fatigue crack that initiated in the web aft face. Though the origin area was slightly damaged by post-event related impacts, nearby secondary cracks consistent with fatigue did not show any damage or microstructural anomalies. At this point in the evaluation, the fatigue crack initiated earlier than predicted and the combination of factors needed to result in an intergranular fracture origin region have not been fully identified.

Observations

- Cross-sections of the GE90 HPC showing the part geometry and location of the fatigue crack can be seen in Figures 2 and 3.
- Optical examination of the fracture surfaces revealed a single heat-tinted, thumbnail-shaped fracture extending into the web outer rim transition region with features consistent with **fatigue** (Figures 4-10, 23, 24, 26-28). No fatigue cracks were found in the seal teeth or inertia weld.
    - The fatigue region extended in a circumferential/axial plane and was initially planar for approximately **0.62 inch** long then extended at a slant angle for a total combined length of approximately **1.72 inches**, prior to transitioning to overstress fracture (Figures 6-8, 10-11).
    - The fatigue crack initiated from the **aft face** of the web and both the inboard and outboard faces were damaged by post-fracture impact damage (Figures 11, 12, 27-29).
    - The fatigue area was approximately **0.950 inch** inboard of the slot bottom (Figure 9). This was at a location where the web was thinnest and was approximately **0.15** inch inboard of the allowable machining mismatch on the forward face of the web (shown in mounts- Figures 26, 57 and 63).
- Scanning electron microscope (SEM) examination of both mating fracture surfaces revealed that the primary fracture **initially propagated** with **intergranular** features to a depth of approximately **7-10 mils** (with local variation), consistent with **hold-time fatigue** (Figures 13-18 and 30-34). The very aft surface/origin area of the outboard fracture had approximately 3 mils of surface damage and the inboard fracture approximately 1 mil of damage, consistent with post-fracture, event-related impact damage (Figure 29). The crack then transitioned to **transgranular, striated** areas that decreased in density progressing through the thickness, consistent with **LCF** (Figures 17-19, with views of the transition area also shown in in Figures 32-36).
    - Based on interpretable striations the fatigue fracture is estimated to have grown from the base of the intergranular region to the end of the striated region (10-105 mils) in **over 5,000 cycles** by multiple estimates (does not include the initial intergranular region)- Figure 20.
- Energy dispersive spectroscopy (EDS) analysis of the fracture only showed elements consistent with oxidized **alloy 718** (EDS 1 and 2- Figure 21; EDS 5- Figure 29). On the outboard fracture origin area the **secondary impact** damage was consistent with an **Al-base alloy** containing Zn and Mg (EDS 4- Figure 22), with smeared base metal nearby (EDS 3). By comparison the impact on the inboard side fracture was consistent with a **Ni-based** alloy, but the peak heights were not an exact match for DA718 (EDS 6- Figure 29).

Observations

• A series of step polishes were made in an axial/radial metallographic mount prepared through the inboard fracture half and a single polish into the outboard fracture half, which showed the following (Figures 37-62):

- No metallurgical anomalies were found in the base material in the as-polished condition and a typical distribution of carbides was observed, which often intersected the surface. In those areas the carbides were often oxidized and partially removed, leaving depressions/pits up to **0.5 mil deep** (Figures 41 and 42).
- The electrolytic phosphoric etch did not reveal any heat affected zones, consistent with the lack of thermal damage.
- The Kalling's etch showed that the microstructure was consistent with properly processed DA718 material with fine grains with an approximate average grain size of **ASTM 11** and occasional grains as-large-as **ASTM 7**, both conforming to the requirements of C50TF81. The structure had a typical matrix of γ with unresolvable γ'' and γ', with dispersed δ Ni_3Nb precipitates, angular gold TiN particles, and random Nb-carbo-nitrides.
- Vickers (500g load) micro-hardness readings taken from the inboard mount (converted to Rockwell C scale for convenience) ranged between **HRC 46-48**, conforming to the requirements of C50TF81. The measurements taken near the aft and forward faces were similar (Figure 55).
- By mating the fracture surface mounts the level of work in the aft corner of the fractures did not match, also consistent with secondary impact damage (Figure 62).
- EDS, microprobe, Auger, high-resolution SEM, and transmission electron microscopy (TEM) examination of the intergranular region did not identify any foreign detrimental species, only **oxidized base material** (Figs. 39. 43. 67-93).
- High resolution SEM/EDS analysis showed **depleted Cr and Fe ahead of the crack tips** at the branching portions of the intergranular fracture (therefore rich in Ni), with the **crack** being rich in base metal oxides (Figures 78-87). This was found as close as 1 mil from the aft face (closest analyzable area).
- More detailed TEM examination of 2 branched cracks from the intergranular fracture showed that there was oxidation ahead of the crack tips with preferential formation of Al and Ti-rich oxides ahead of Fe-Cr rich spinel oxide structure. A γ phase lean in γ'/γ'' forming elements was present ahead and adjacent to the crack tip. Both the crack tip structures were consistent with **hold-time fatigue crack growth** under low oxygen partial pressure (Figures 88-93).
- Microprobe analysis of the base metal adjacent to the intergranular fracture (and in the mount on the opposite side of the disk) revealed a composition consistent with the requirement of alloy 718, though it was slightly enriched in Nb near the surface carbide (Figure 73).

Observations

• SEM examination showed that on the aft web face **within 16 mils** of the fatigue fracture were **secondary cracks** at the base of etched/oxidized carbides (Figures 94-96 and 98). These circumferential cracks were up to approximately **3 mils** long and were up to **0.5 mil deep** (based on the metallographic mounts). Secondary cracks were not observed further inboard (Figure 97), on the corresponding forward face, except for a single crack at/next to the cyclic tensile fracture (Figure 99), nor on either face on the opposite side of the disk (Figures 100 and 101). Cracks extending on opposing 45 degree planes were found near the rim fracture ends, consistent with event-induced shear cracks (Figures 102-104).

- Focused ion beam (FIB) trenches made into the sides of 2 secondary cracks near the fatigue fracture showed growth from the base of oxidized/etched carbides. The cracks tended to be branched/meandering, generally extending normal to the surface, but the level of oxidation at the crack tips was relatively thick/rounded, consistent with blunted cracks (Figures 105, 106, 108, 114, 116). Based on the level of oxidation and orientation the cracks were consistent with pre-existing **fatigue** cracks (not event-related).
- SEM/EDS analysis of the secondary cracks revealed only base metal oxides with no detrimental species (Figs. 107, 109, 115).
- Step-polishes were made into the same 2 secondary cracks and they showed similar meandering/branching features, that were more transgranular in some areas and more intergranular in others (Figures 111, 112, 116-121). **No damage/microstructural anomalies** were found and the cracks were up to **0.5 mil** deep.

• Visual examination of the stage 8 surfaces showed variation in the shot peening appearance based on location. On the forward side (that had direct line-of-sight) it was more uniform and pronounced than the aft side (Figure 64). On the aft side near the bore the peening looked similar to the forward side (not shown), but progressing radially outward the apparent coverage and/or intensity decreased with minimal distortion/deformation of the machining lines in the web.

• A circumferential mount made near the fatigue region showed distorted surface grain structure in a single direction on both the forward and aft faces of the web, consistent with a turning operation. From optical examination on the forward side the surface grains were locally distorted by approximately **0.5 mil**, whereas on the aft side by approximately **0.2 mil** (Figures 65 and 66). Follow-on electron backscatter diffraction (EBSD) examination showed that the worked grains were approximately **4.1 mils** deep on the forward face and **1.6-2.0 mils** deep on the aft face (described later). On the aft face approximately 11 turning lines were measured in 0.1 inch, consistent with acceptable machining parameters.

• All other fractures on the spool were consistent with overstress. In the stage 10 aft cone arm was a separate 360 degree fracture where the wall thickness was reduced by rubbing (with a visible heat tint), consistent with event-related damage as the spool moved aft against the static structure/CDP seal (Appendix A).

Observations

Residual Stress

• Residual stress measurements were taken on both the forward and aft web faces (in a radial plane at/near and slightly inboard of the fracture) of the event disk and 2 comparison disks of similar vintage and with similar peening features (see Appendix B showing the surface of S/N GWNHA139 and Appendix C1).

- The data showed that the comparison disks had a more compressive layer on the **forward** web exhibiting profiles with a shape/depth meeting typical expectations for a shot-peened part with the parameters used (Appendix C2). For the event part, the residual stress profiles that were within 0.3-0.5 inch of the fracture were less compressive, while a profile 1.6 inch further inboard radially was more compressive, closer to the comparison disk profiles.
- On the **aft** web all disks had a differing compressive profiles than expected. The stress gradient was very steep initially and was only lightly compressive within 1-2 mils of the surface, with 1 event disk profile having up to 50 ksi of tensile stress (Appendix C3). These profiles and surface variation are consistent with GE experience for as-turned surfaces (with little or no peening).

Low Cycle Fatigue Tests

• *Internal Specimens*: Radial internal sheet specimens were manufactured from the event and comparison stage 8 disk webs and tested at 1000°F. The results from both webs were nearly equivalent with most data being at/near GE average life curves, and the outlier was above minimum requirements (Appendix D1- left). Circumferential smooth bar specimens made from the bore of both disks showed comparable results at/near GE average life curves (Appendix D1- right).

• *Surface Specimens*: Radial sheet specimens were tested from comparison disk S/N GWNHA139 with an as-manufactured aft surface with similar peening to the event disk. The fatigue lives were at/near the GE average curve for DA718 (Appendix D2).

Surface Work/Strain

• Metallographic mounts were submitted to GE GRC to examine the event spool surface to see if there was additional work near the fracture/secondary cracks that may have been pre-existing (beyond machining/peening expectations). Using high-contrast SEM backscatter and EBSD imaging showed that the **forward** face of the web had a uniform level of work/strain approximately **4.1 mils deep**, whereas on the **aft** face it was estimated between **1.6-2.0 mils**, consistent with differences in peening observed on the part (Appendix E2 and E3).

• The secondary crack analyzed adjacent to the main fatigue fracture did not show any additional/differing work/strain compared to the baseline surface (left images in Appendix E2 and E3; both in E4). Note that the rectangular missing material at the secondary crack surface was the result of the prior examination FIB process.

GE90 HPC Cross-section

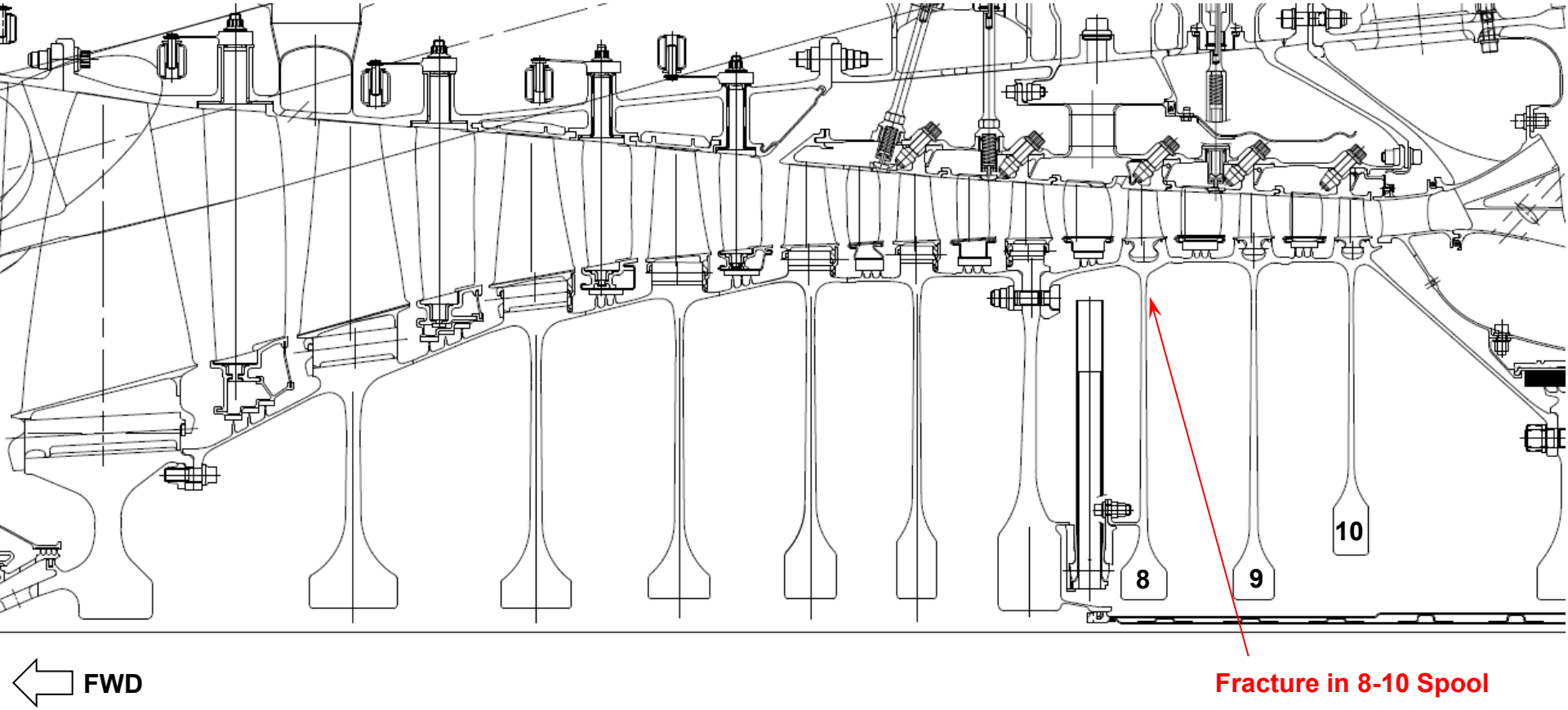

Figure 2: Schematic of the GE90 HPC cross-section showing the geometry of the 8-10 spool and the location where the primary fatigue crack was found in the stage 8 disk web near the rim.

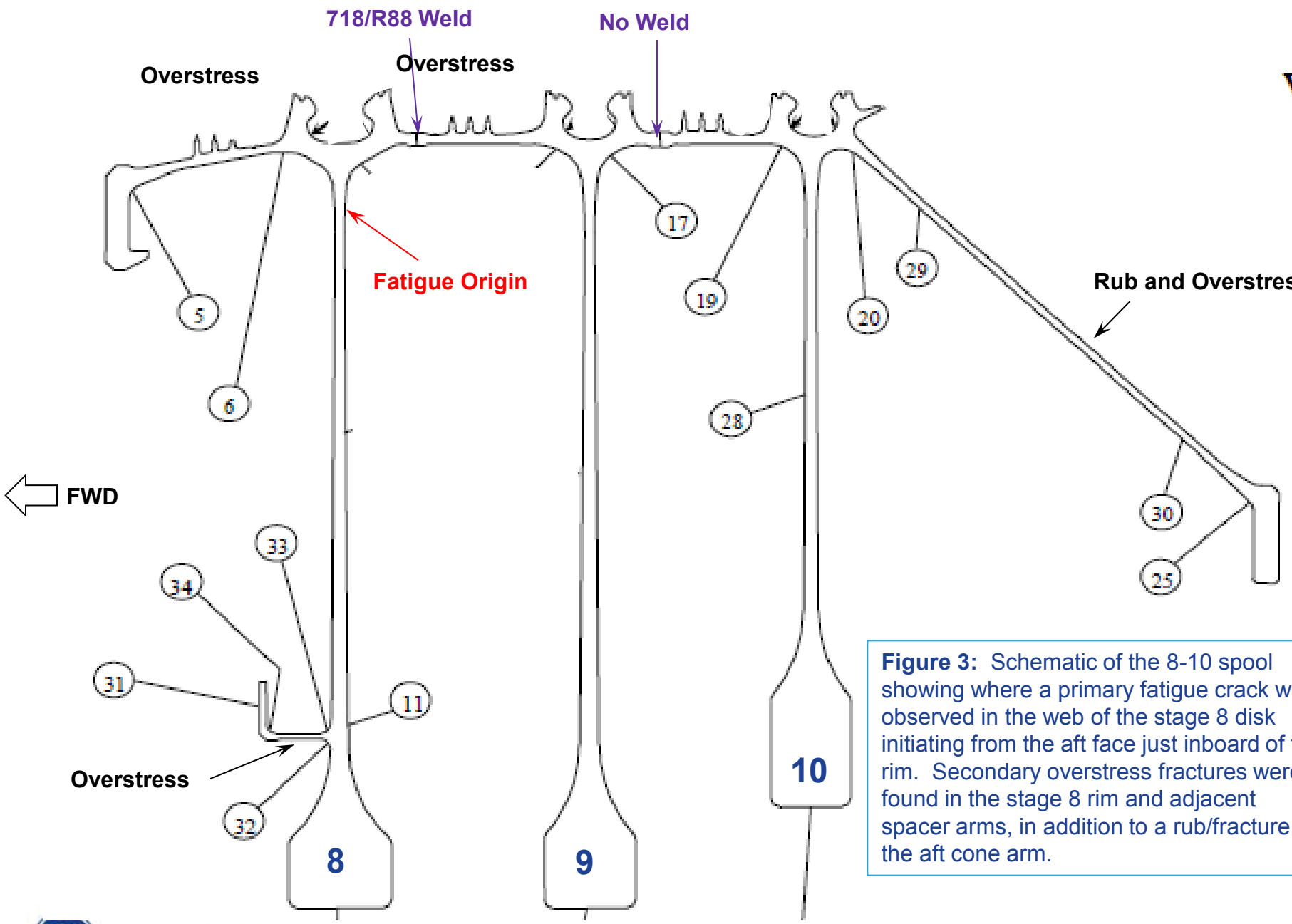

Figure 3: Schematic of the 8-10 spool showing where a primary fatigue crack was observed in the web of the stage 8 disk initiating from the aft face just inboard of the rim. Secondary overstress fractures were found in the stage 8 rim and adjacent spacer arms, in addition to a rub/fracture in the aft cone arm.

Findings from NTSB Investigation in Washington, DC Lab

Sept 14 & 15, 2015

Data generated by Donald Kramer, NTSB
(Also see NTSB Materials Laboratory Factual Report 15-131)

Figure 4: Overall optical view of the liberated fragments of the stage 8 disk rim that were recovered on-site and were returned to the NTSB laboratory for examination. Approximately 4 of 7 feet of the rim were recovered (remaining rim was still on disk). A circumferential fatigue crack was found in the web near the rim and all other fractures were consistent with overstress.

Figure 5: Optical view of the portion of the liberated stage 8 rim piece containing the fatigue fracture in the web (not visible).

Figure 6: Optical view of the portion of the liberated stage 8 rim piece containing the fatigue fracture in the web (tinted area).

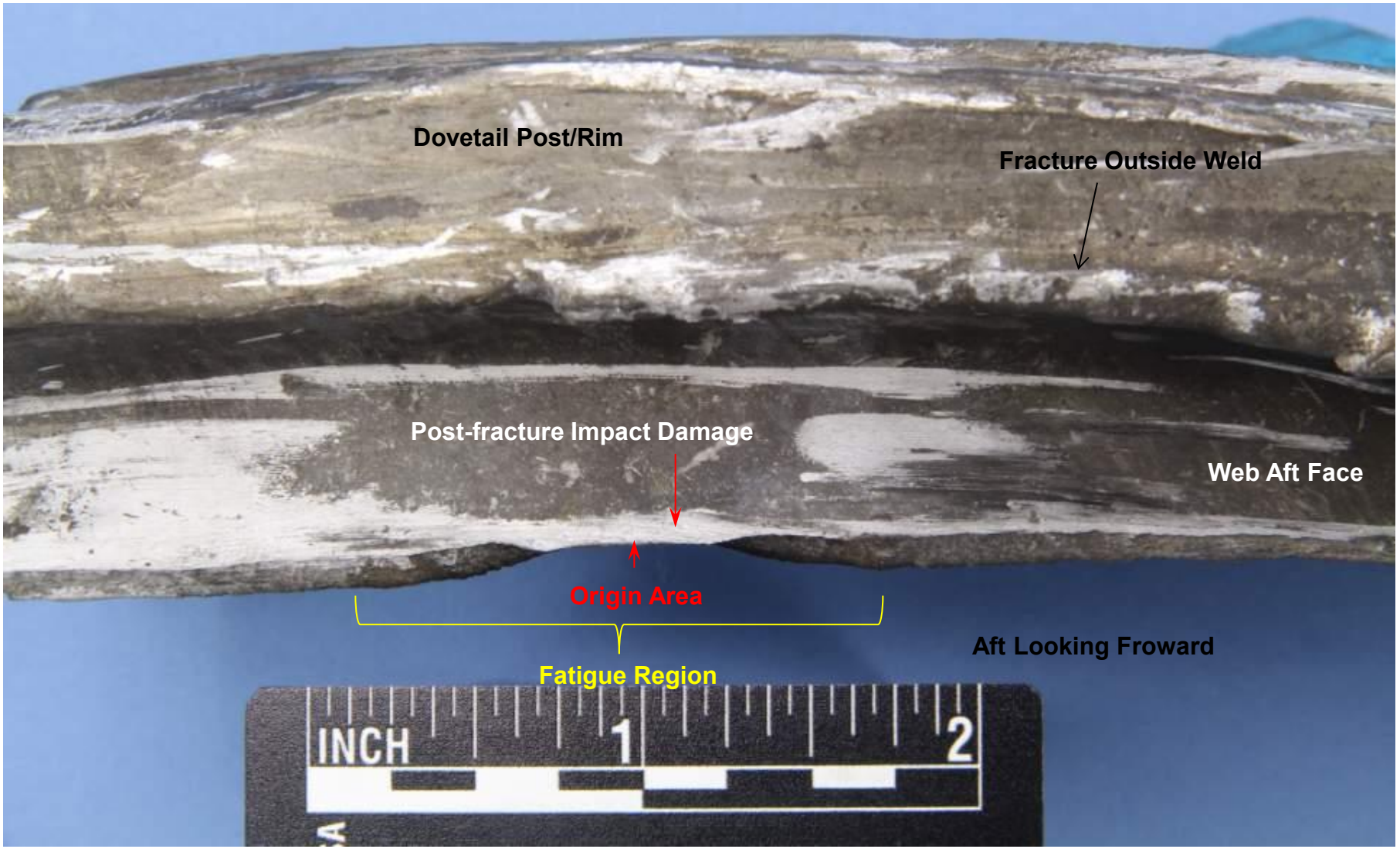

Figure 7: View of the aft side of the web showing the region of fatigue that was initially planar and then grew at a slant angle. The aft face near the origin was damaged by post-fracture impact damage (white debris).

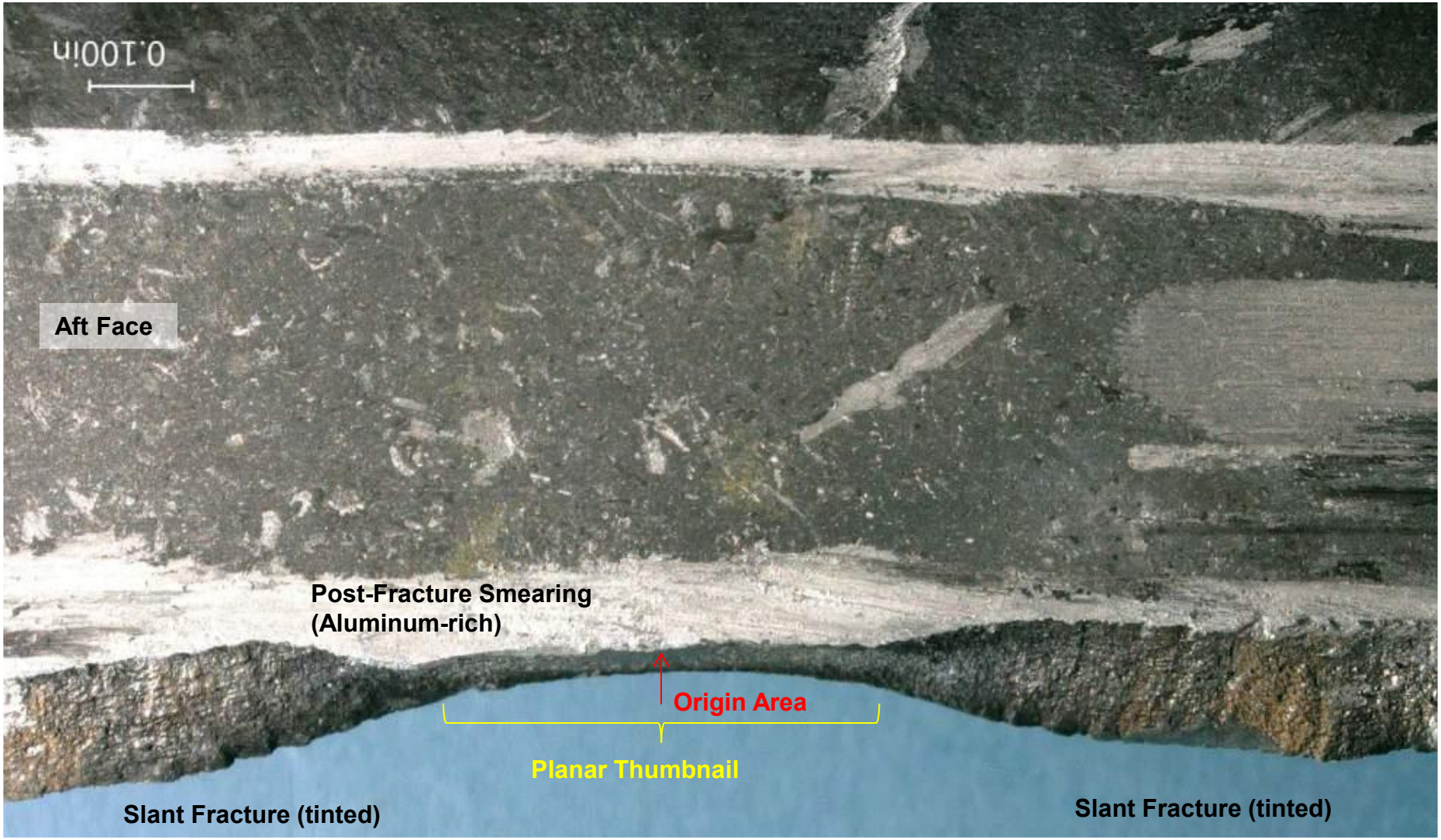

Figure 8: Higher magnification view of the fatigue fracture showing the initial planar region (approximately 0.62 inch long circumferentially) and the adjacent slant fracture region consistent with cyclic tensile that reached a total length of approximately 1.72 inch, prior to transitioning the overstress.

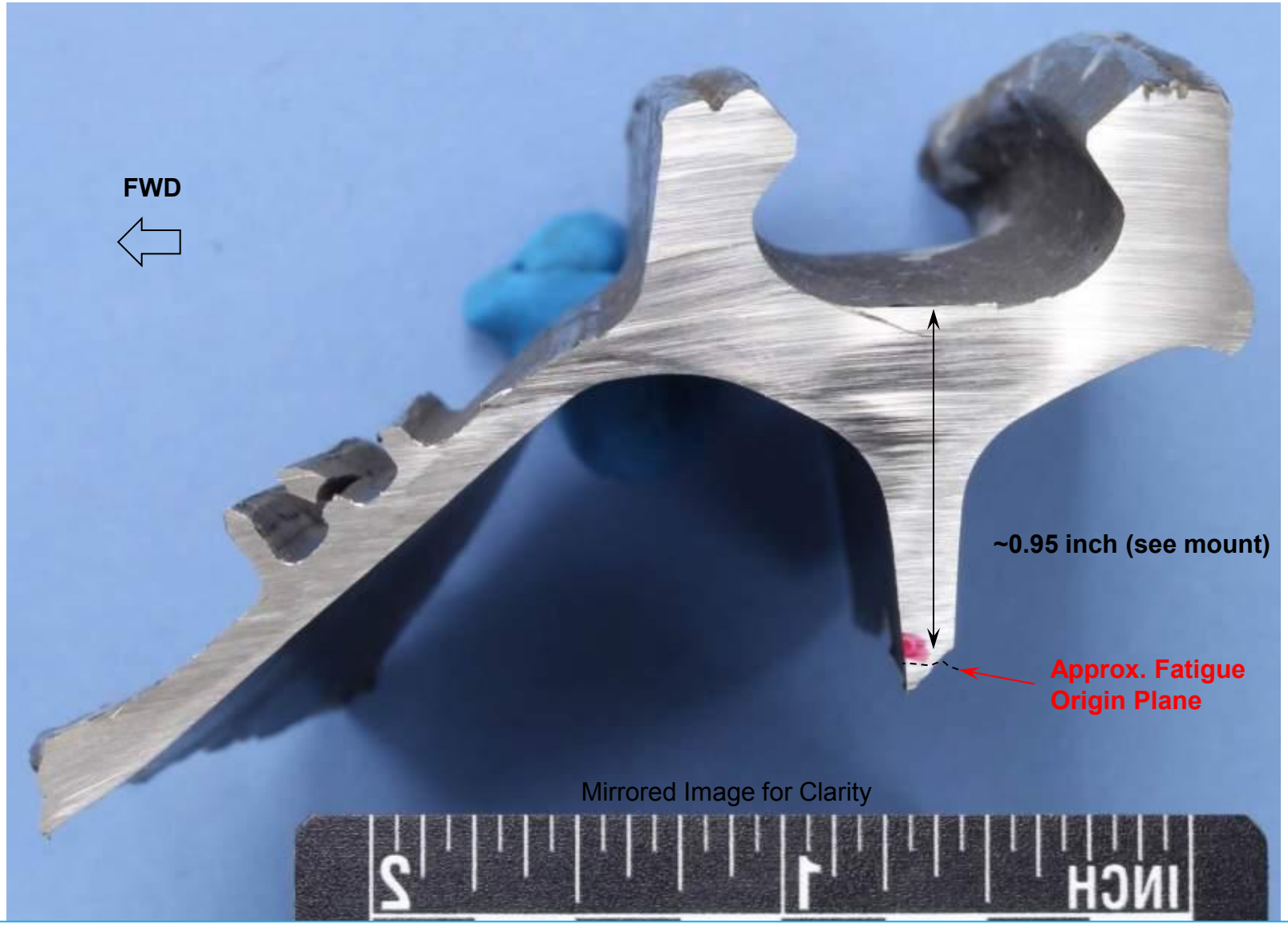

Figure 9: Optical view of a lab-cut section of the outboard liberated piece showing that the fatigue fracture was located approximately 0.95 inch inboard of the slot bottom in the thinnest portion of the web near the rim (better view shown in metallographic mount).

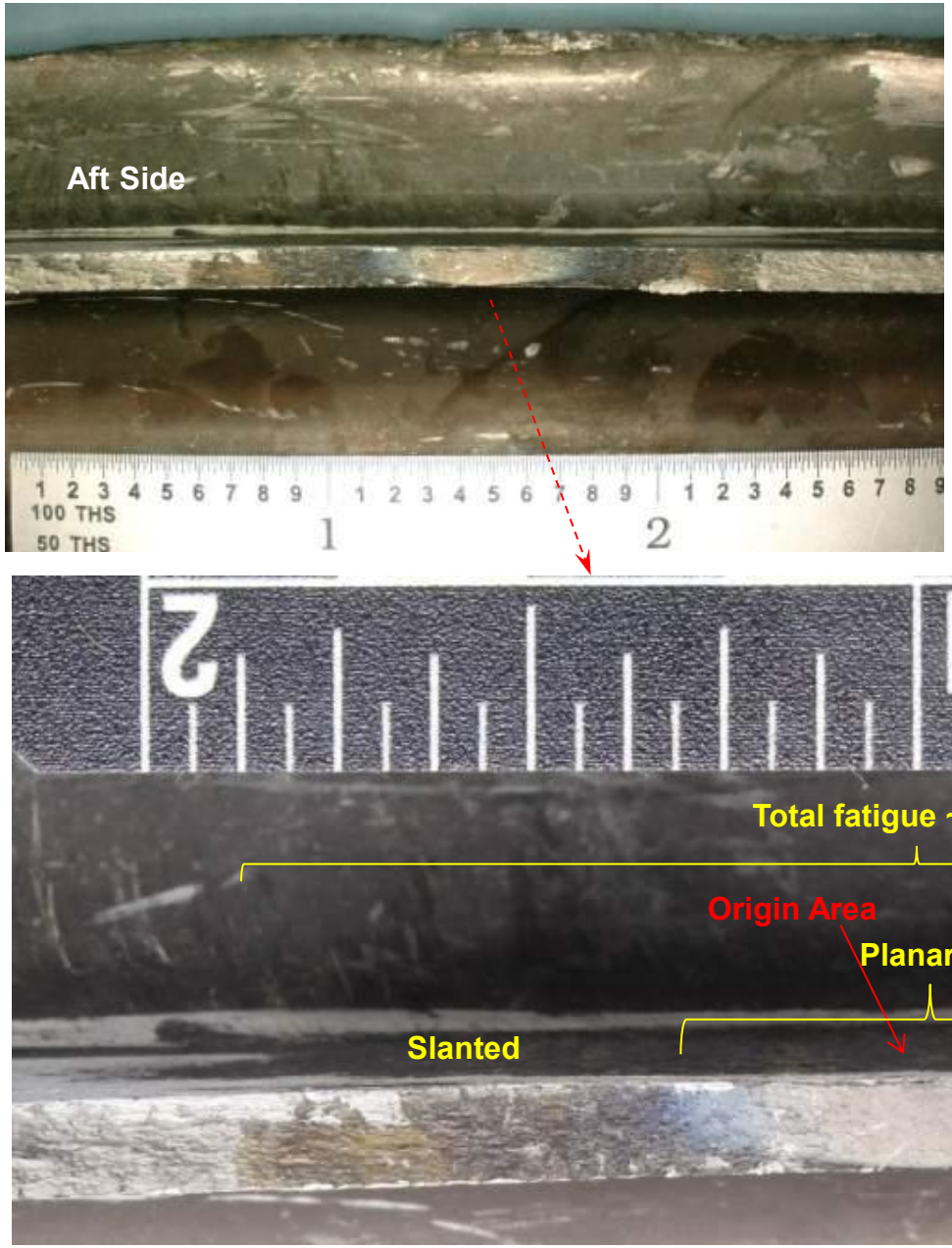

Figure 10: Optical views at varying magnification of the web fracture showing a thumbnail-shaped region normal to the surface with varying tinting, consistent with fatigue, initiating from the aft web face.

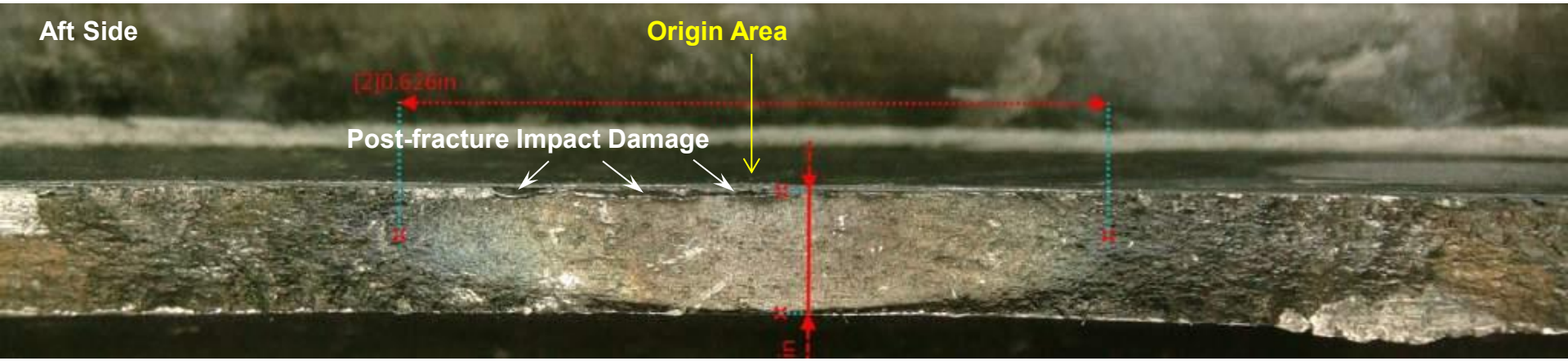

Figure 11: Higher magnification optical view showing the variation in tinting and changes in morphology on the fracture. The initial 0.62 inch portion of fatigue was planar until it progressed through the wall thickness. The fracture then continued with a rougher morphology at a slant angle, consistent with a cyclic tensile region.

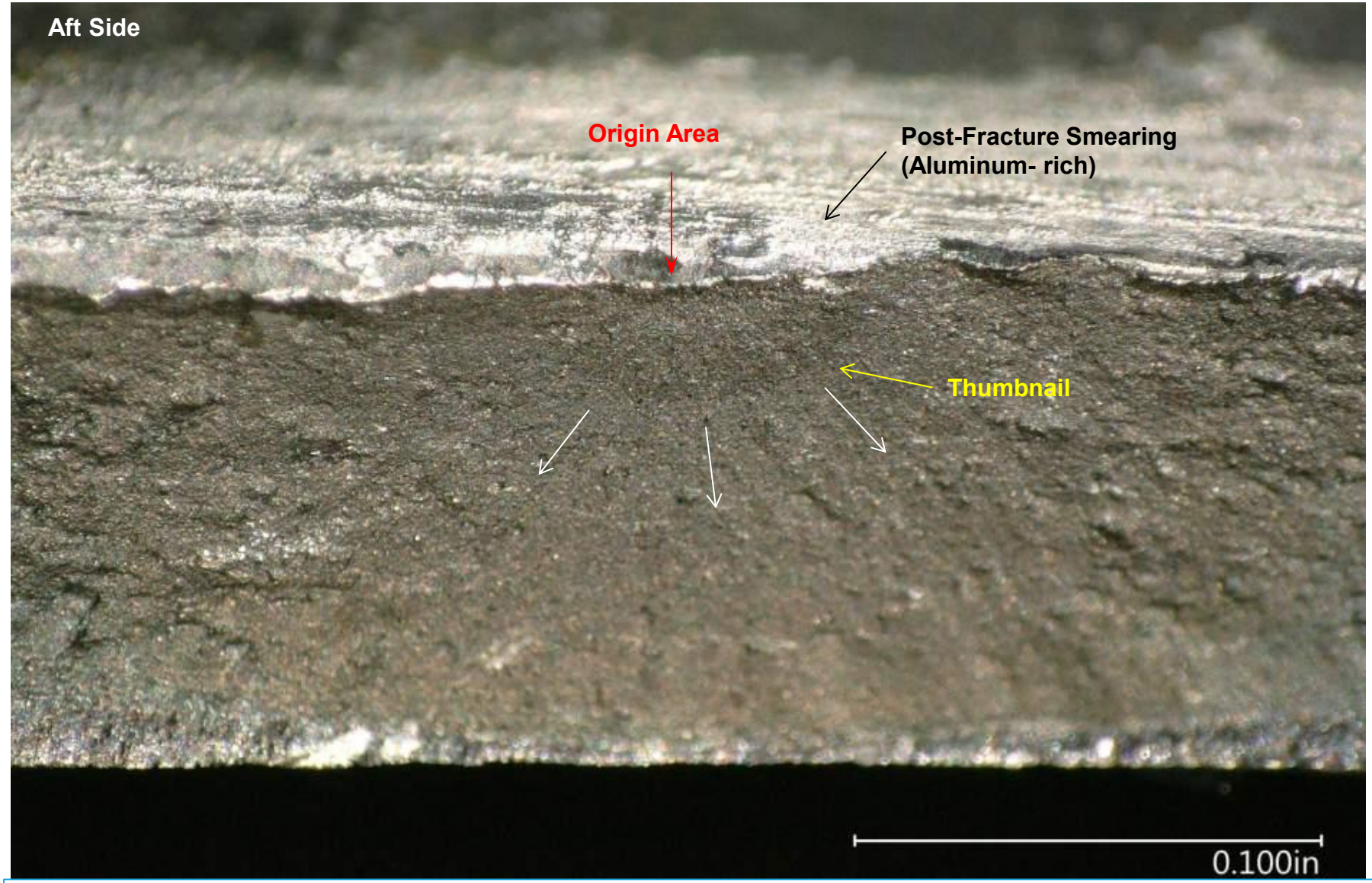

Figure 12: Higher magnification angled view of the planar fatigue region showing a small thumbnail beach-mark in the early portions of the propagation (showing the crack shape in the early stages of growth). The fracture at the aft face/origin was deformed upward by post-fracture impact damage.

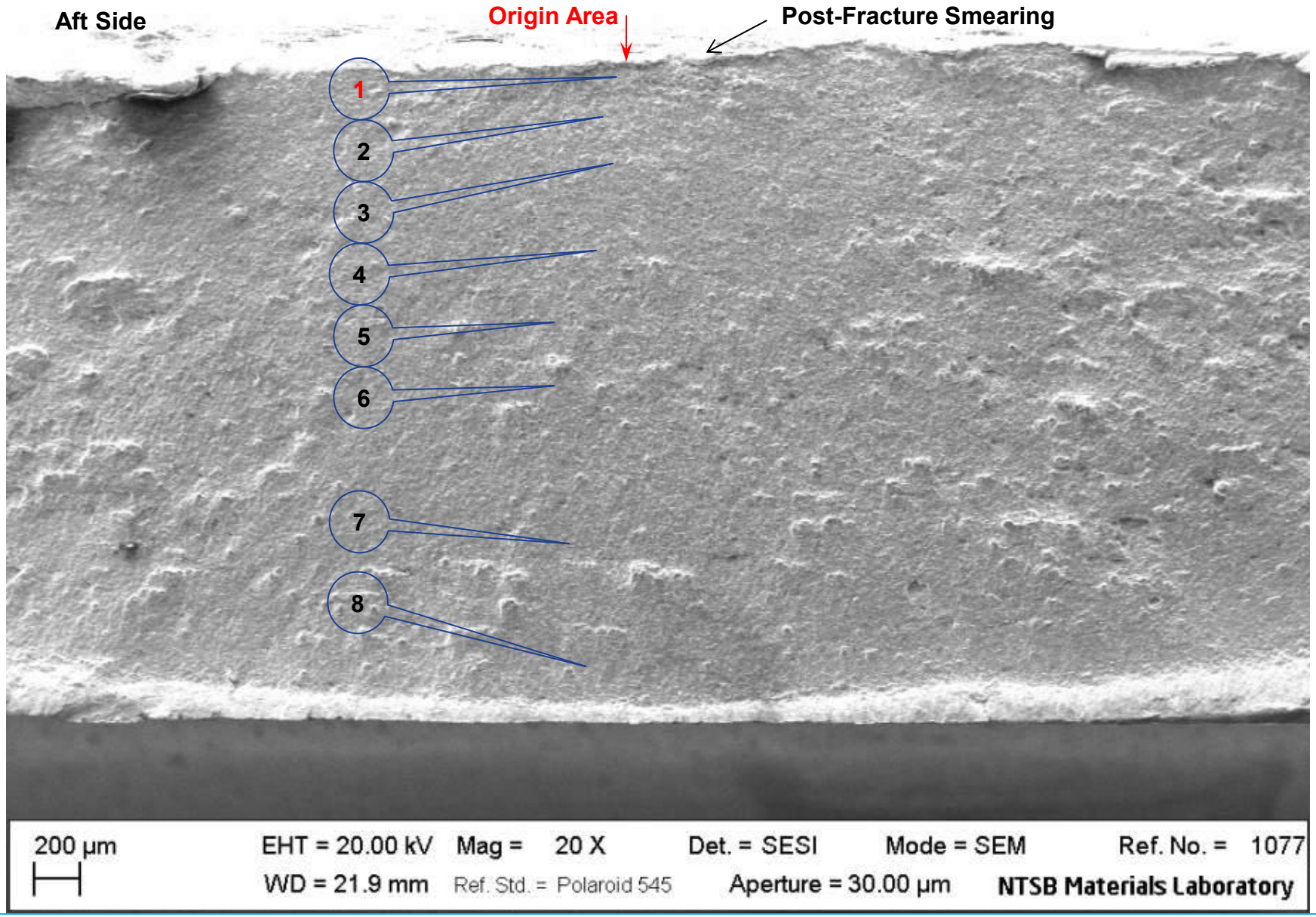

Figure 13: Low magnification SEM map of the outboard fracture areas examined further: in area 1 the fracture was intergranular and in areas 2-8 the features were transgranular with striations that decreased in density.

AREA 1

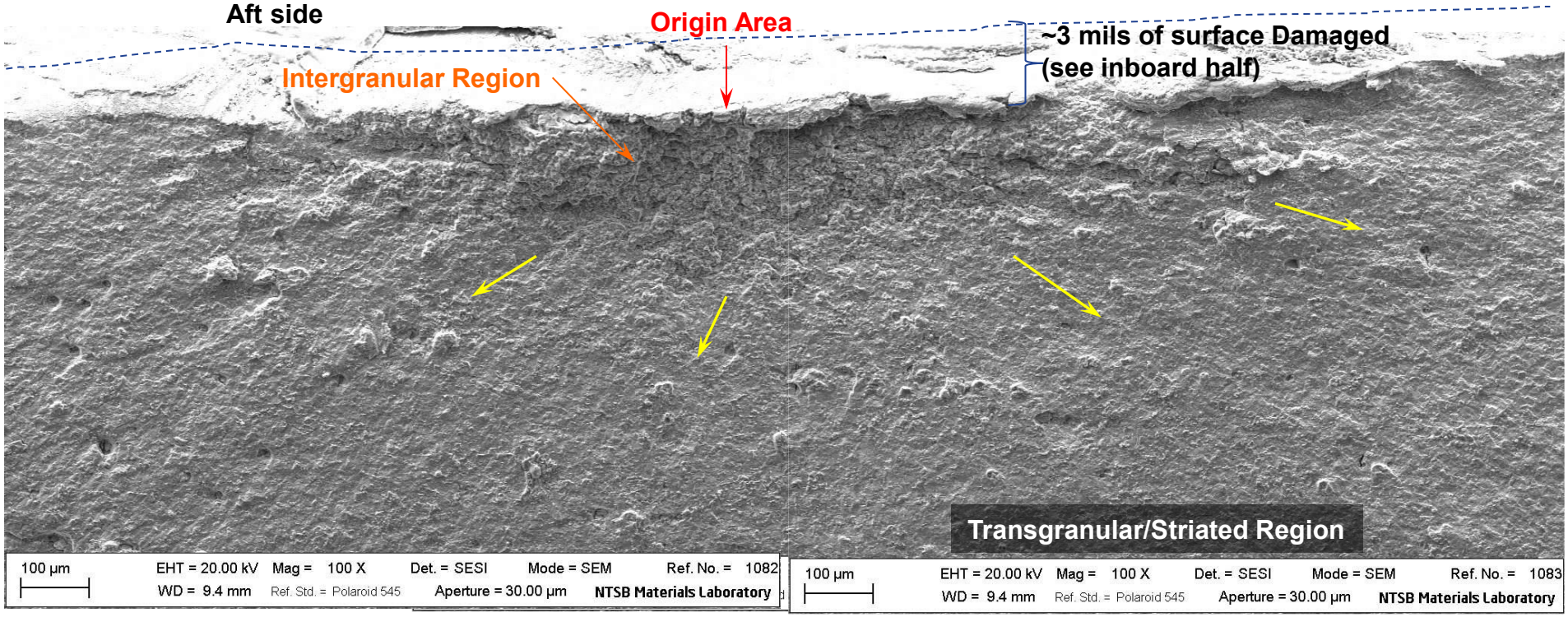

Figure 14: Intermediate magnification SEM view of the origin area showing that there was an initial region of intergranular growth prior to transitioning to transgranular/striated growth. The aft surface/origin area was damaged by post-fracture impact smearing, estimated to be approximately 3 mils deep on the outboard half.

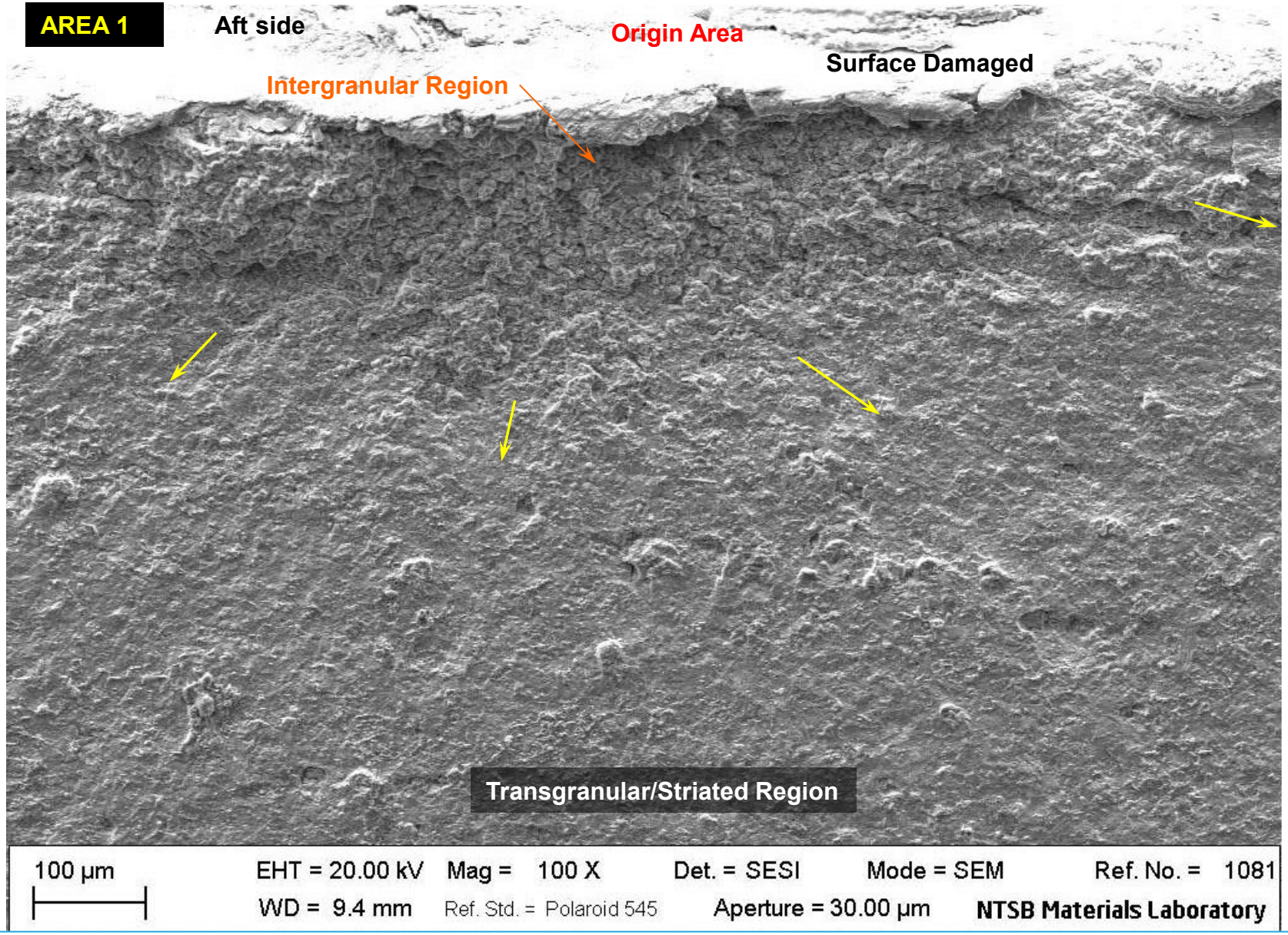

Figure 15: Intermediate magnification SEM view of the origin area showing that there was an initial region of intergranular growth prior to transitioning to transgranular/striated features.

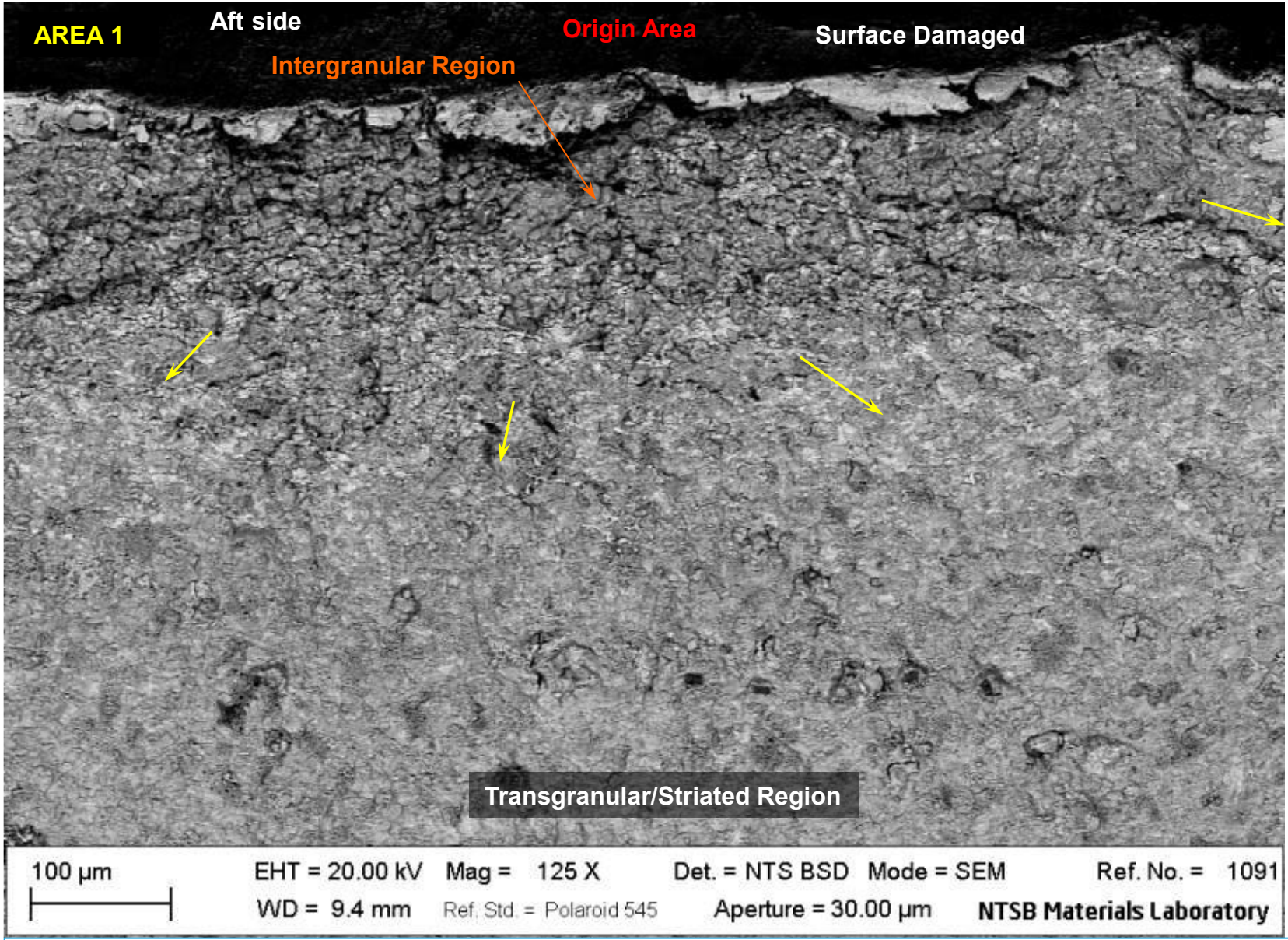

Figure 16: Similar view of the fracture in backscatter imaging mode showing the changes in morphology from intergranular to transgranular with no material anomalies observed. The post-fracture smearing is also visible at the aft surface.

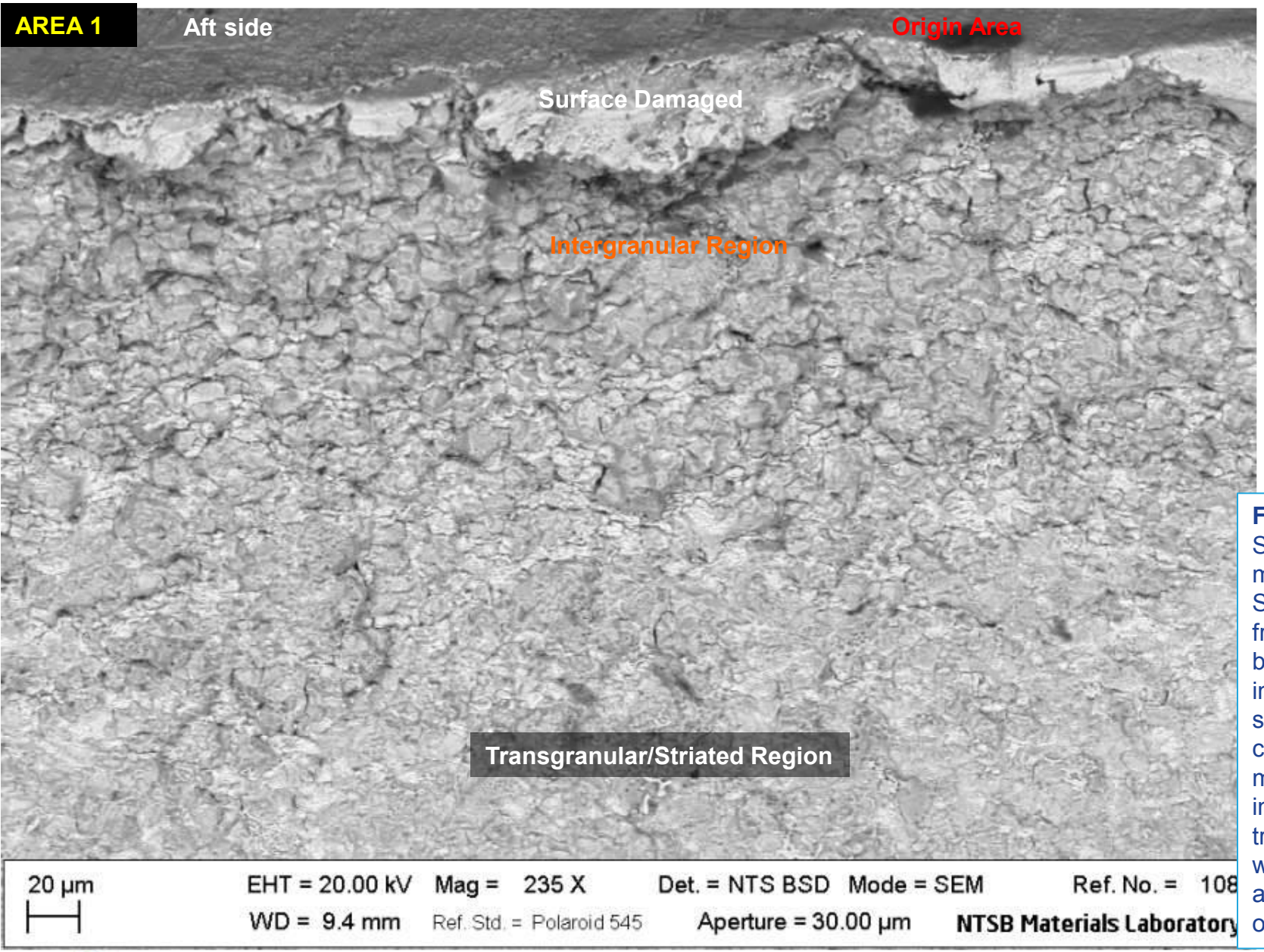

Figure 17: Slightly higher magnification SEM view of the fracture in backscatter imaging mode showing the changes in morphology from intergranular to transgranular with no material anomalies observed.

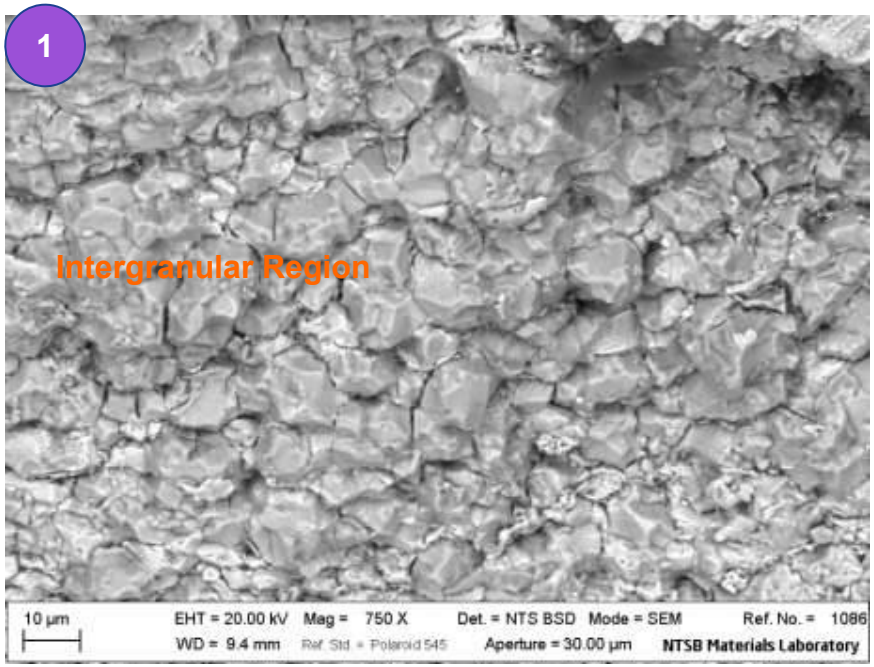

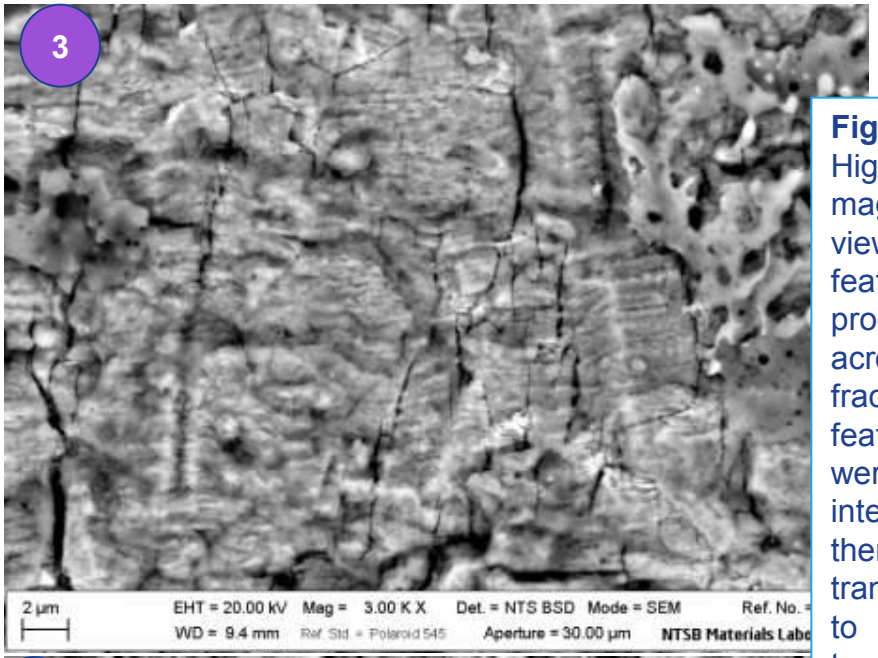

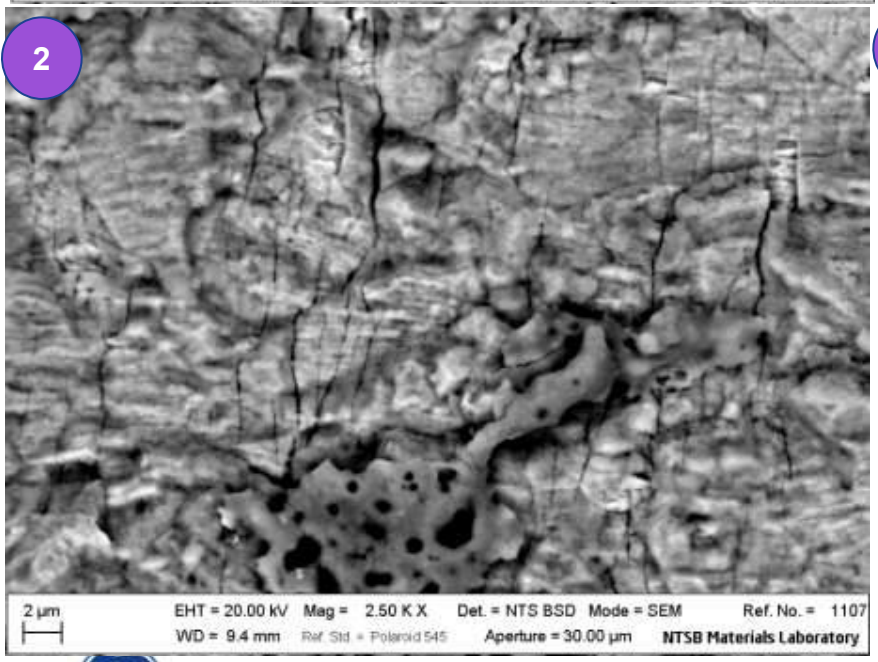

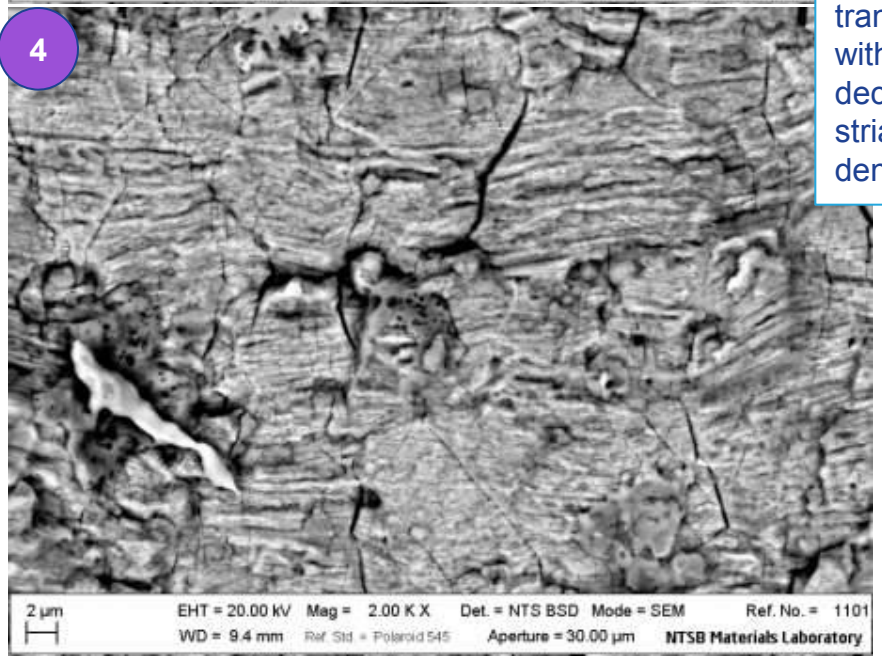

Figure 18: Higher magnification views of the features progressing across the fracture. The features were initially intergranular, then transitioned to transgranular with decreasing striation densities.

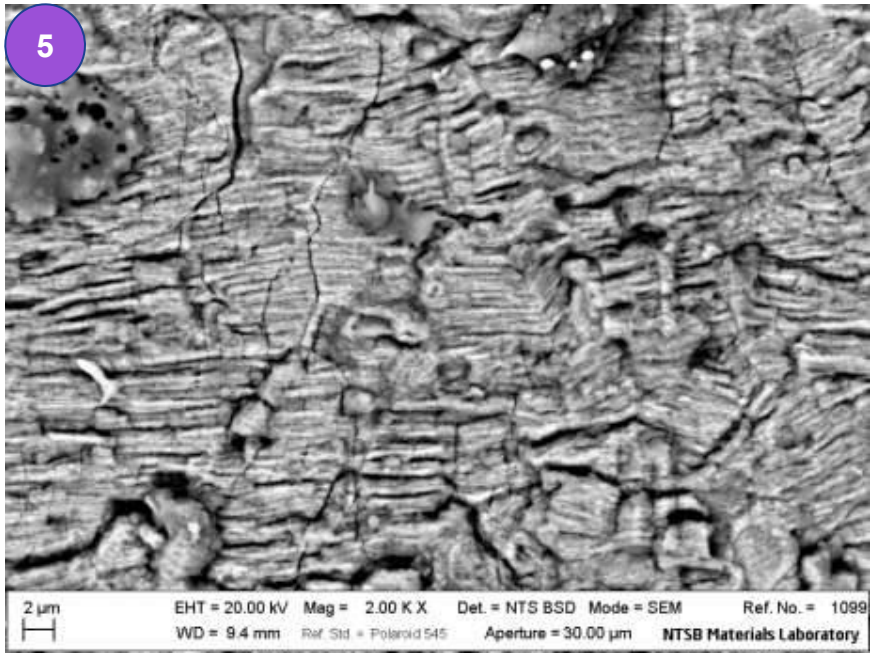

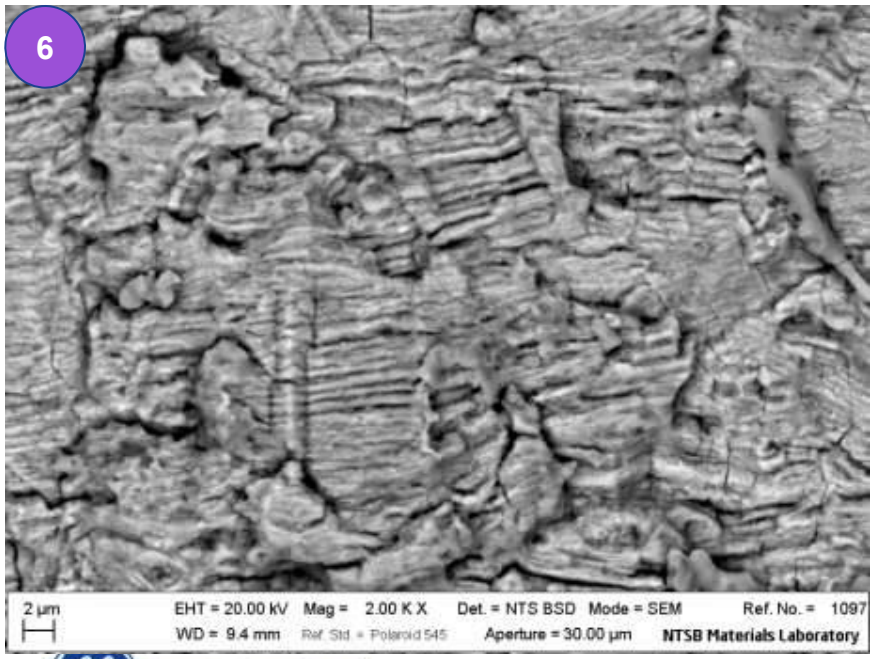

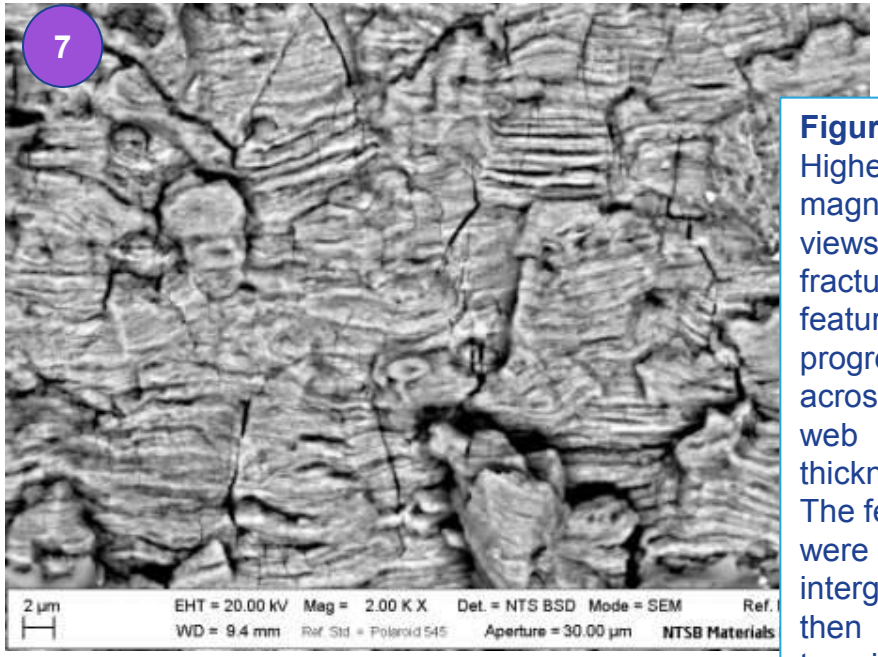

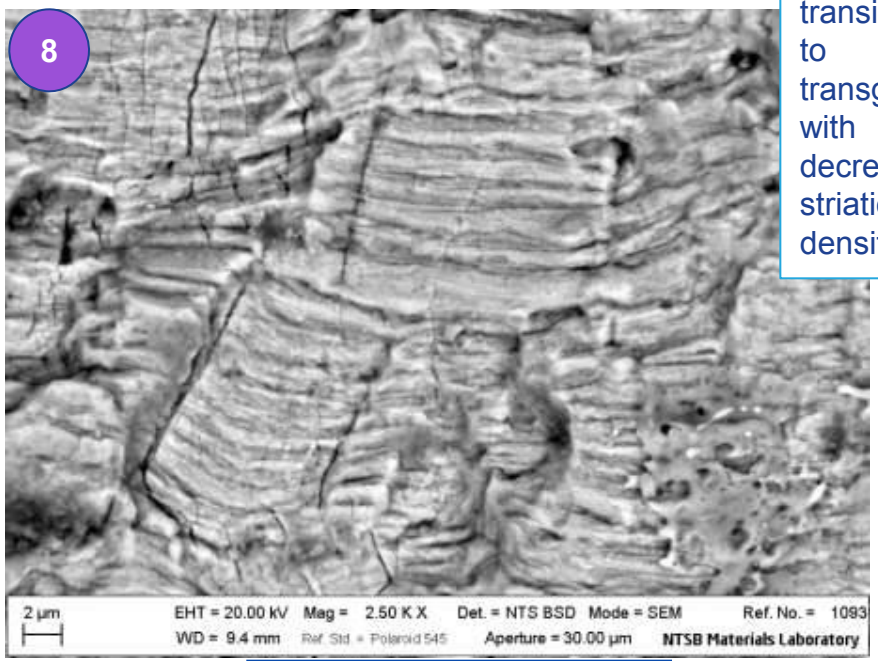

Figure 19: Higher magnification views of the fracture features progressing across the web thickness. The features were initially intergranular, then transitioned to transgranular with decreasing striation densities.

Striation Density

Note: Estimates from base of intergranular region

$$Y := \int_{0.01}^{0.115} 2751.1 \cdot x^{-0.915}\, dx$$

$$Y = 5.049 \times 10^{3}$$

$$Y1 := \int_{0.01}^{0.115} 1928.1 \cdot x^{-1.057}\, dx$$

$$Y1 = 5.716 \times 10^{3}$$

INTERGRANUAL4R REGION

y = 1928.1x^-1.057
R² = 0.8436

y = 2751.1x^-0.915
R² = 0.7289

Striations/inch

Distance From Oriign (inch)

Figure 20: The striation data was plotted as a function of depth by two evaluators (red and blue points) and both showed a decreasing striation density, consistent with LCF growth. From the base of the intergranular region (bulk around 10 mils) the crack was estimated to have grown between 5-5.7K cycles (**not including the intergranular region**).

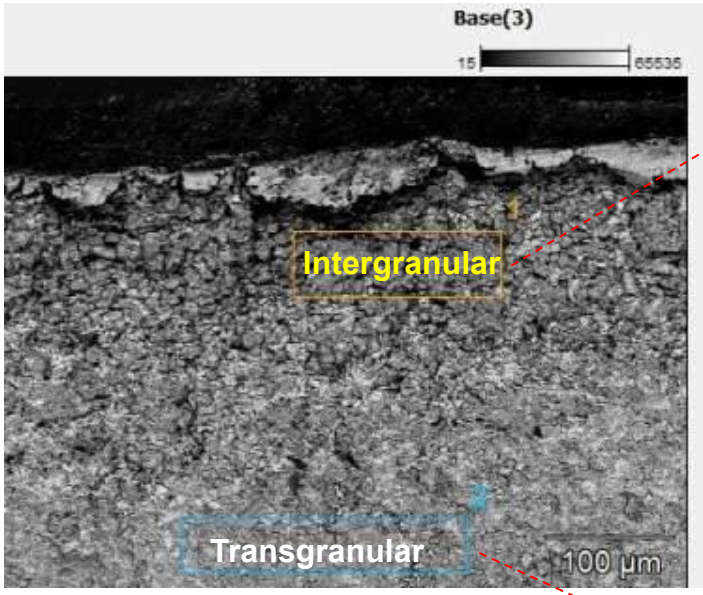

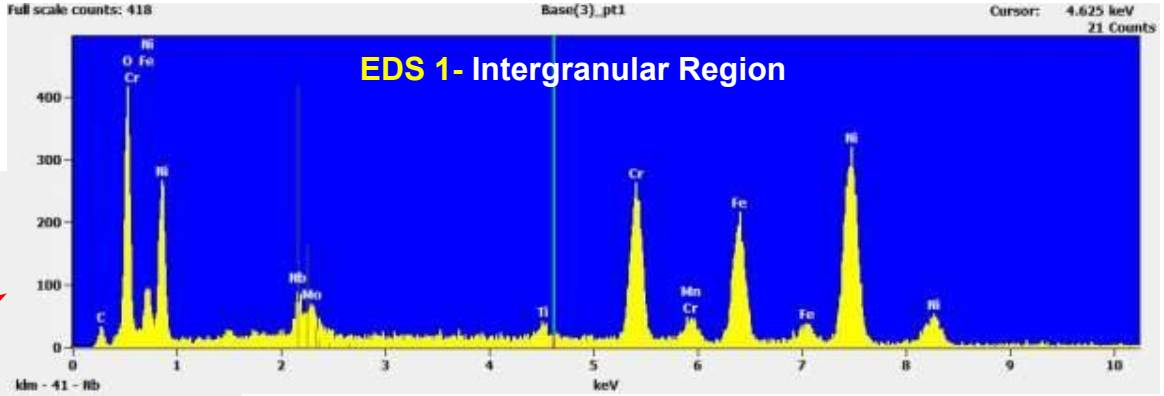

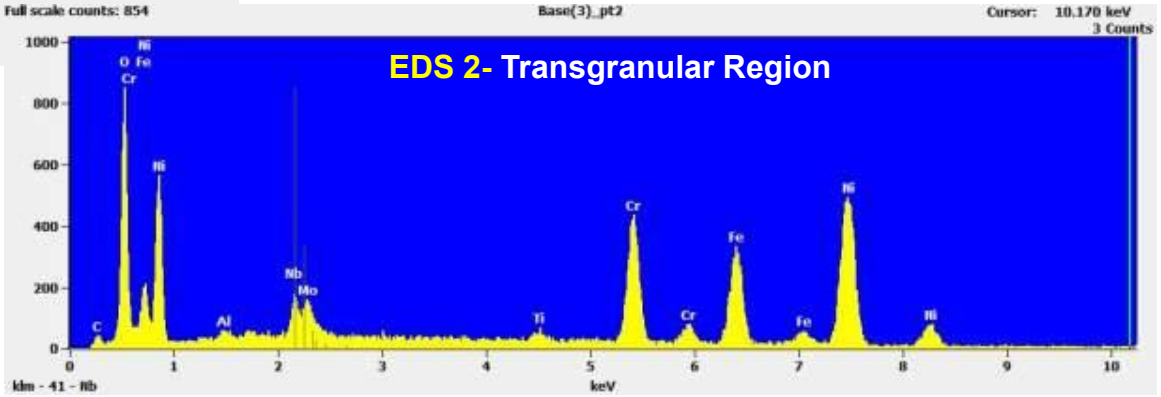

Figure 21: Energy dispersive spectroscopy analysis showed that in both the intergranular and transgranular areas spectra consistent with the requirement of alloy 718 were observed (per C50TF81), with the addition of oxygen. No detrimental species were found.

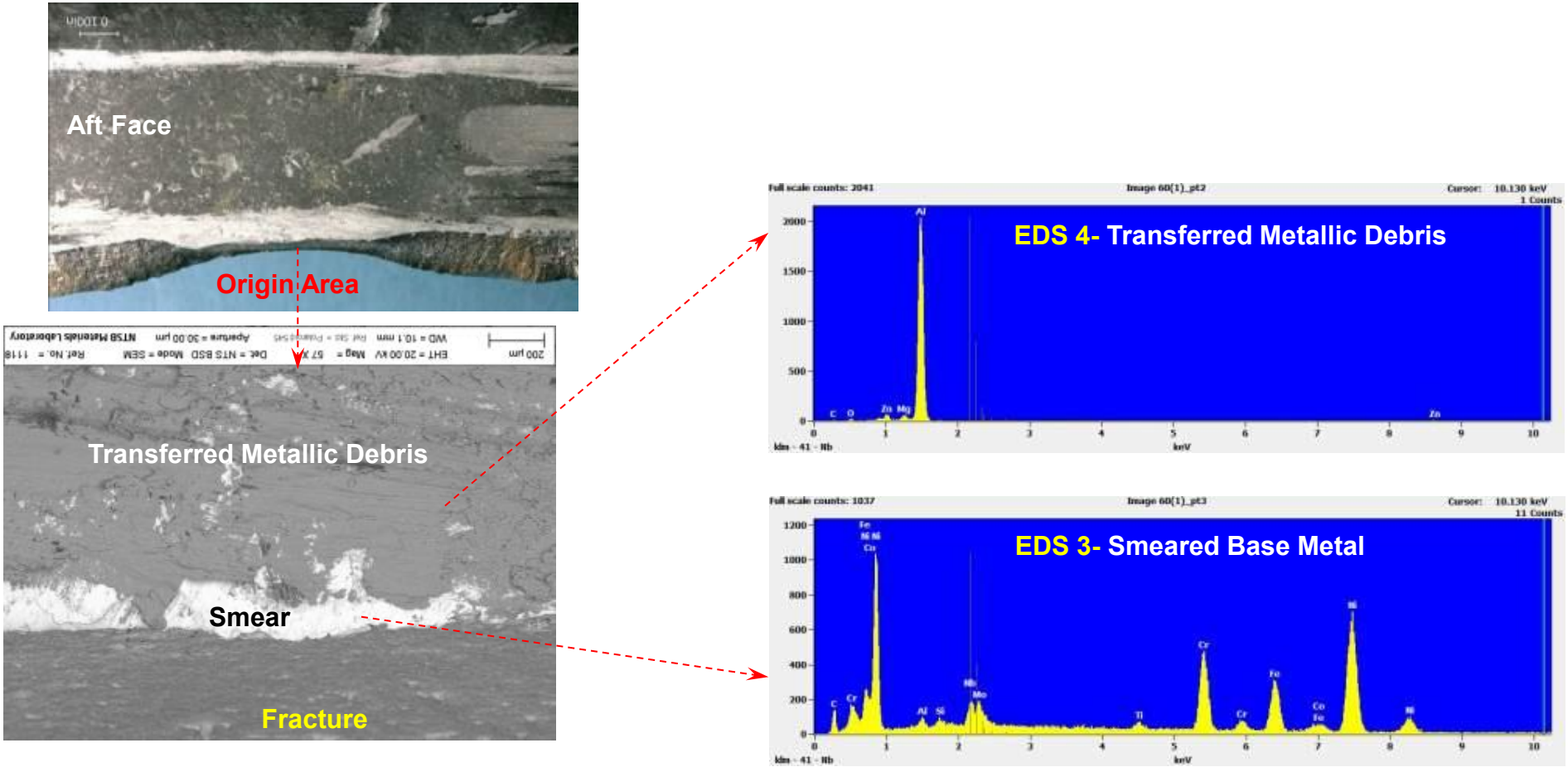

Figure 22: EDS analysis of debris on the aft outer web surface showed that in the smeared area adjacent to the fracture alloy 718 base metal elements were observed (EDS 3), with superimposed aluminum-rich transferred material containing small peaks of Zn and Mg (EDS 4).

Findings from NTSB Investigation in GE Lab

From Sept 23rd, 2015

Data generated by William Rossey, GE

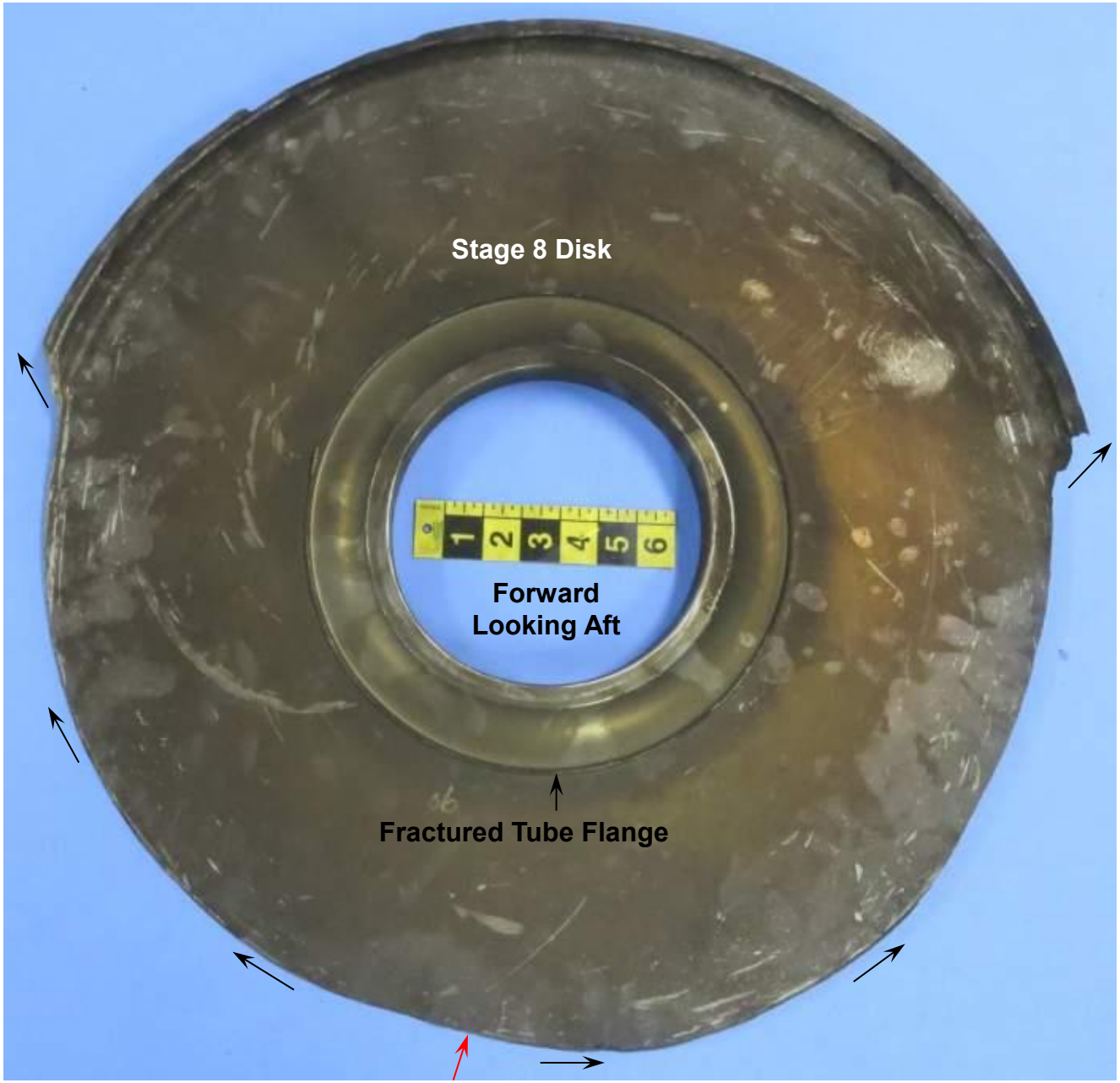

Figure 23: Optical view of the fractured stage 8 disk from the 8-10 spool after removal from the engine. The disk liberated approximately 60 percent of the rim and a single fatigue area was found near the center of the liberated region. All other areas of the fracture were consistent with overstress, including the forward tube flange near the bore.

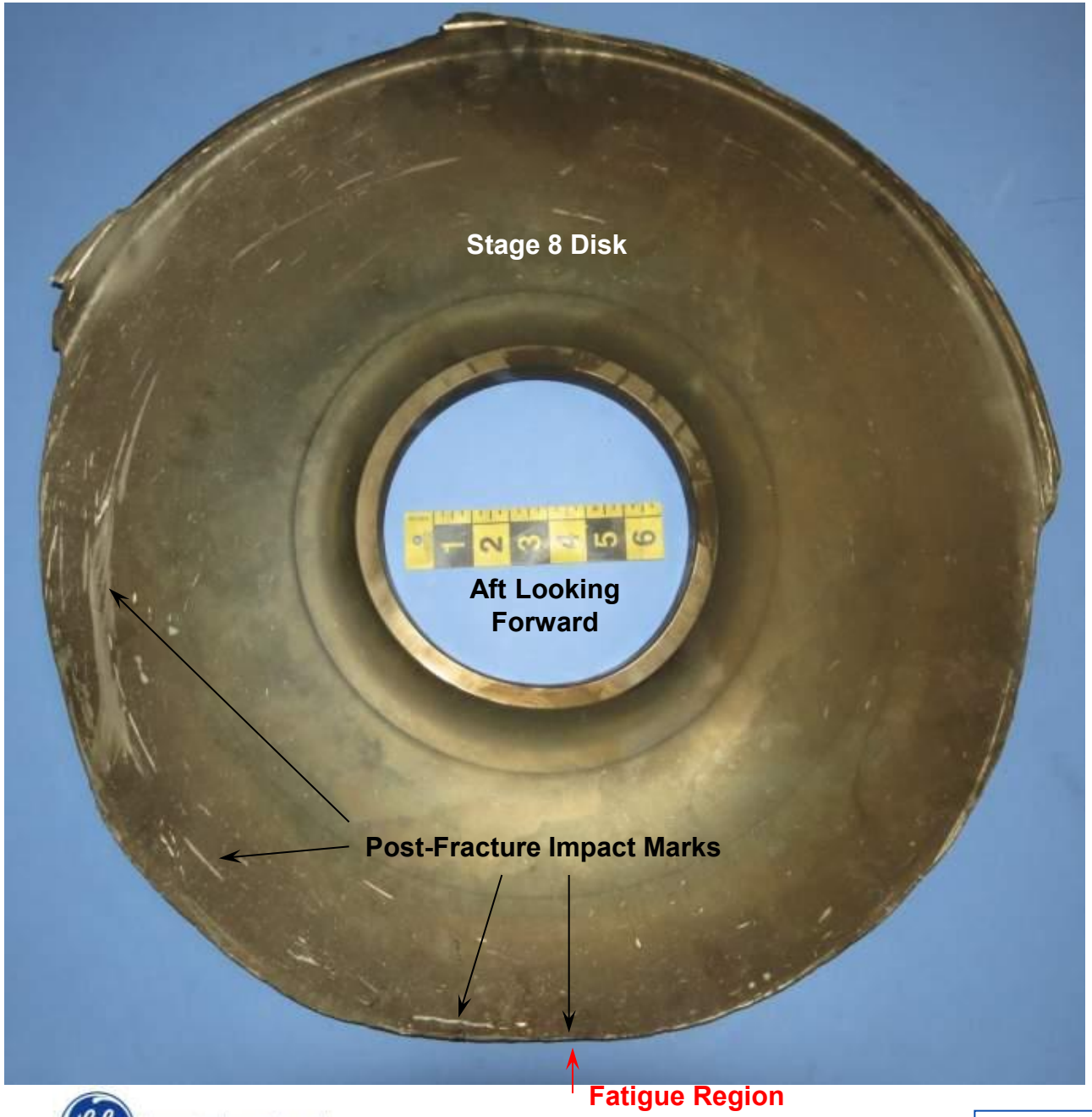

Figure 24: View of the corresponding aft side of the disk, which showed multiple circumferential impact/smearing marks, consistent with event-related impacts, including some at the origin area (shown in more detail later).

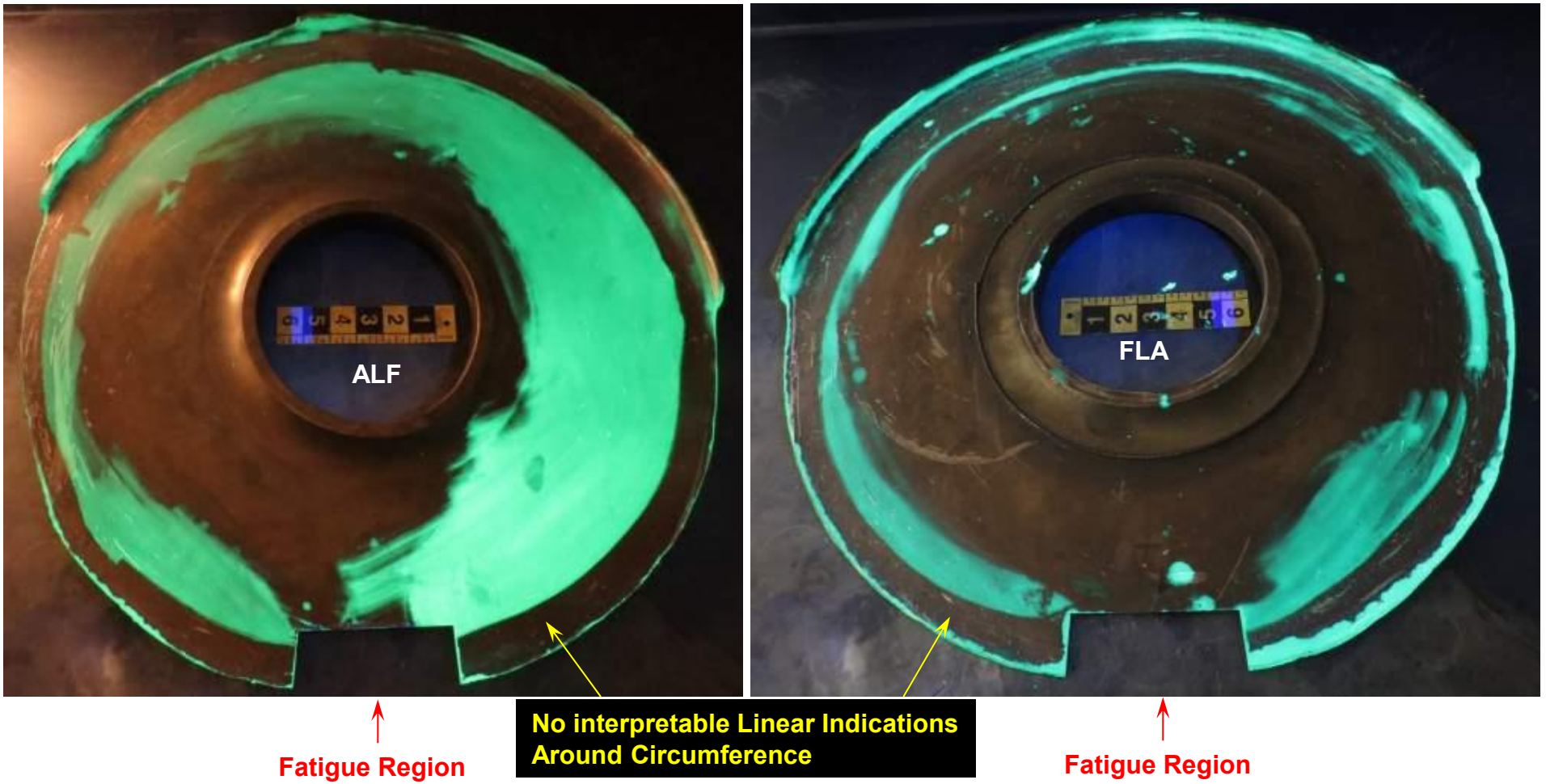

Figure 25: A local FPI inspection of a 1.5 inch band around the part adjacent to the fracture plane did not reveal any additional interpretable linear indications/cracks.

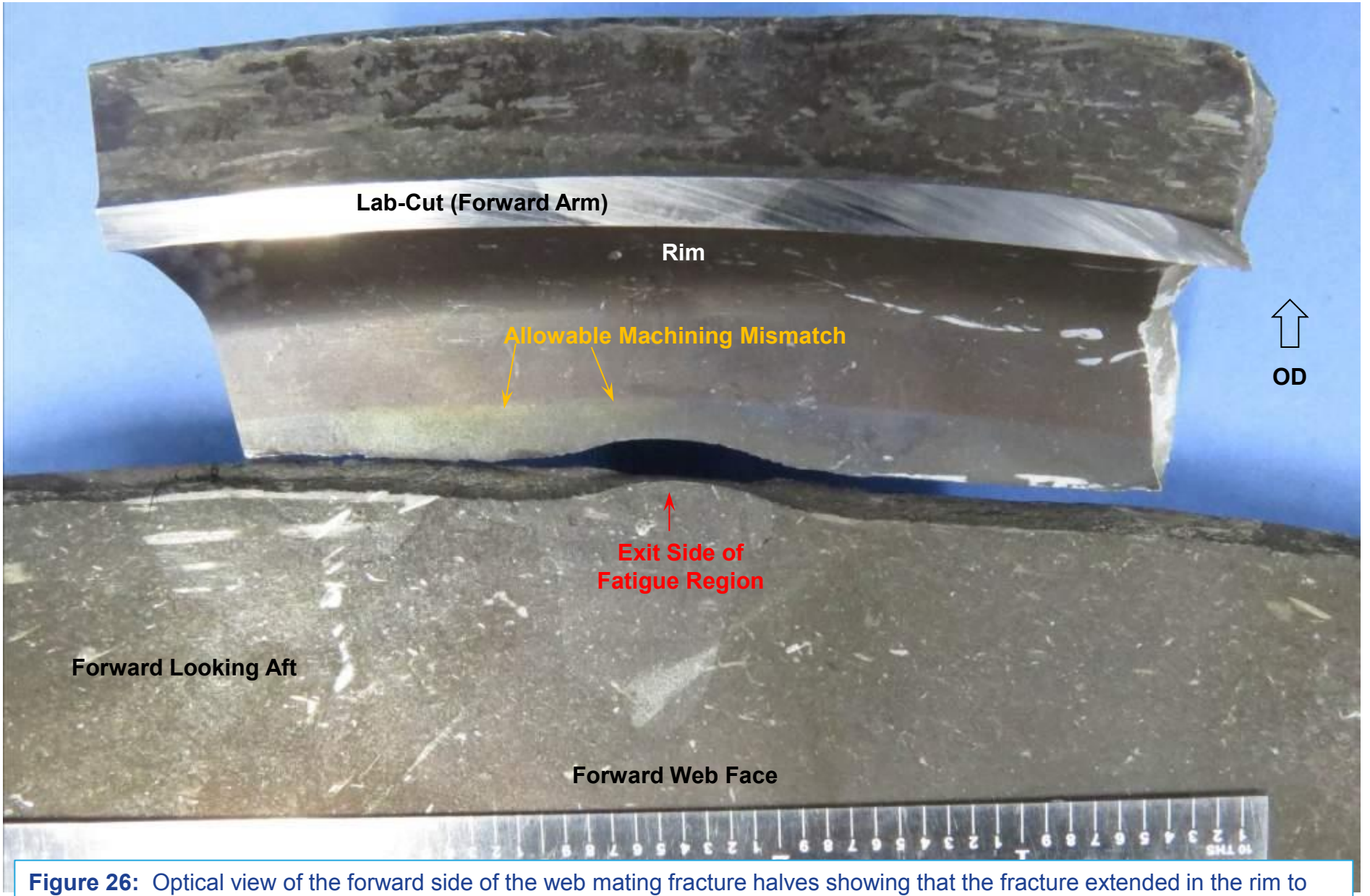

Figure 26: Optical view of the forward side of the web mating fracture halves showing that the fracture extended in the rim to web transition region, approximately 0.15 inch inboard of the machining mismatch.

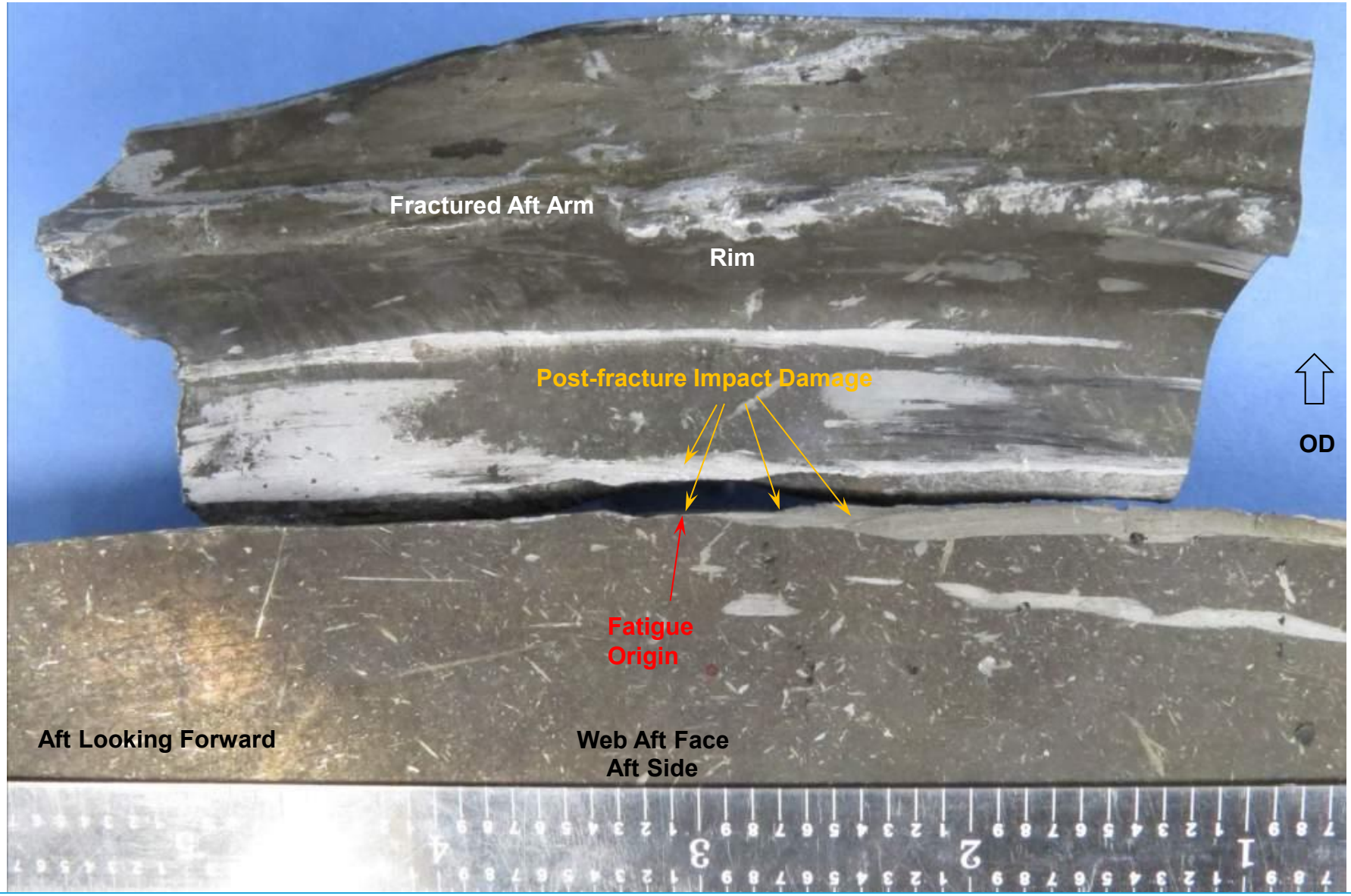

Figure 27: Optical view of the aft side of the web mating fracture halves showing that the fracture extended in the rim to web transition area. Both aft faces of the web at the origin area were damaged by post-fracture impact smearing damage.

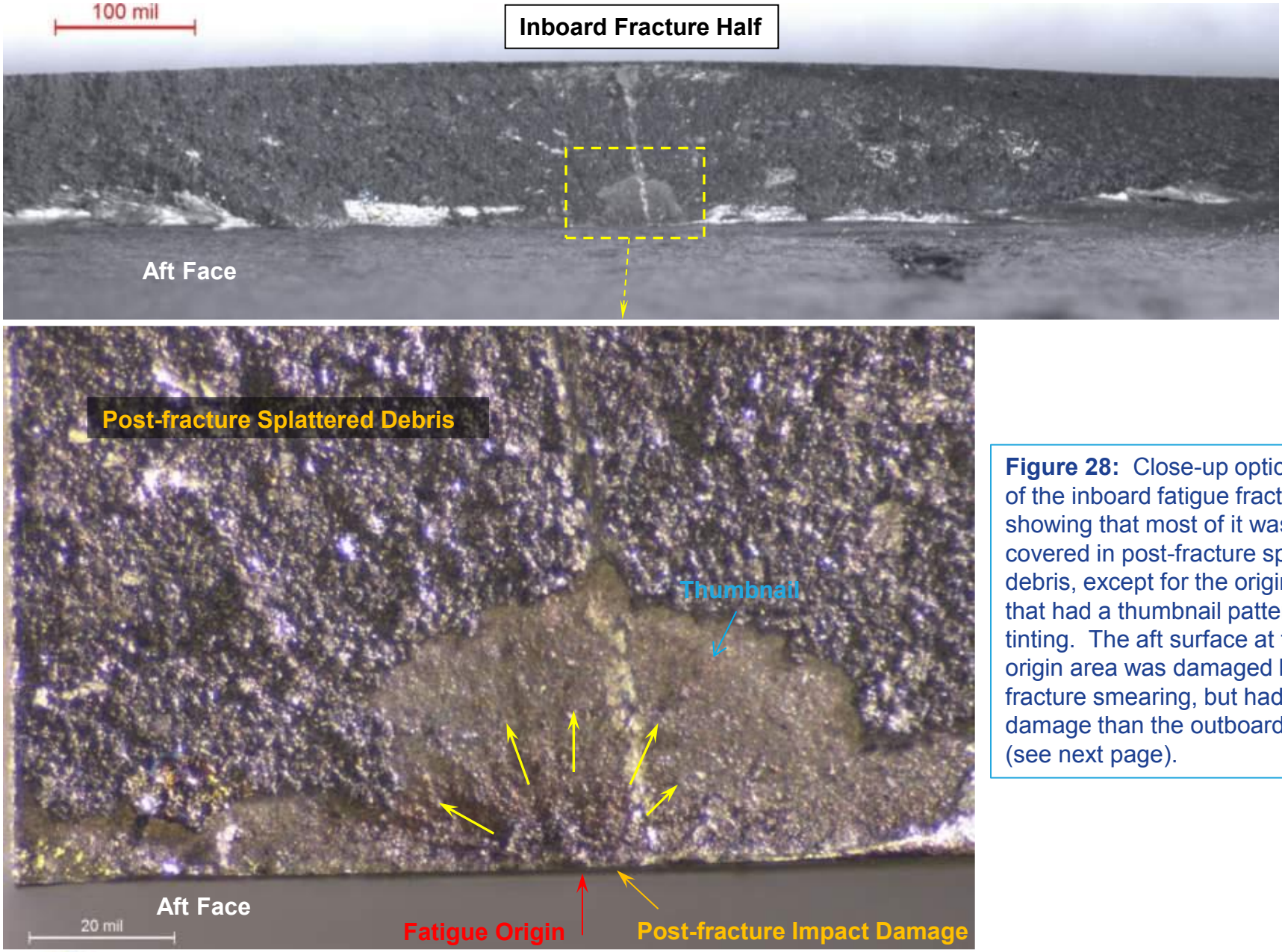

Figure 28: Close-up optical view of the inboard fatigue fracture showing that most of it was covered in post-fracture splattered debris, except for the origin area that had a thumbnail pattern and tinting. The aft surface at the origin area was damaged by post-fracture smearing, but had less damage than the outboard side (see next page).

Figure 29: Side-by-side SEM views at similar magnifications of the mating fracture surface origin areas showing that the outboard half had approximately 3 mils of damage at the surface compared to approximately 1 mil of damage on the inboard half. EDS spectra showed that the fracture surface intergranular region was consistent with oxidized 718 (EDS 5), while on the inboard post-fracture impacted area a Ni-based alloy with similar elements was observed (EDS 6).

Mating Outboard Fracture Half

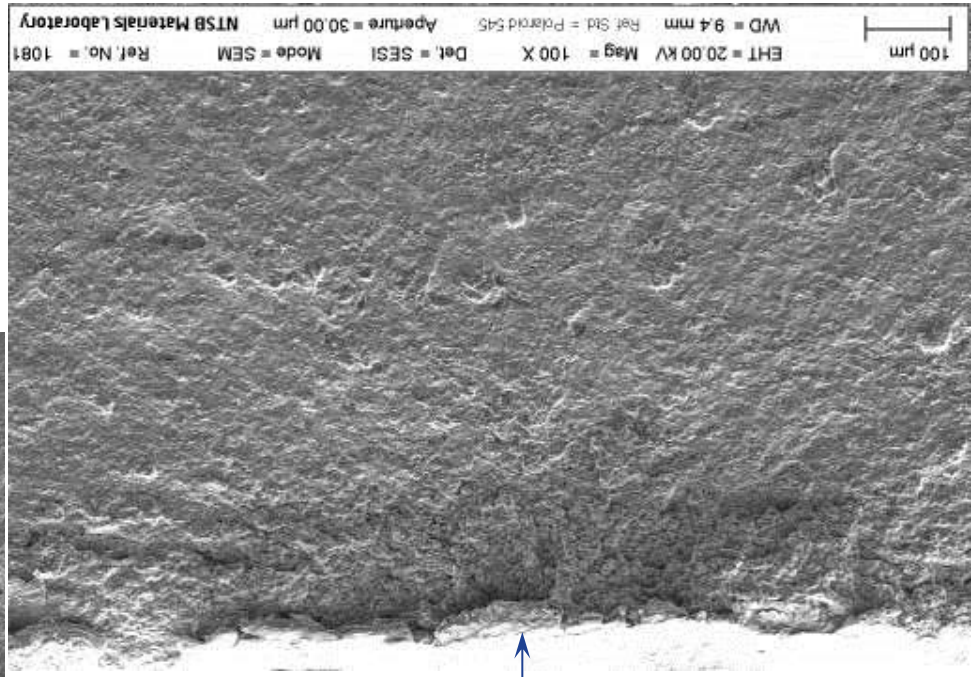

Inboard Fracture Half

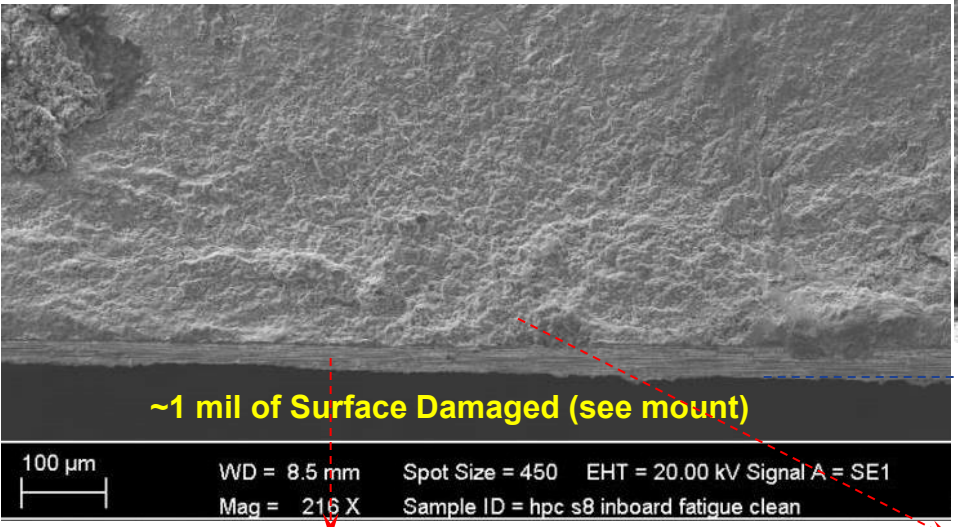

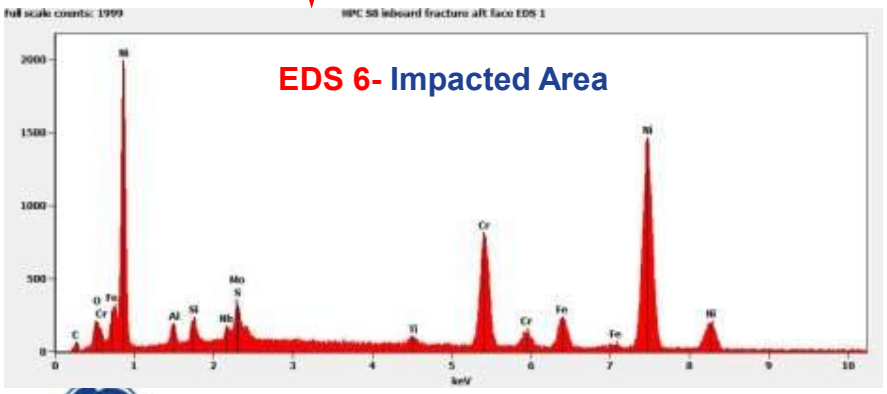

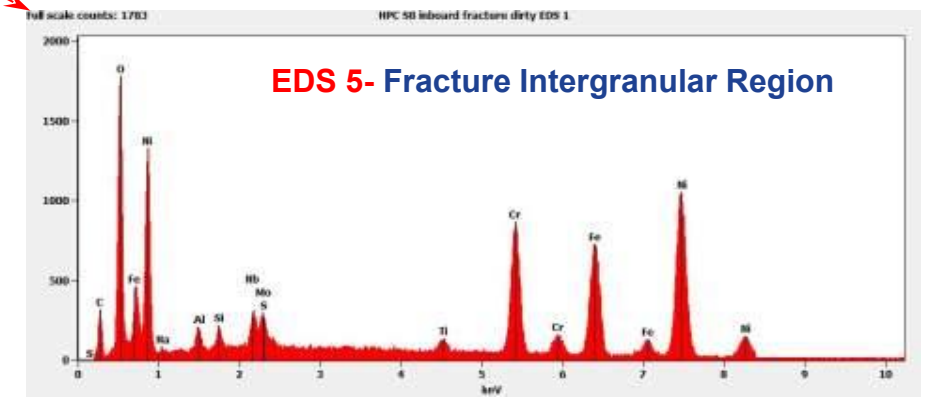

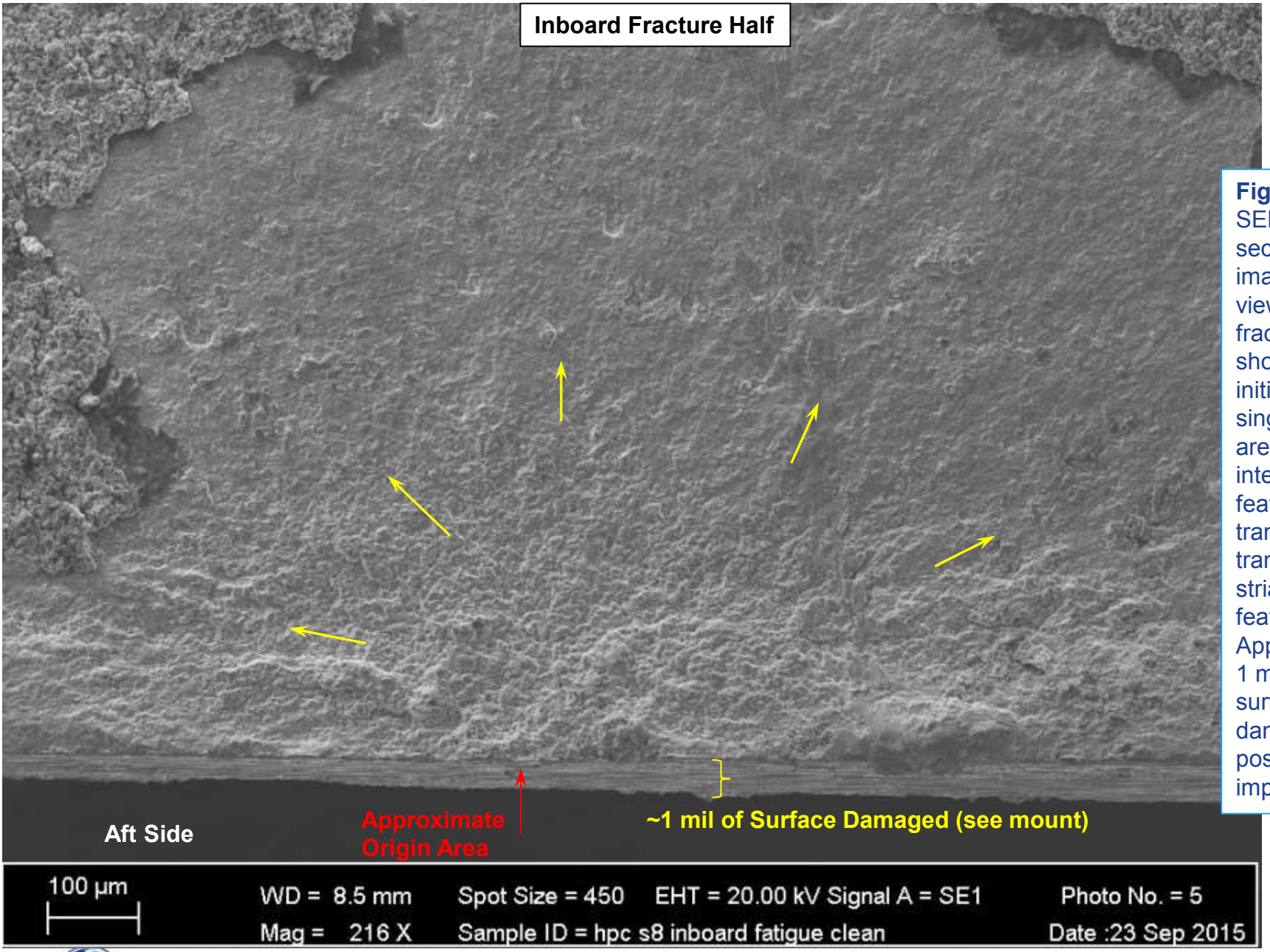

Figure 30: SEM secondary imaging mode view of the fracture showing initiation from a single origin area that had intergranular features, that transitioned to transgranular/ striated features. Approximately 1 mil of the surface was damaged by post-fracture impact.

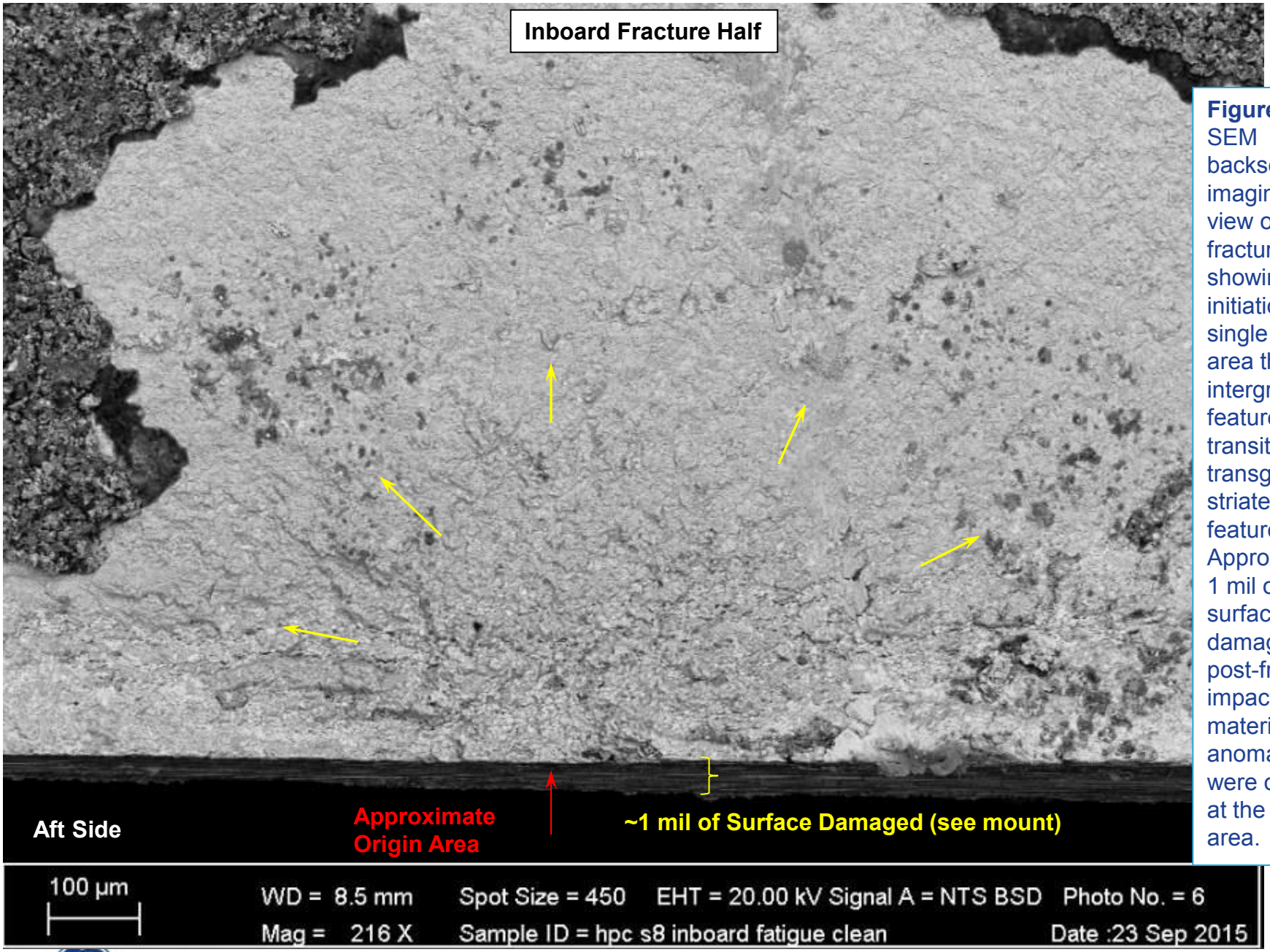

Figure 31: SEM backscatter imaging mode view of the fracture showing initiation from a single origin area that had intergranular features, that transitioned to transgranular/ striated features. Approximately 1 mil of the surface was damaged by post-fracture impact. No material anomalies were observed at the origin area.

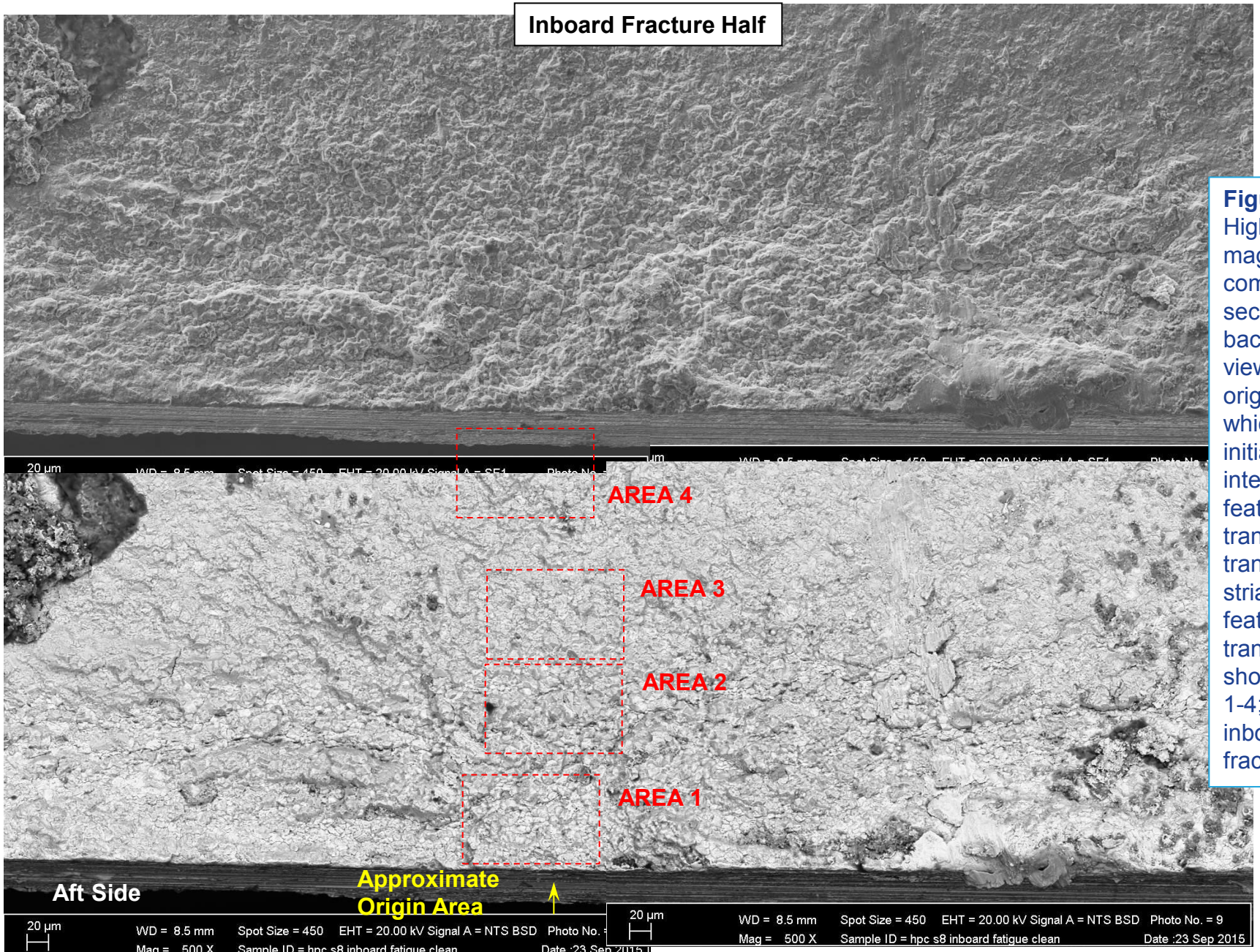

Figure 32: Higher magnification comparison secondary and backscatter views of the origin area which showed initially intergranular features that transitioned to transgranular/ striated features (the transition is shown in areas 1-4; also see inboard fracture).

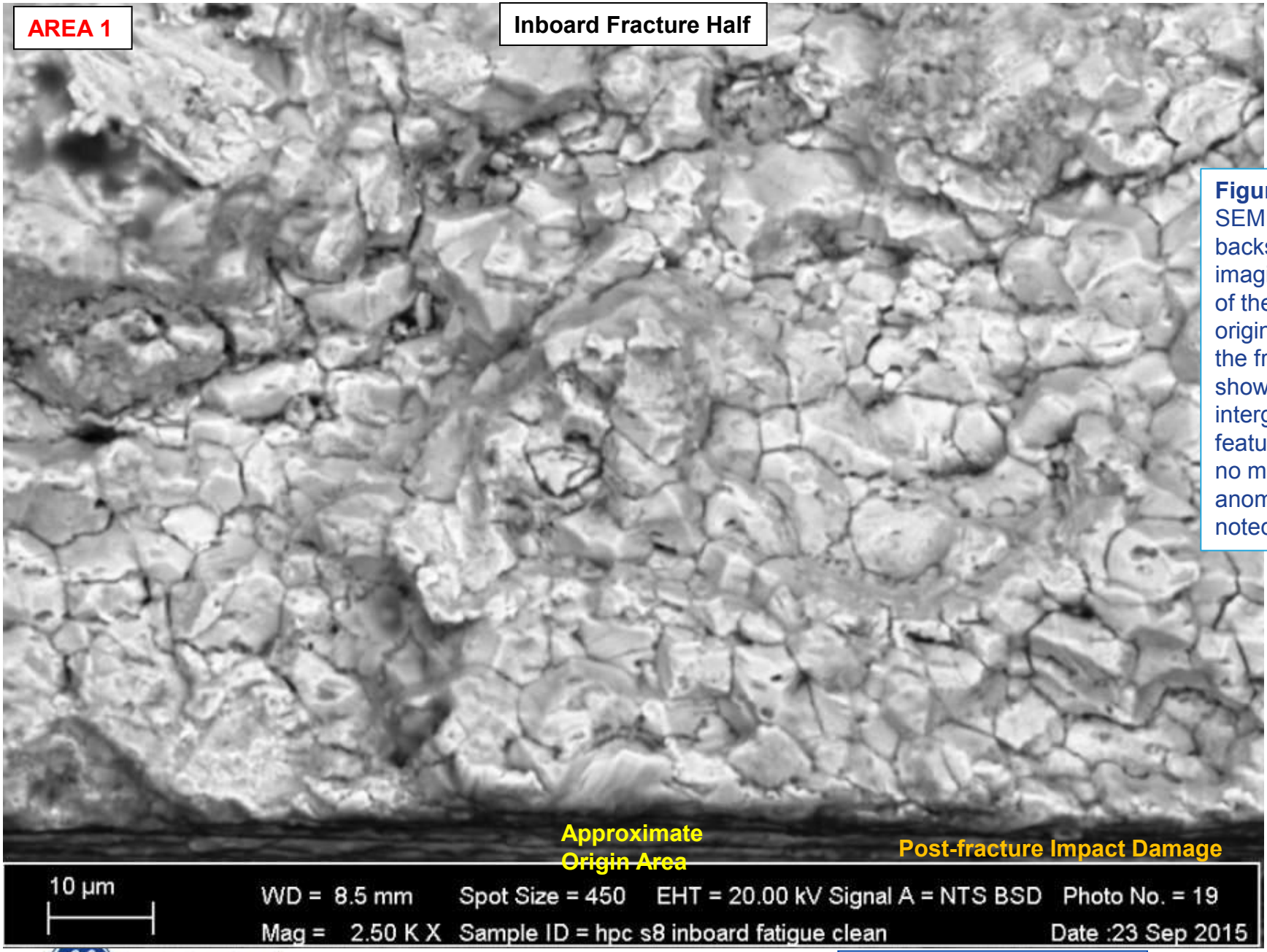

Figure 33: SEM backscatter imaging mode of the general origin area of the fracture showing intergranular features with no material anomalies noted.

AREA 2

Inboard Fracture Half

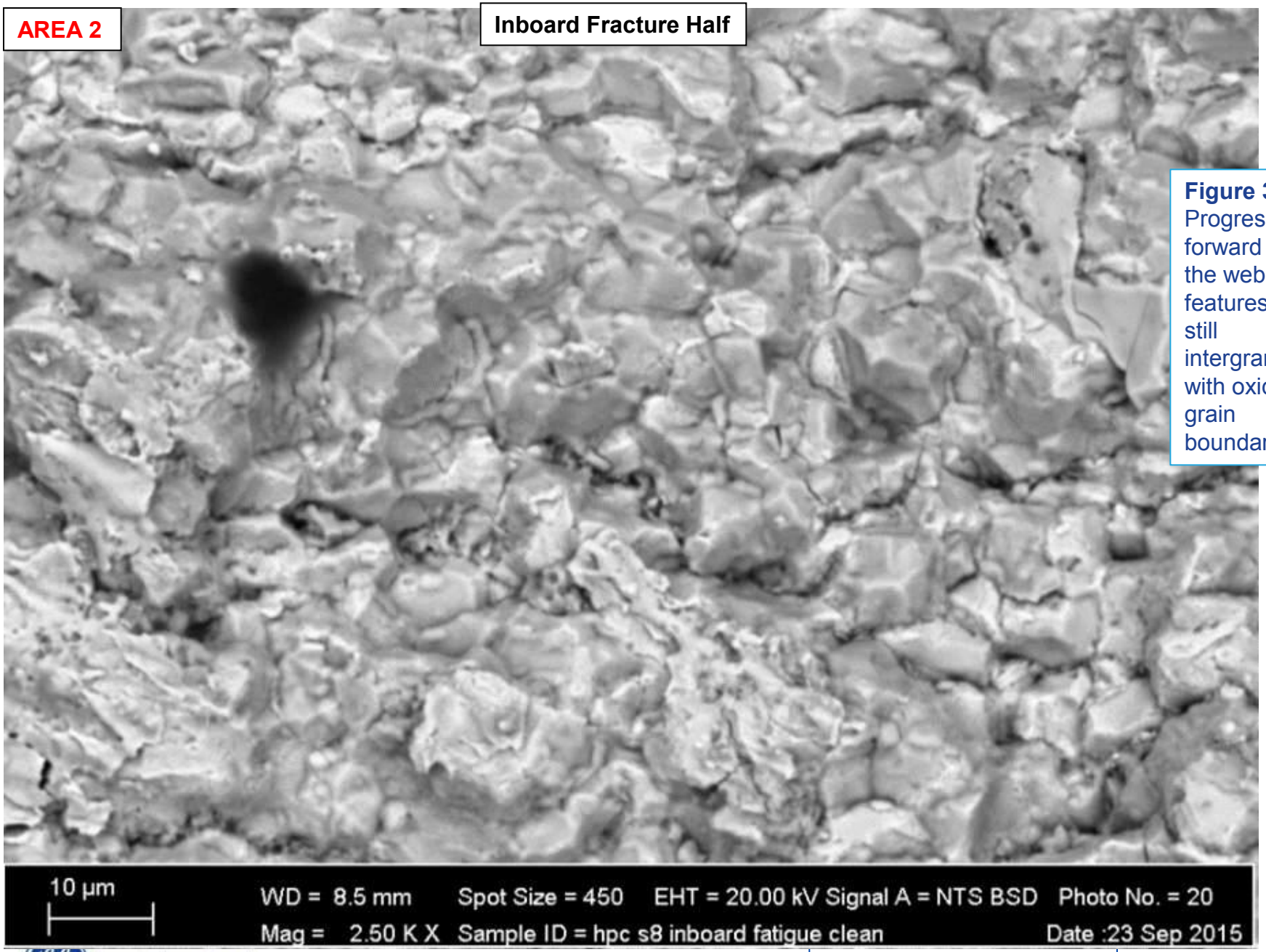

Figure 34: Progressing forward across the web the features were still intergranular with oxidized grain boundaries.

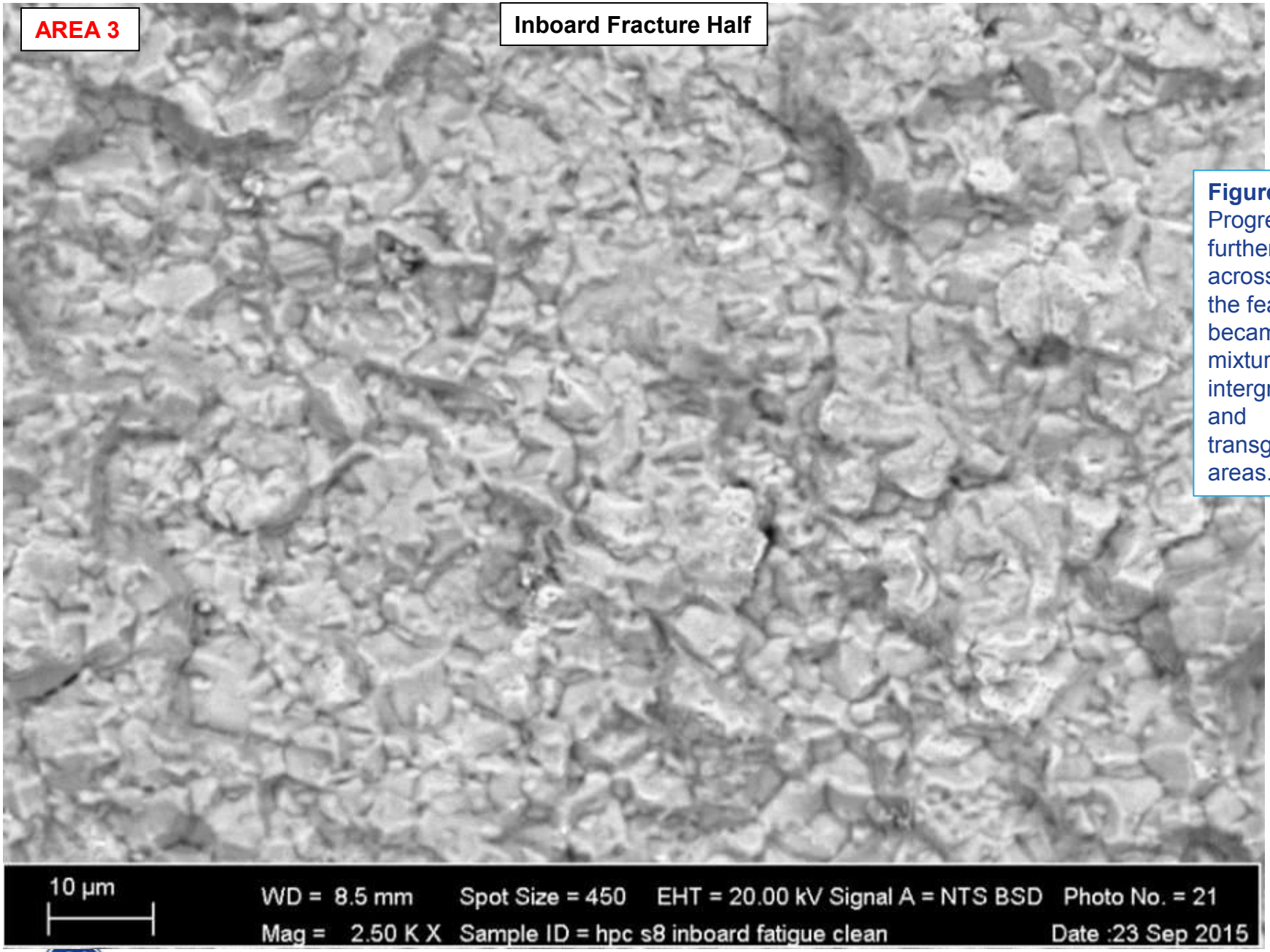

Figure 35: Progressing further forward across the web the features became a mixture of intergranular and transgranular areas.

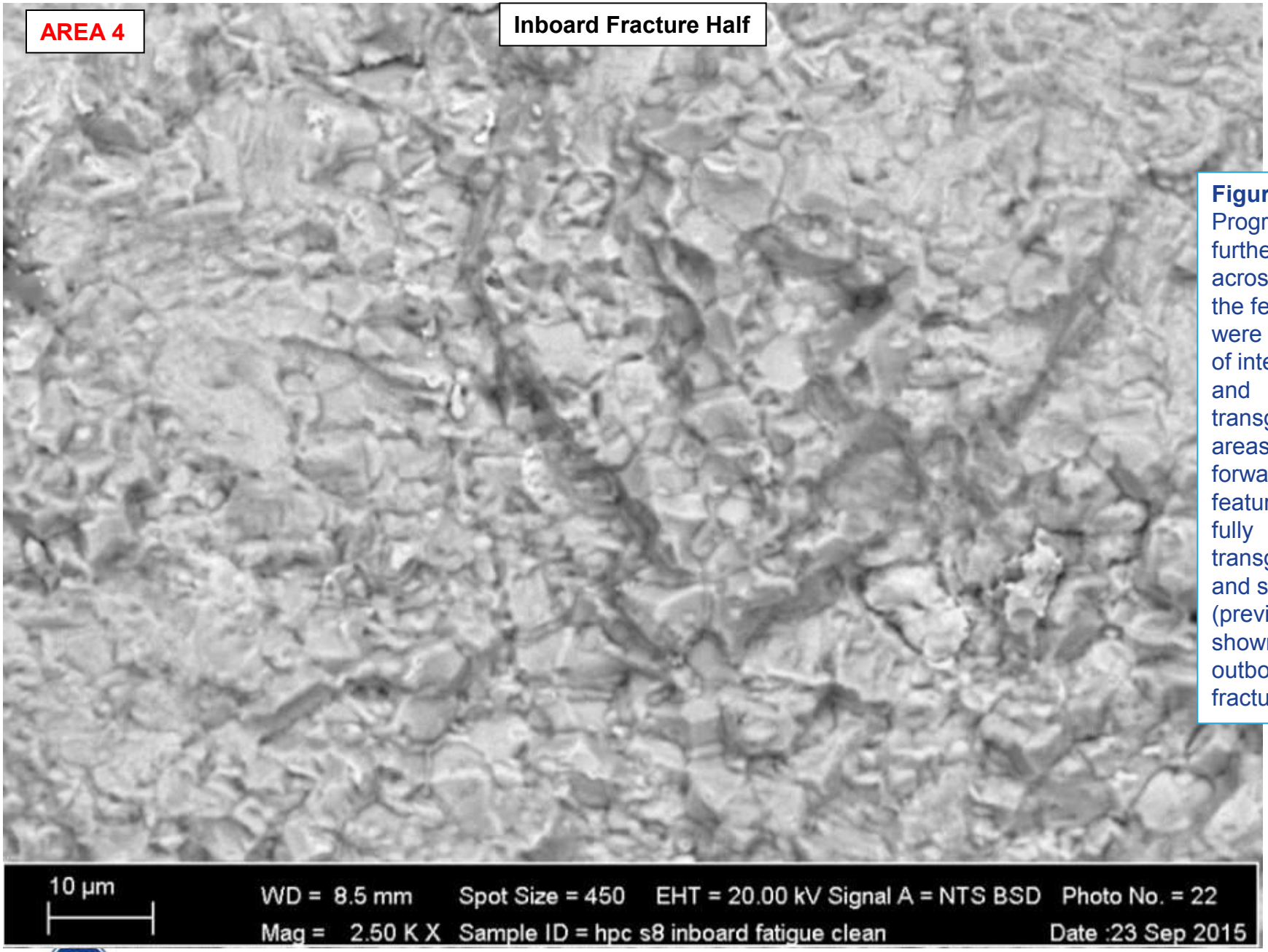

Figure 36: Progressing further forward across the web the features were a mixture of intergranular and transgranular areas. Further forward the features were fully transgranular and striated (previously shown on outboard fracture).

Metallographic Mounts of Inboard Fracture

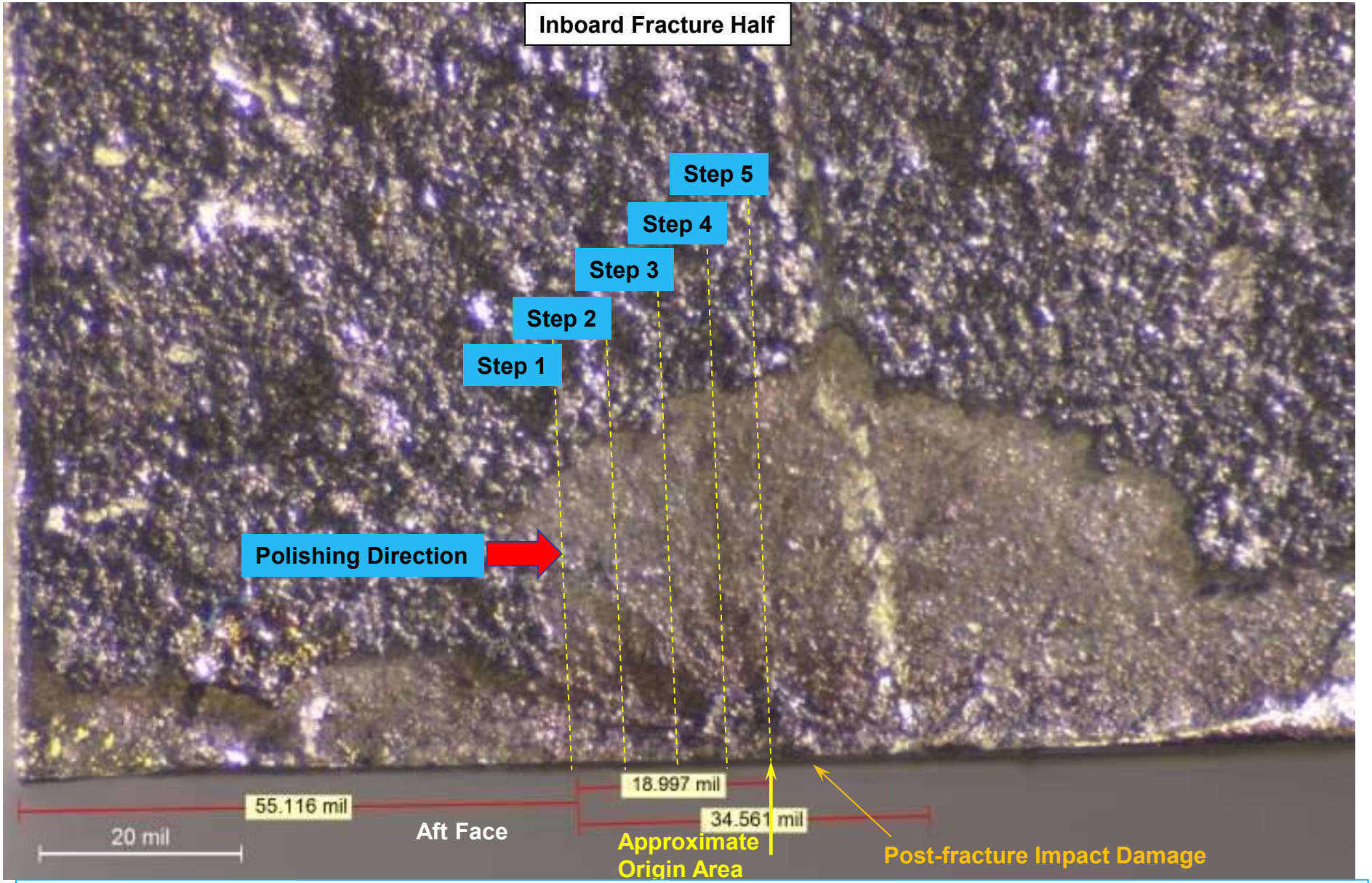

Figure 37: Map showing where a series of step polishes were made across the inboard fracture half metallographic mount. The 5th step was approximately in the plane of the origin area.

Inboard Fracture Half

1st Step Polish

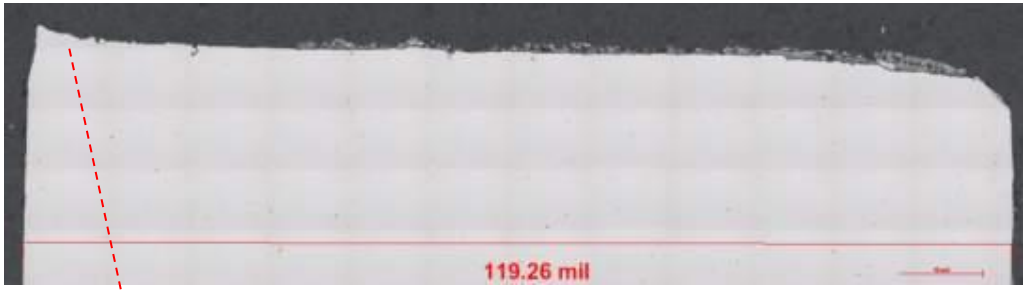

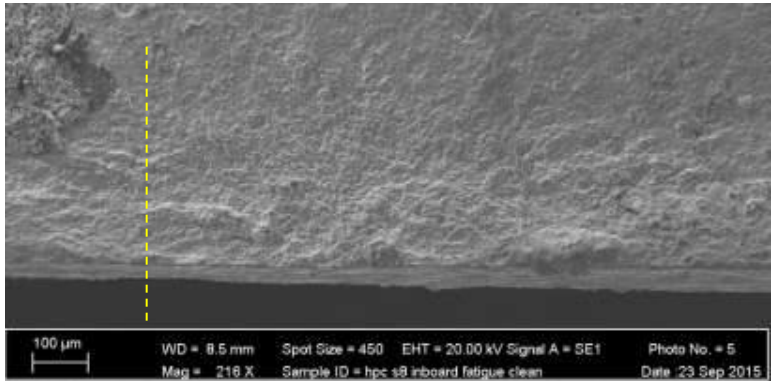

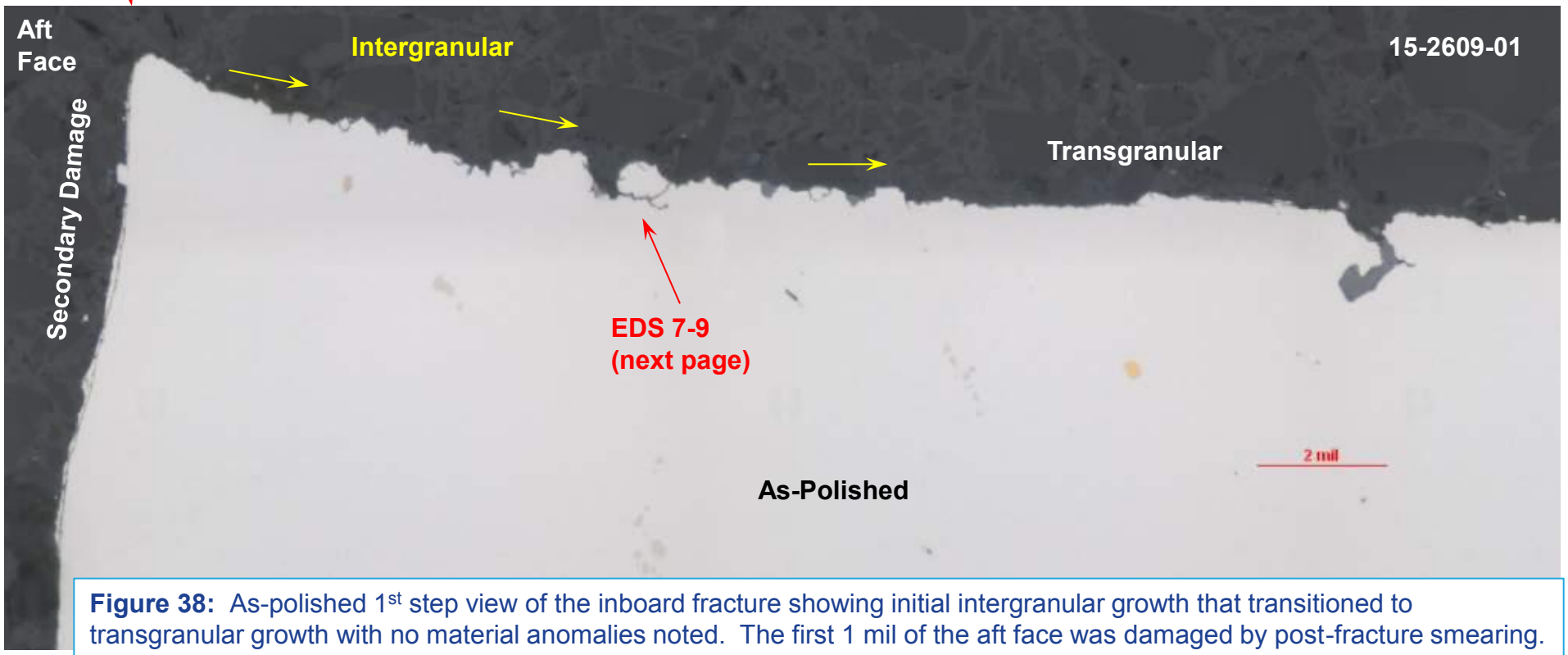

Figure 38: As-polished 1st step view of the inboard fracture showing initial intergranular growth that transitioned to transgranular growth with no material anomalies noted. The first 1 mil of the aft face was damaged by post-fracture smearing.

Inboard Fracture Half **1st Step Polish**

Image Mirrored for Clarity

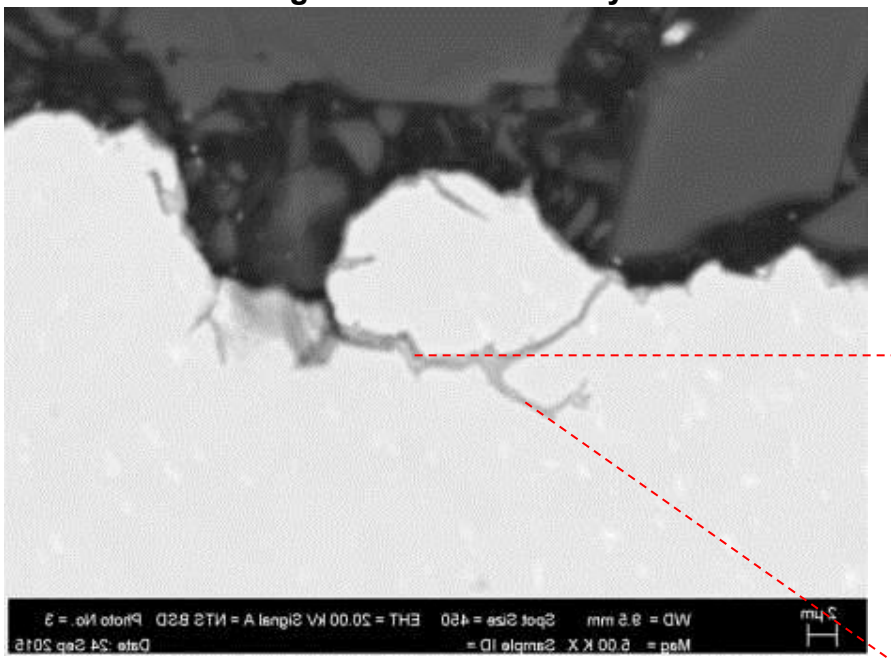

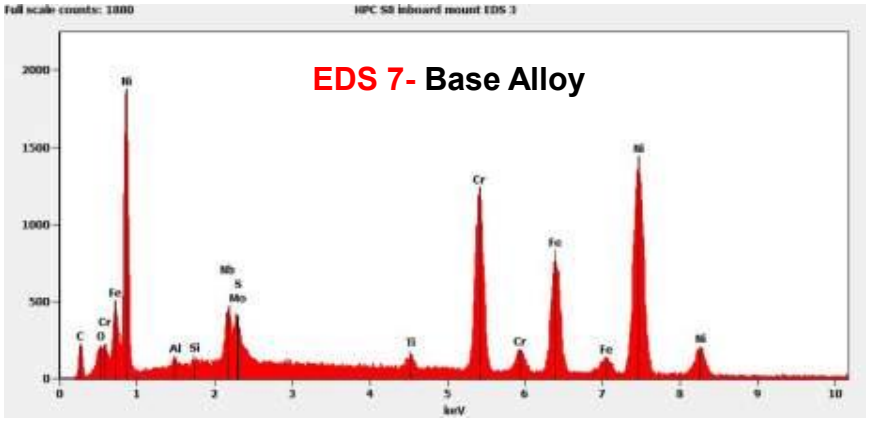

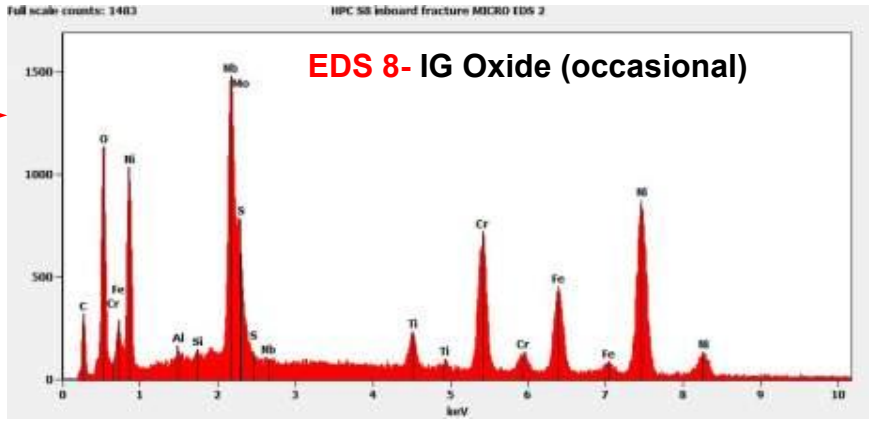

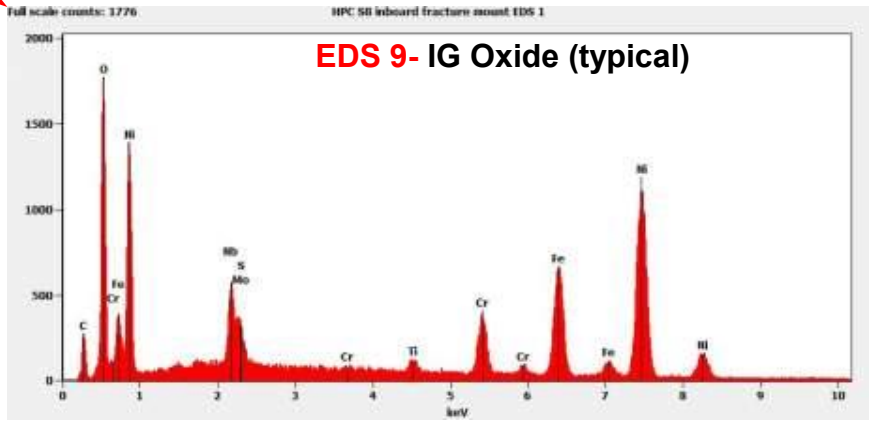

Figure 39: SEM/EDS examination of the intergranular surface oxides. The base material was consistent with the requirement of alloy 718 (EDS 7), while at the grain boundaries only elements consistent with oxidized base material were observed (EDS 9), with occasional areas richer in Nb, consistent with local delta phase oxidation (EDS 8).

Figure 40: As-polished 2nd step view of the inboard fracture showing initial intergranular growth that transitioned to transgranular growth with no material anomalies noted. The first 1 mil of the aft face was damaged by post-fracture smearing. Inboard of the fracture along the face were surface-connected carbides that were etched/oxidized up to approximately 0.3 mil deep locally.

Inboard Fracture Half

3rd Step Polish

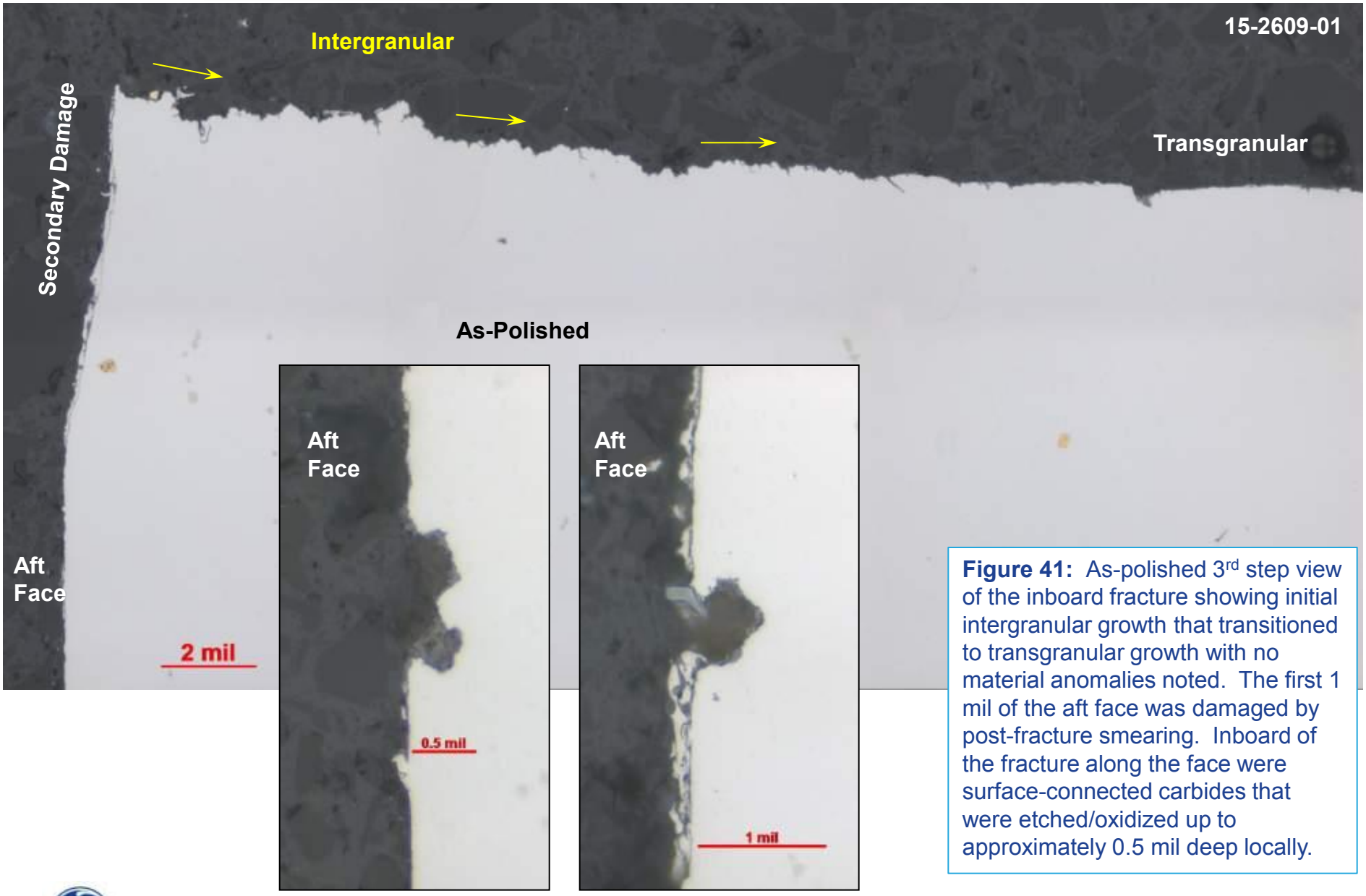

Figure 41: As-polished 3rd step view of the inboard fracture showing initial intergranular growth that transitioned to transgranular growth with no material anomalies noted. The first 1 mil of the aft face was damaged by post-fracture smearing. Inboard of the fracture along the face were surface-connected carbides that were etched/oxidized up to approximately 0.5 mil deep locally.

Inboard Fracture Half | 4th Step Polish

Intergranular

Transgranular

Secondary Damage

EDS 11-13
(next page)

As-Polished

Aft Face

2 mil

0.5 mil

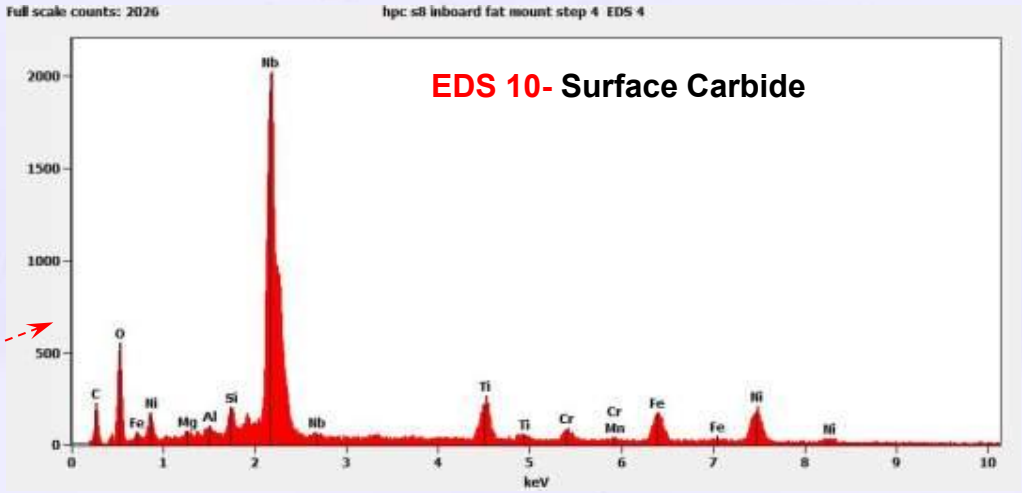

Figure 42: As-polished 4th step view of the inboard fracture showing initial intergranular growth that transitioned to transgranular growth with no material anomalies noted. The first 1 mil of the aft face was damaged by post-fracture smearing. Inboard of the fracture along the face were surface-connected carbides that were etched/oxidized up to approximately 0.2 mil deep locally. EDS analysis confirmed the surface "pit" was consistent with oxidized Nb-rich carbides (EDS 10).

4th Step Polish (~origin)

Image Mirrored for Clarity

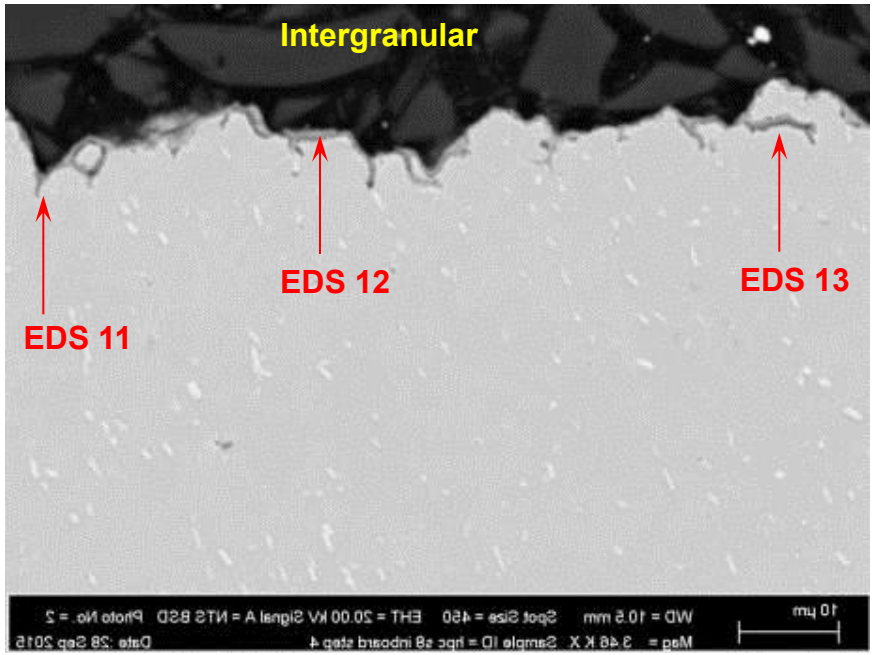

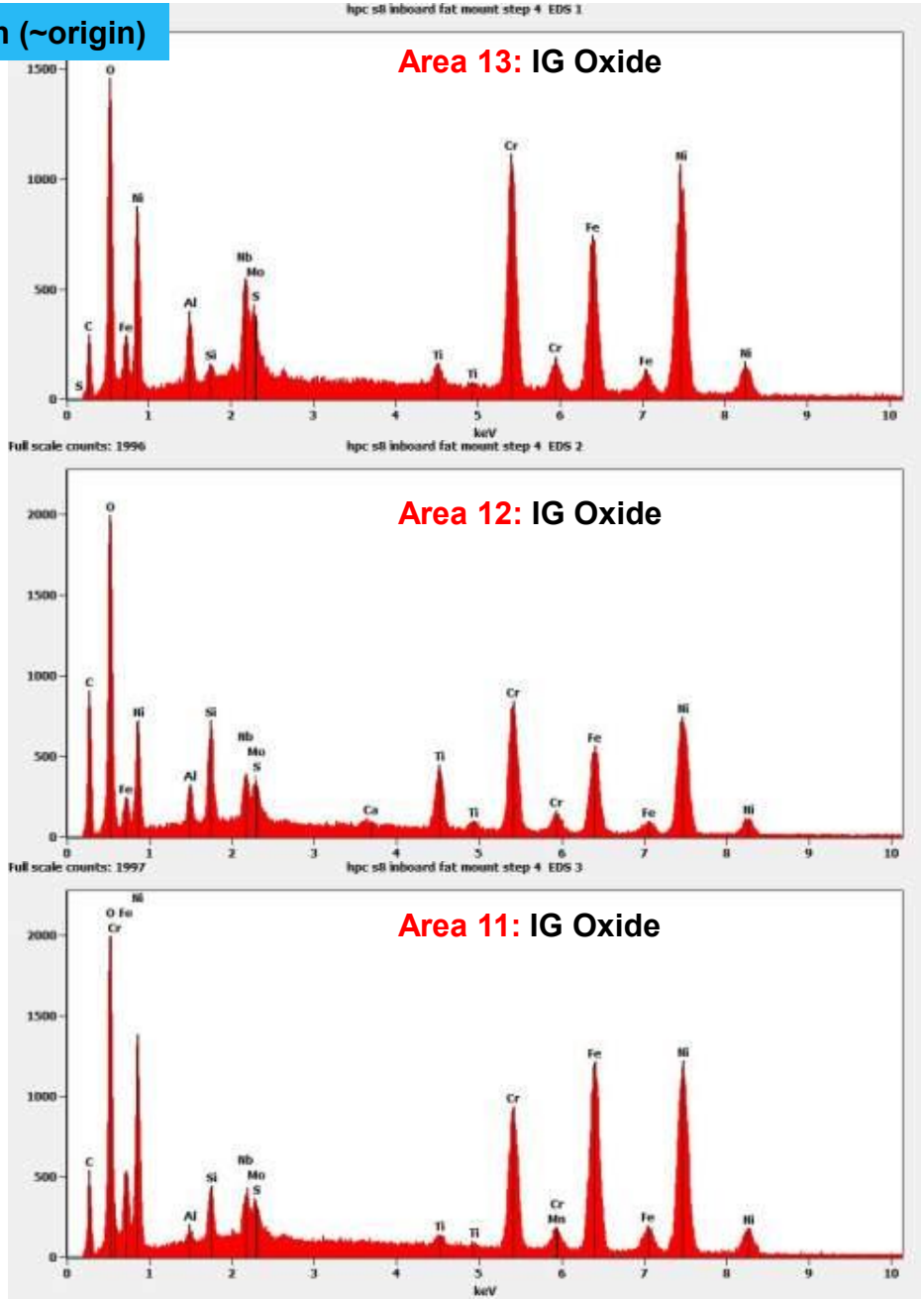

Figure 43: EDS analysis of the fracture in the intergranular region only showed elements consistent with base metal material oxides with no detrimental species found (EDS 11-13).

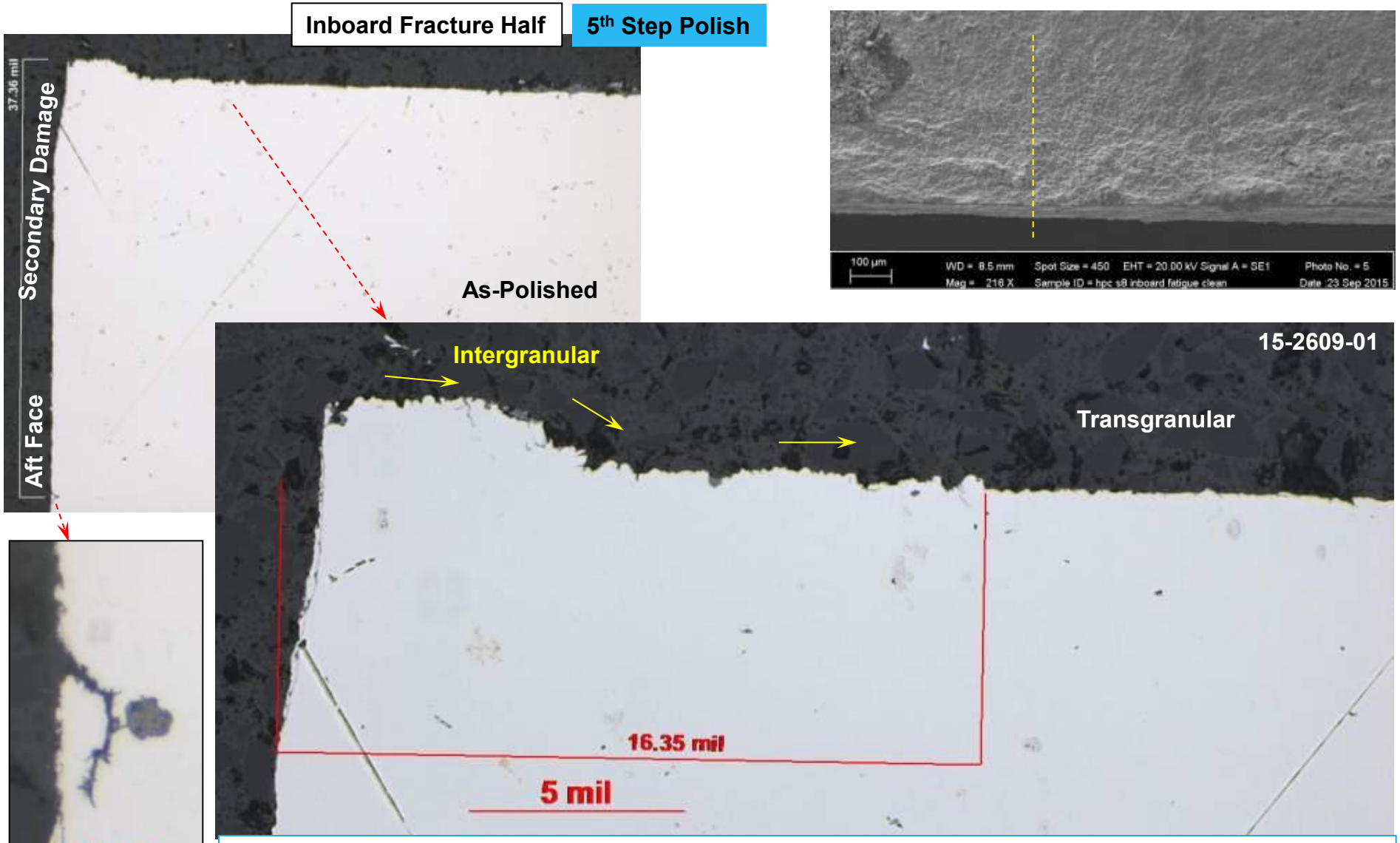

Figure 44: As-polished 5th step view of the inboard fracture through the approximate origin area showing initial intergranular growth that transitioned to transgranular growth with no material anomalies noted. The first 1 mil of the aft face was damaged by post-fracture smearing. In the current plane of polish the predominantly intergranular region was up to 16 mils deep.

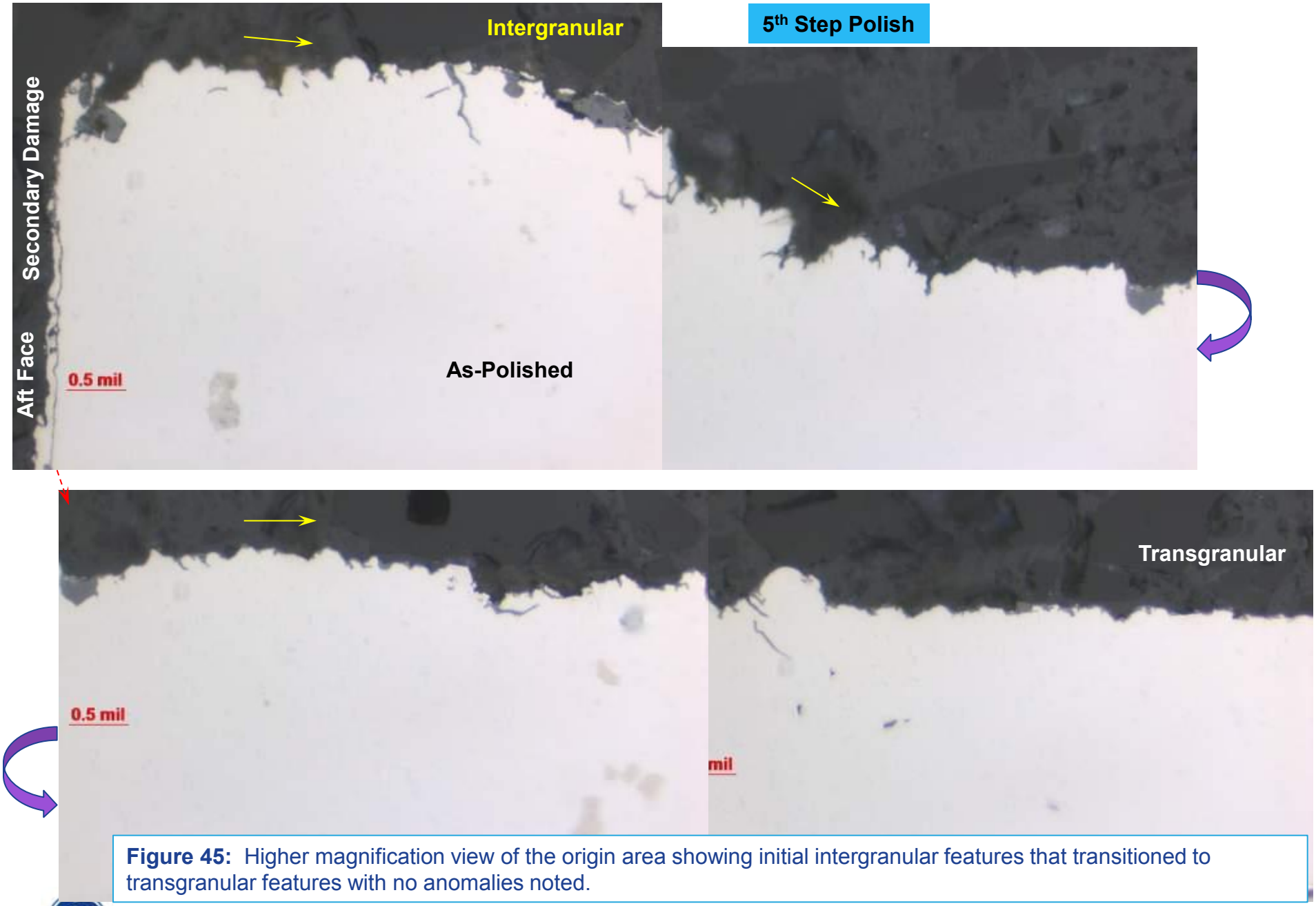

Figure 45: Higher magnification view of the origin area showing initial intergranular features that transitioned to transgranular features with no anomalies noted.

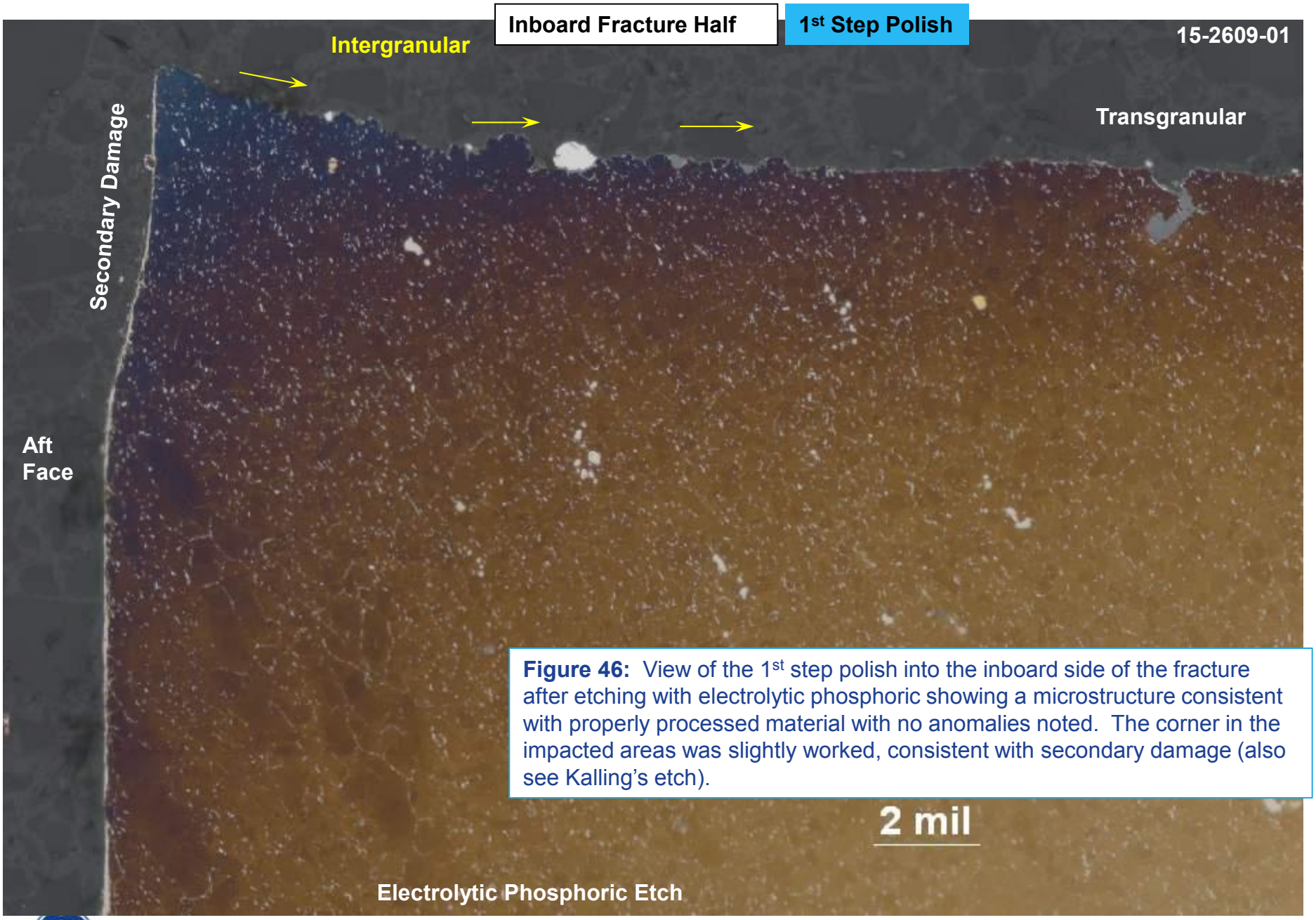

Figure 46: View of the 1st step polish into the inboard side of the fracture after etching with electrolytic phosphoric showing a microstructure consistent with properly processed material with no anomalies noted. The corner in the impacted areas was slightly worked, consistent with secondary damage (also see Kalling's etch).

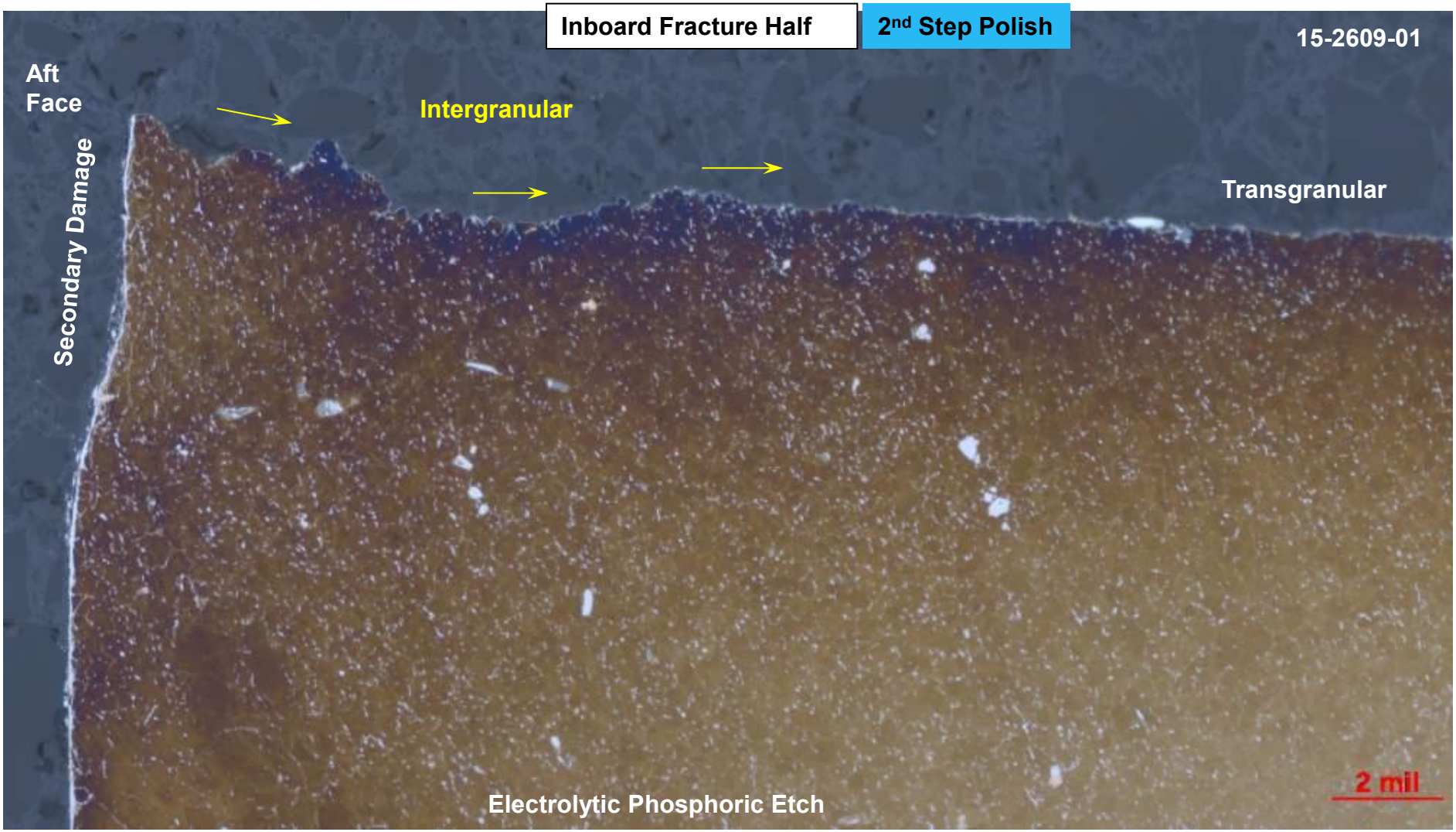

Figure 47: View of the 2nd step polish into the inboard side of the fracture after etching with electrolytic phosphoric showing a microstructure consistent with properly processed material with no anomalies noted. The corner in the impacted areas was slightly worked, consistent with secondary damage (also see Kalling's etch).

Figure 48: View of the 3rd step polish into the inboard side of the fracture after etching with electrolytic phosphoric showing a microstructure consistent with properly processed material with no anomalies noted. The corner in the impacted areas was slightly worked, consistent with secondary damage (also see Kalling's etch).

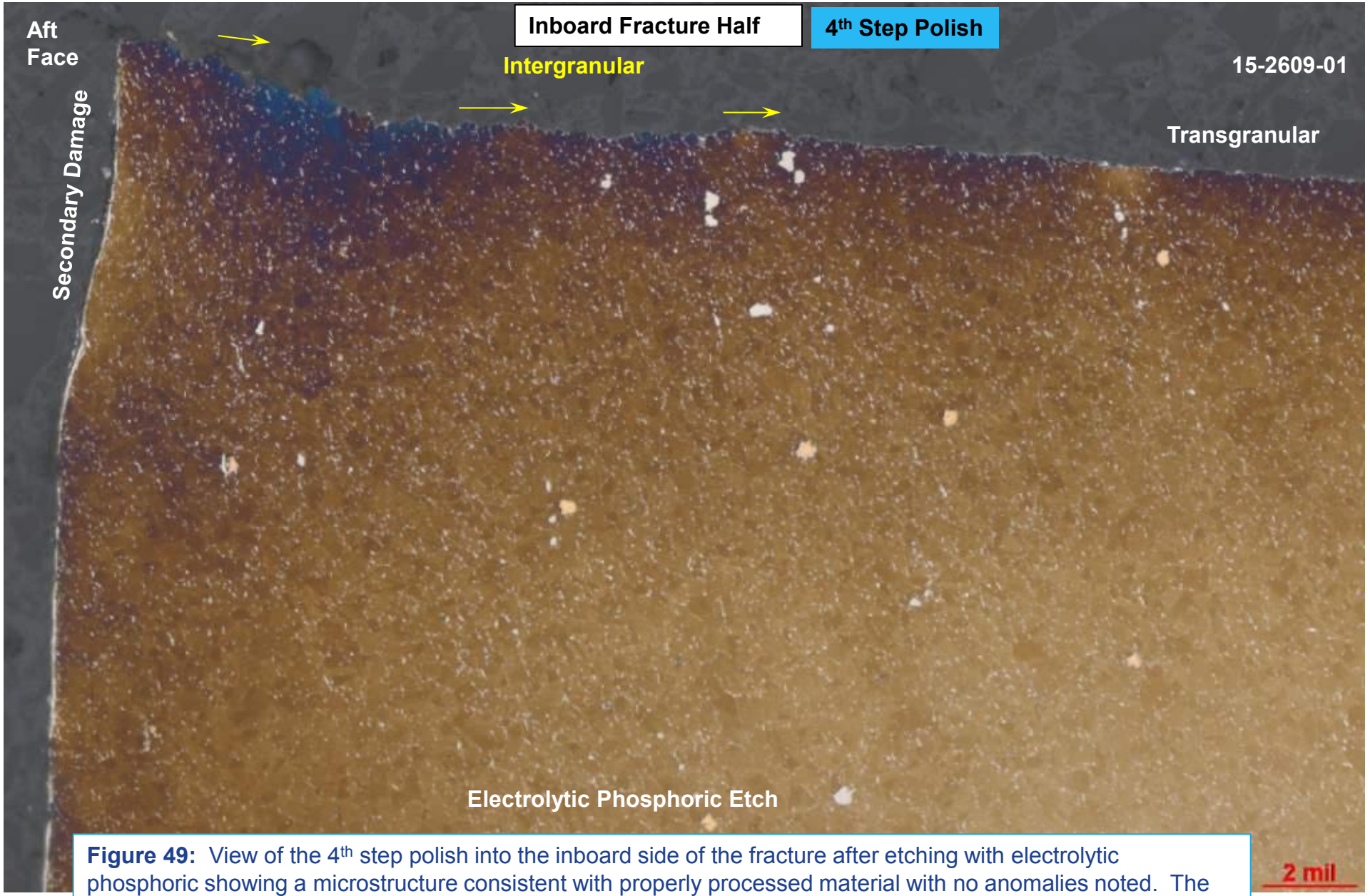

Figure 49: View of the 4th step polish into the inboard side of the fracture after etching with electrolytic phosphoric showing a microstructure consistent with properly processed material with no anomalies noted. The corner in the impacted areas was slightly worked, consistent with secondary damage (also see Kalling's etch).

Inboard Fracture Half | 5th Step Polish

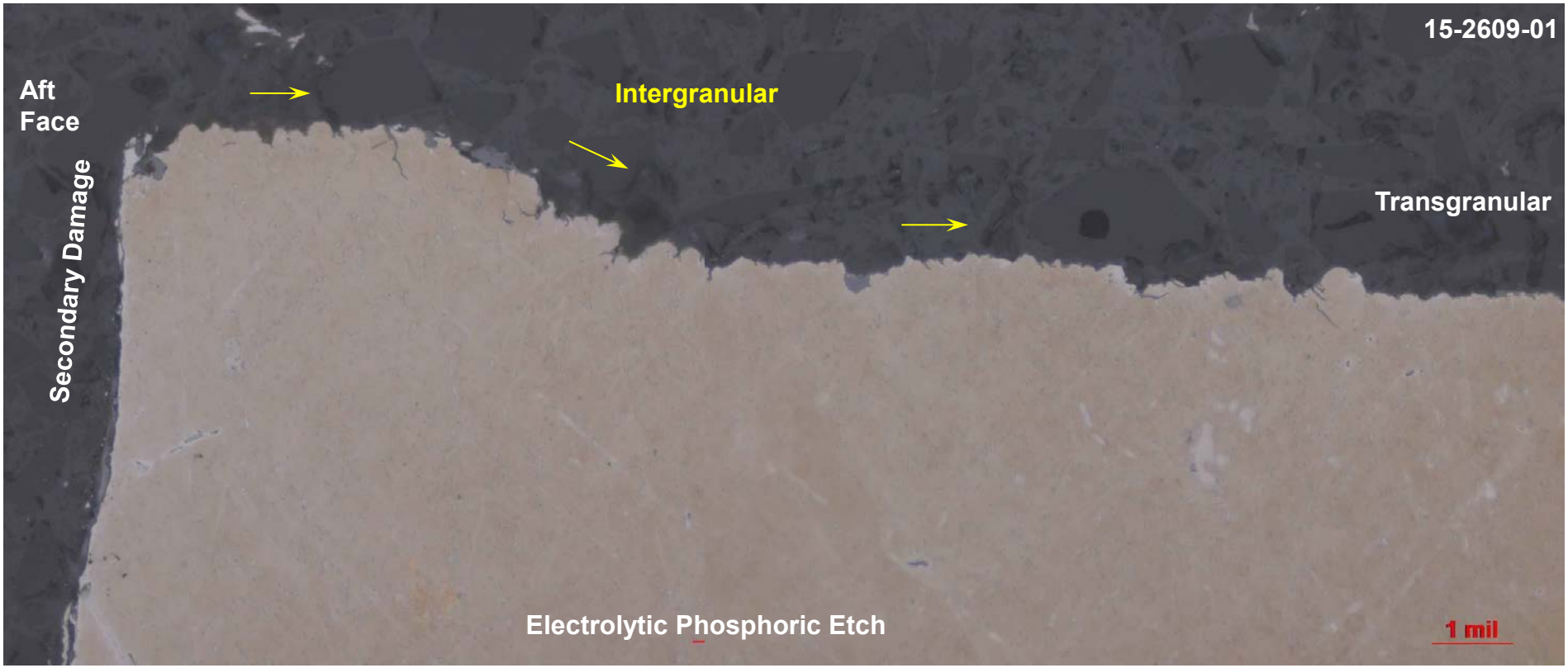

Figure 50: View of the 5th step polish into the inboard side of the fracture after etching with electrolytic phosphoric showing a microstructure consistent with properly processed material with no anomalies noted. The corner in the impacted areas was slightly worked, consistent with secondary damage (also see Kalling's etch in next few pages).

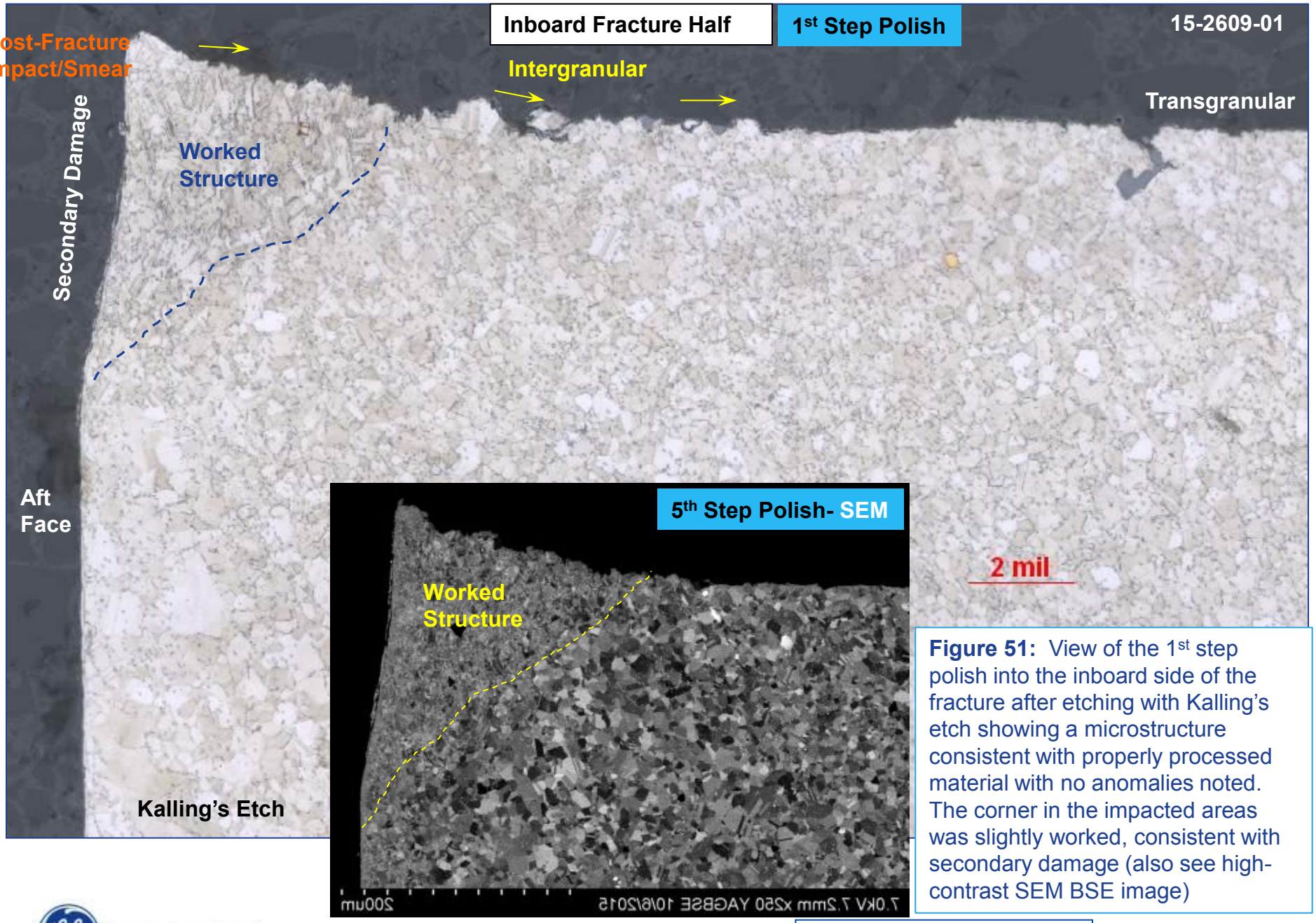

Figure 51: View of the 1st step polish into the inboard side of the fracture after etching with Kalling's etch showing a microstructure consistent with properly processed material with no anomalies noted. The corner in the impacted areas was slightly worked, consistent with secondary damage (also see high-contrast SEM BSE image)

Inboard Fracture Half | 2nd Step Polish

Figure 52: View of the 2nd step polish into the inboard side of the fracture after etching with Kalling's etch showing a microstructure consistent with properly processed material with no anomalies noted. The corner in the impacted areas was slightly worked, consistent with secondary damage.

Inboard Fracture Half | 3rd Step Polish

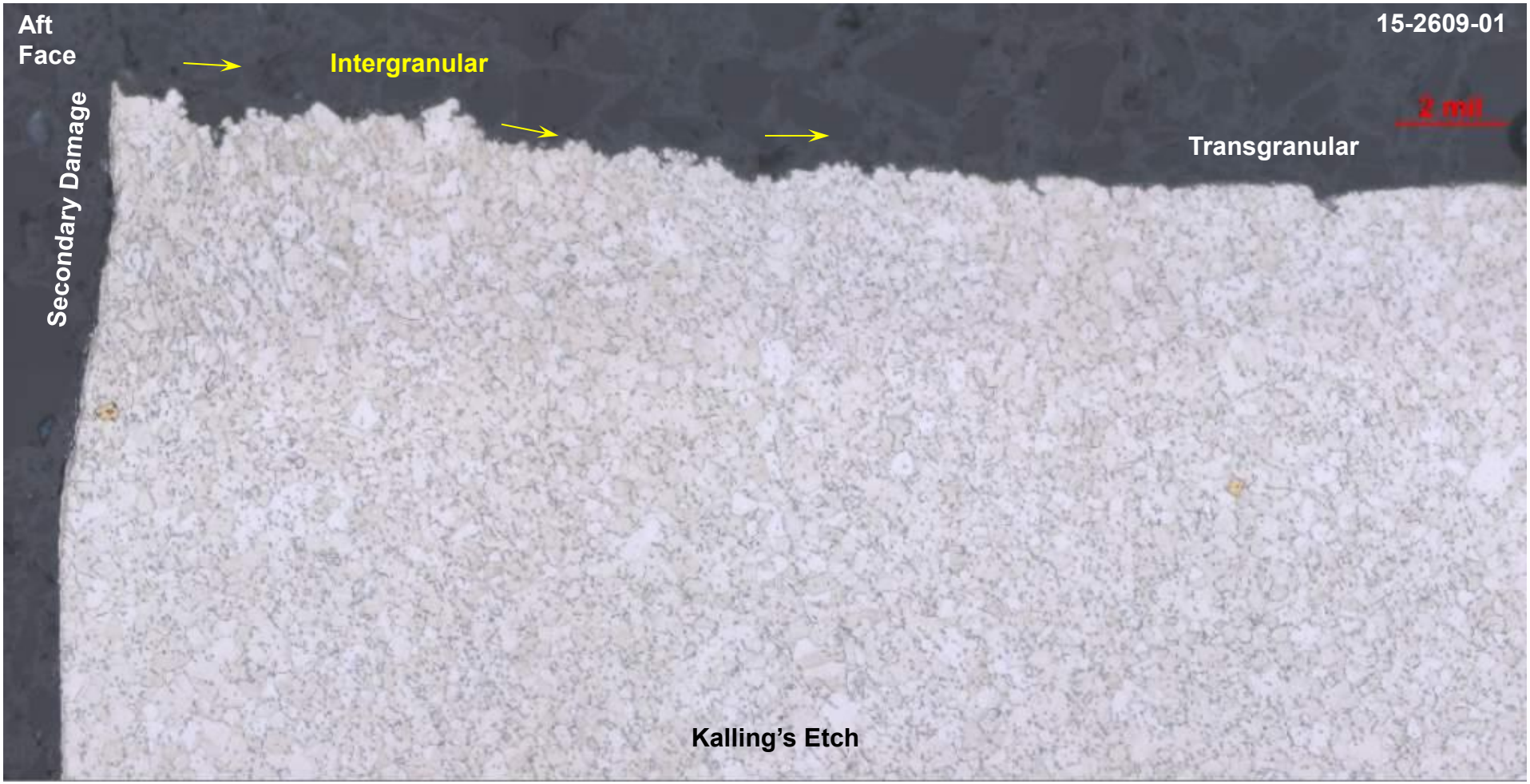

Figure 53: View of the 3rd step polish into the inboard side of the fracture after etching with Kalling's etch showing a microstructure consistent with properly processed material with no anomalies noted. The corner in the impacted areas was slightly worked, consistent with secondary damage.

Inboard Fracture Half | 4th Step Polish

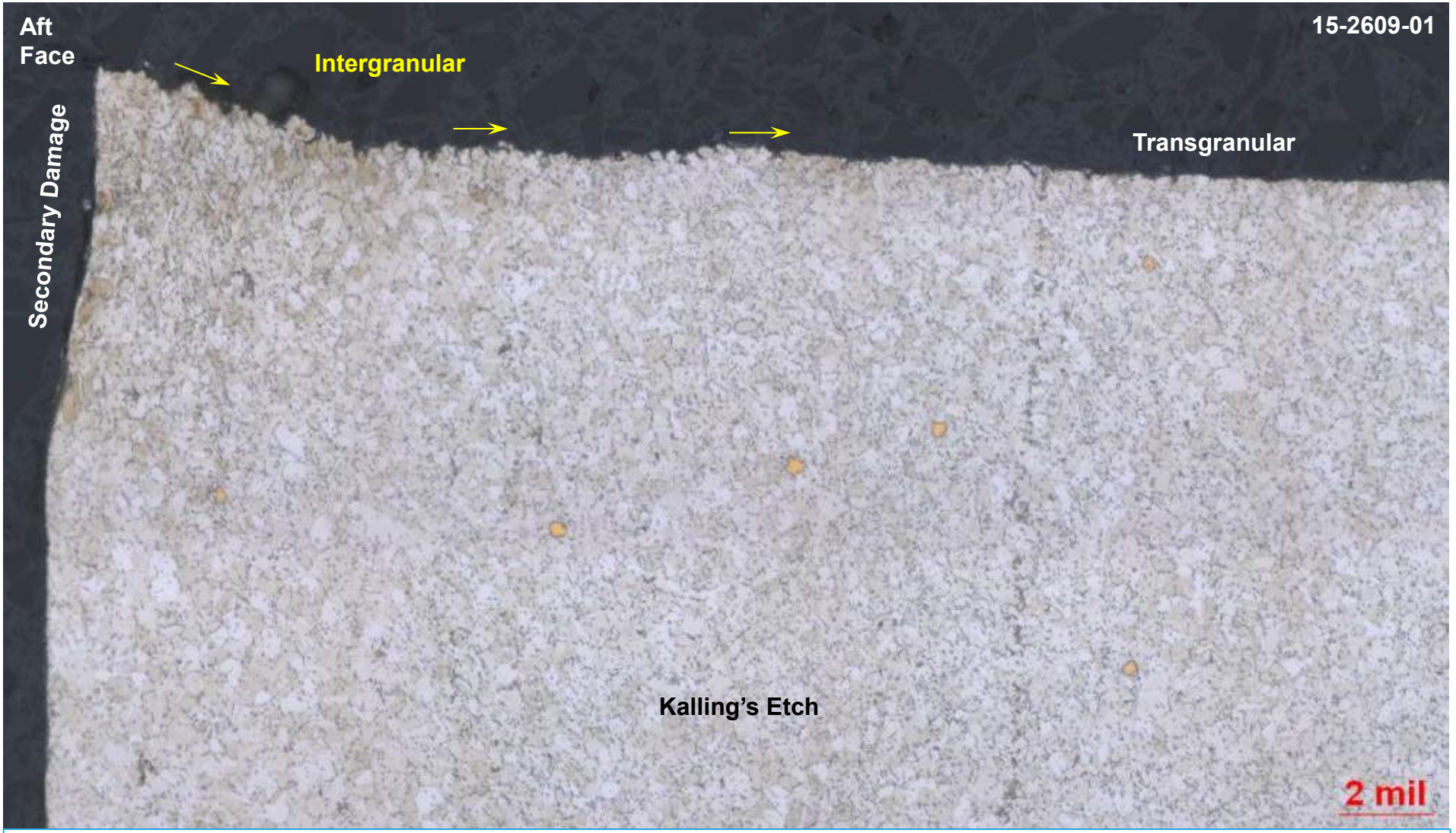

Figure 54: View of the 4th step polish into the inboard side of the fracture after etching with Kalling's etch showing a microstructure consistent with properly processed material with no anomalies noted. The corner in the impacted areas was slightly worked, consistent with secondary damage.

Inboard Fracture Half | 4th Step Polish

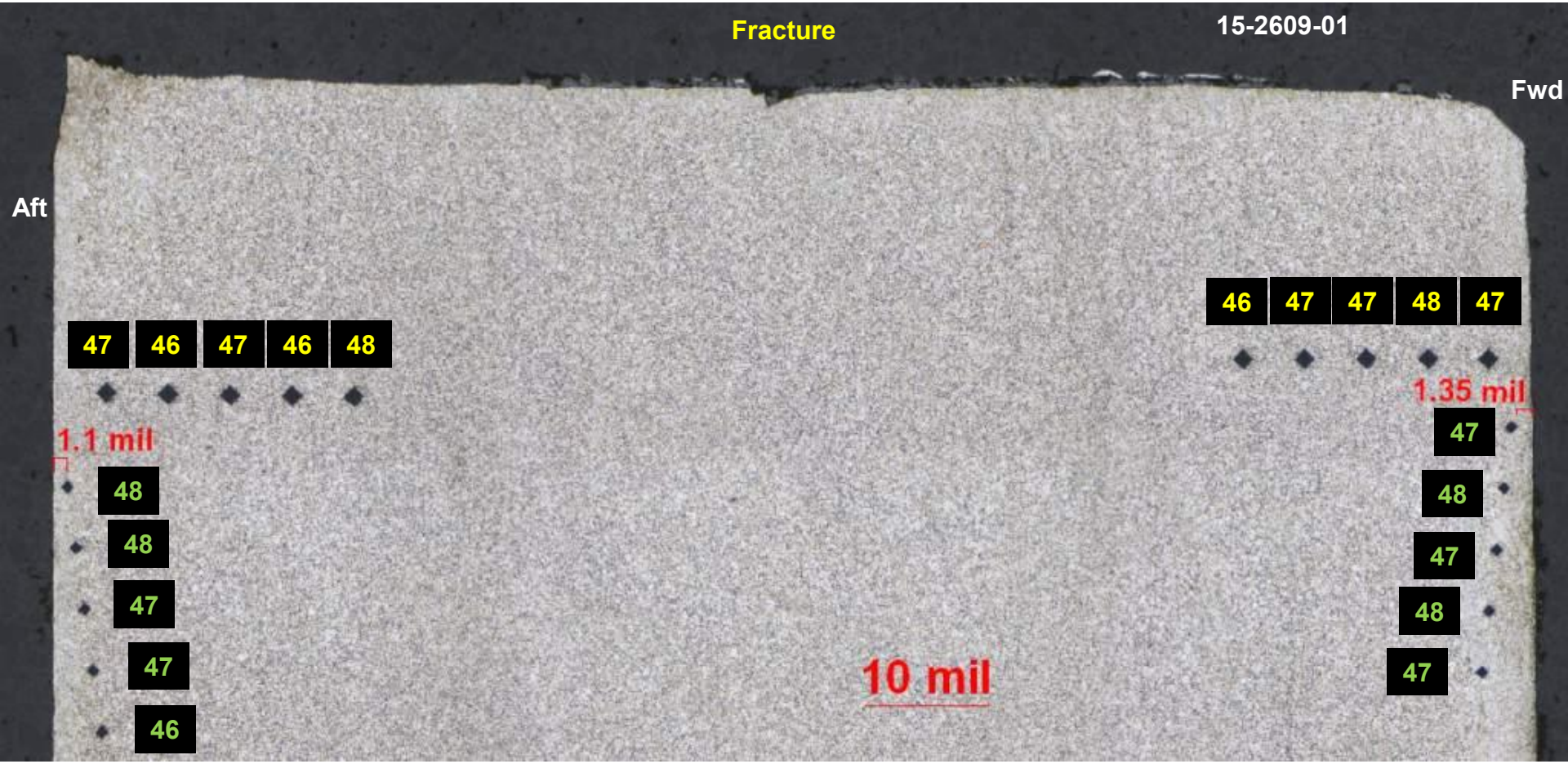

Figure 55: Micro-hardness measurements taken near the forward and aft faces ranged between HRC 46-48 and conformed to the requirement of C50TF81.

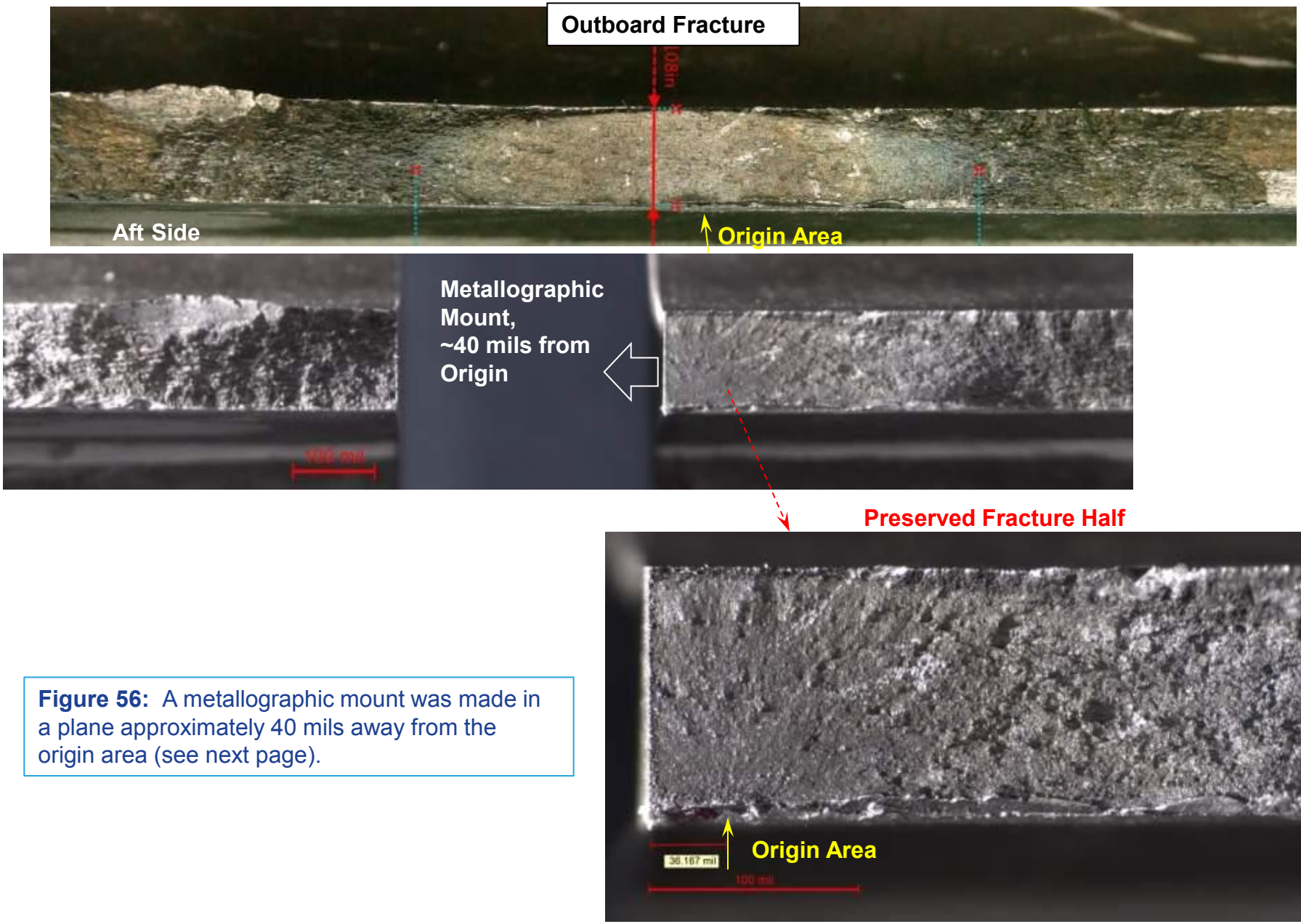

Figure 56: A metallographic mount was made in a plane approximately 40 mils away from the origin area (see next page).

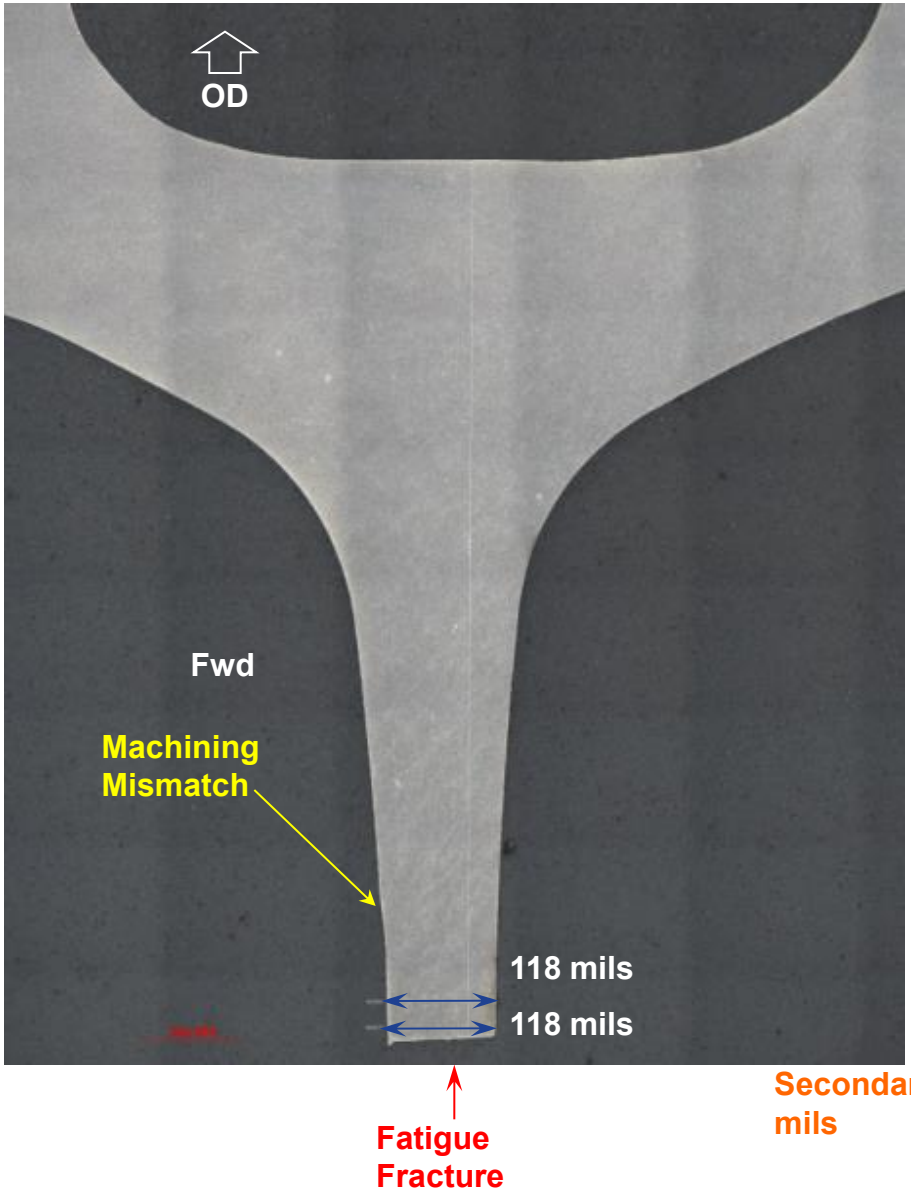

Figure 57: A metallographic made into the outboard fracture showed that it extended from the aft side of the web approximately 0.950 inch from the slot bottom at the web transition area where the wall thickness was reduced to approximately 0.118 inch. Secondary cracks were found within 16 mils of the main fatigue fracture further inboard.

Outboard Fracture

Figure 58: The as-polished metallographic mount into the outboard fracture showed that there were no material anomalies in the base structure. The aft corner/origin area fracture was more damaged than the inboard side, but the underlying base structure had less damage/work (see etched mount).

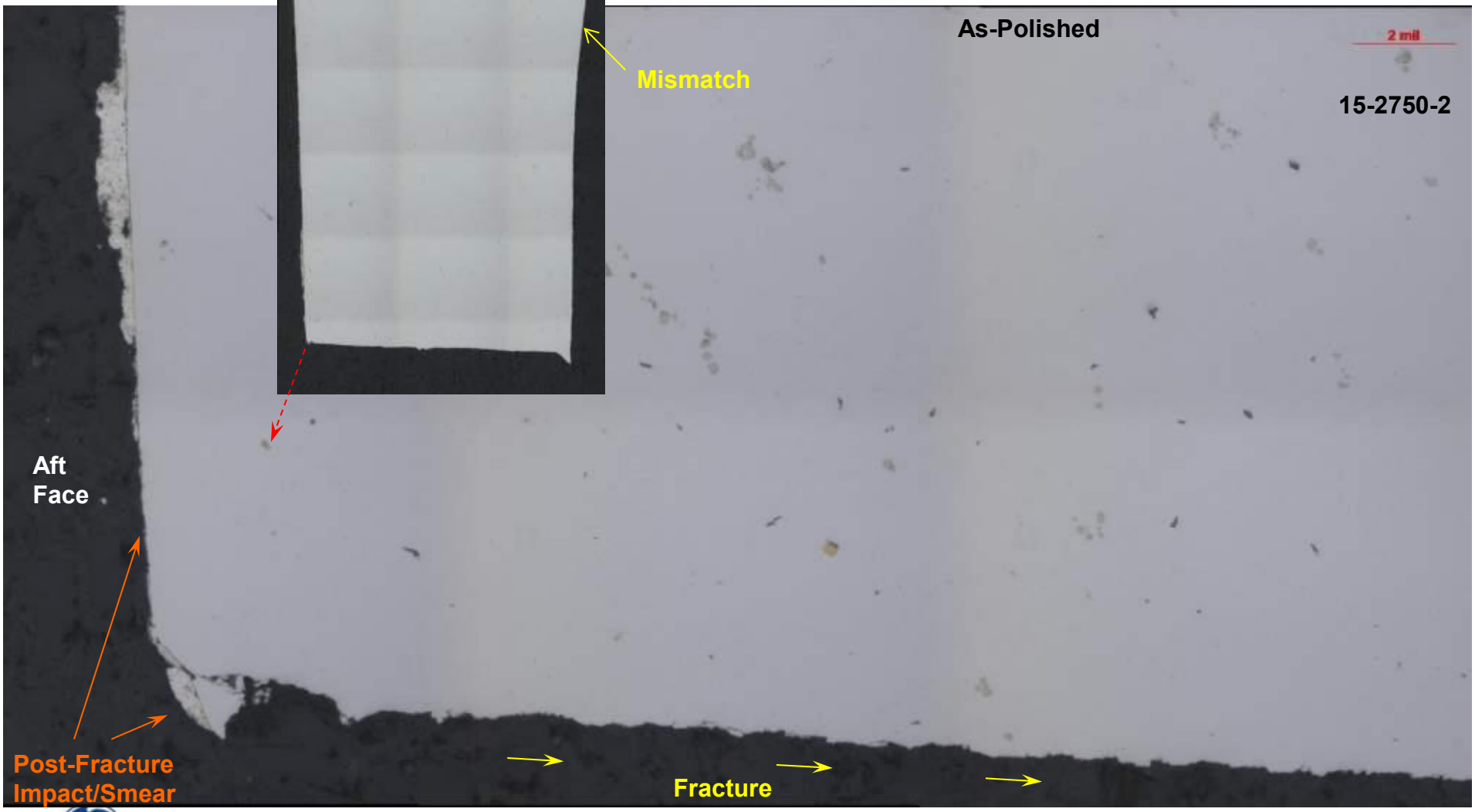

Outboard Fracture

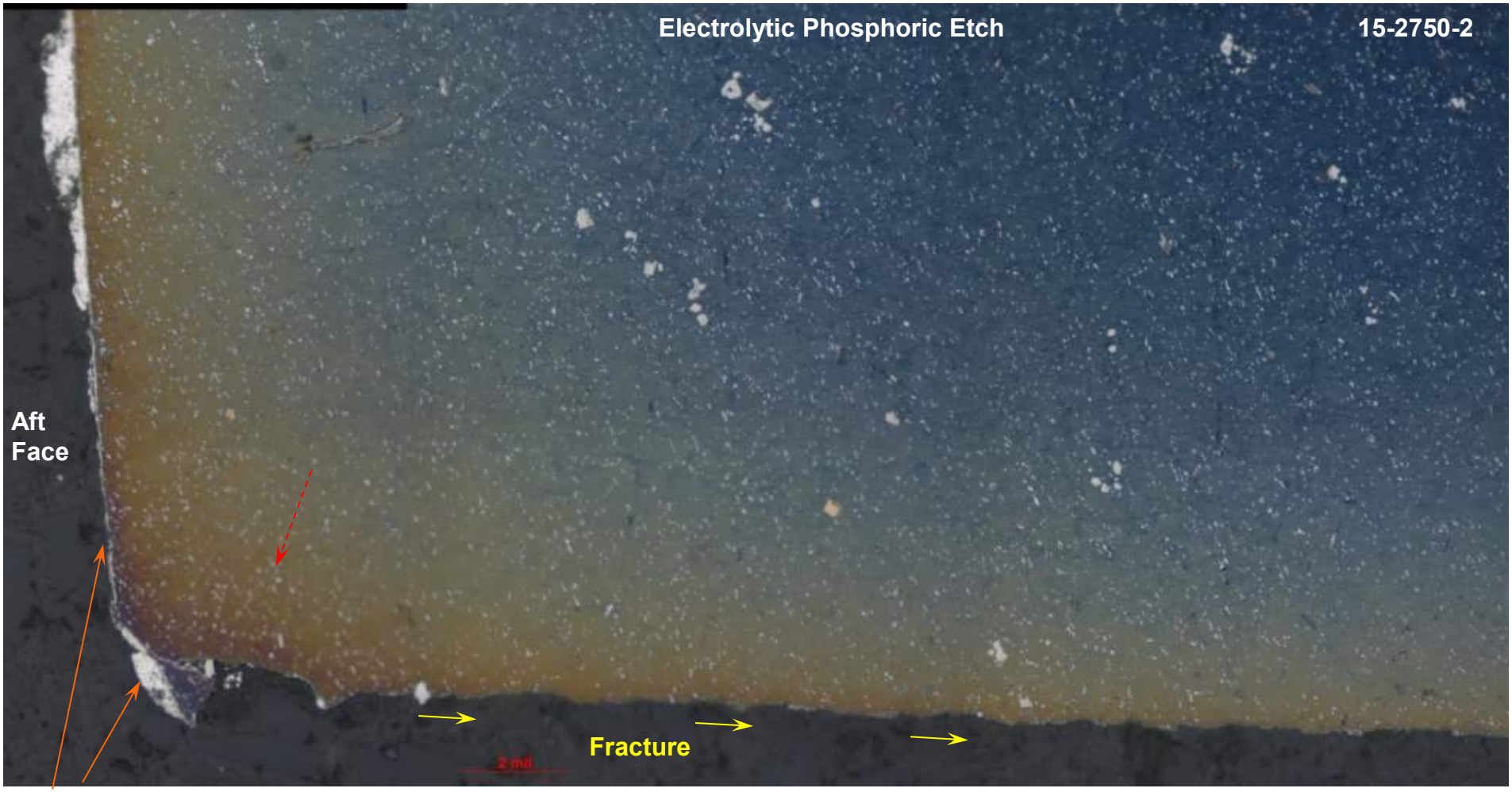

Figure 59: The etched metallographic mount into the outboard fracture showed that there were no material anomalies in the base structure. The aft corner/origin area fracture was more damaged than the inboard side, but the underlying base structure had less damage/work (see Kalling's etch)

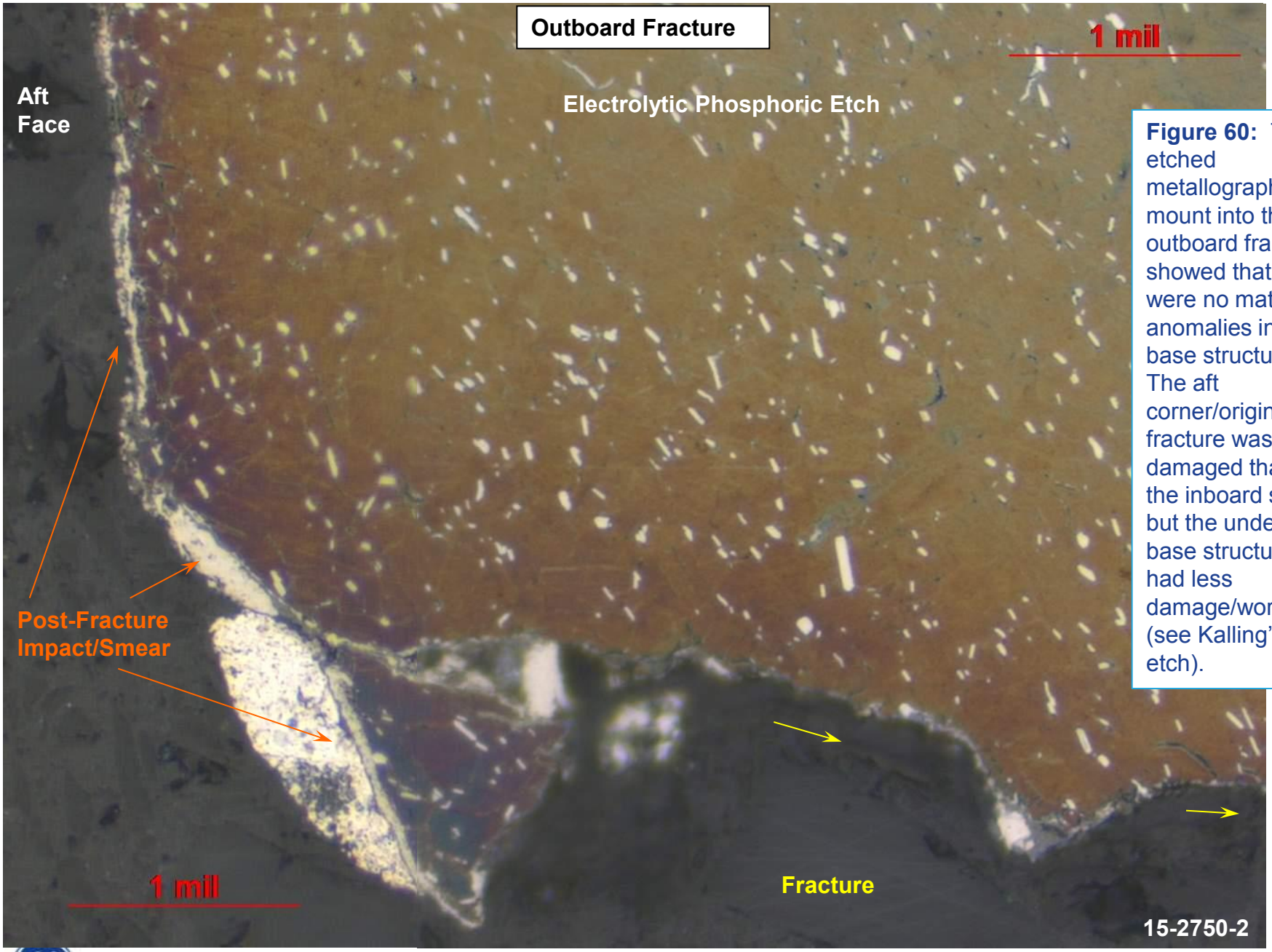

Figure 60: The etched metallographic mount into the outboard fracture showed that there were no material anomalies in the base structure. The aft corner/origin area fracture was more damaged than the inboard side, but the underlying base structure had less damage/work (see Kalling's etch).

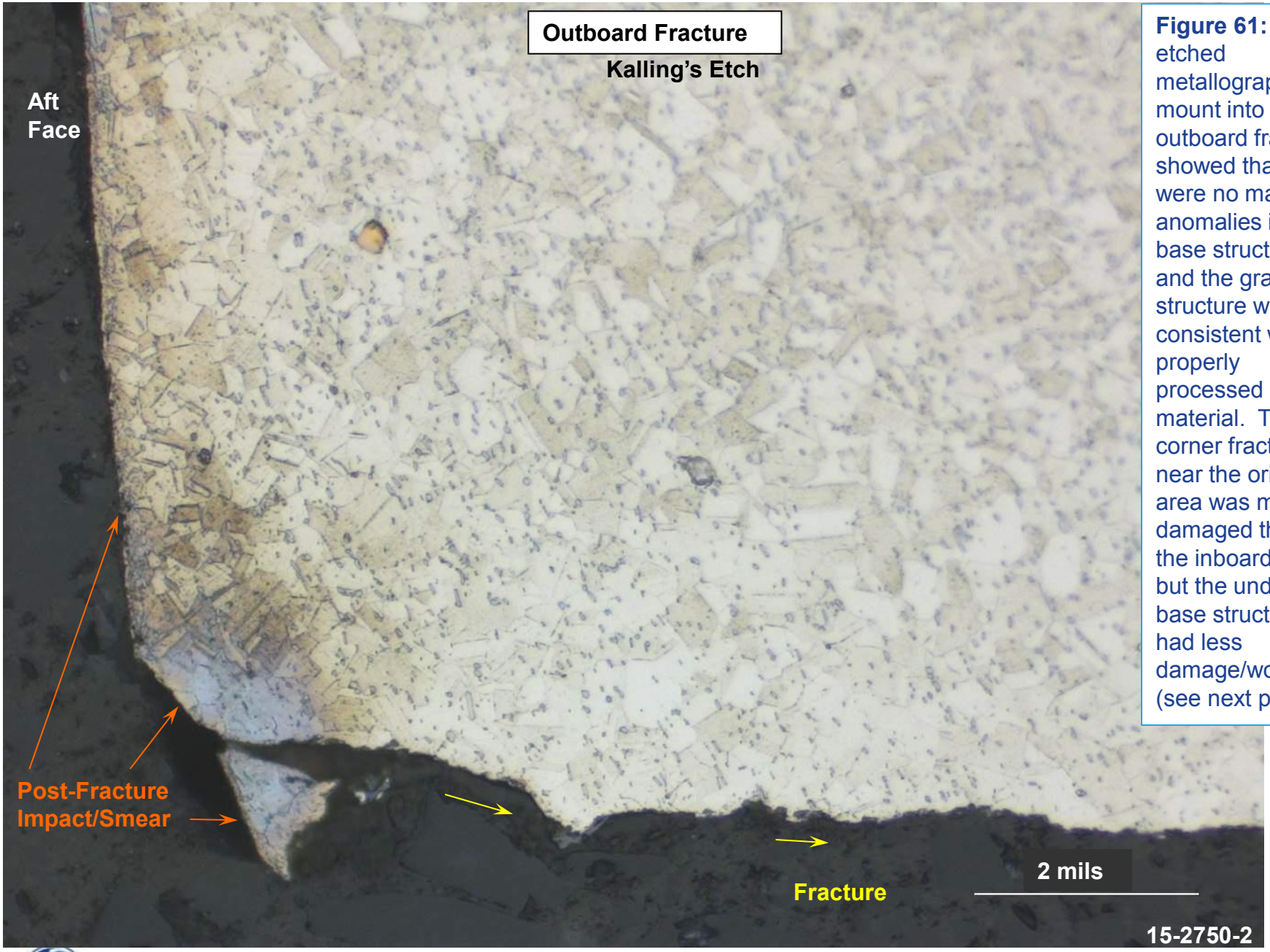

Figure 61: The etched metallographic mount into the outboard fracture showed that there were no material anomalies in the base structure and the grain structure was consistent with properly processed material. The aft corner fracture near the origin area was more damaged than the inboard side, but the underlying base structure had less damage/work (see next page).

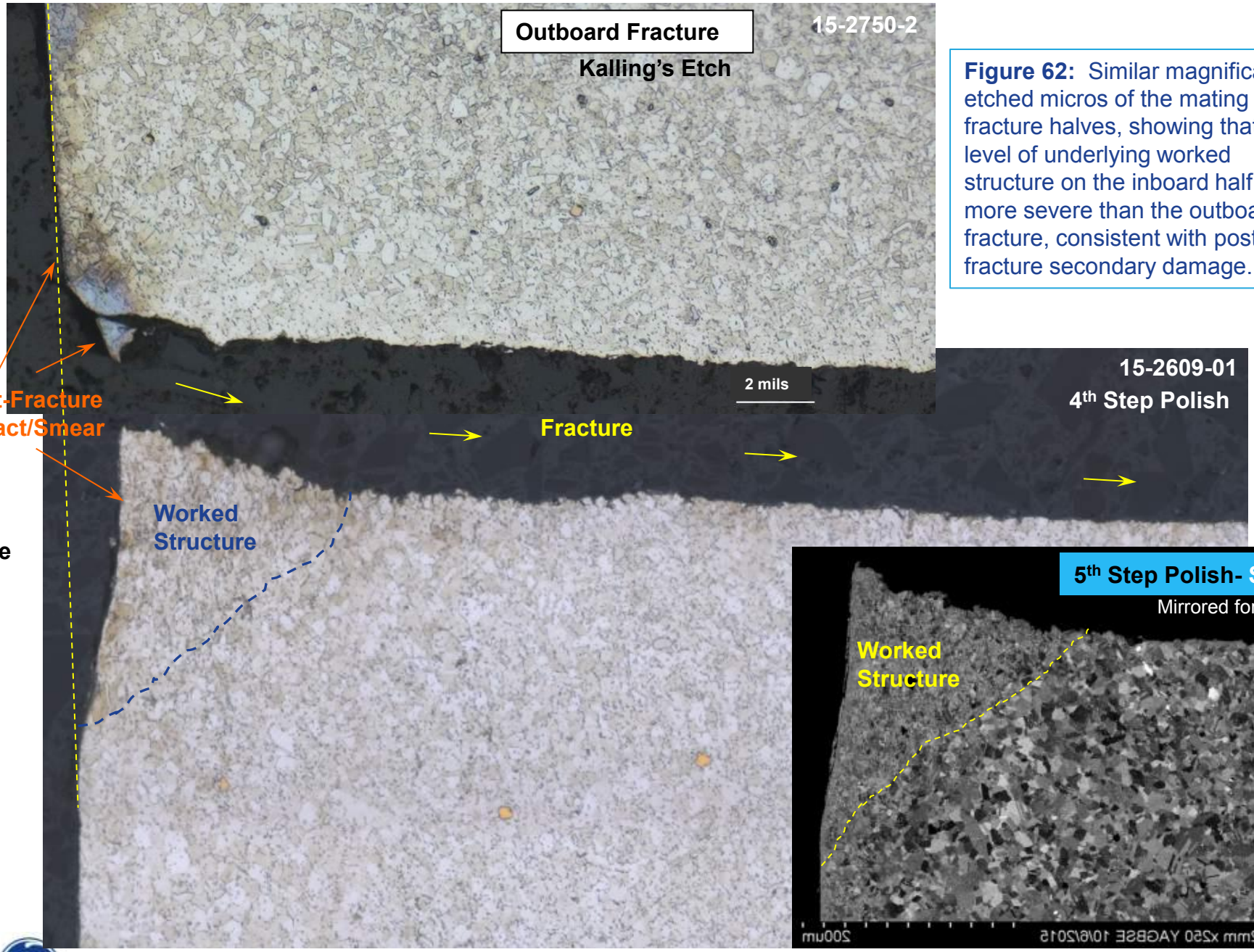

Figure 62: Similar magnification etched micros of the mating fracture halves, showing that the level of underlying worked structure on the inboard half was more severe than the outboard fracture, consistent with post-fracture secondary damage.

Mount on Diametrically Opposite Side of Disk

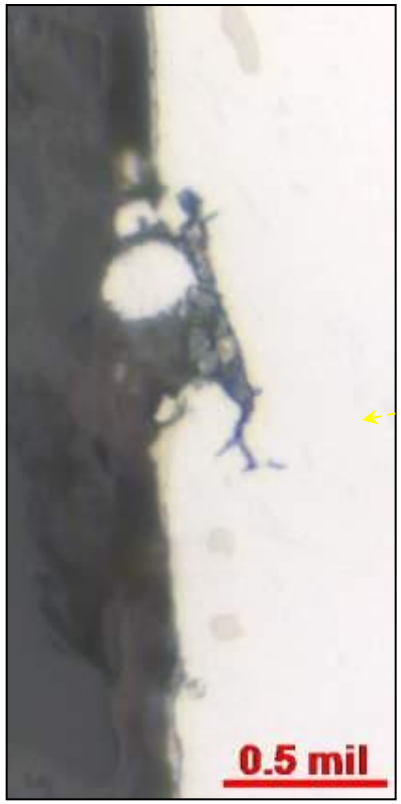

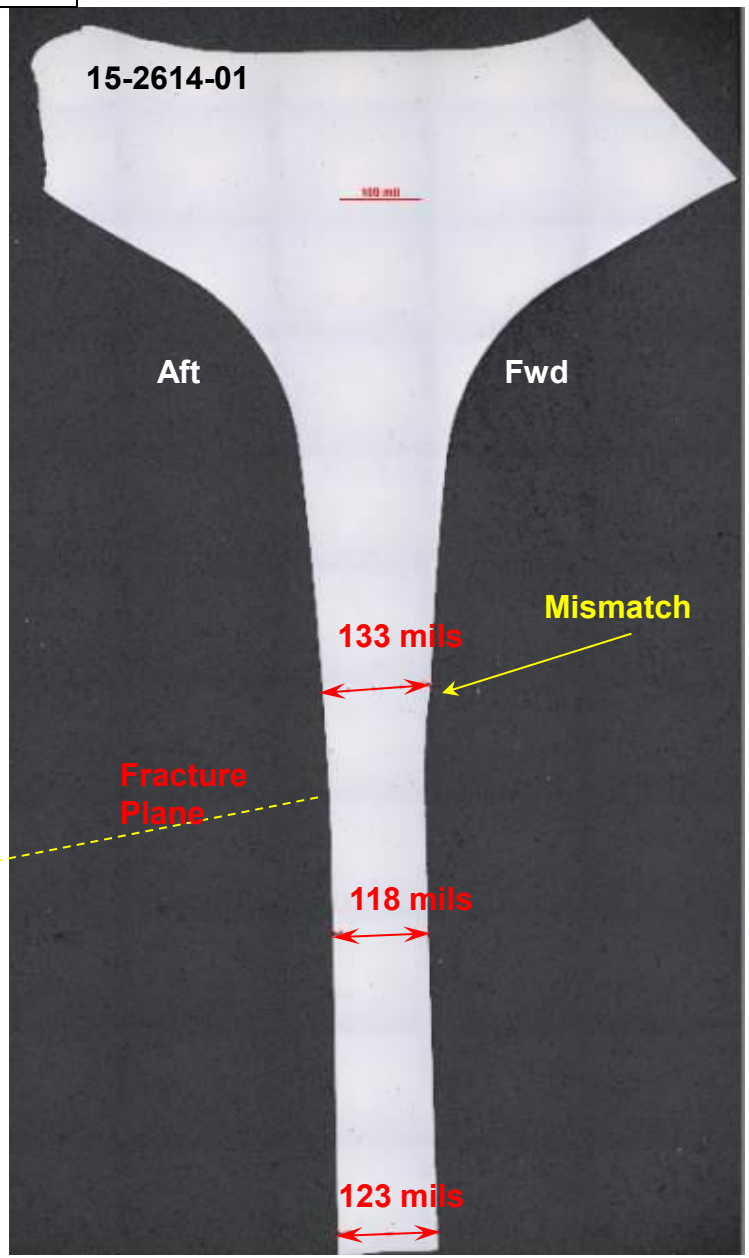

Figure 63: A mount made on the diametrically opposed side of the disk showed that the fracture was at the web to rim transition area where the wall thickness was approximately 0.118 inch (thinnest region of web). On the forward side an allowable mismatch was observed further outboard.

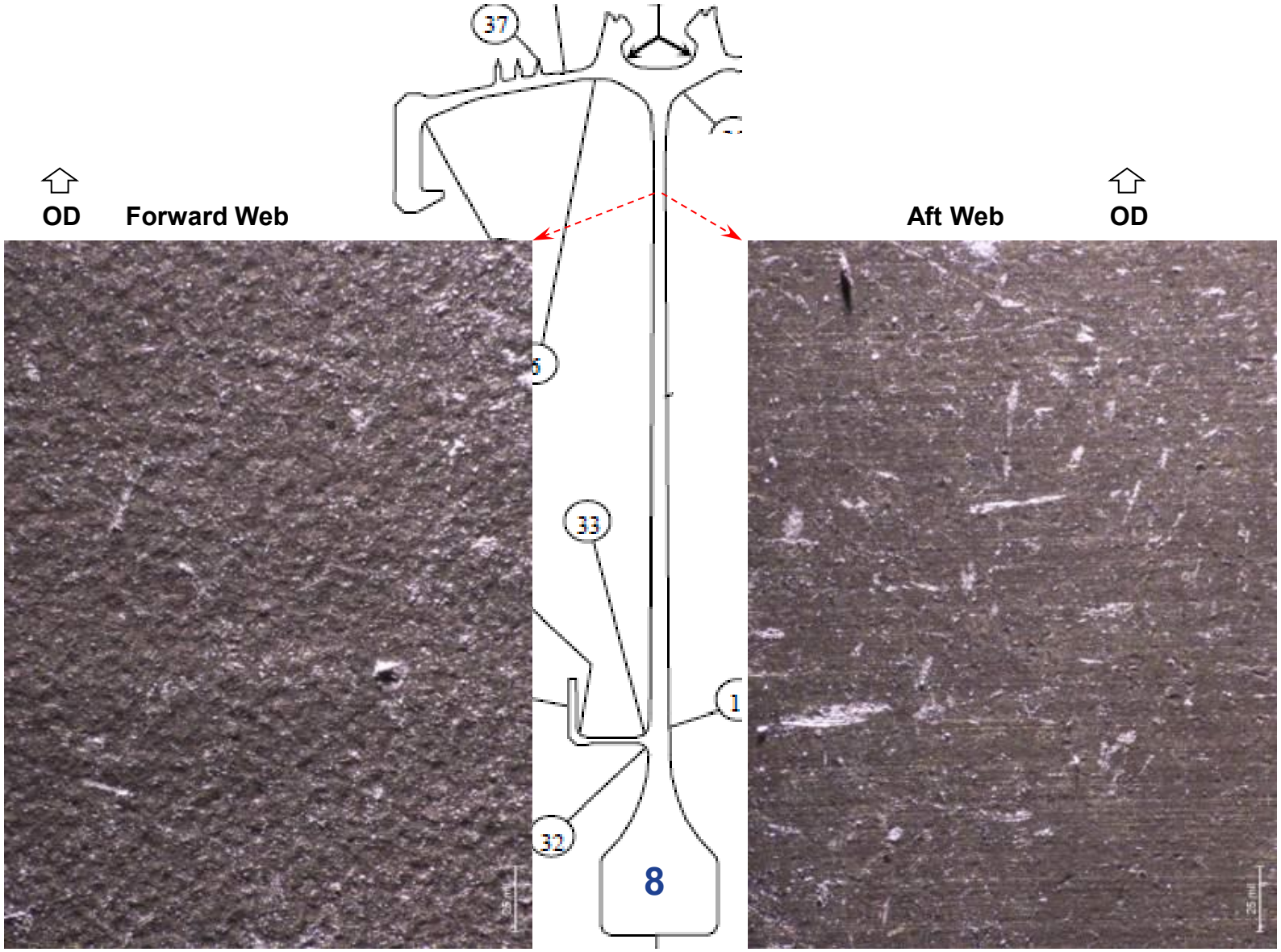

Figure 64: Optical views at similar magnifications of the forward and aft web surfaces in a similar radial plane as the fracture. The images showed that the peening on the forward side was more pronounced than the aft side.

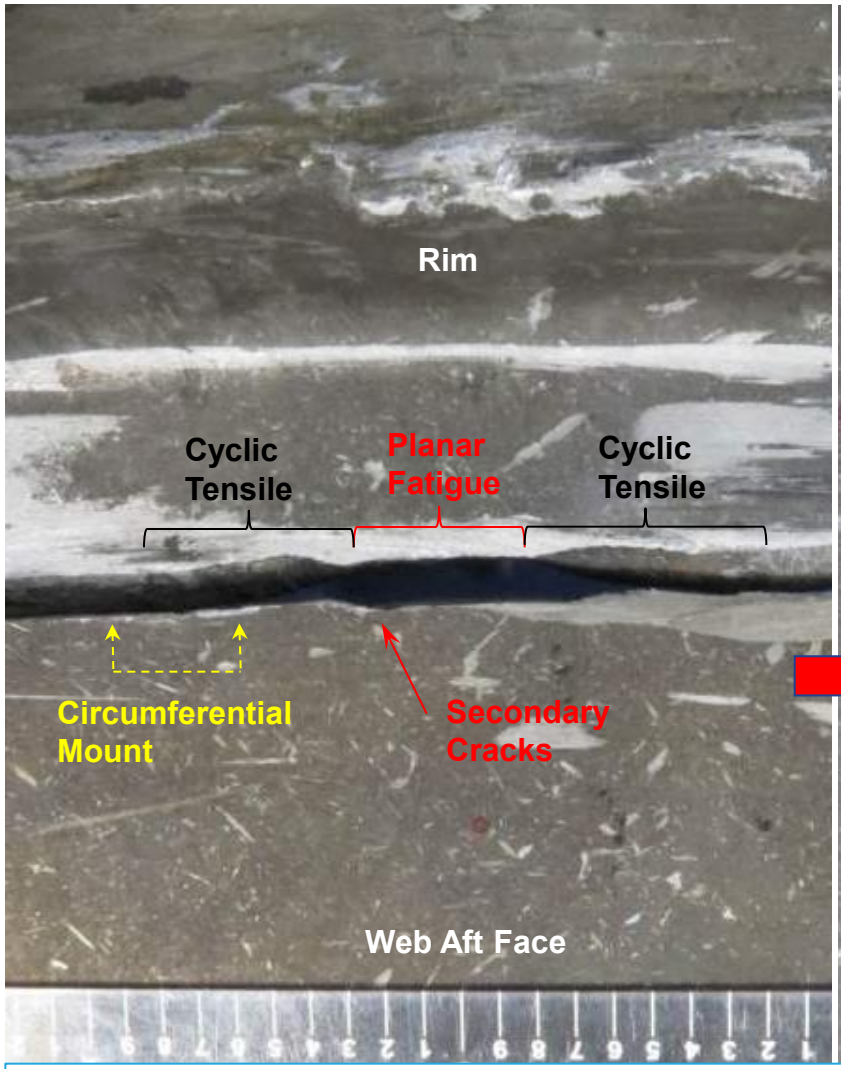

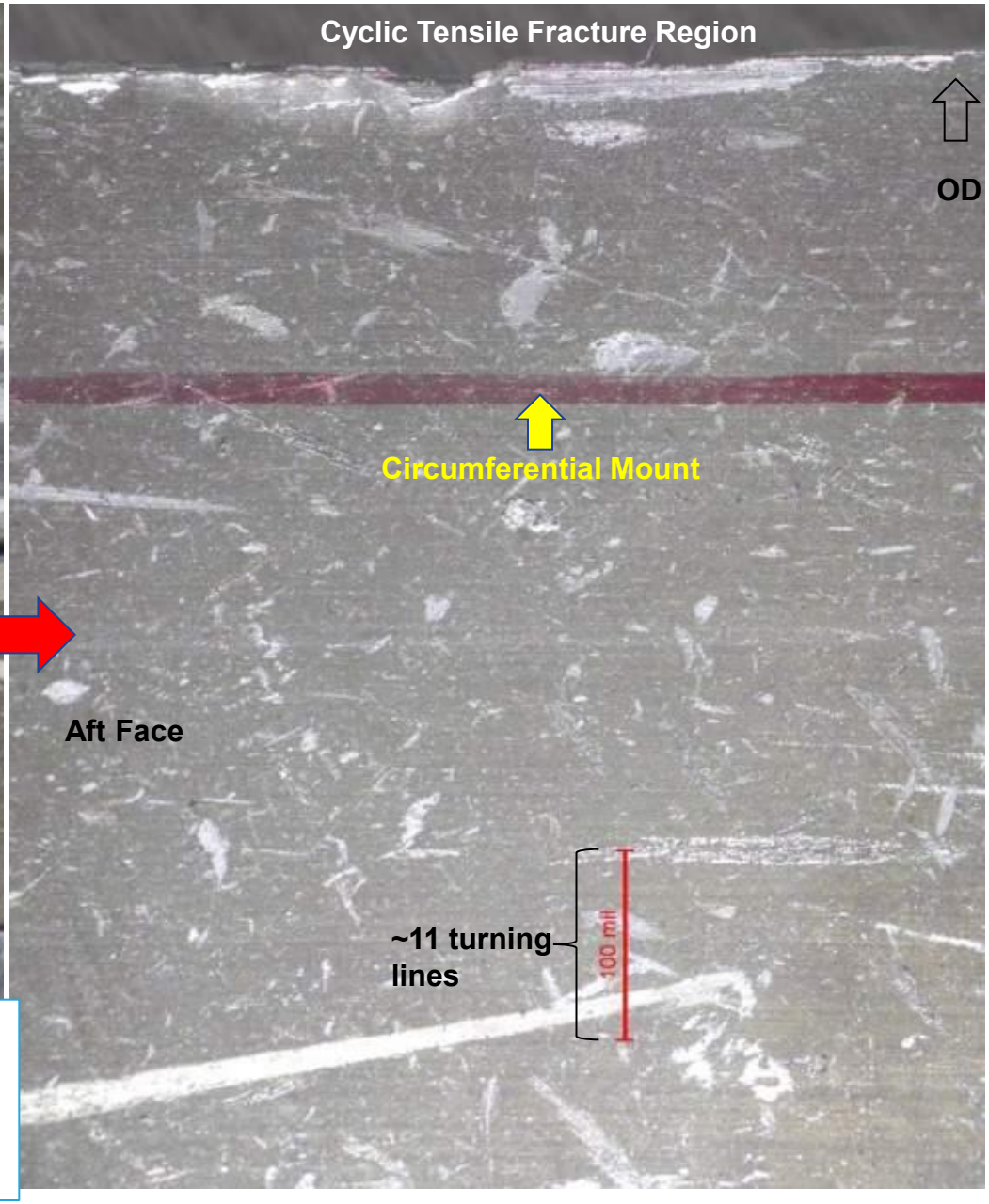

Figure 65: Optical views of the aft face of the web showing where a circumferential mount was made to assess the machined surfaces. The right image shows that approximately 11 turning lines were observed within 0.1 inch.

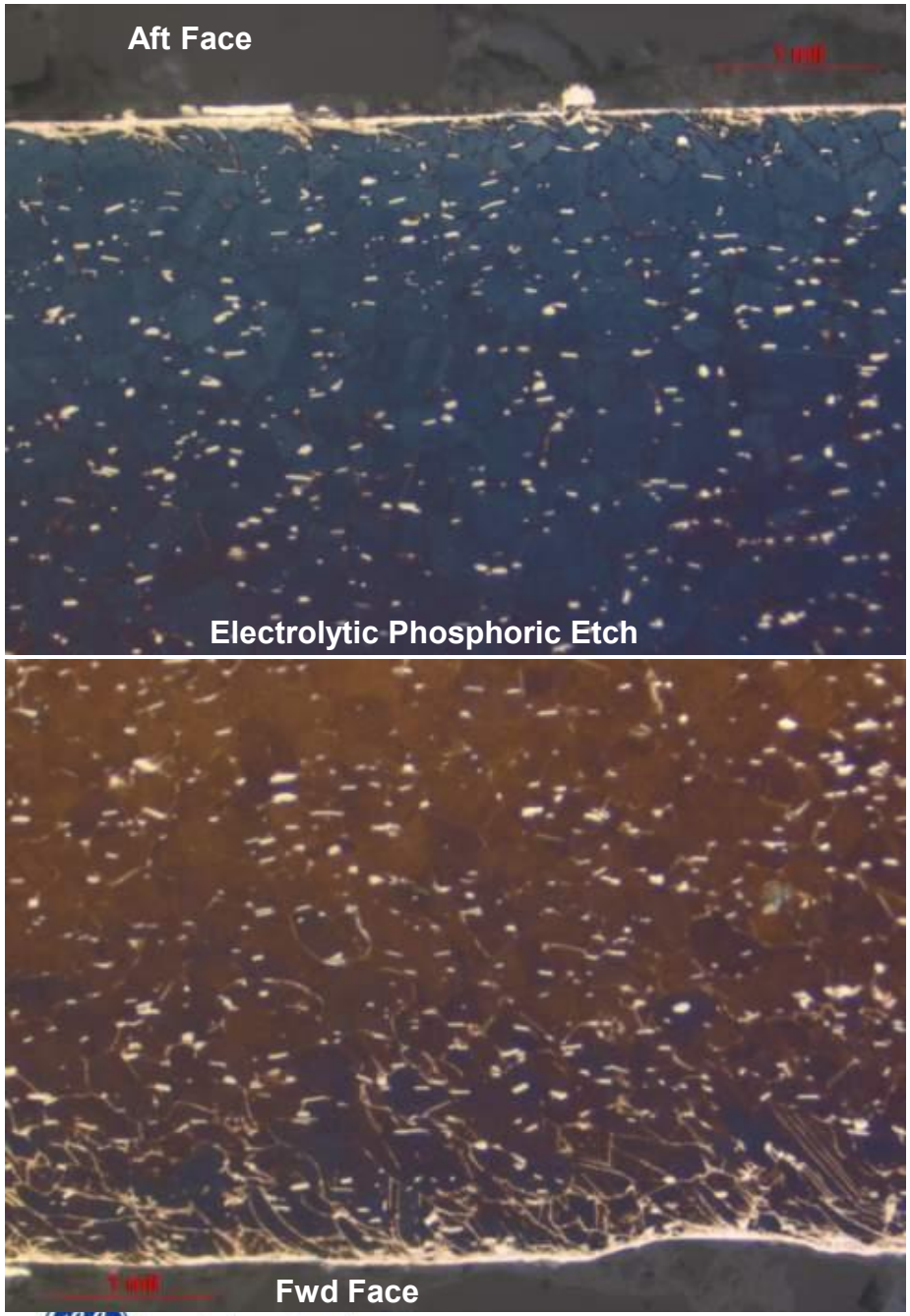

Figure 66: A circumferential mount made in the vicinity of the fatigue region showed that on the aft side distorted grains from turning were visible to a depth of approximately 0.2 mil, compared to approximately 0.5 mil on the forward face (the worked structure was shown to be deeper by EBSD- see Appendix E).

Further Examination of Inboard Fracture Intergranular Region

Microprobe- GE Aviation
High Res SEM/EDS, Auger, & TEM – GE GRC

Microprobe

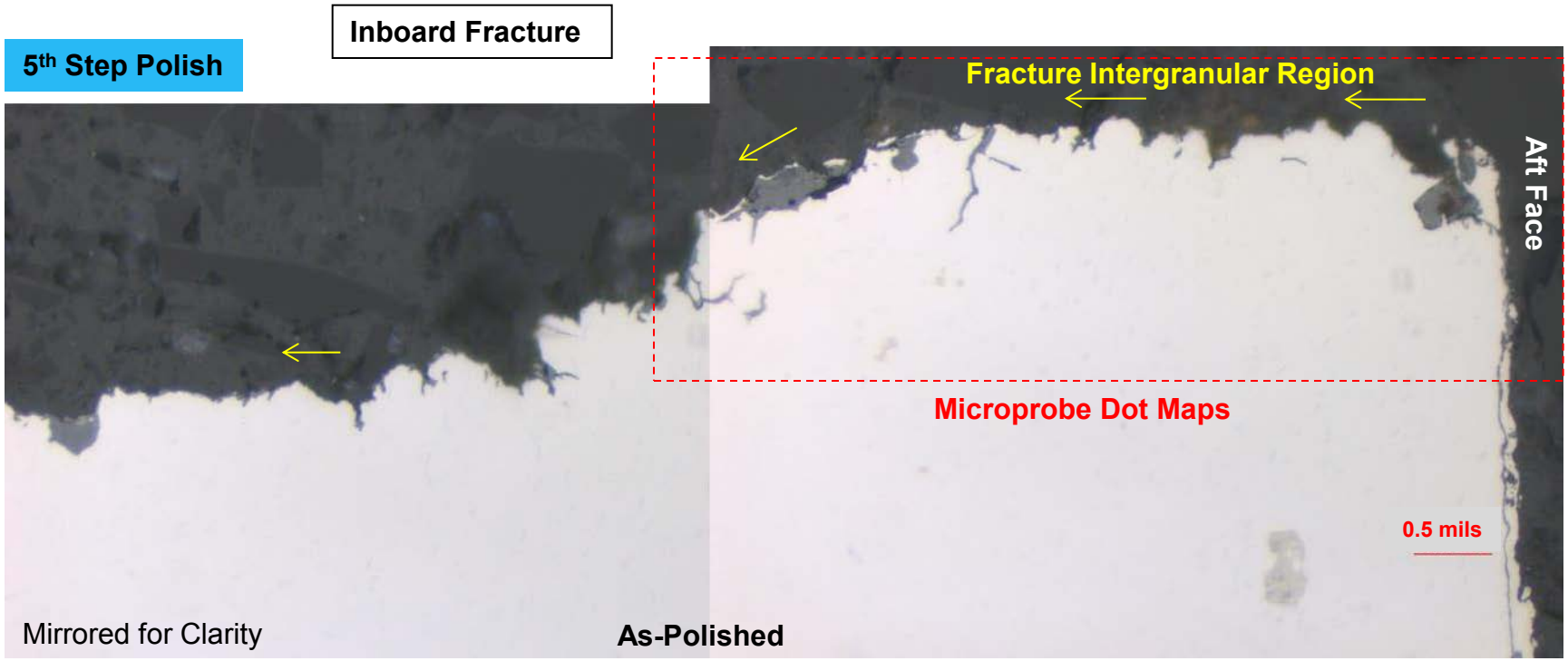

Figure 67: Two dot maps regions were generated with by microprobe analysis. The first one was a higher resolution scan of the origin area near the aft face (area shown above) and a second was a slightly larger area of the fracture (see Figure 70).

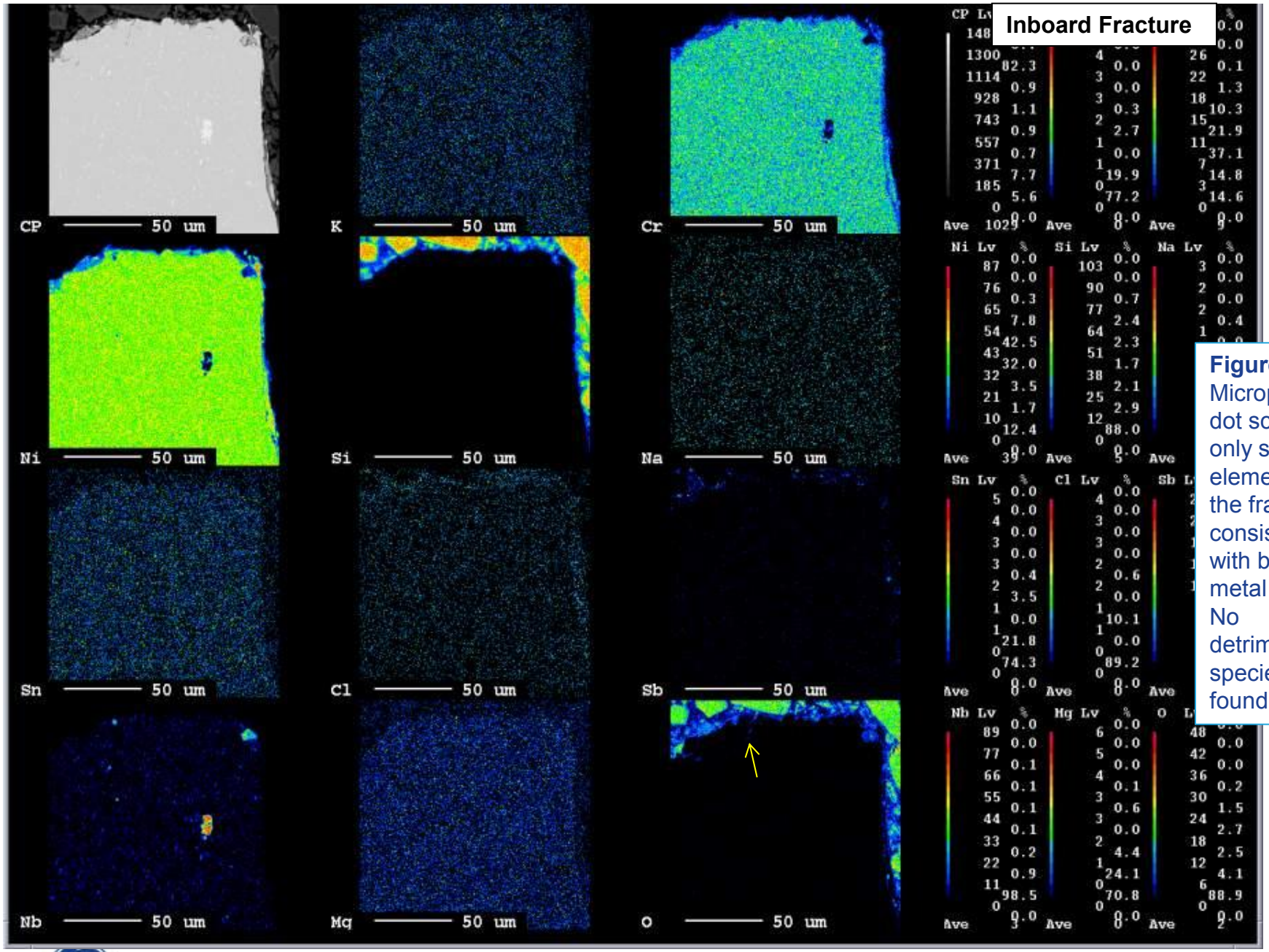

Figure 68: Microprobe dot scans only showed elements on the fracture consistent with base metal oxides. No detrimental species were found.

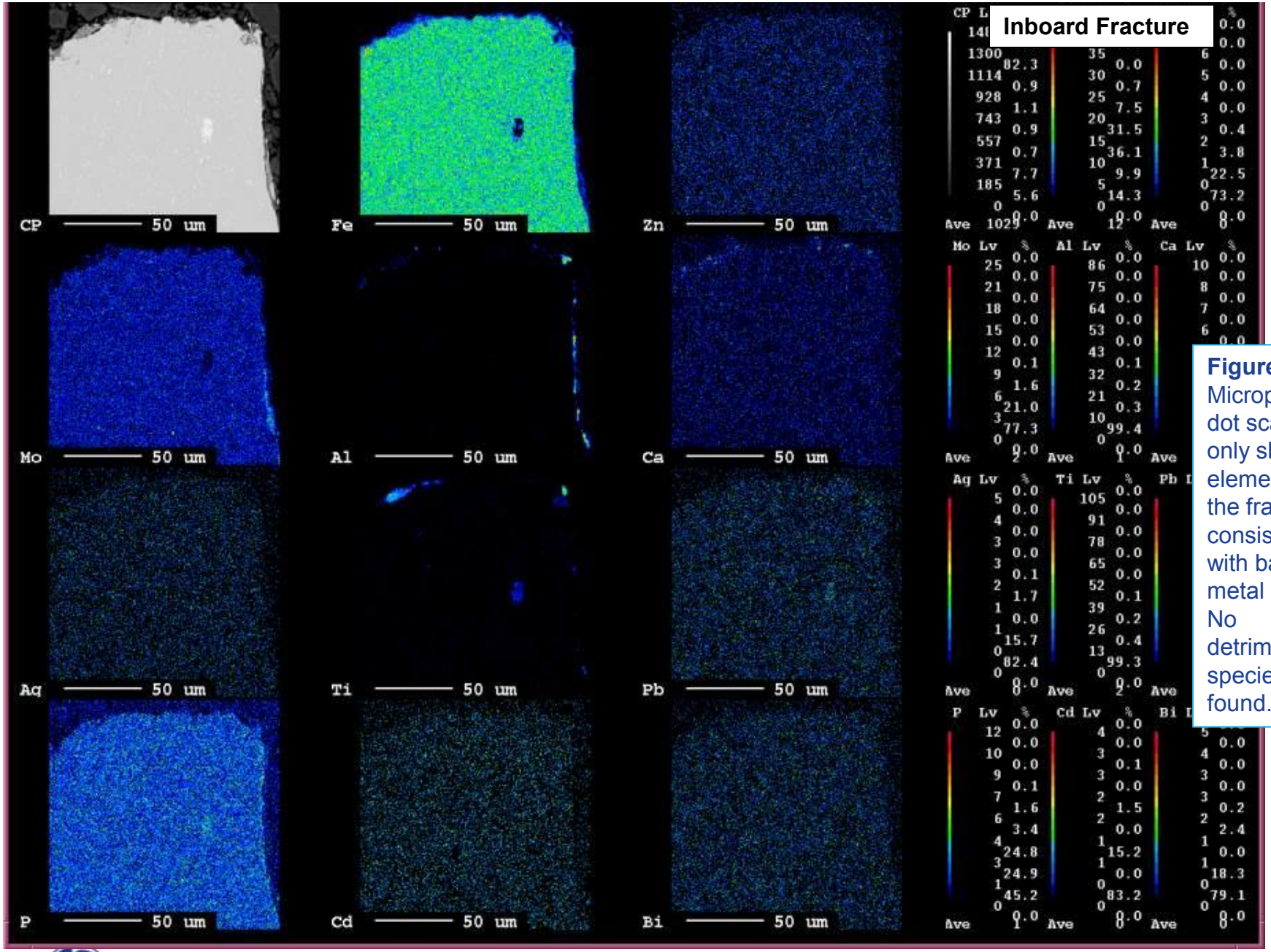

Figure 69: Microprobe dot scans only showed elements on the fracture consistent with base metal oxides. No detrimental species were found.

Inboard Fracture

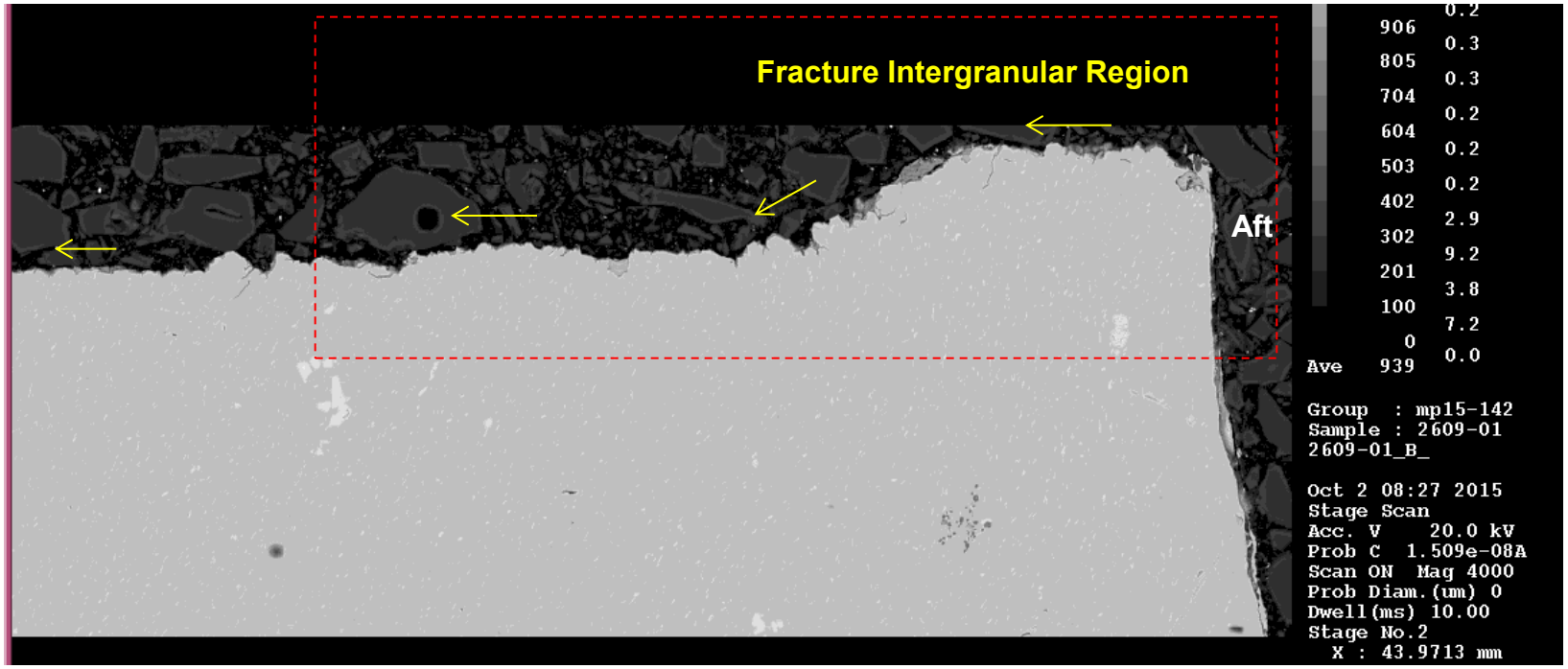

Figure 70: SEM image showing the location of the second microprobe dot map, which included a slightly larger area of the intergranular portion of the fracture.

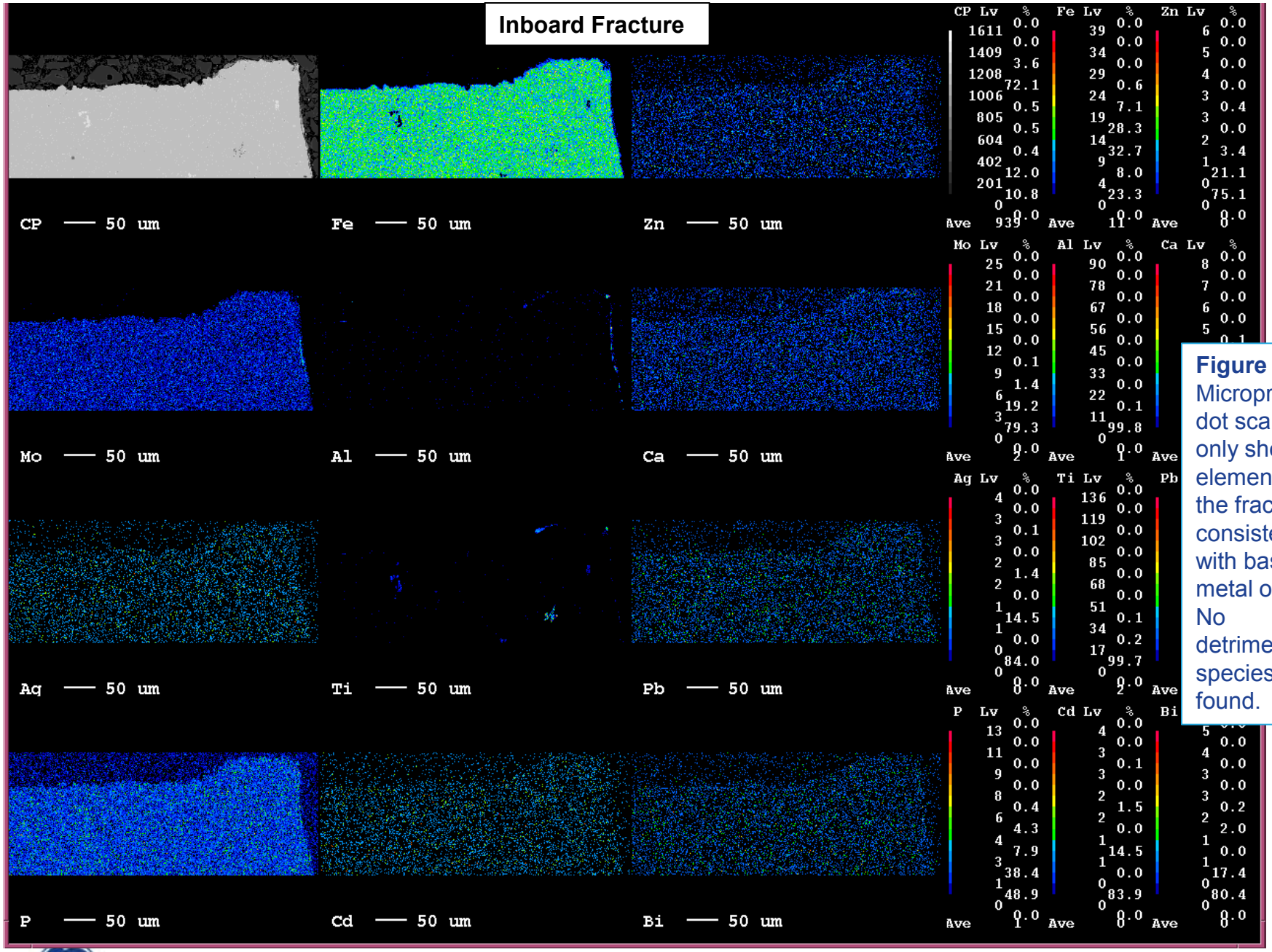

Figure 71: Microprobe dot scans only showed elements on the fracture consistent with base metal oxides. No detrimental species were found.

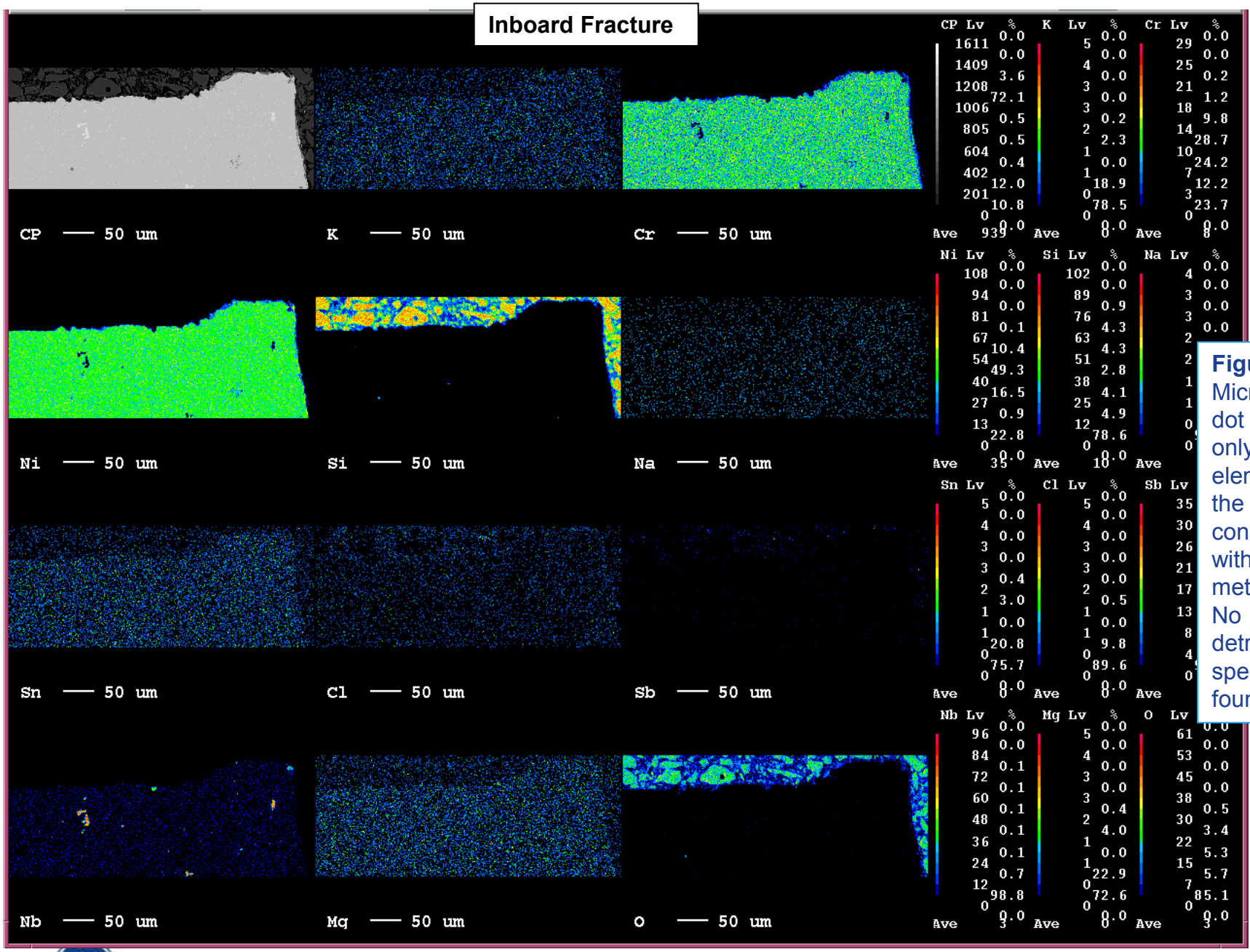

Figure 72: Microprobe dot scans only showed elements on the fracture consistent with base metal oxides. No detrimental species were found.

Inboard Fracture

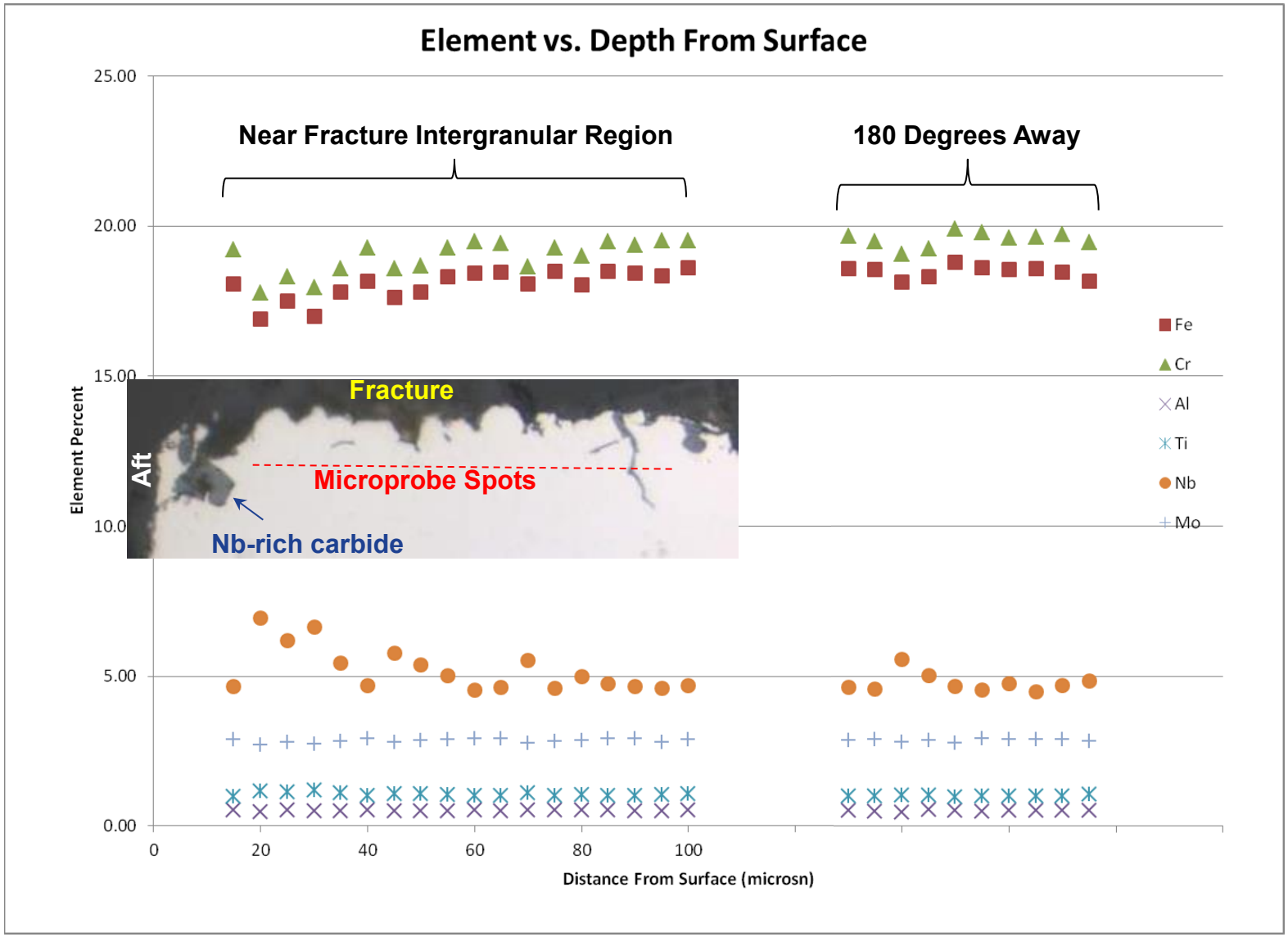

Figure 73: Microprobe compositional readings were taken across the base material near the fracture showed slightly elevated Nb (near a carbide) compared to the baseline deeper into the part and on the opposite side of the disk. No Nb-lean areas were found and the readings were within the expected range for the alloy.

Auger

GE GRC

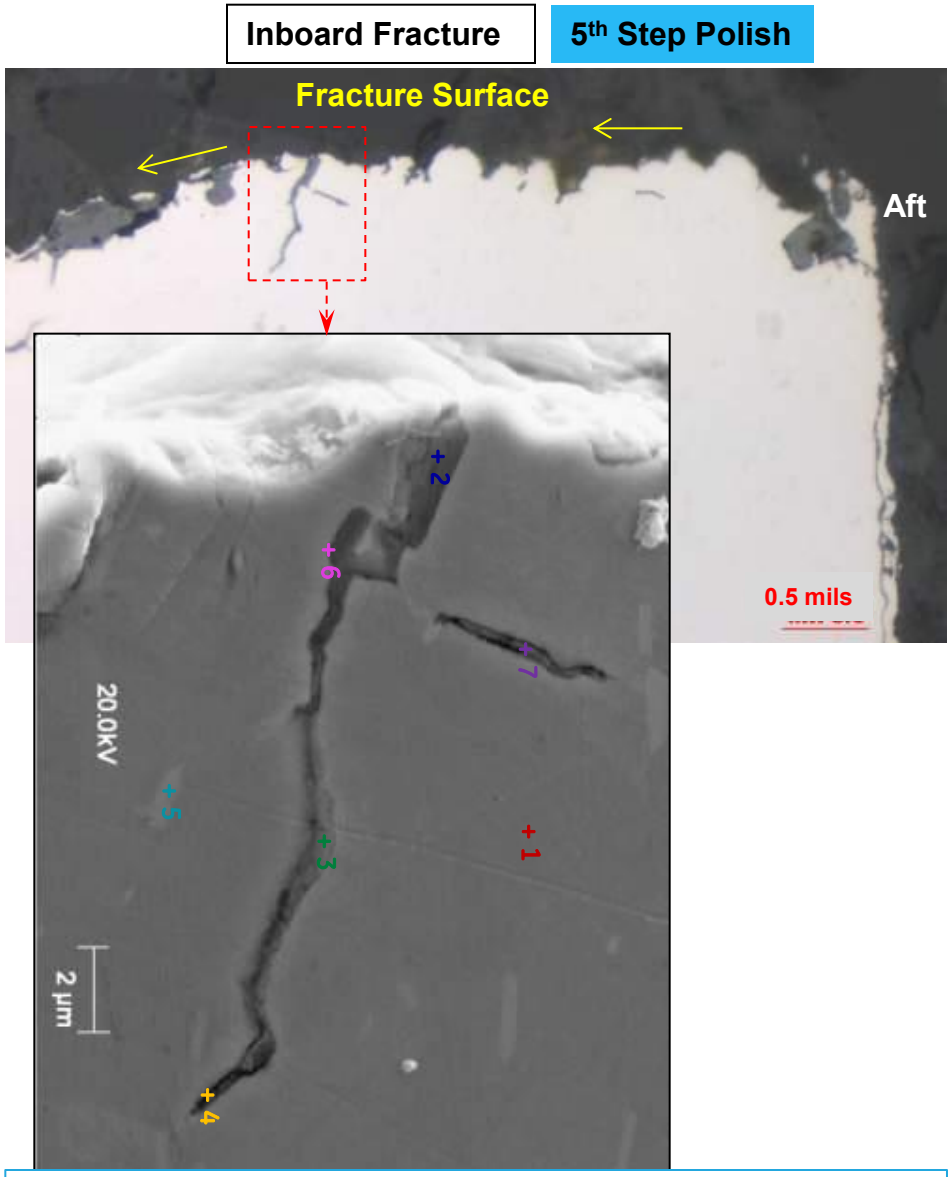

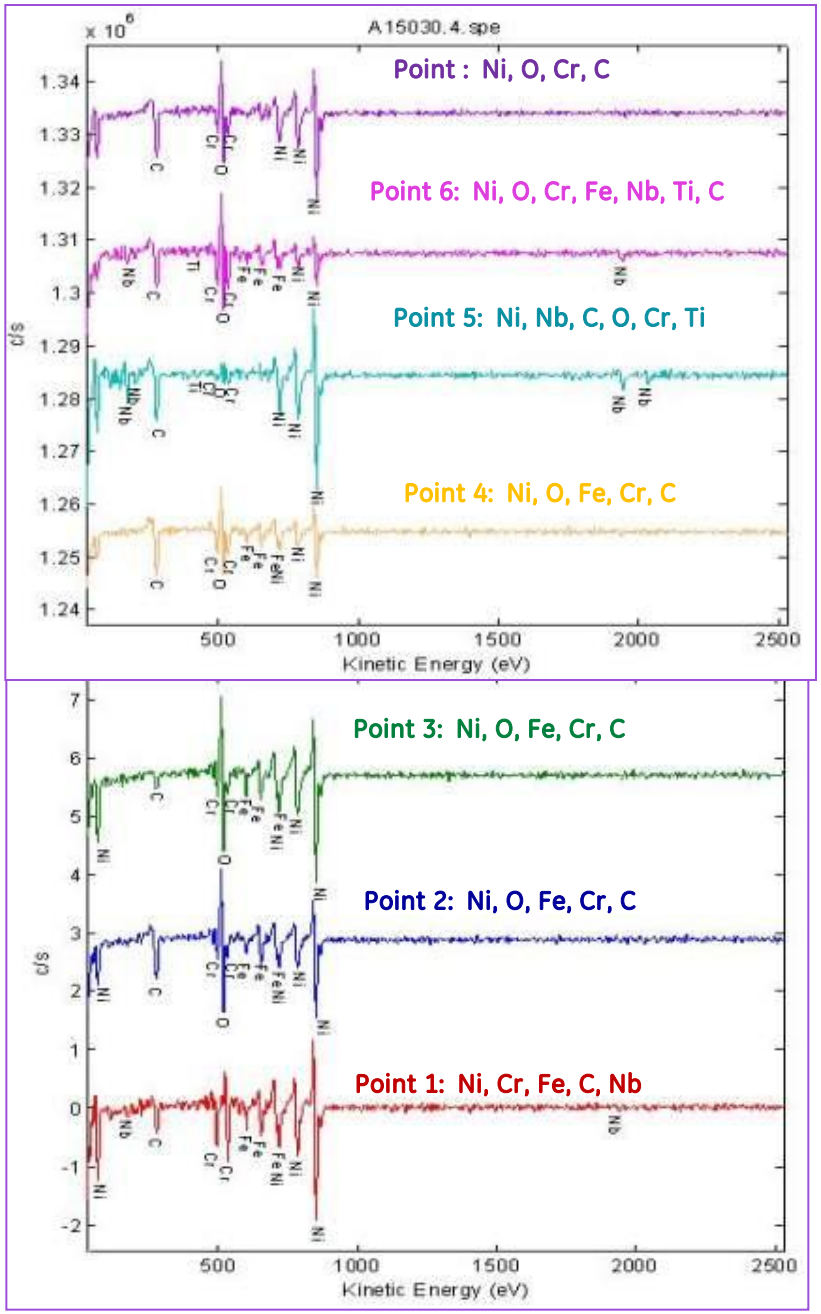

Figure 74: Seven areas of the fracture surface intergranular branch spike were analyzed by Auger and only base metal oxides were found with no detrimental species.

Inboard Fracture | **5th Step Polish**

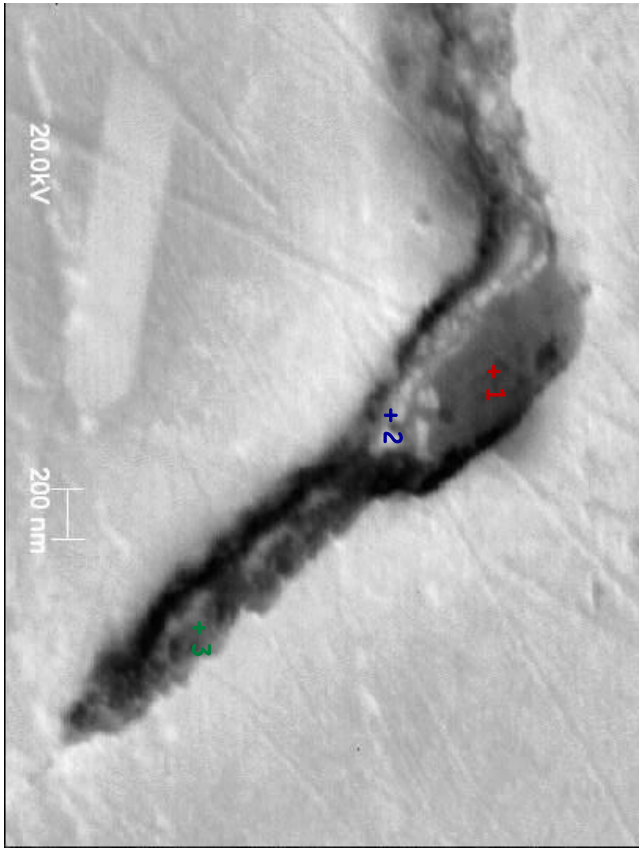

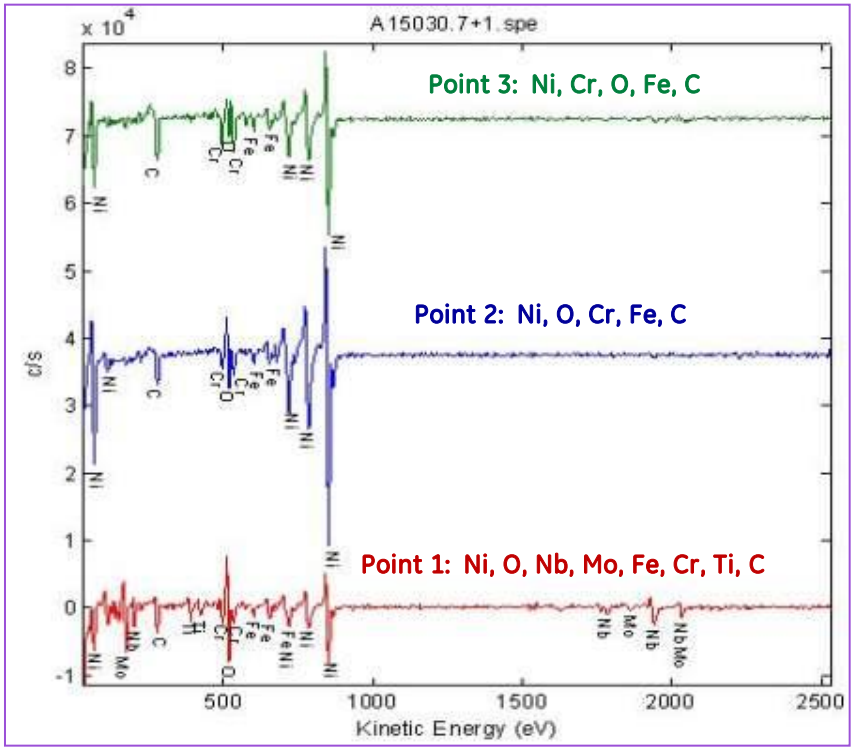

Figure 75: Additional examination of the branched crack only showed base metal oxides with no detrimental species.

Inboard Fracture **5th Step Polish**

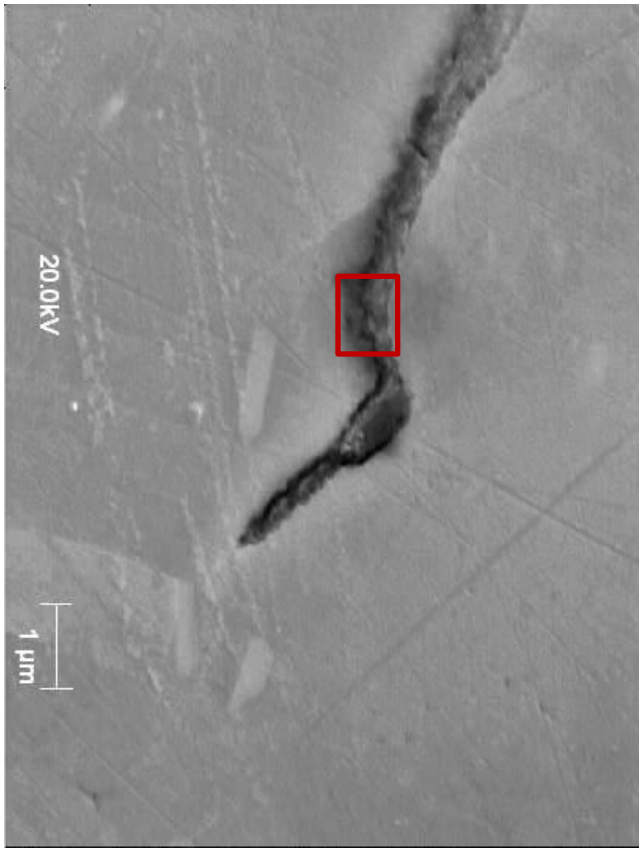

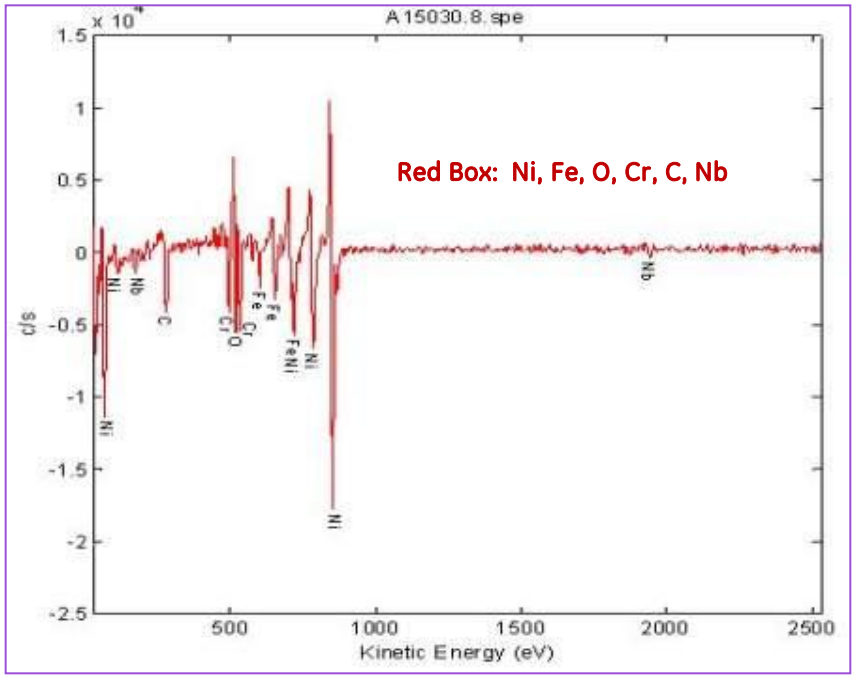

Figure 76: Additional examination of the branched crack only showed base metal oxides with no detrimental species.

Inboard Fracture **5th Step Polish**

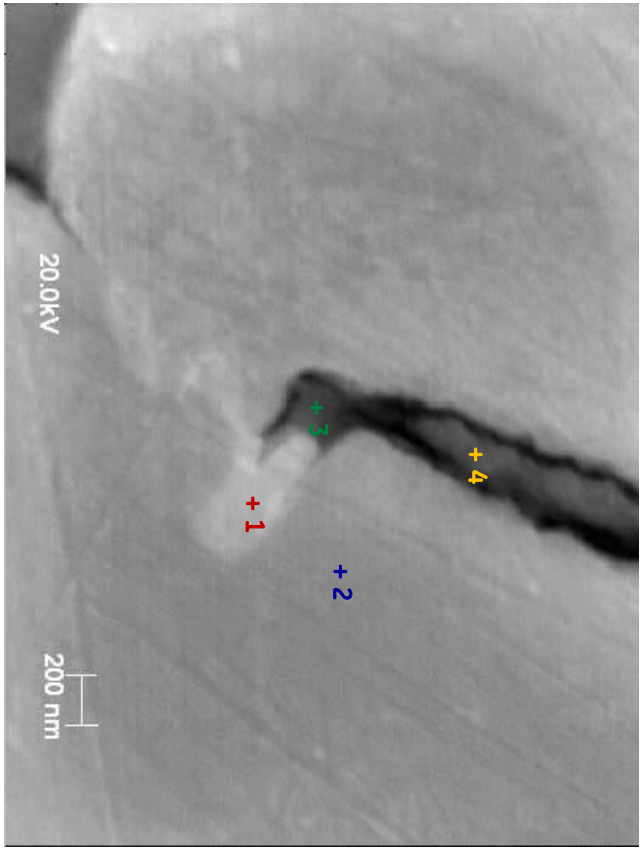

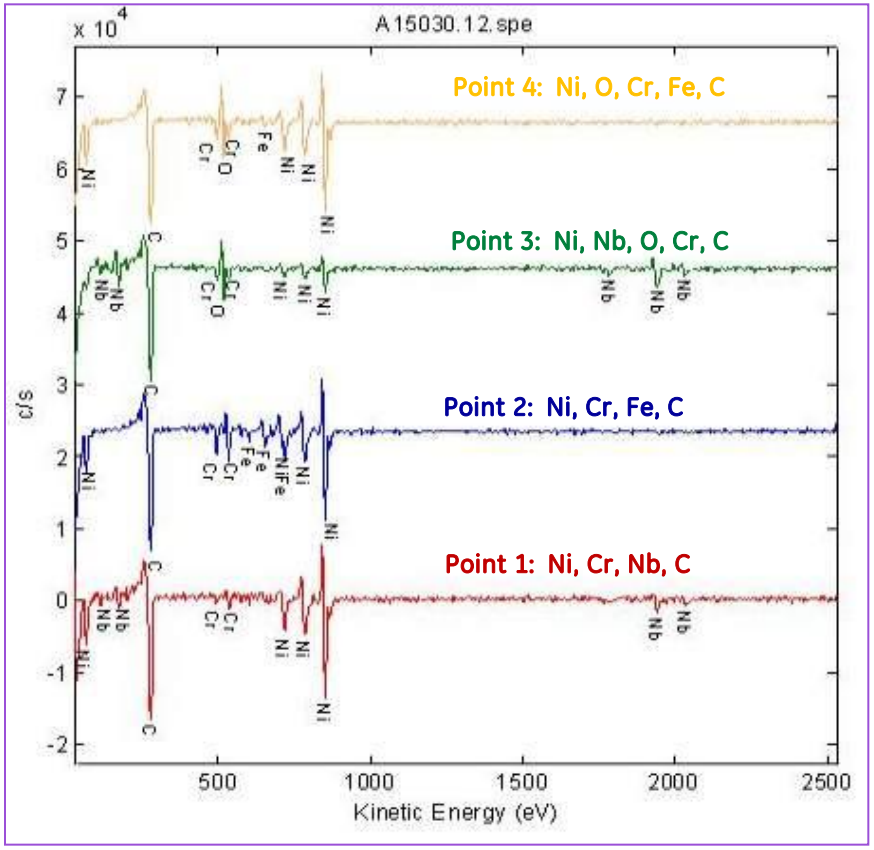

Figure 77: Additional examination of the branched crack only showed base metal oxides with no detrimental species.

High Res SEM Work

GE GRC

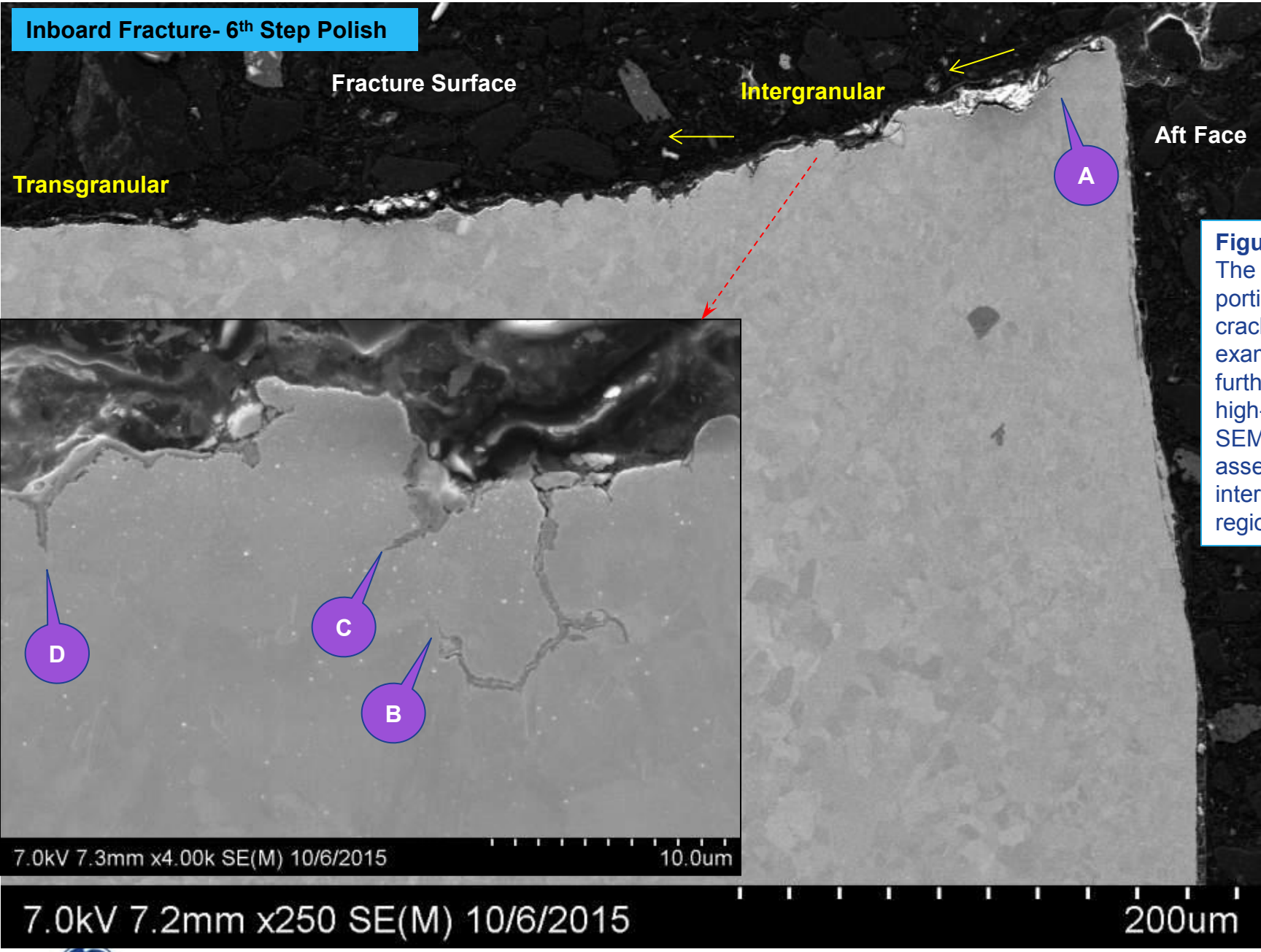

Figure 78: The initial portion of the crack was examined further with high-resolution SEM to further assess the intergranular region.

AREA A- ~1 mil from Surface

Inboard Fracture

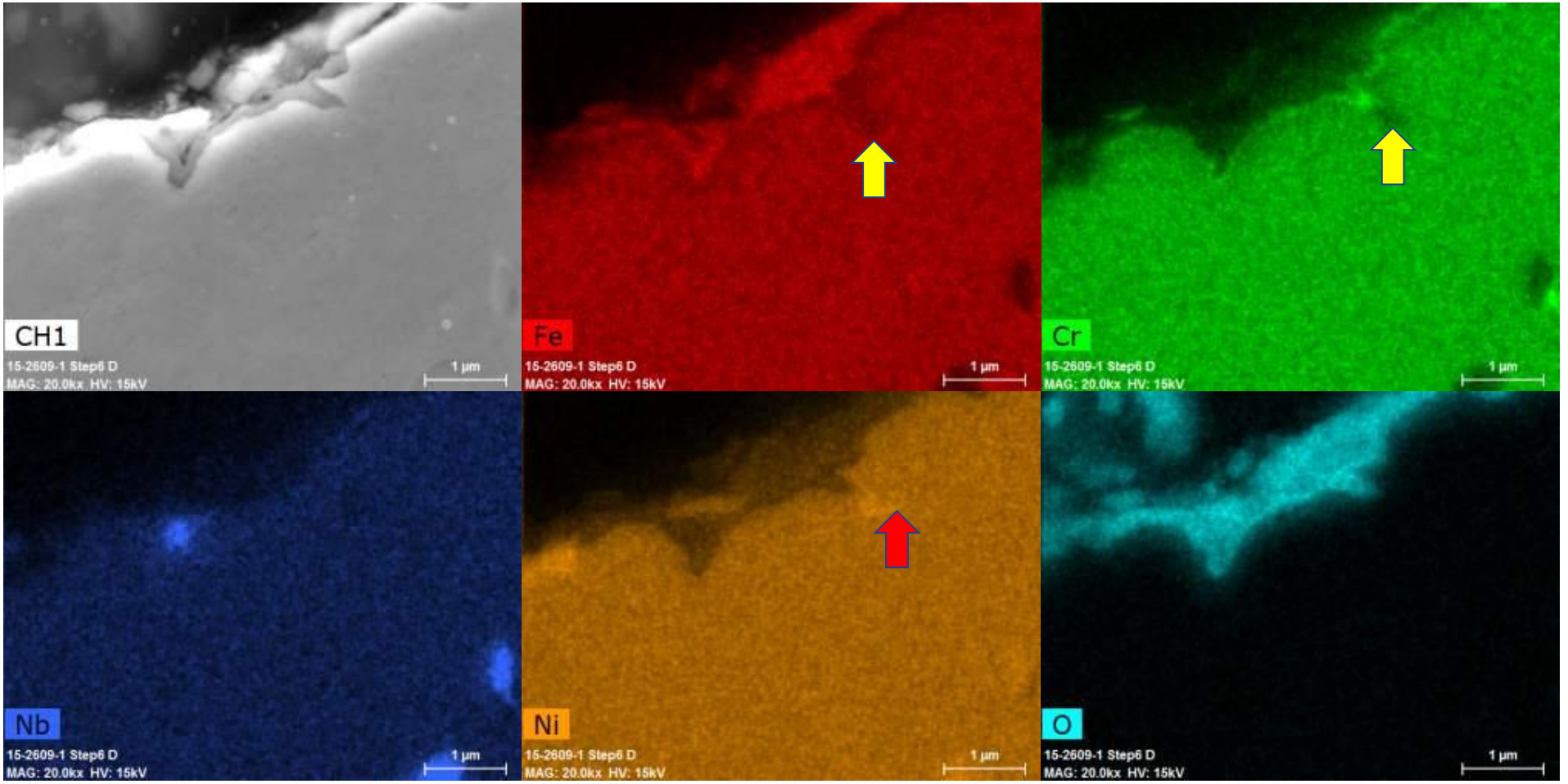

Figure 79: The compositional dot-maps showed that at the fracture branched crack approximately 1 mil from the aft surface was depleted in Fe and Cr ahead of the crack front (yellow arrows) and therefore, richer in Ni (red arrow). The crack itself only contained base metal oxides and no detrimental species were found.

AREA A- ~1 mil from Surface

Inboard Fracture

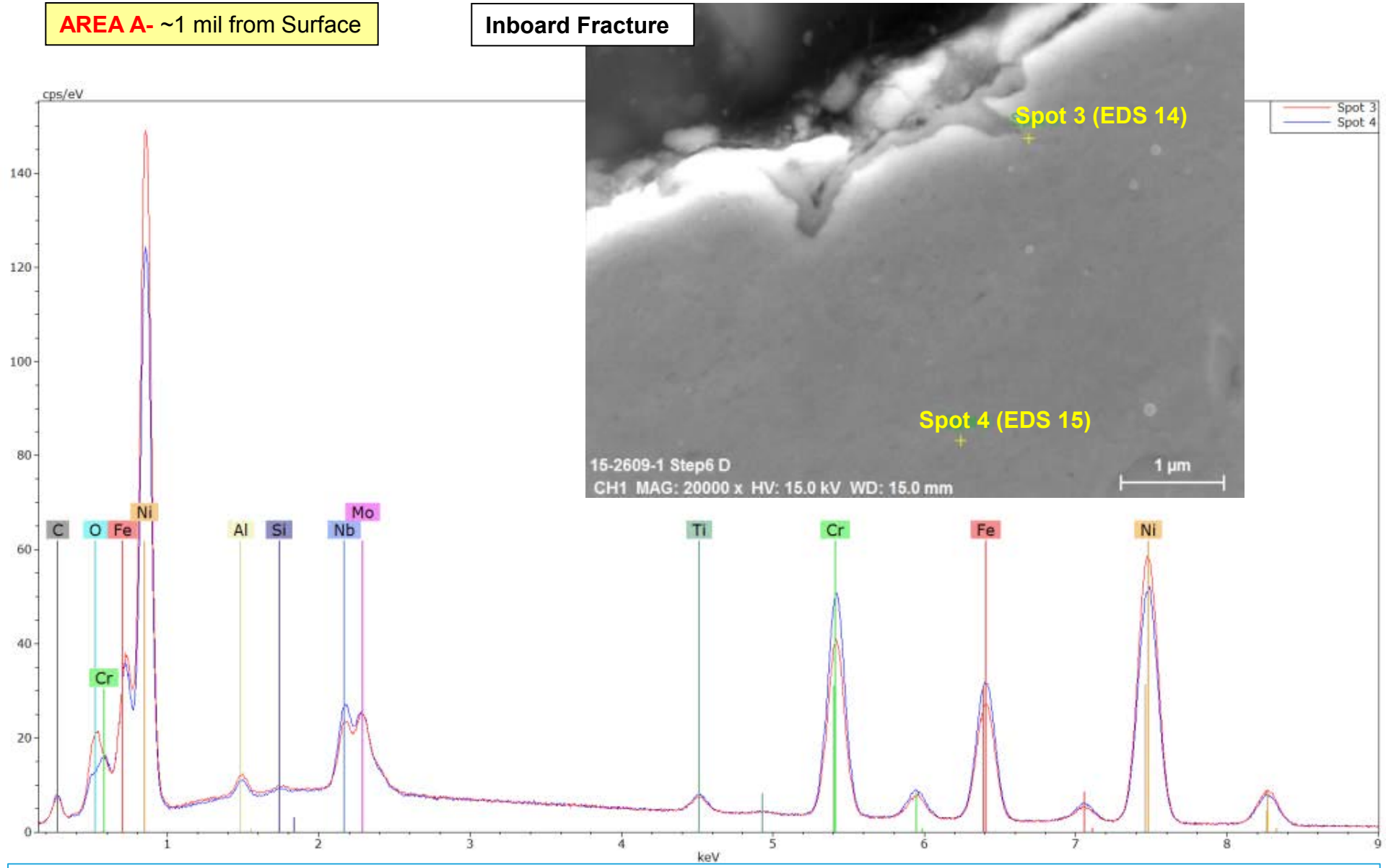

Figure 80: Superimposed EDS spectra of the baseline (spot 4- EDS 15) and region ahead of the crack-tip (spot 3- EDS 14), showed that the latter was depleted in Fe and Cr, and richer in Ni.

Inboard Fracture

AREA B- ~4 mils from Surface

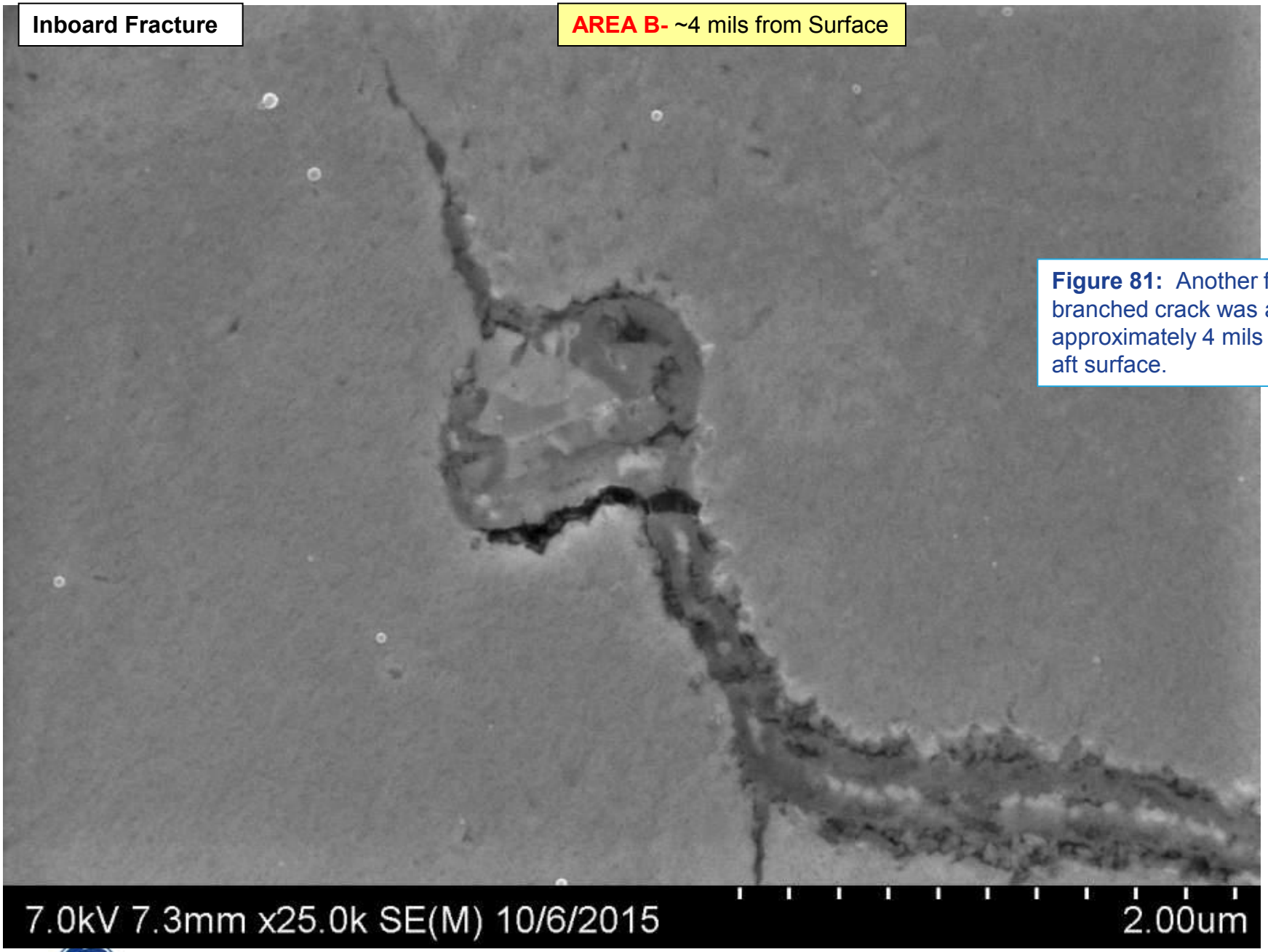

Figure 81: Another fracture branched crack was analyzed approximately 4 mils from the aft surface.

AREA B- ~4 mils from Surface

Inboard Fracture

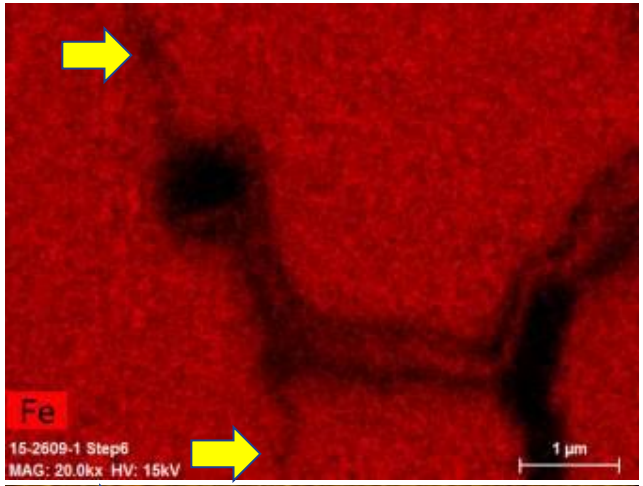

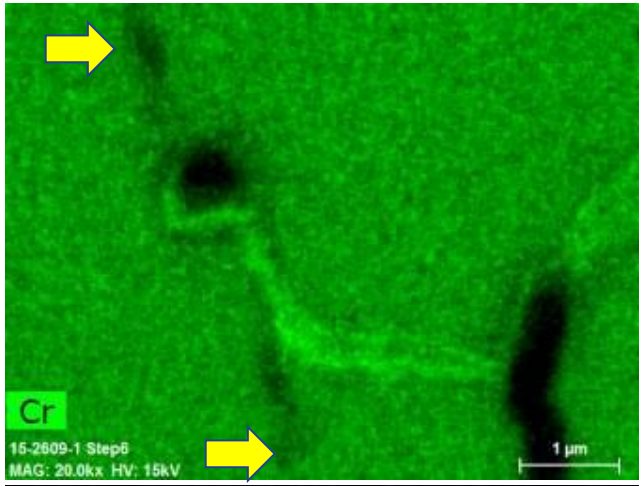

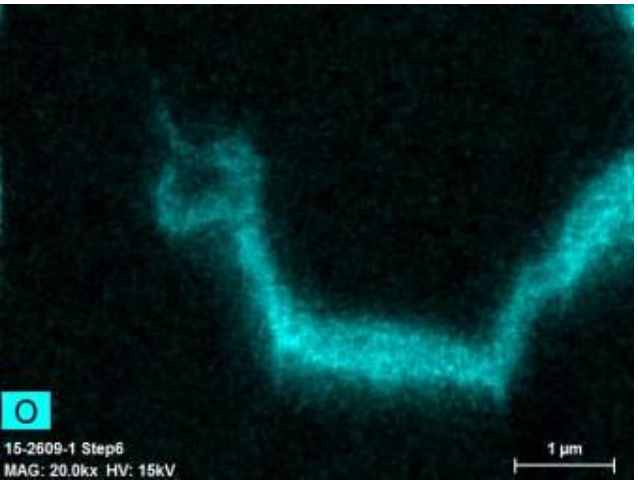

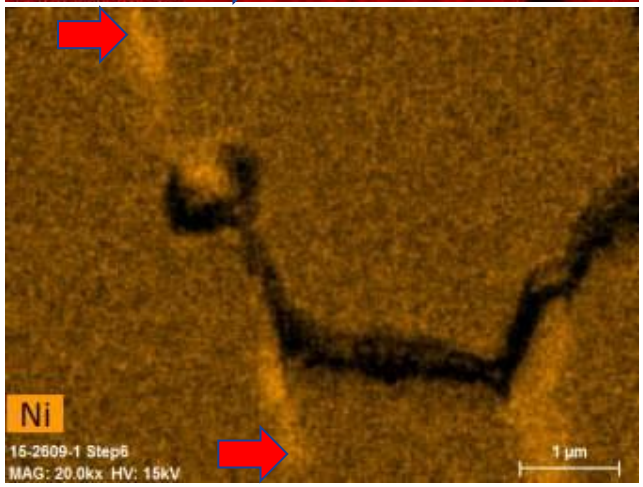

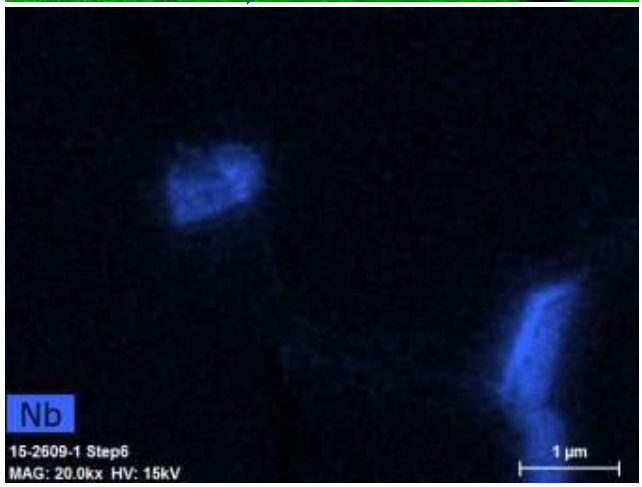

Figure 82: The compositional dot-maps showed that at the fracture branched crack approximately 4 mils from the aft surface was depleted in Fe and Cr ahead of the crack front (yellow arrows) and therefore, richer in Ni (red arrow). The crack itself only contained base metal oxides and no detrimental species were found.

AREA B- ~4 mils from Surface

Inboard Fracture

Spot 1	1.34	Al 0.42	Si 0.08	Ti 0.81	Cr 15.36	Fe 15.29	Ni 61.55	Nb 3.52	Mo 2.97
Spot 2	1.30	Al 0.49	Si 0.10	Ti 1.05	Cr 19.16	Fe 18.69	Ni 53.31	Nb 4.34	Mo 2.87

Ahead of Crack Base

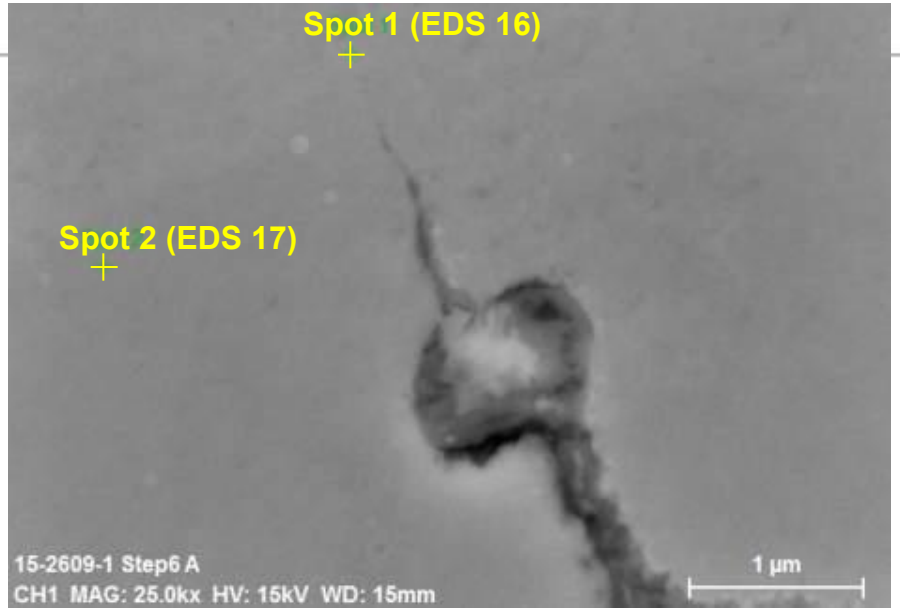

Figure 83: Superimposed EDS spectra of the baseline (spot 2- EDS 17) and region ahead of the crack-tip (spot 1- EDS 16), showed that the latter was depleted in Fe and Cr, and richer in Ni (also shown in table with semi-quantitative readings).

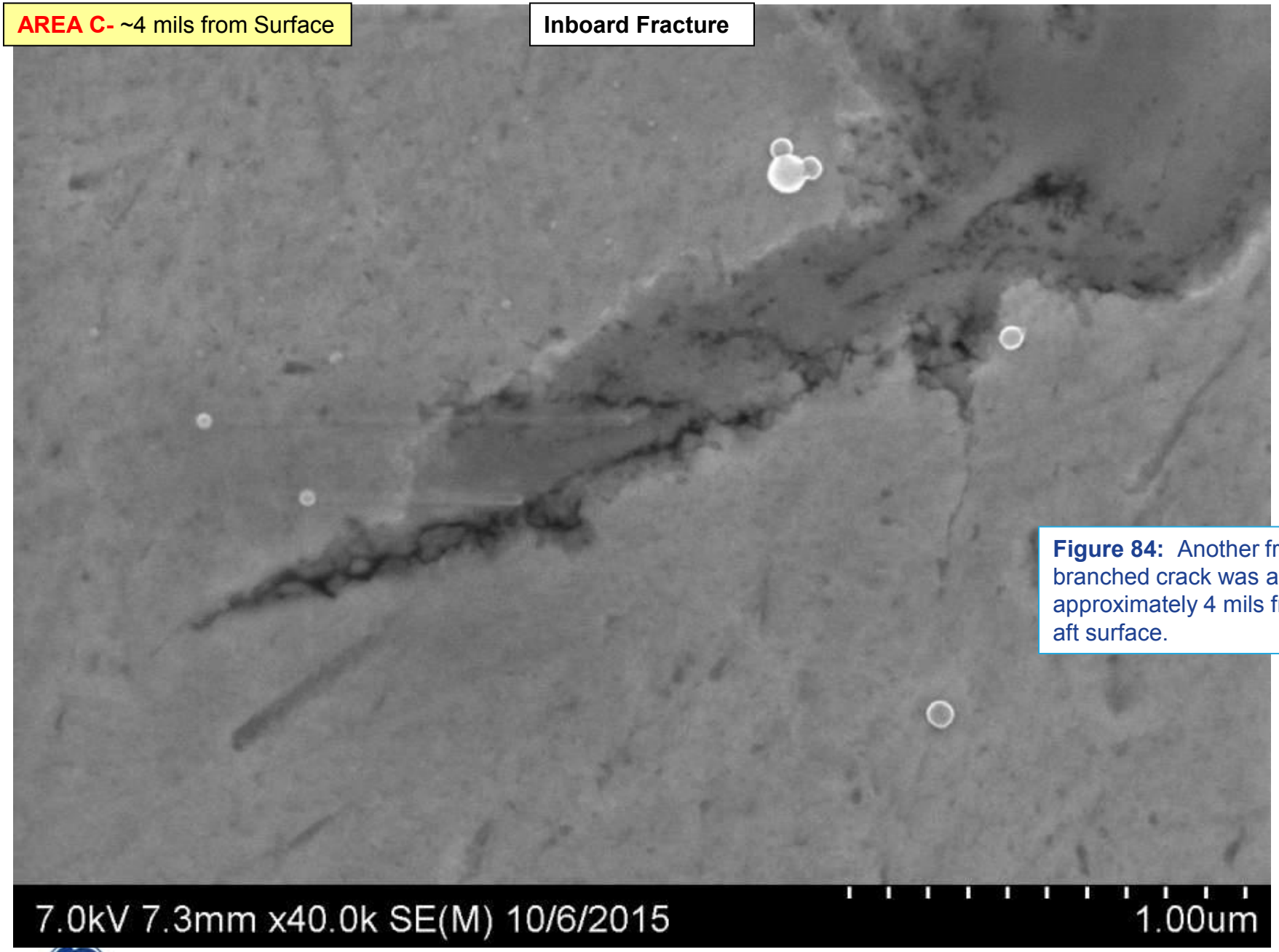

Figure 84: Another fracture branched crack was analyzed approximately 4 mils from the aft surface.

AREA C- ~4 mils from Surface

Inboard Fracture

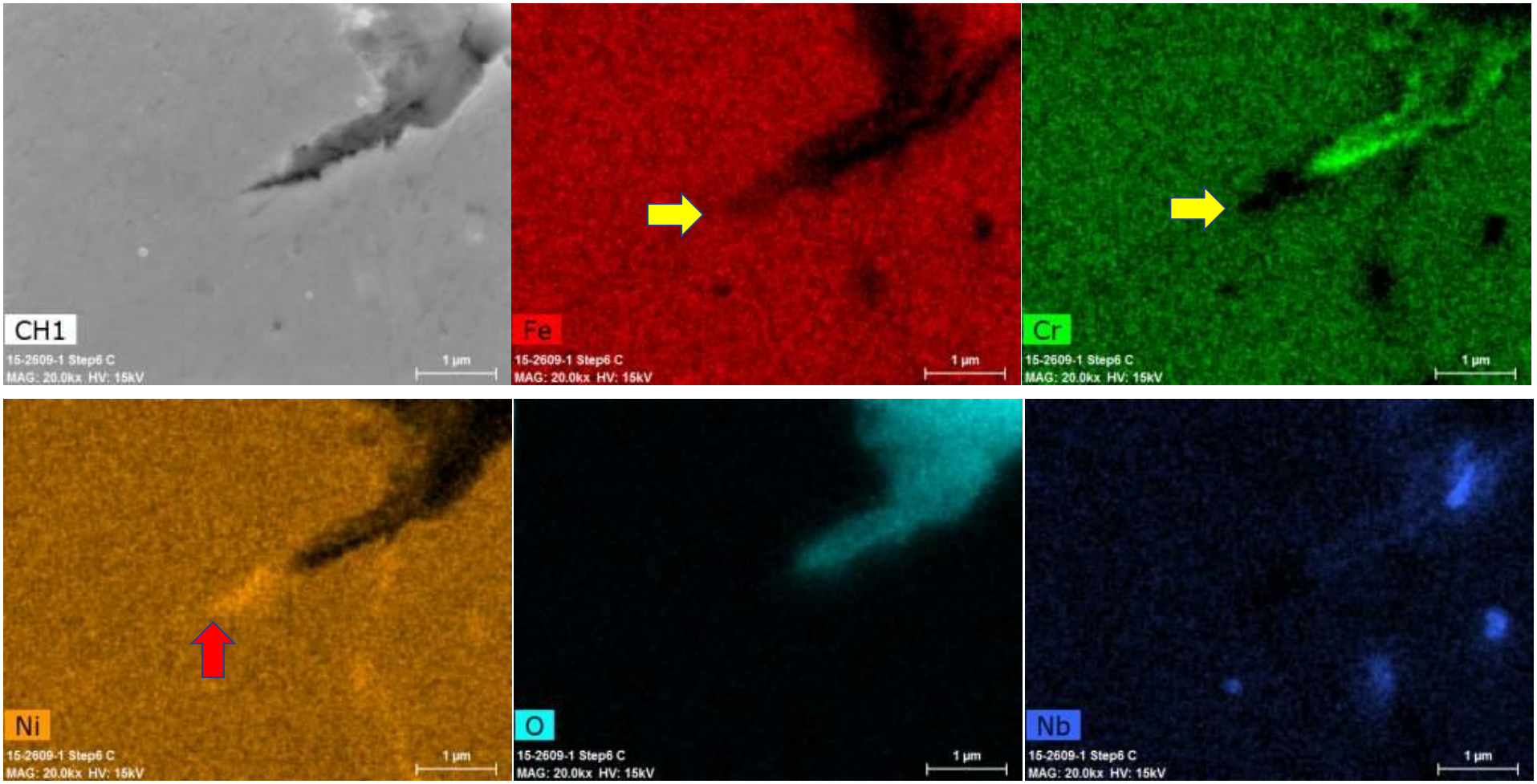

Figure 85: The compositional dot-maps showed that at the fracture branched crack approximately 4 mils from the aft surface was depleted in Fe and Cr ahead of the crack front (yellow arrows) and therefore, richer in Ni (red arrow). The crack itself only contained base metal oxides and no detrimental species were found.

AREA D- ~5 mils from Surface

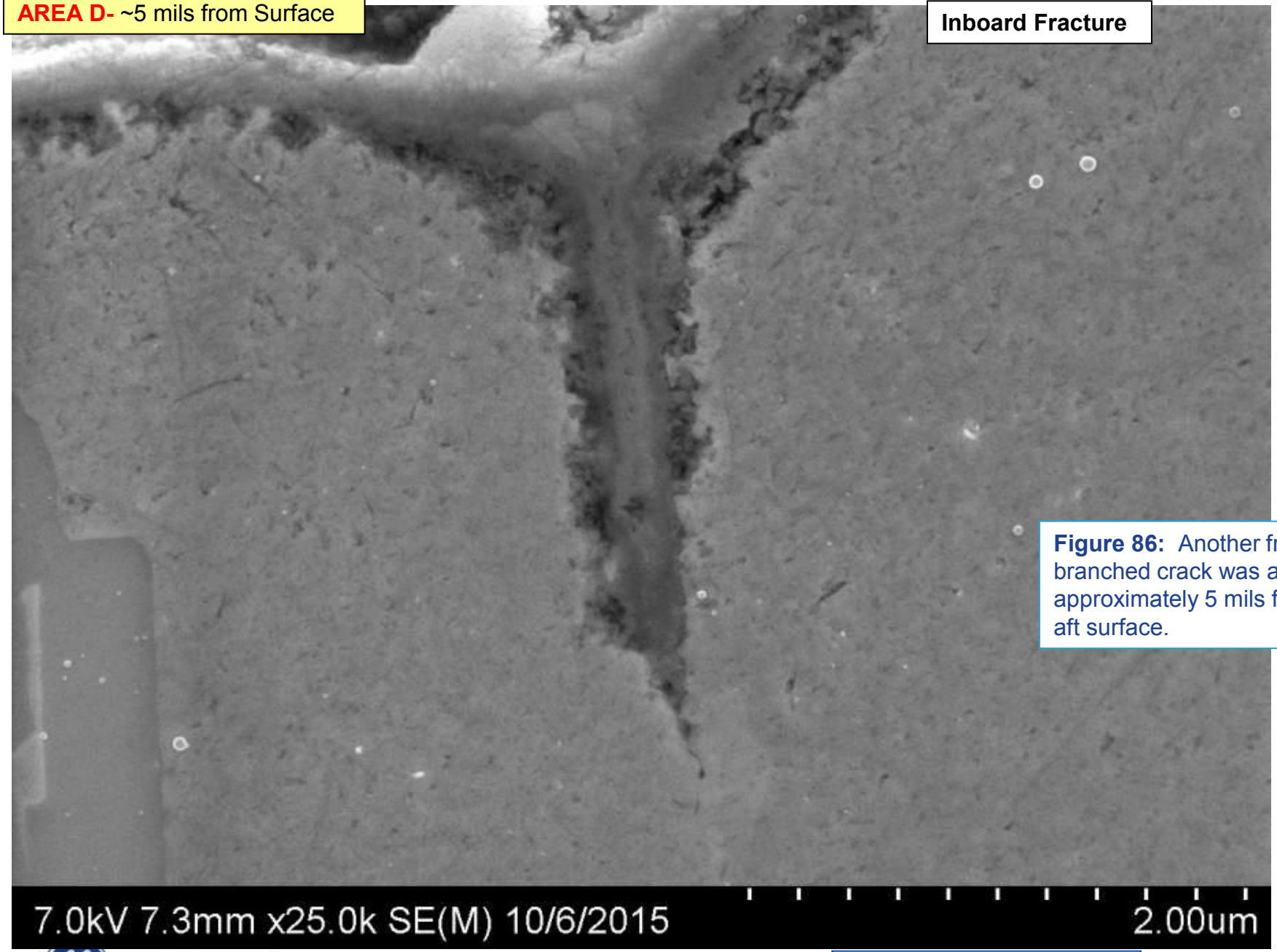

Figure 86: Another fracture branched crack was analyzed approximately 5 mils from the aft surface.

AREA D- ~5 mils from Surface

Inboard Fracture

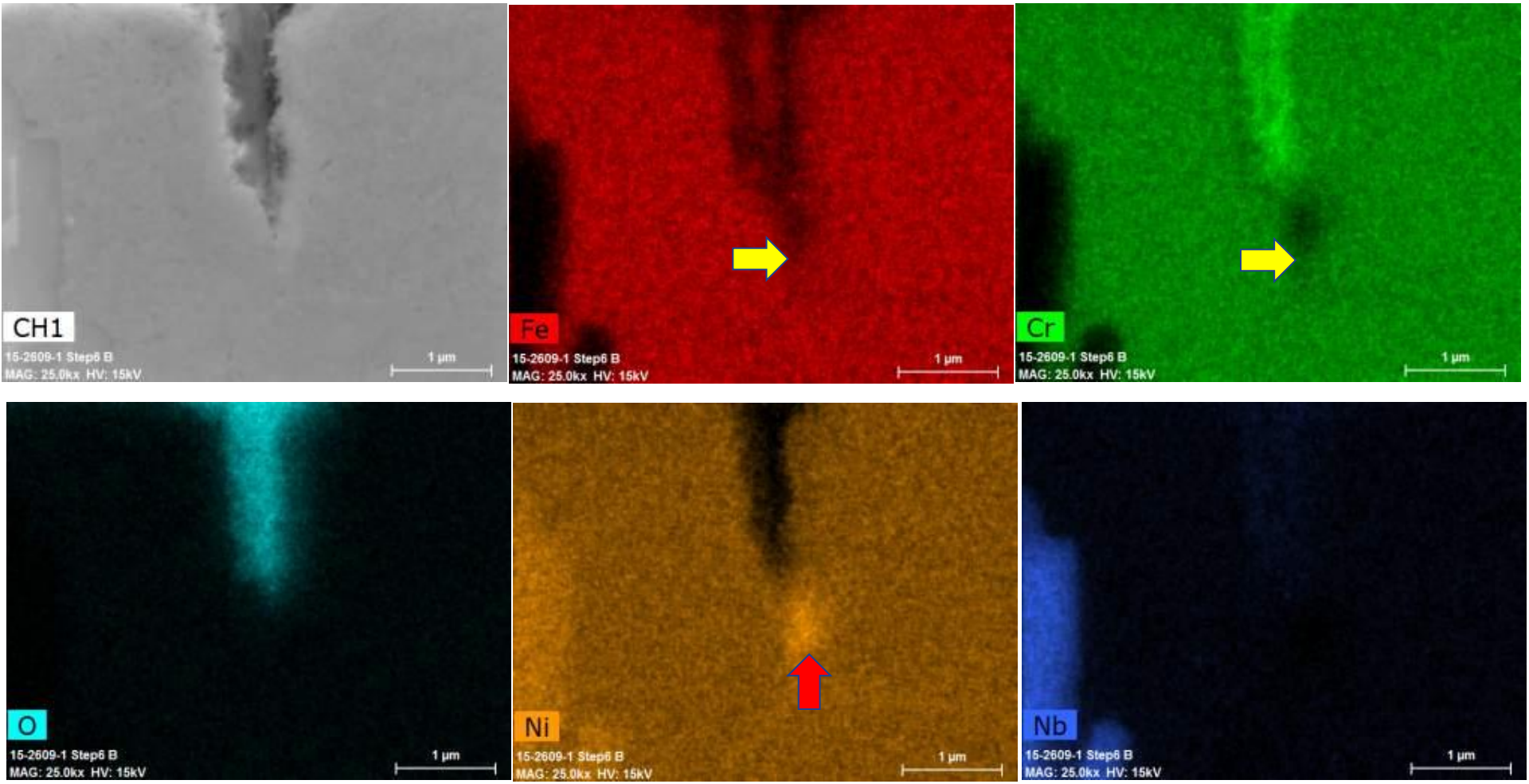

Figure 87: The compositional dot-maps showed that at the fracture branched crack approximately 4 mils from the aft surface was depleted in Fe and Cr ahead of the crack front (yellow arrows) and therefore, richer in Ni (red arrow). The crack itself only contained base metal oxides and no detrimental species were found.

TEM

GE GRC

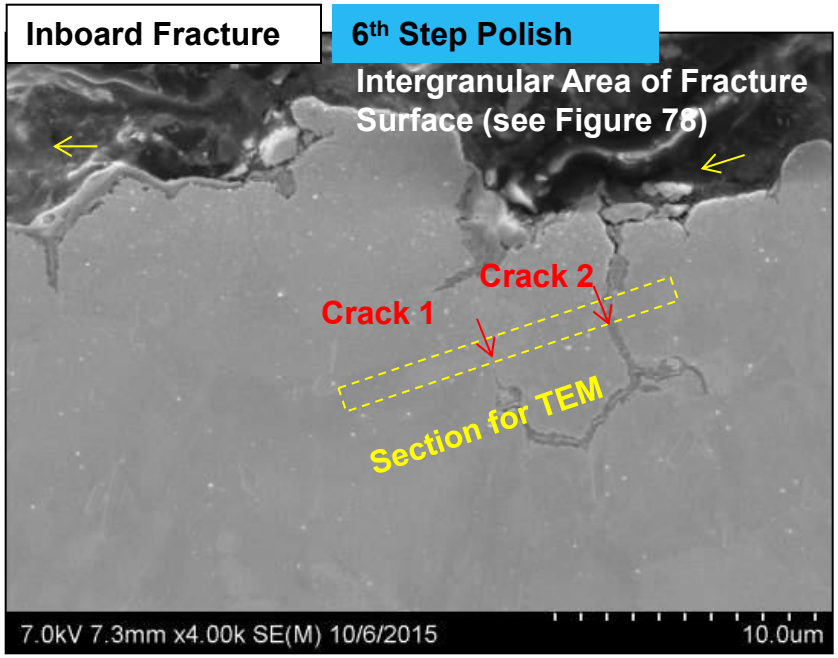

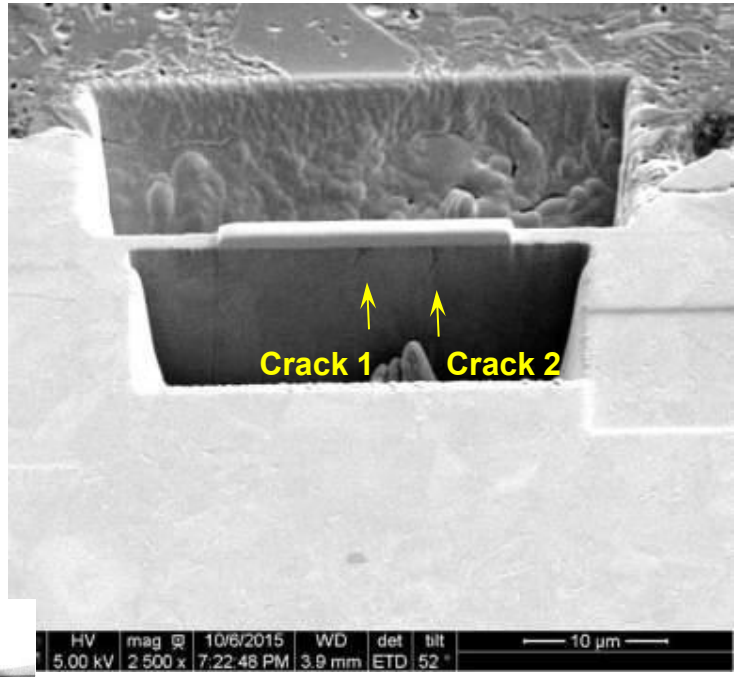

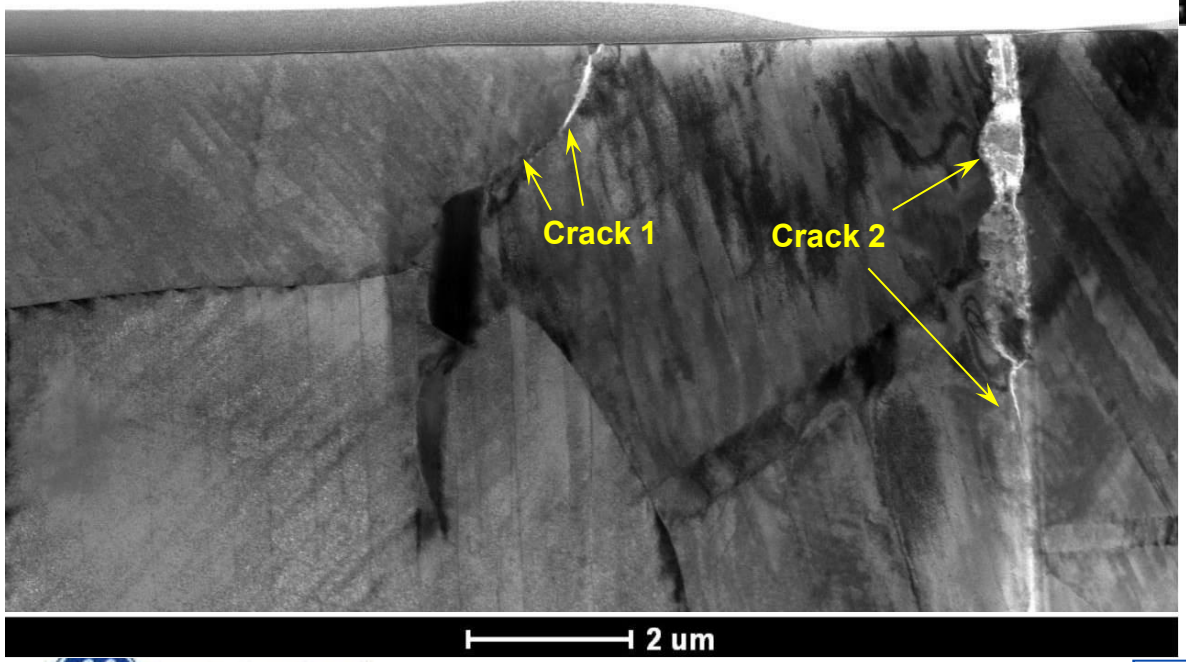

Figure 88: Views of the FIB section removed for TEM analysis that included 2 cracks from the intergranular fracture.

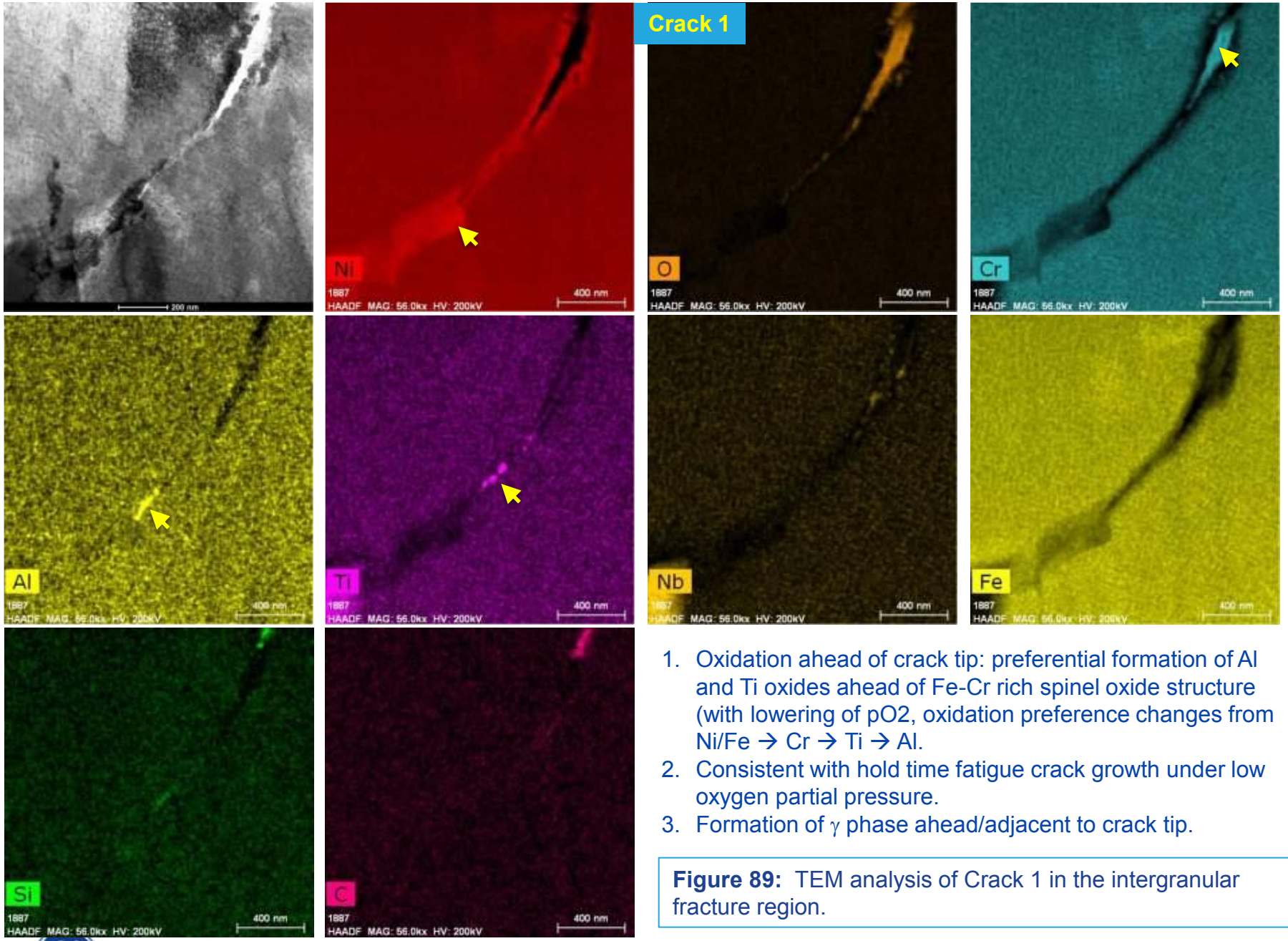

1. Oxidation ahead of crack tip: preferential formation of Al and Ti oxides ahead of Fe-Cr rich spinel oxide structure (with lowering of pO2, oxidation preference changes from Ni/Fe → Cr → Ti → Al.
2. Consistent with hold time fatigue crack growth under low oxygen partial pressure.
3. Formation of γ phase ahead/adjacent to crack tip.

Figure 89: TEM analysis of Crack 1 in the intergranular fracture region.

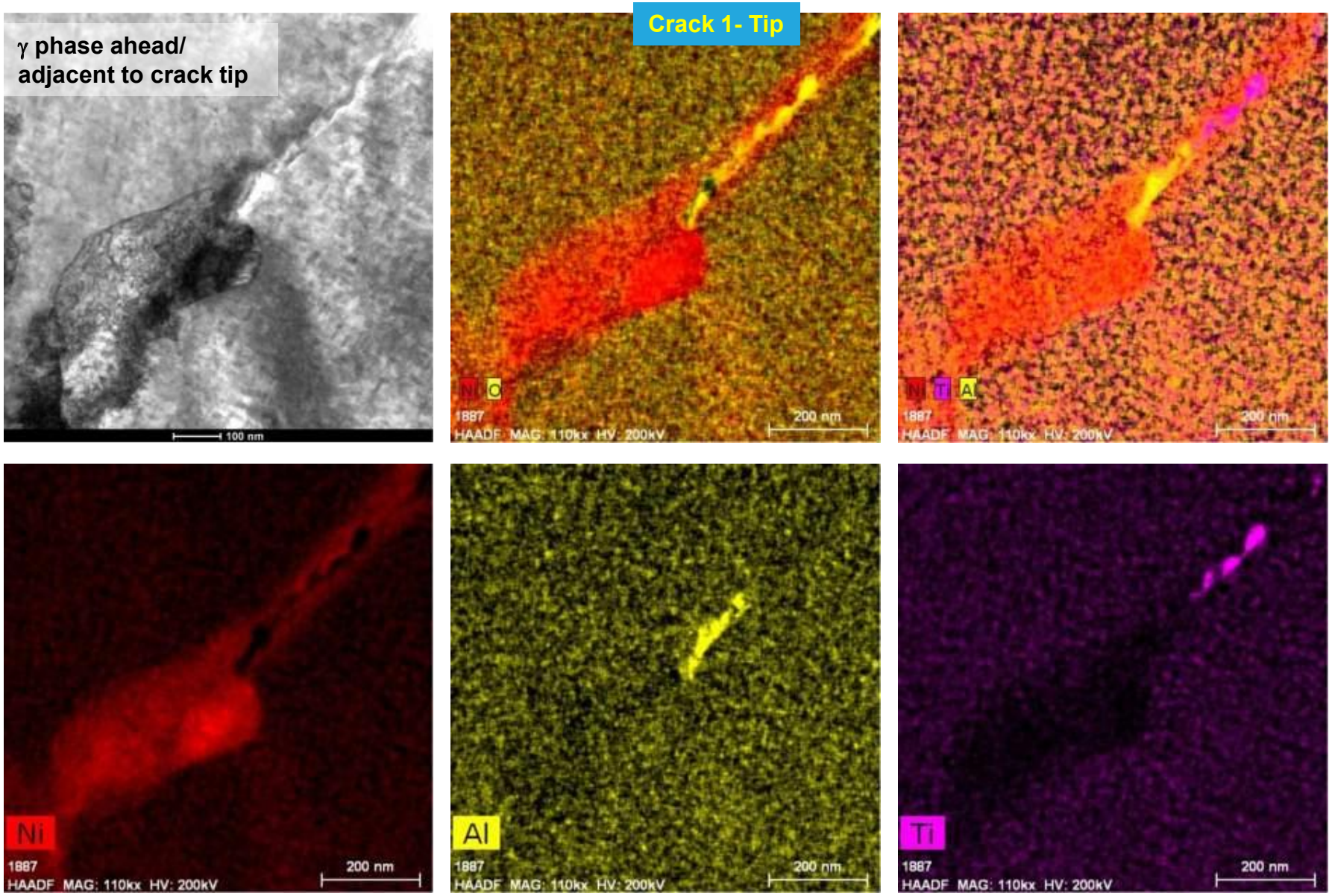

Figure 90: More detailed examination of the tip of crack 1 showing the γ phase ahead/adjacent to crack tip and initial oxides formed.

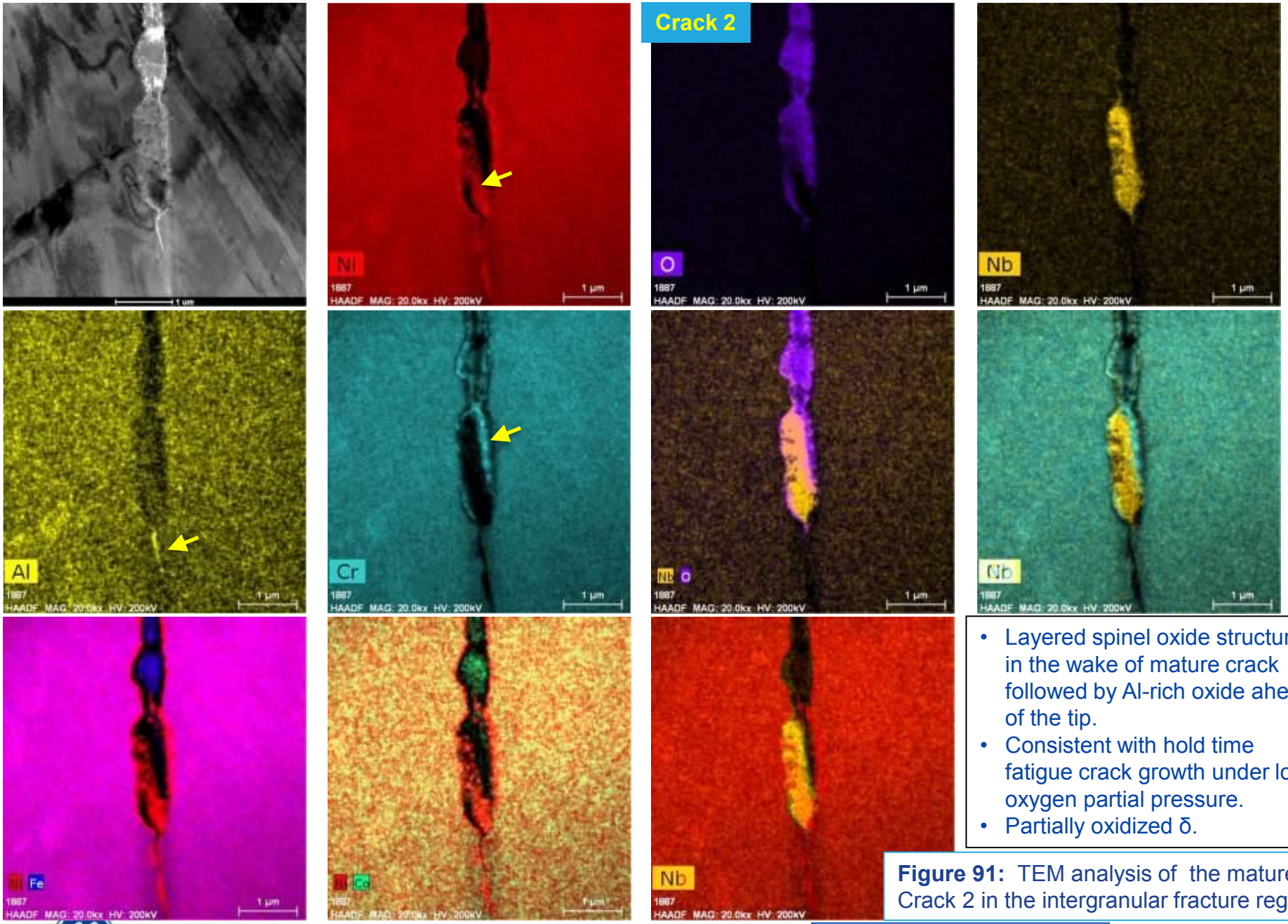

- Layered spinel oxide structure in the wake of mature crack followed by Al-rich oxide ahead of the tip.
- Consistent with hold time fatigue crack growth under low oxygen partial pressure.
- Partially oxidized δ.

Figure 91: TEM analysis of the mature Crack 2 in the intergranular fracture region.

Crack 2

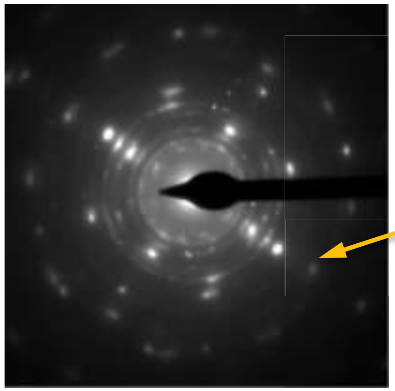

Spinels AB_2O_4
(A,B: Fe, Cr, Ni)

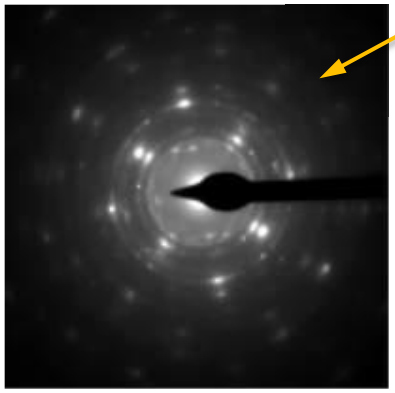

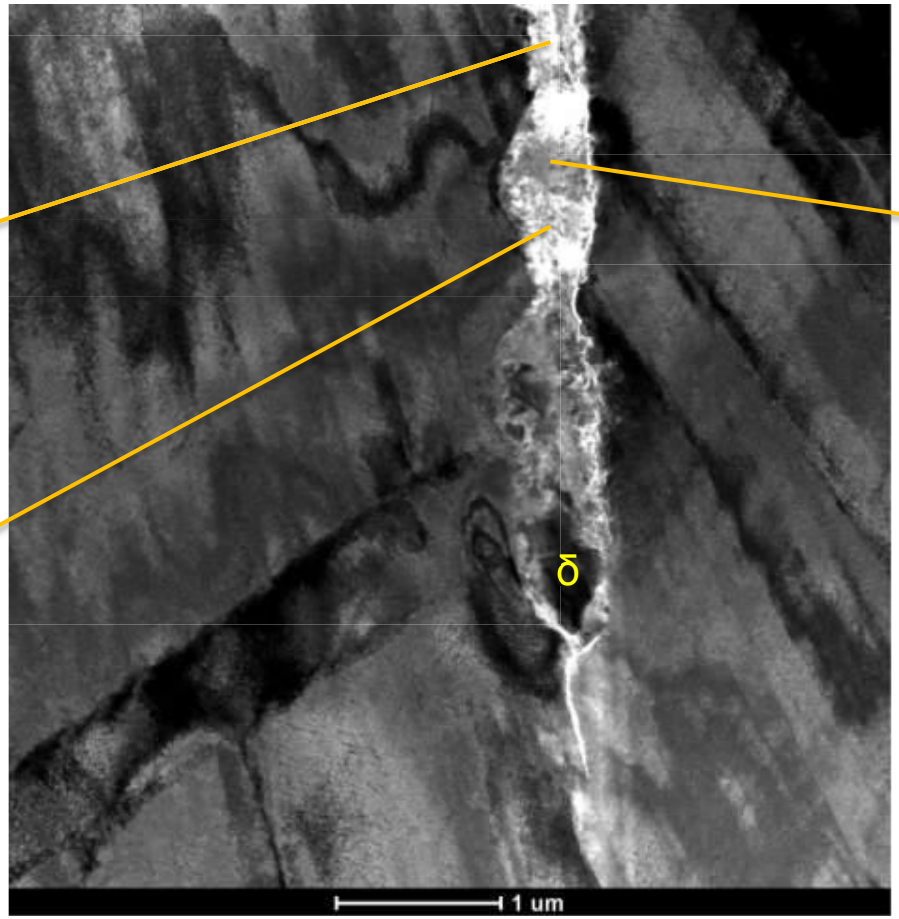

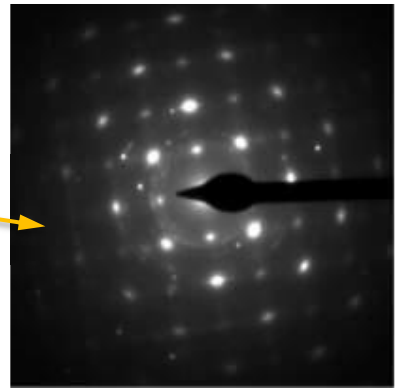

Spinels AB_2O_4
(A,B: Fe, Cr, Ni)

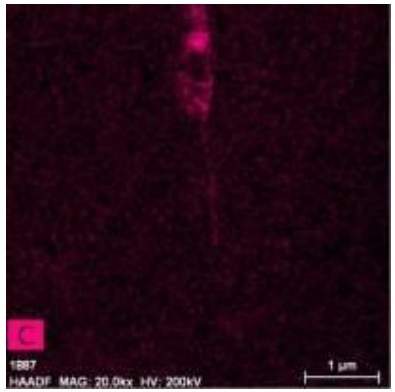

Figure 92: TEM analysis of the mature Crack 2 in the intergranular fracture region.

Crack 2- Tip

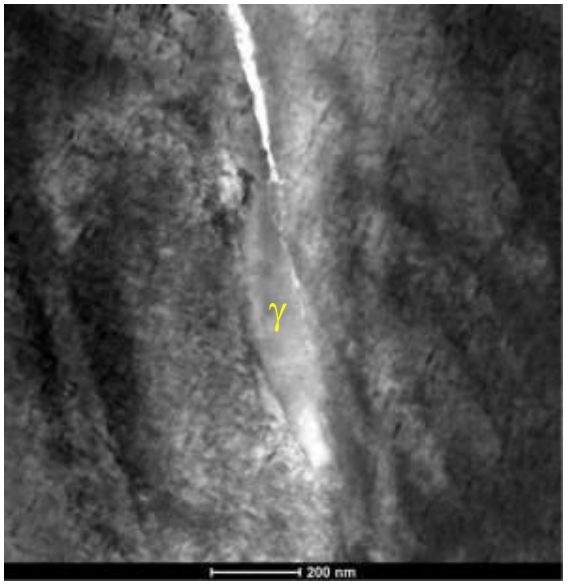

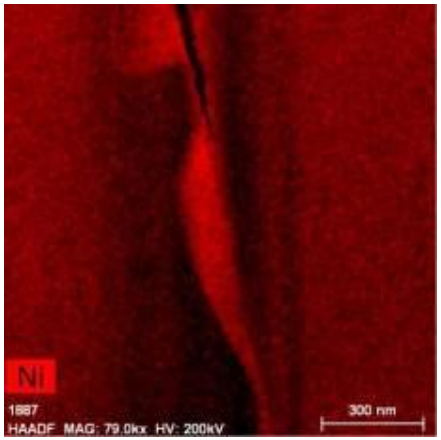

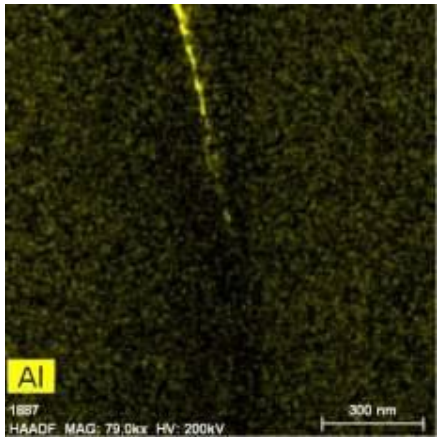

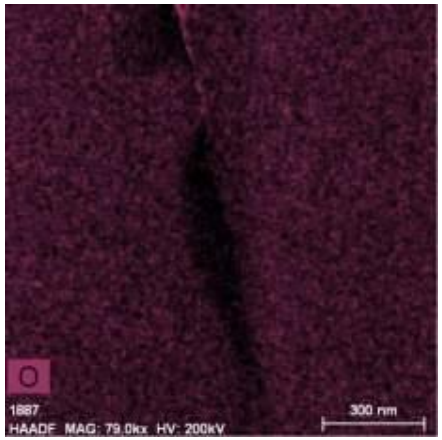

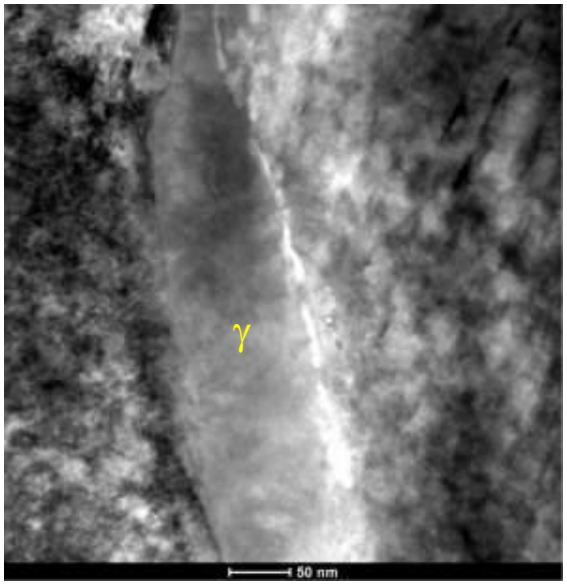

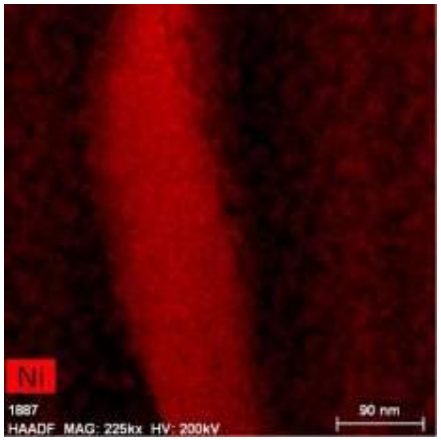

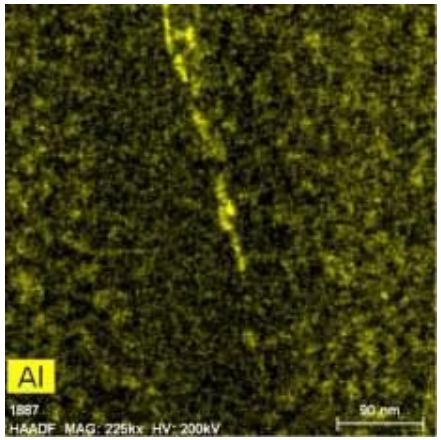

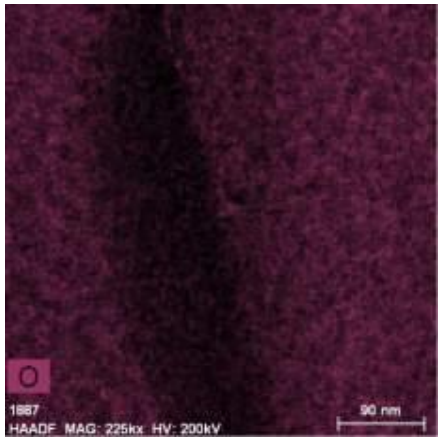

- γ phase ahead/adjacent to crack tip.
- Thin Al-rich oxide ahead of crack tip.

Figure 93: TEM analysis of the tip of Crack 2 in the intergranular fracture region.

Secondary Cracks Adjacent to Fatigue Region

General SEM & Metallographic mounts – GE Aviation
FIB analysis- GE GRC

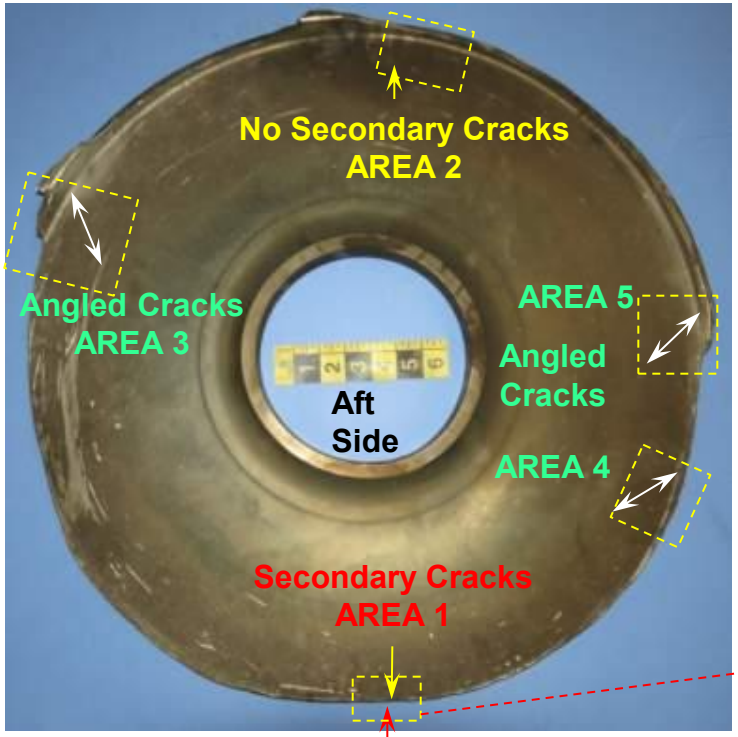

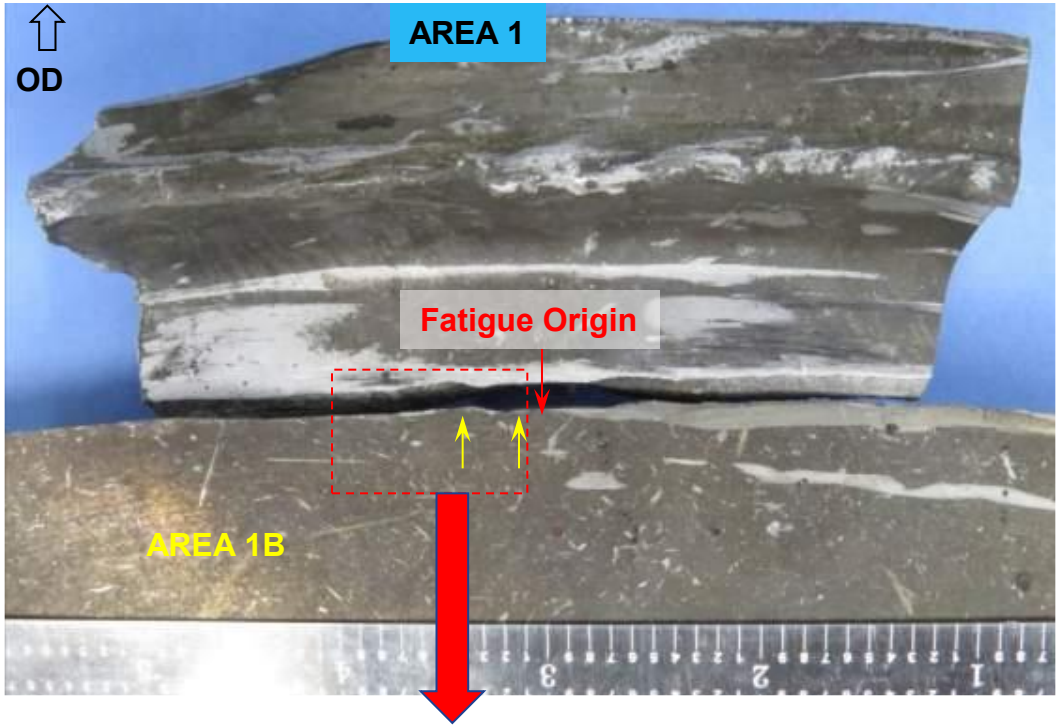

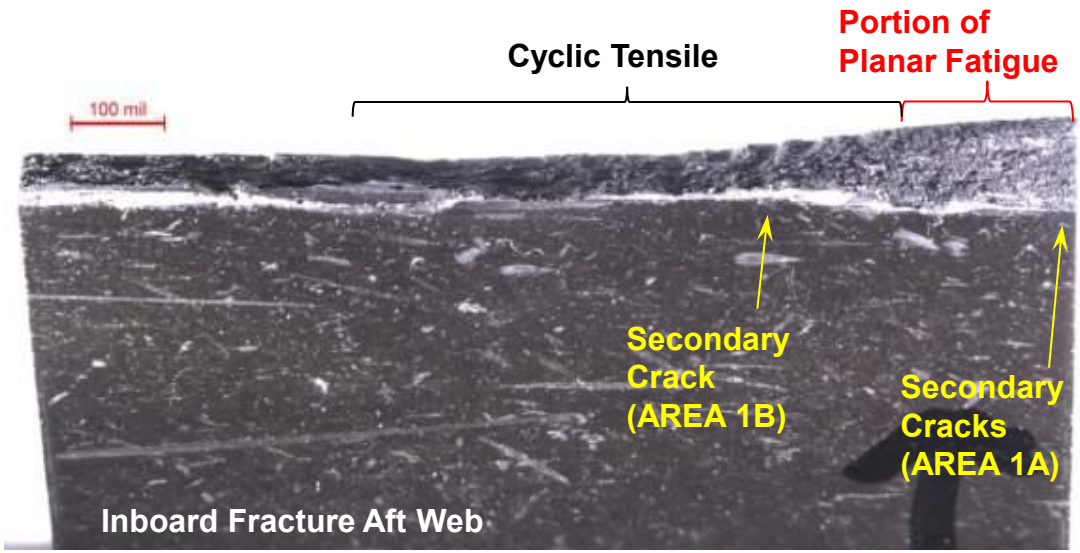

Figure 94: Optical views showing where secondary cracks were observed on the aft web adjacent to the fatigue region. A group of secondary cracks was found just inboard of the planar fatigue region (Area 1A) and 1 crack was observed in the cyclic tensile region, but in a similar radial plane (Area 1B).

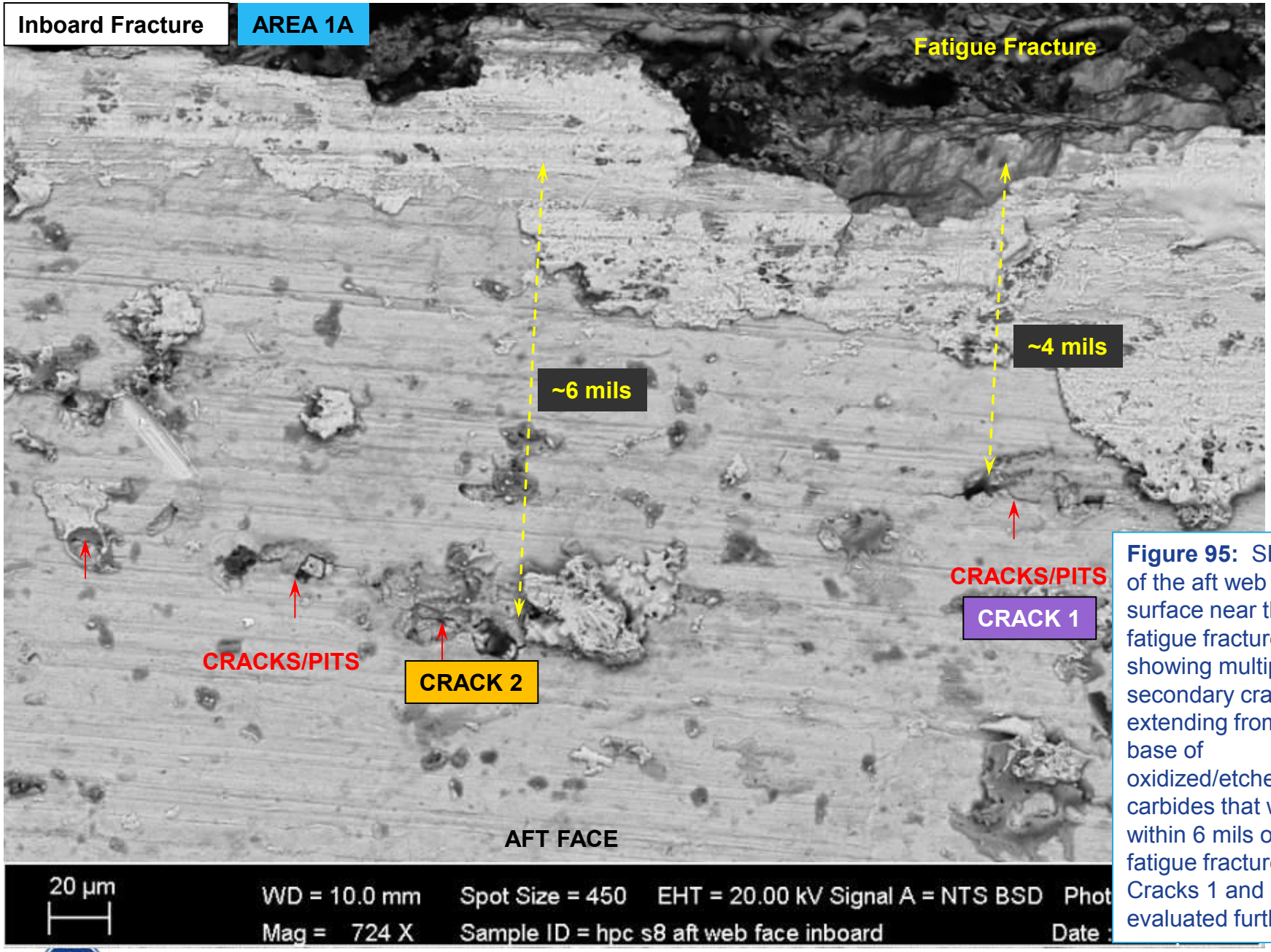

Figure 95: SEM view of the aft web face surface near the fatigue fracture showing multiple secondary cracks extending from the base of oxidized/etched carbides that were within 6 mils of the fatigue fracture locally. Cracks 1 and 2 were evaluated further.

Inboard Fracture **AREA 1A**

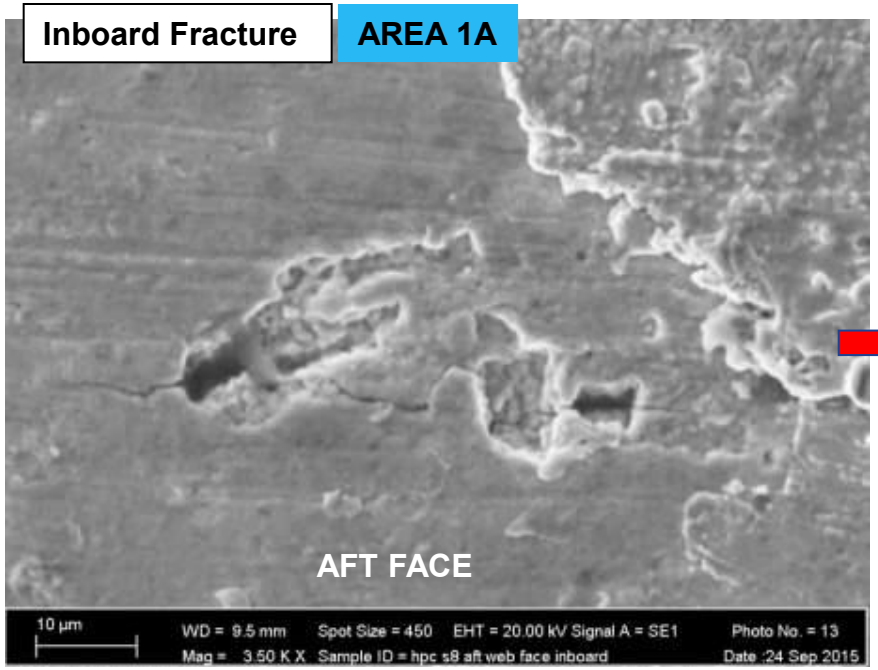

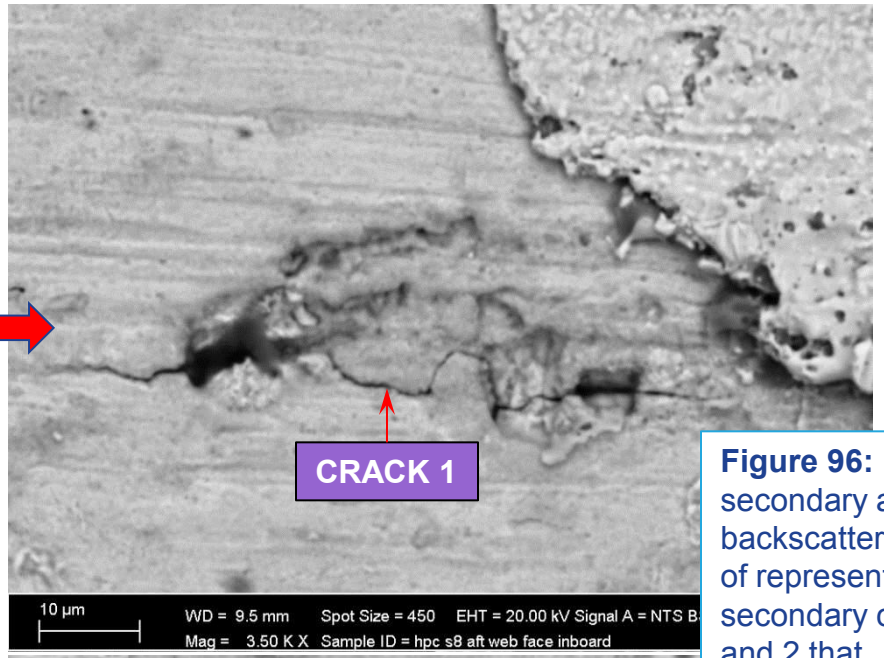

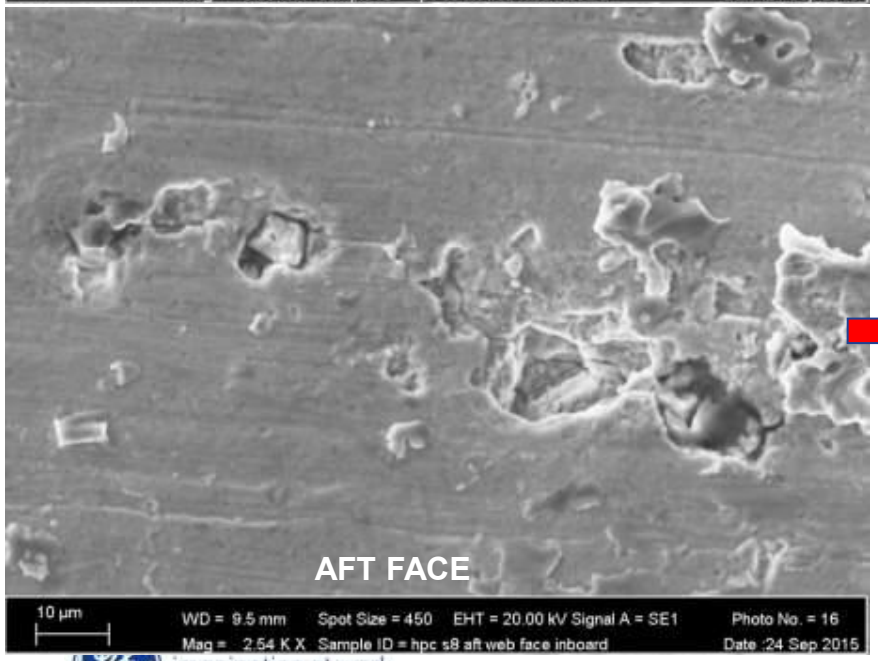

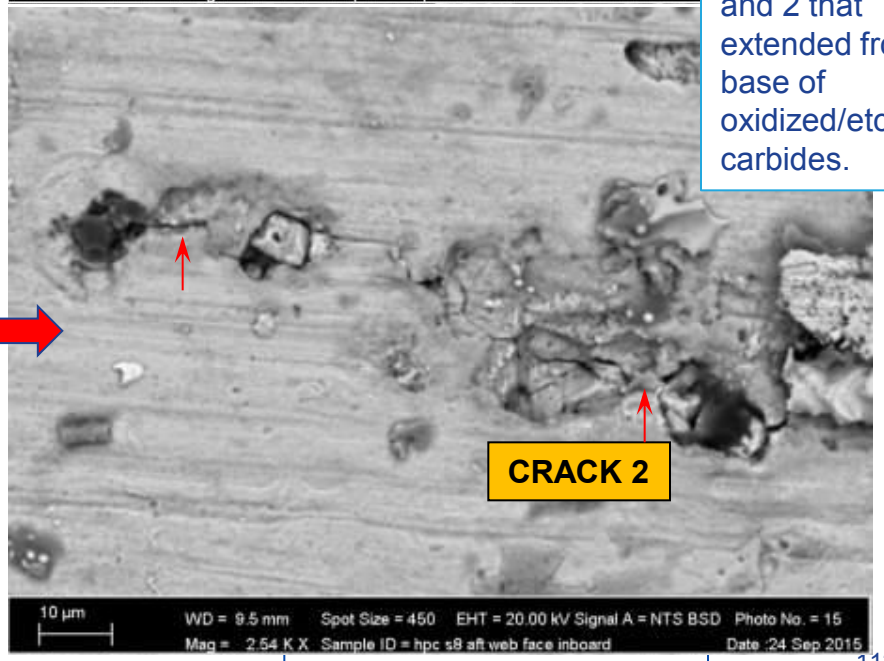

Figure 96: SEM secondary and backscatter images of representative secondary cracks 1 and 2 that extended from the base of oxidized/etched carbides.

Inboard Fracture **AREA 1A**

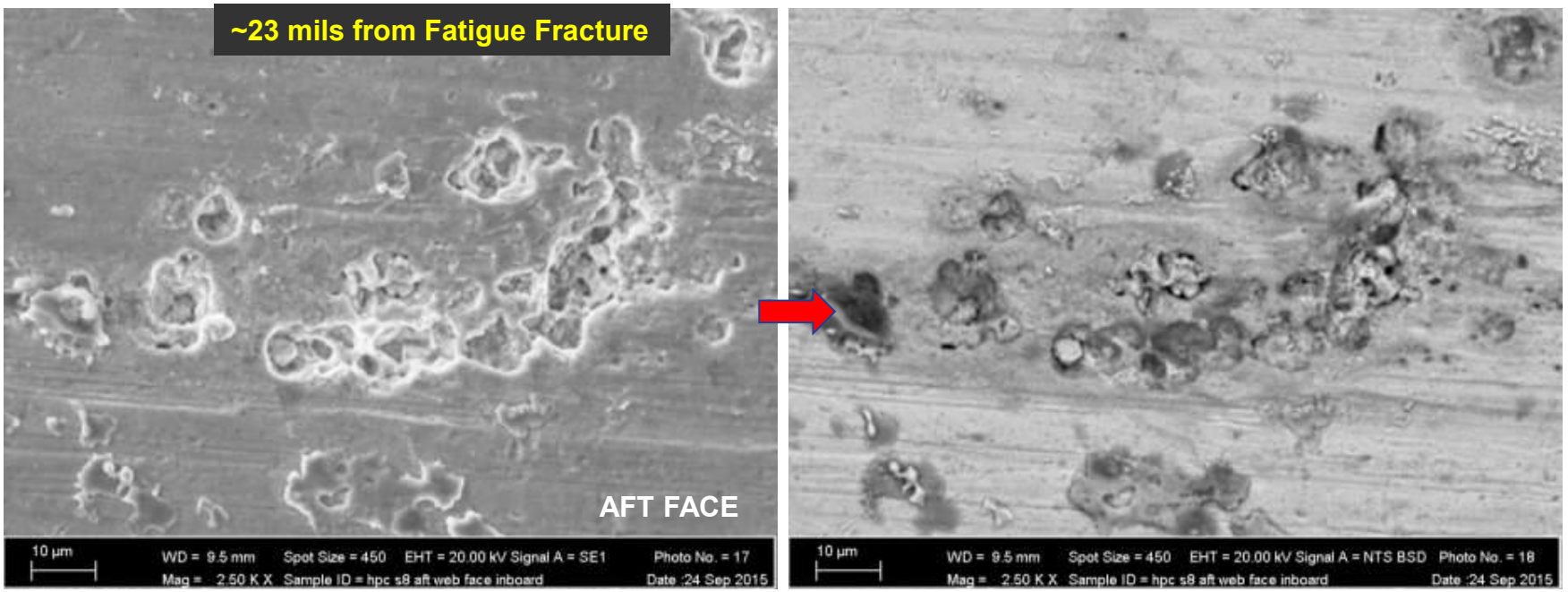

Figure 97: Etched/oxidized carbides were observed throughout the free exposed surfaces, but beyond approximately 16 mils of the fatigue plane (23 mils in above image) no secondary cracks were observed.

Inboard Fracture **AREA 1B**

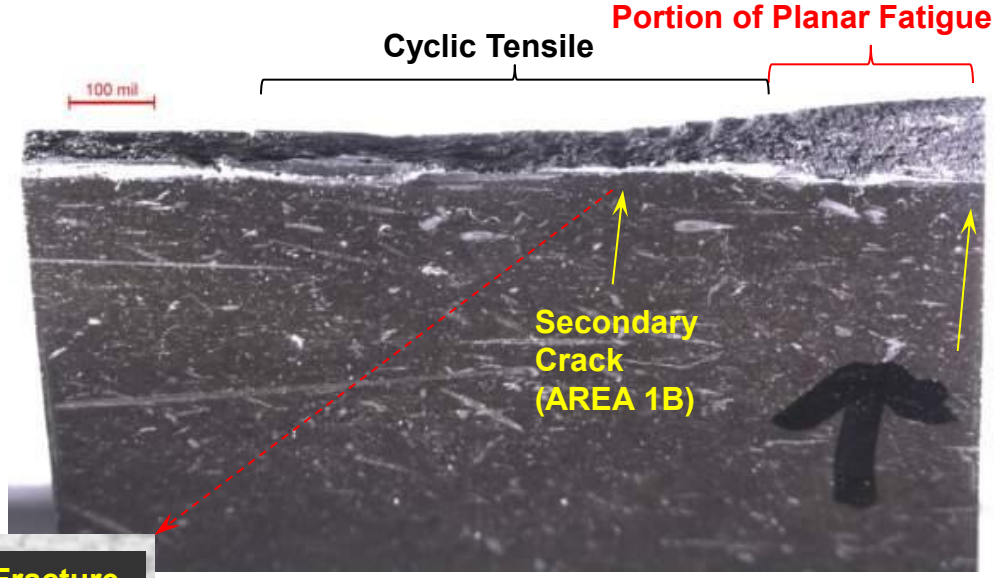

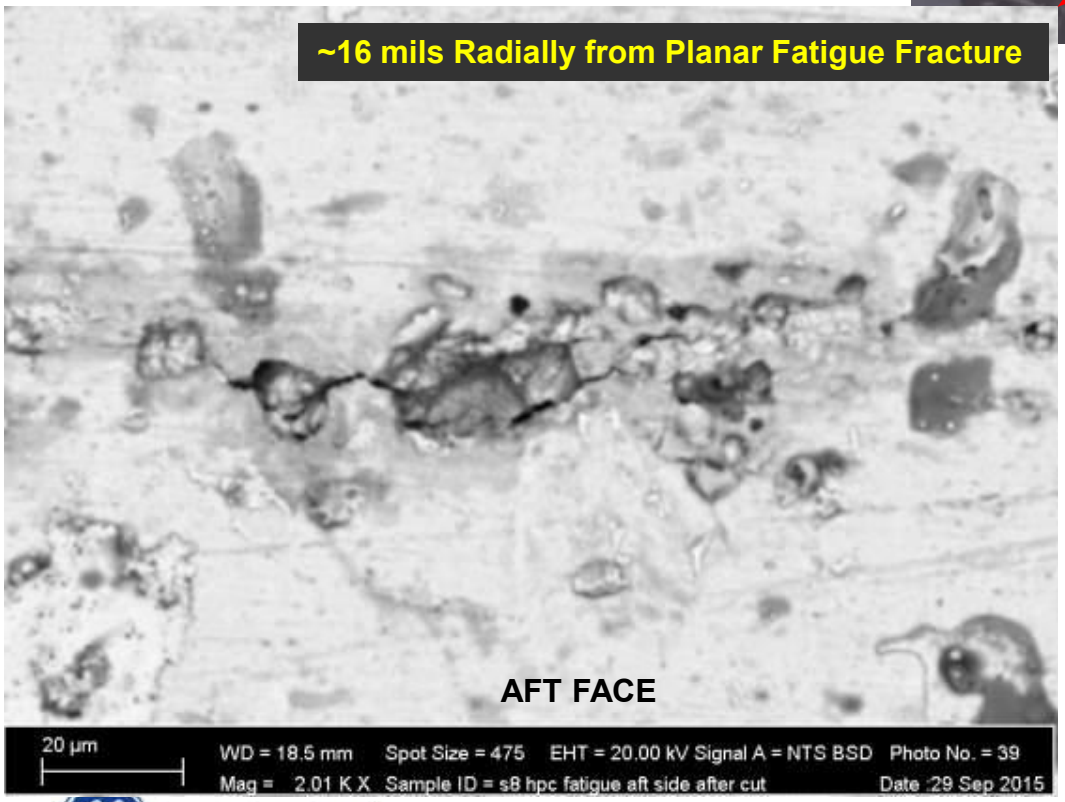

Figure 98: A separate secondary crack was observed in the cyclic tensile region of the web that was approximately 16 mils radially from the planar fatigue region.

Inboard Fracture (Forward Web)

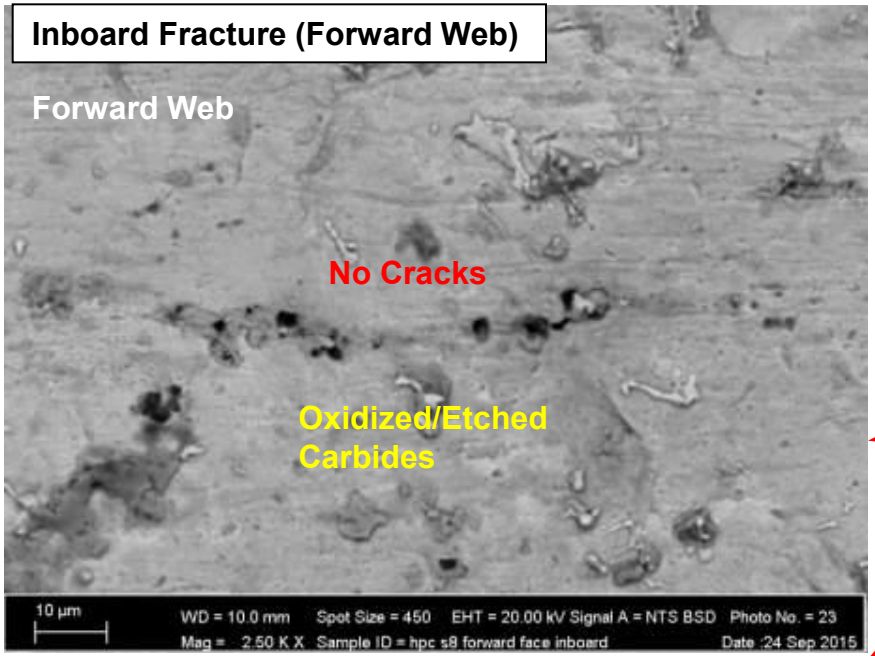

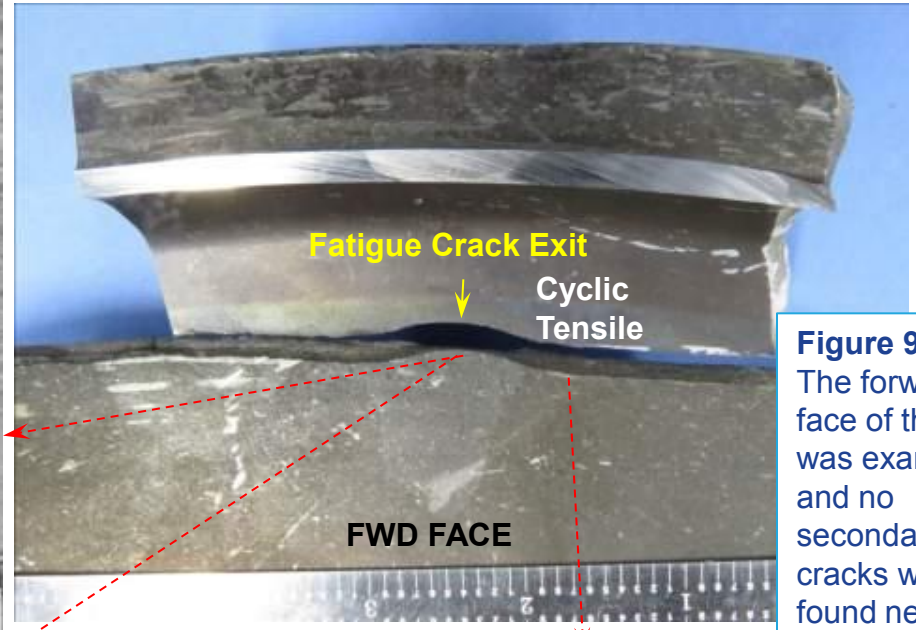

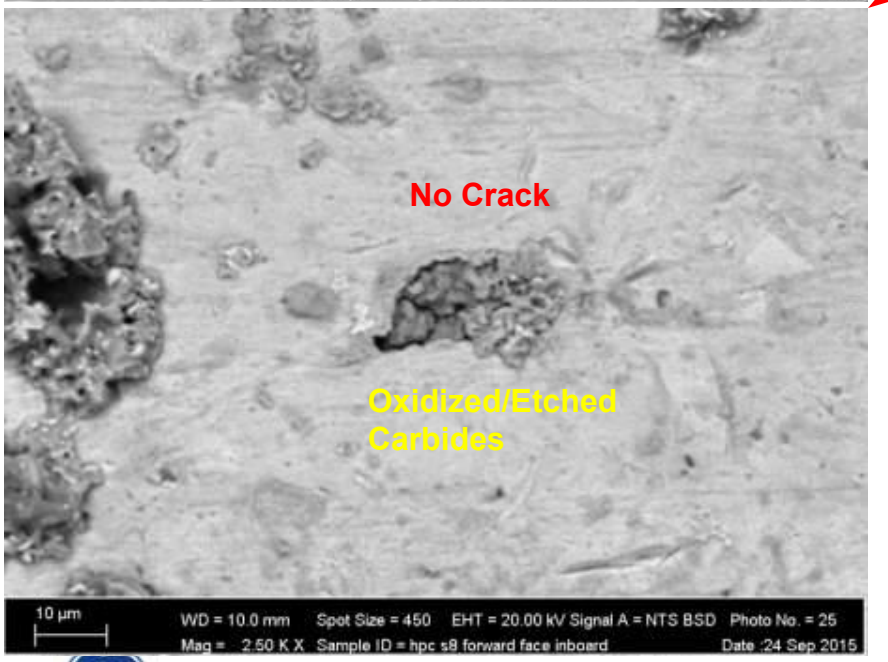

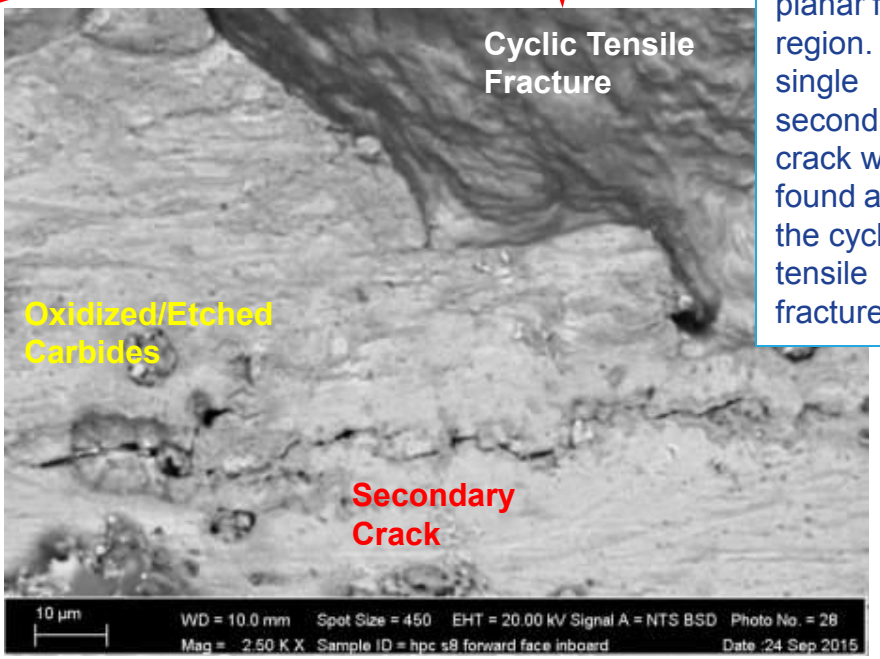

Figure 99: The forward face of the web was examined and no secondary cracks were found near the planar fatigue region. Only a single secondary crack was found at/near the cyclic tensile fracture.

Inboard Fracture (Diametrically Opposed Side) **AREA 2**

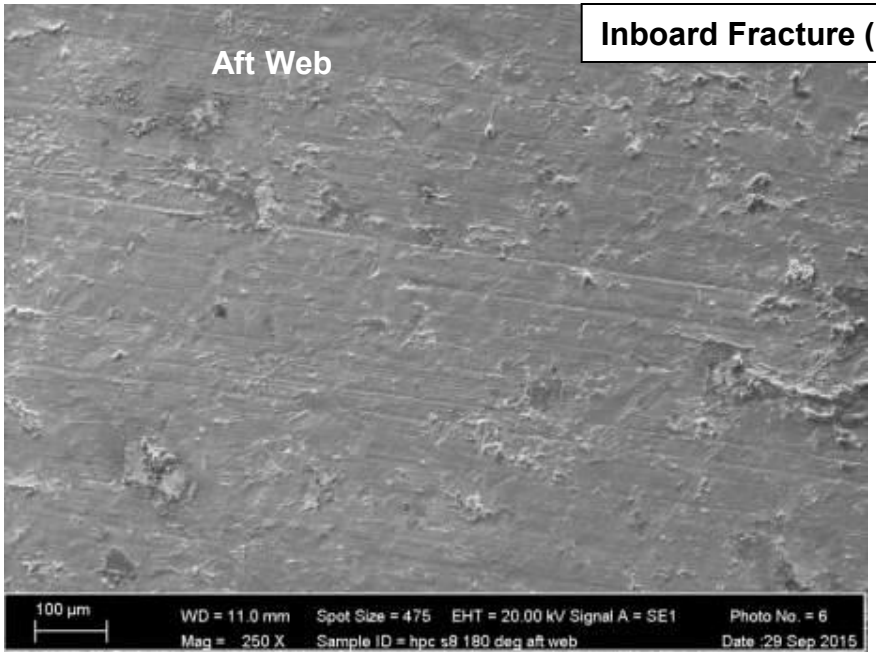

Figure 100: SEM examination showed that on the diametrically opposite side of the disk from the fatigue region there were oxidized/etched carbides with no observable cracks on the aft face in the same radial plane as the facture.

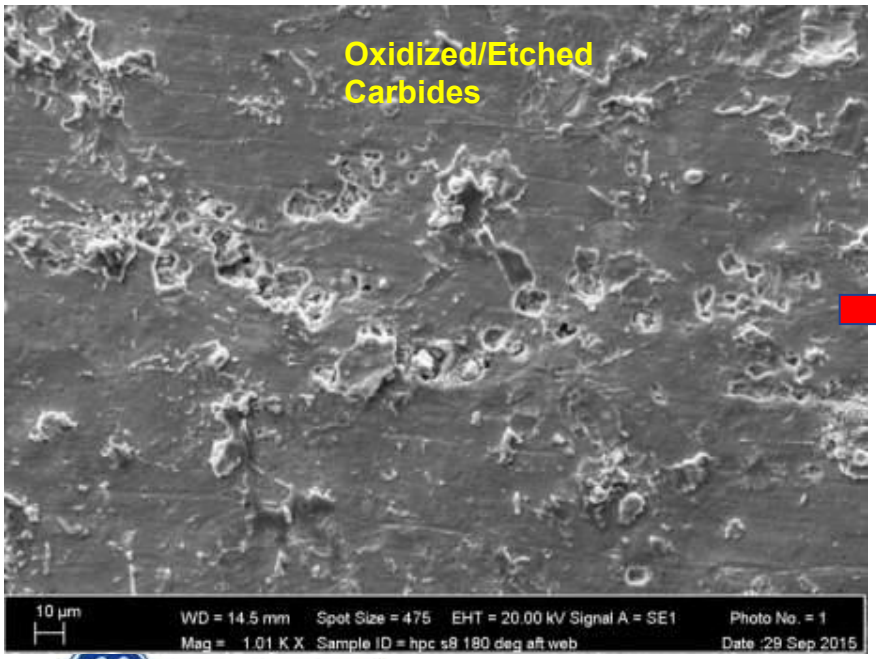

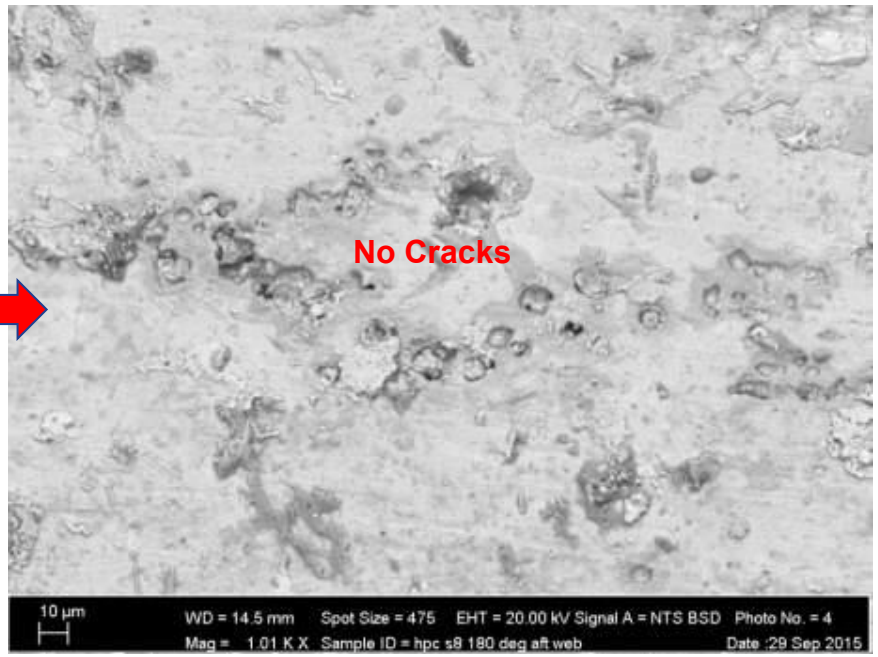

Inboard Fracture (Diametrically Opposed Side) **AREA 2**

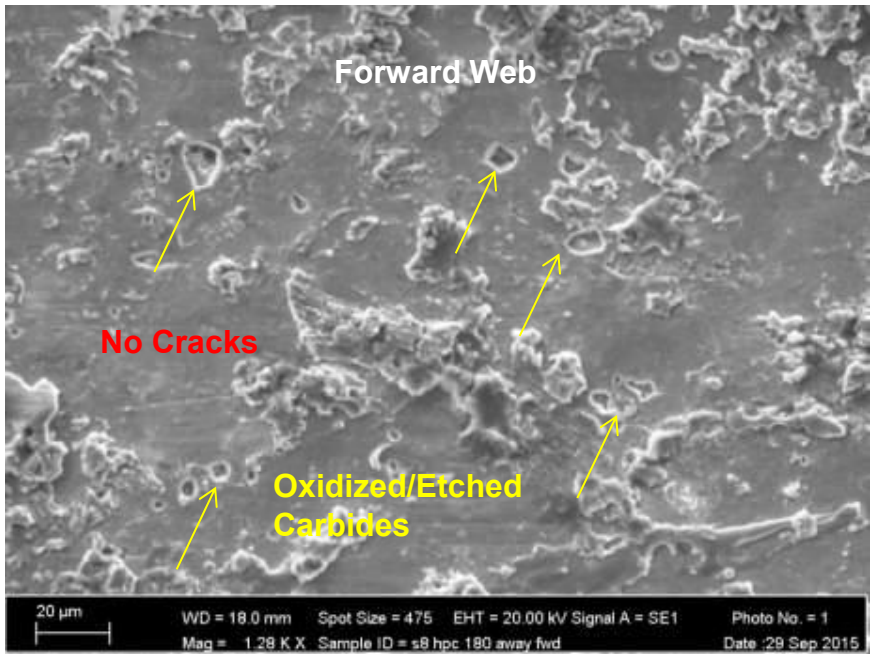

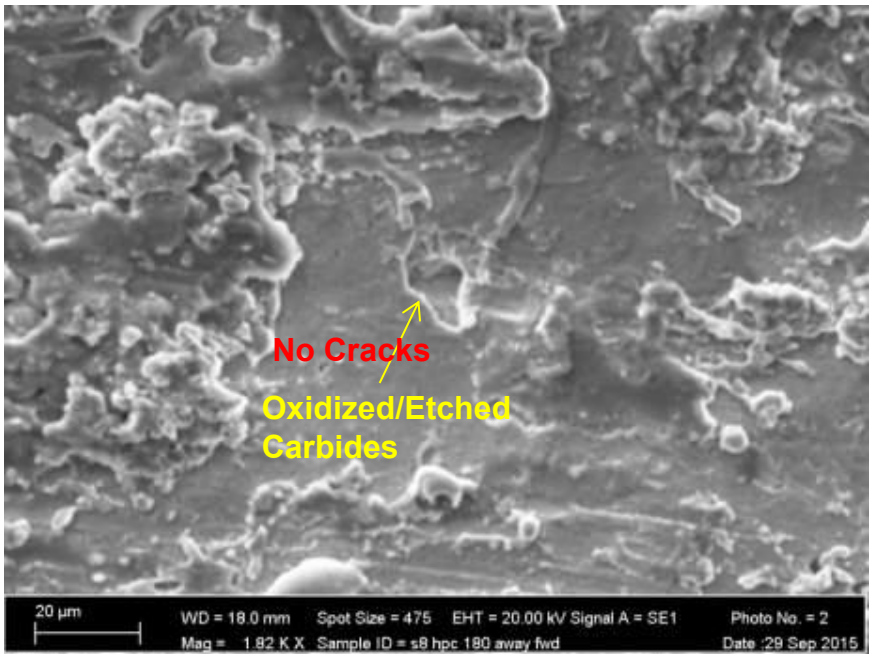

Figure 101: SEM examination showed that on the diametrically opposite side of the disk from the fatigue region there were oxidized/etched carbides with no observable cracks on the forward face in the same radial plane as the facture.

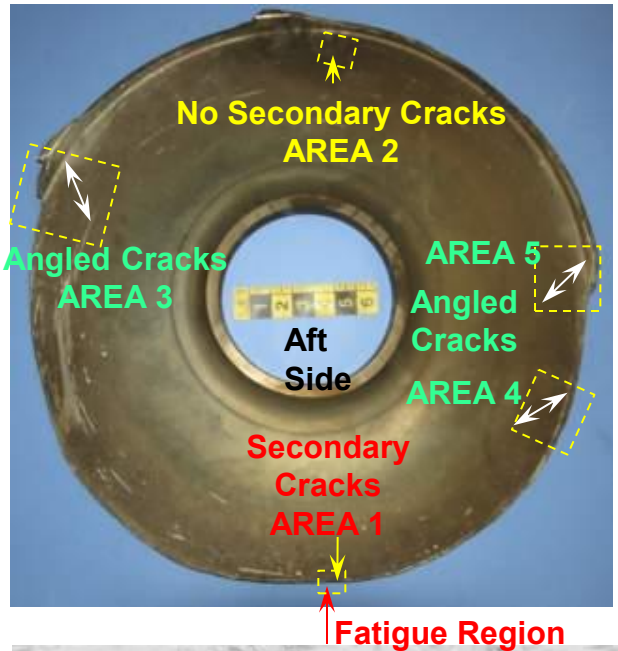

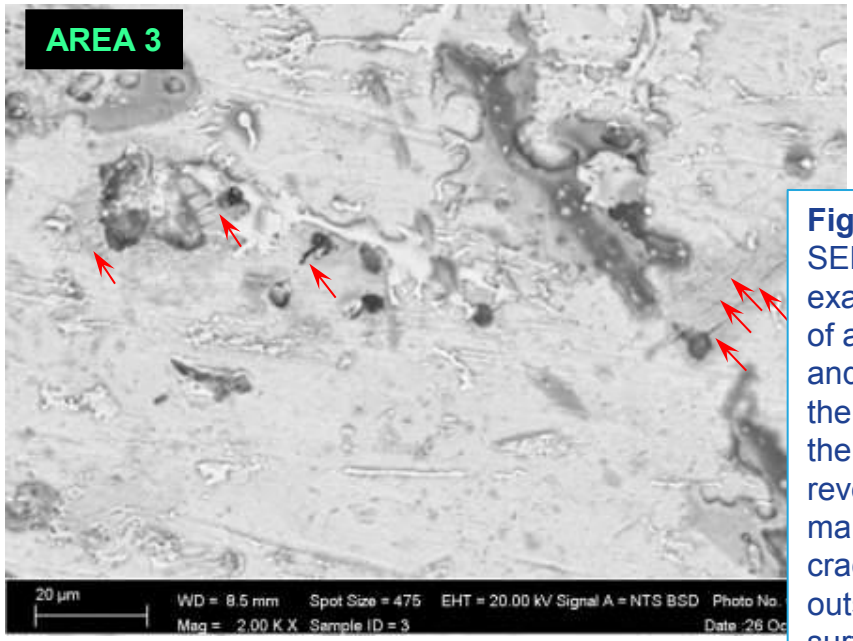

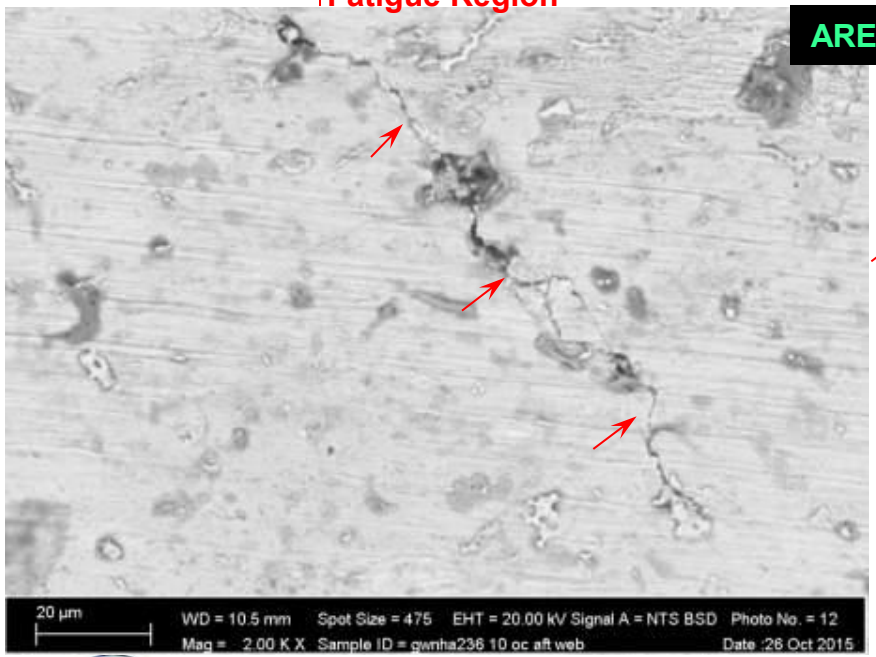

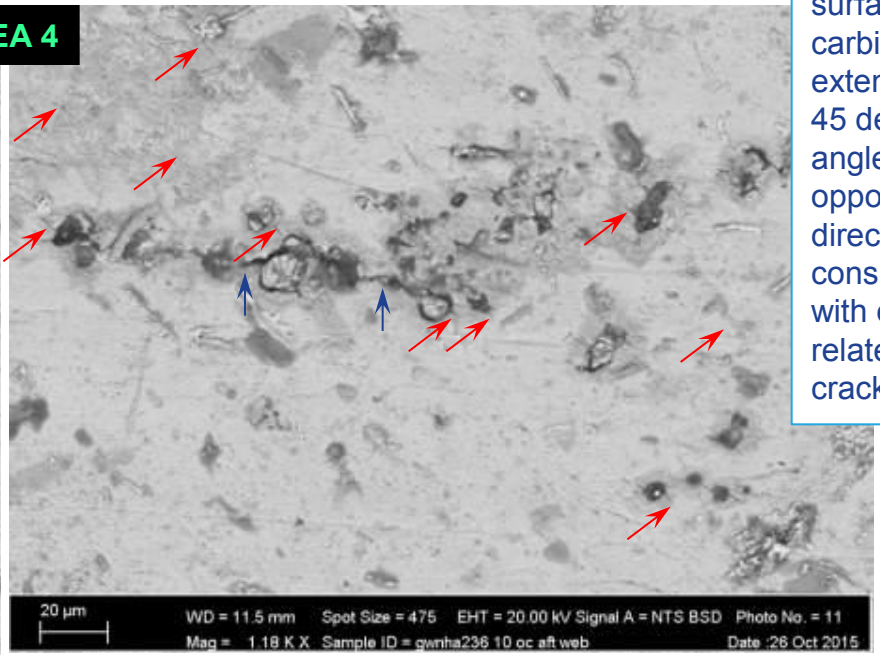

Figure 102: SEM examination of areas 3, 4, and 5 near the ends of the rim tear revealed many small cracks in and outside of surface carbides that extended at 45 degree angles (in opposing directions), consistent with event-related shear cracking.

AREA 4

MT15-2982-01

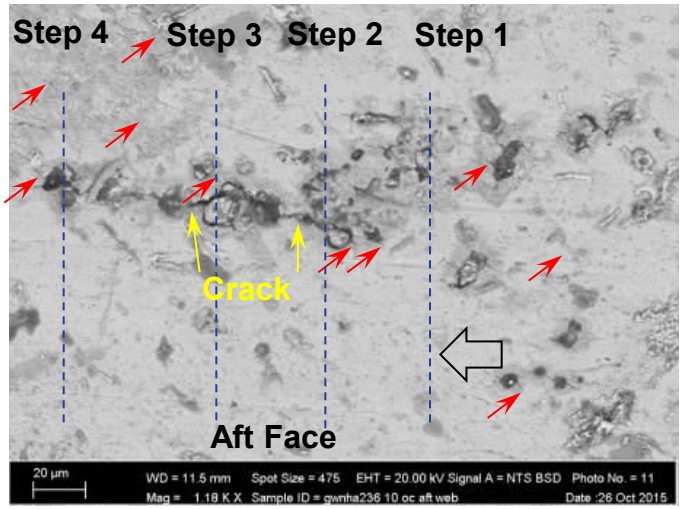

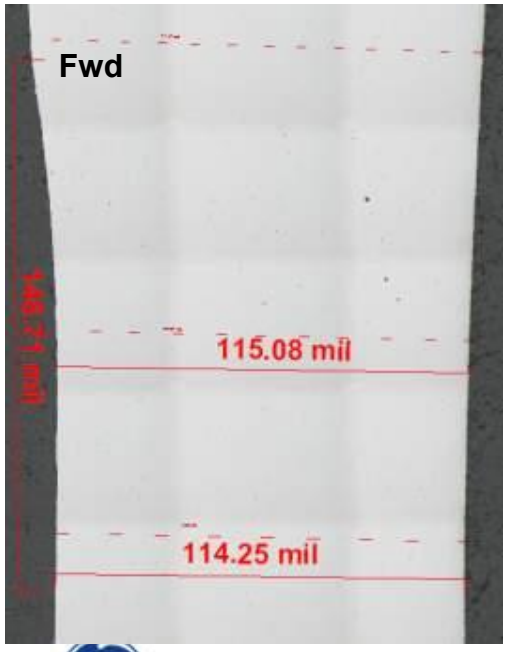

Figure 103: A mount made through one of the cracked areas near the rim fracture end showed that the minimum web wall thickness was reduced to 0.114 inch and multiple polishes could not clearly resolve the small surface cracks on the aft face (lower images), but on the forward face 0.5 mil deep cracks were found that extended at an angle, consistent with event-induced shear cracks.

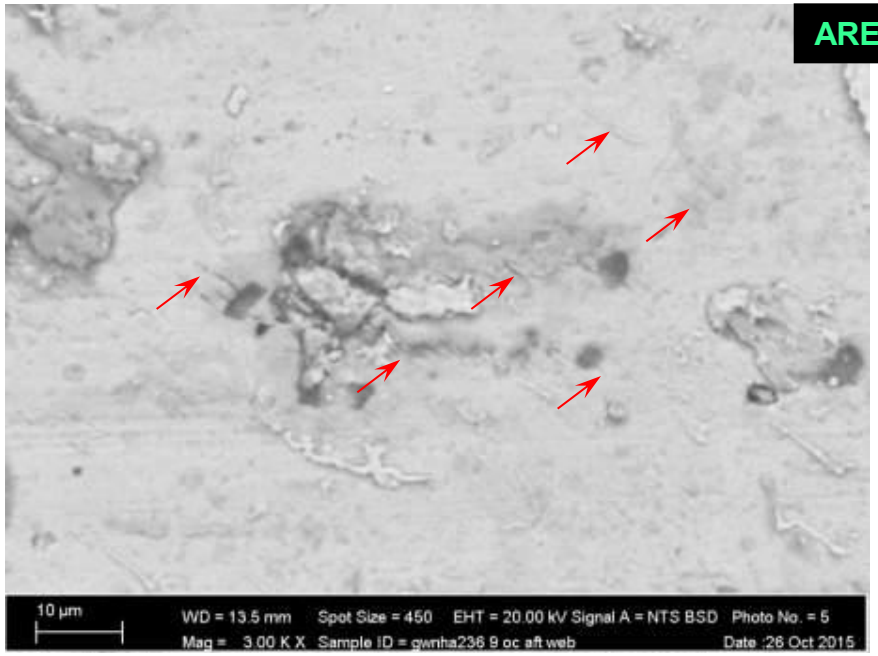

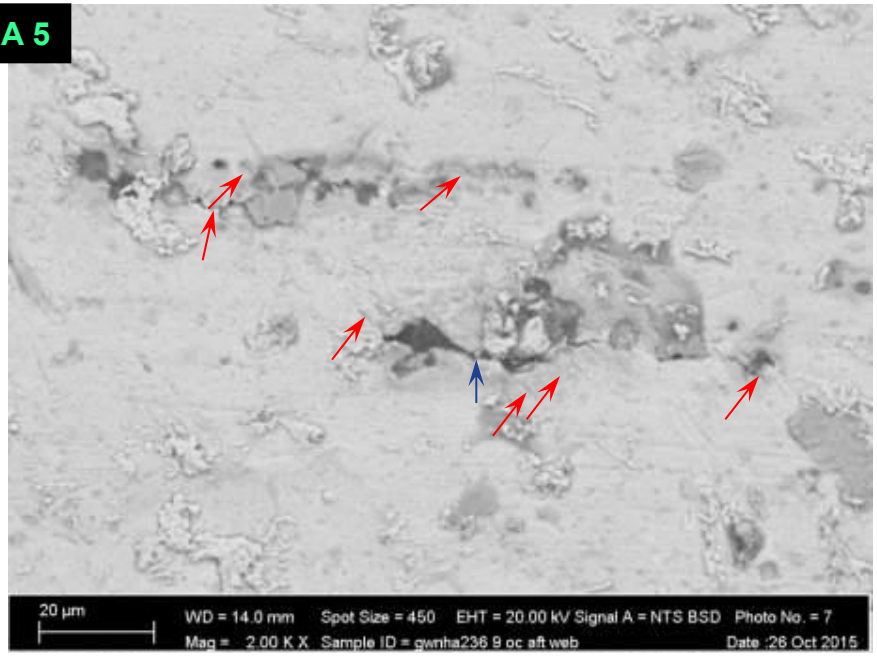

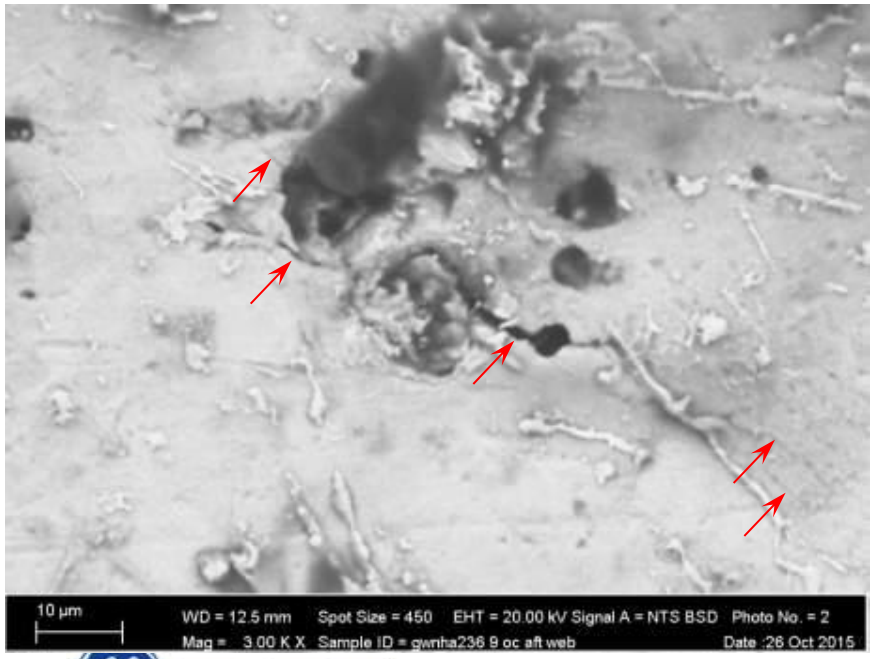

Figure 104: SEM examination of area 5 near the end of the rim tear revealed many small cracks in and outside of surface carbides that extended at 45 degree angles, consistent with event-related shear cracking.

Further Characterization of Secondary Cracks

FIB Sections and Mounts

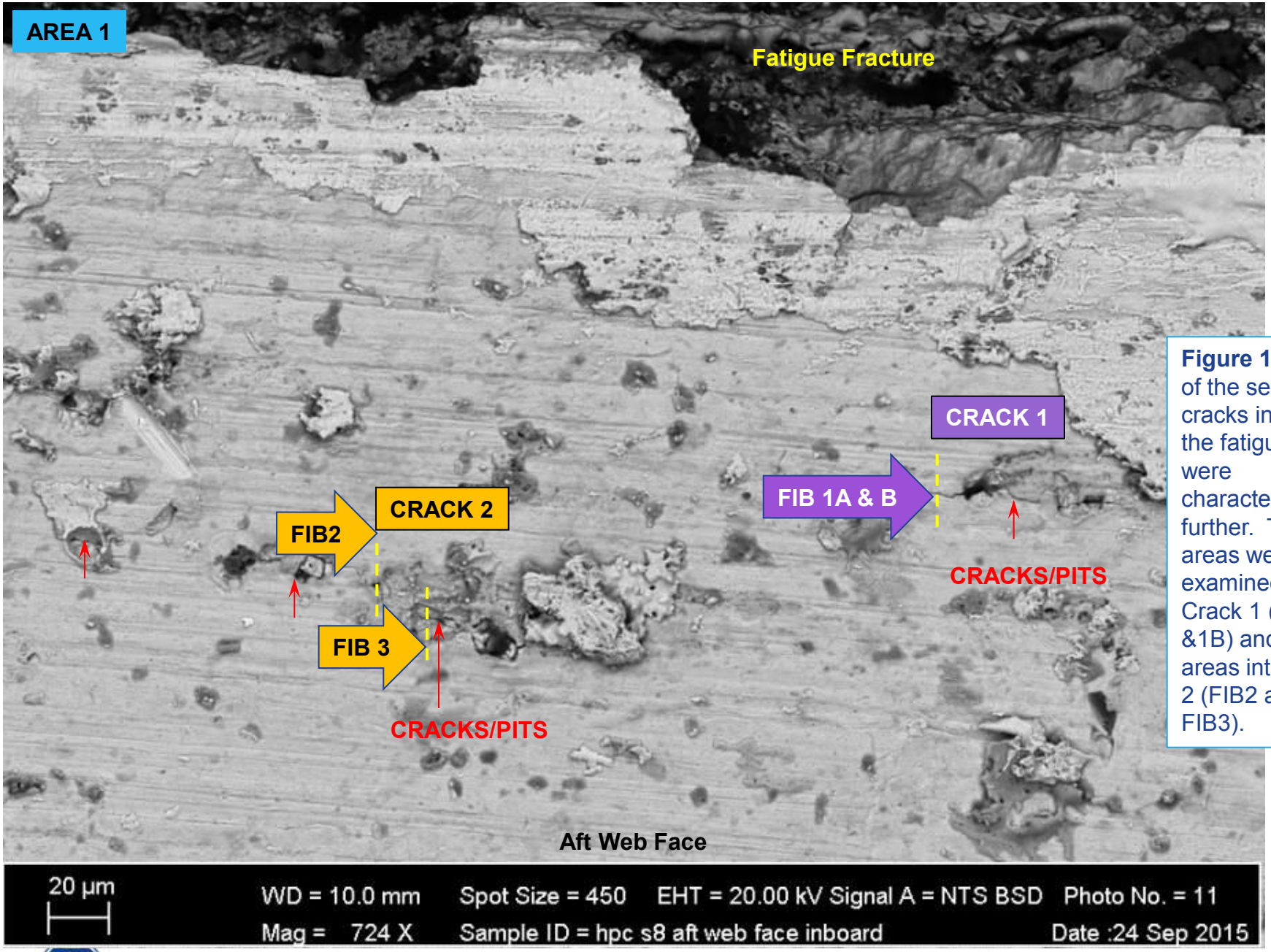

Figure 105: Two of the secondary cracks inboard of the fatigue region were characterized further. Two FIB areas were examined into Crack 1 (FIB 1A &1B) and two areas into Crack 2 (FIB2 and FIB3).

CRACK 1

FIB1A (Deep Trench #1)

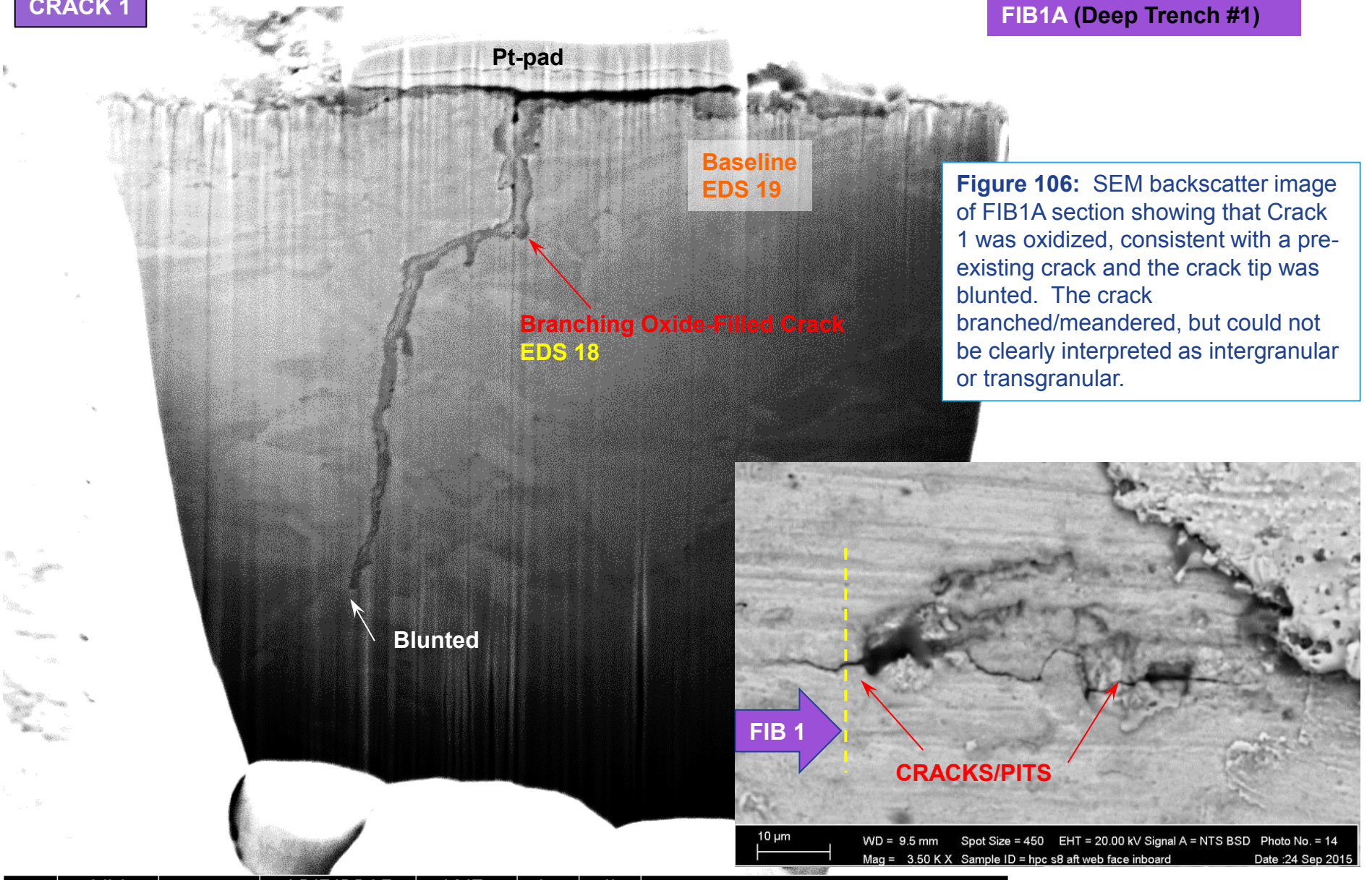

Figure 106: SEM backscatter image of FIB1A section showing that Crack 1 was oxidized, consistent with a pre-existing crack and the crack tip was blunted. The crack branched/meandered, but could not be clearly interpreted as intergranular or transgranular.

CRACK 1 **FIB1A (Deep Trench #1)**

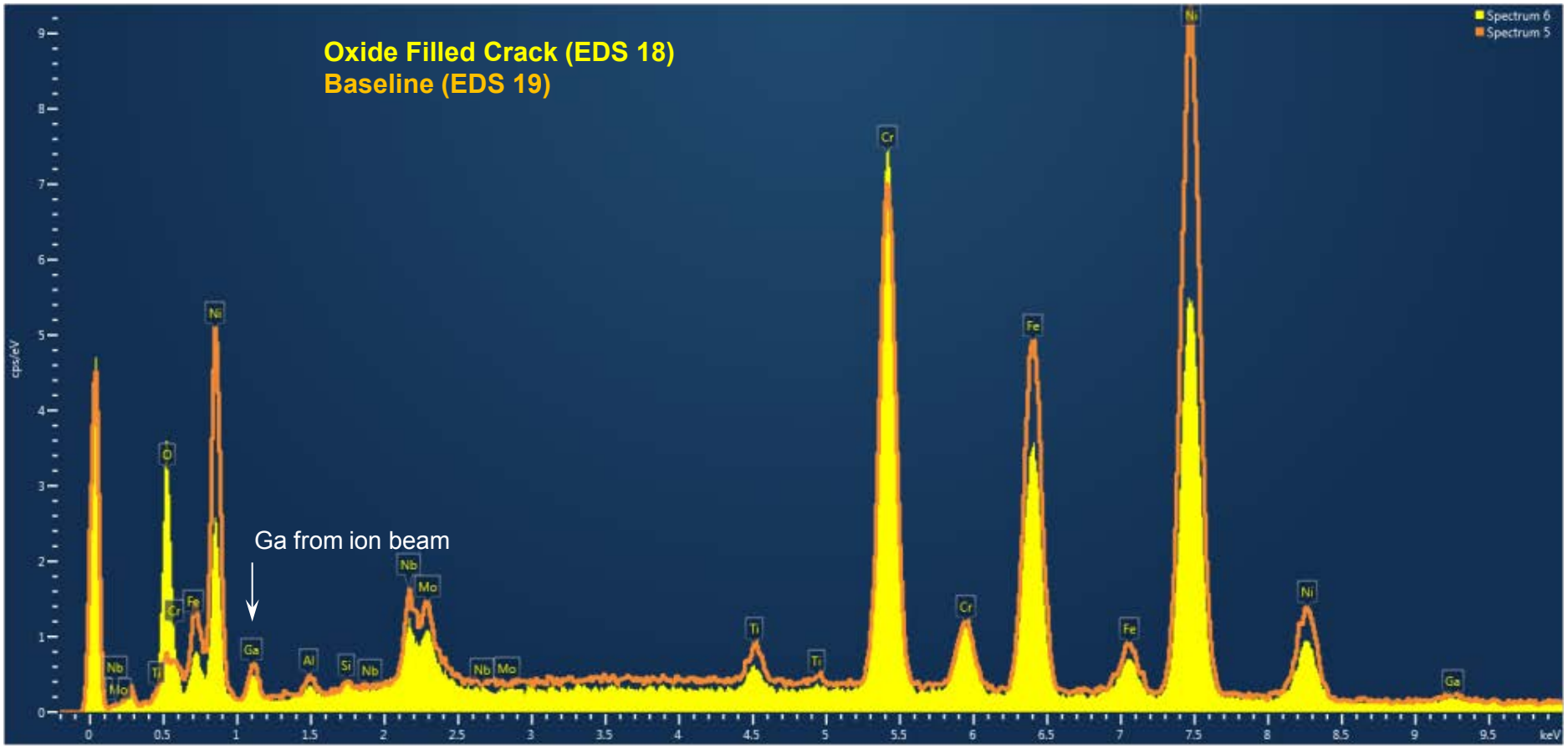

Figure 107: Superimposed EDS spectra showed that the crack only had elements consistent with oxidized base material (EDS 18), with the baseline shown in EDS 19. No detrimental species were found in the oxides.

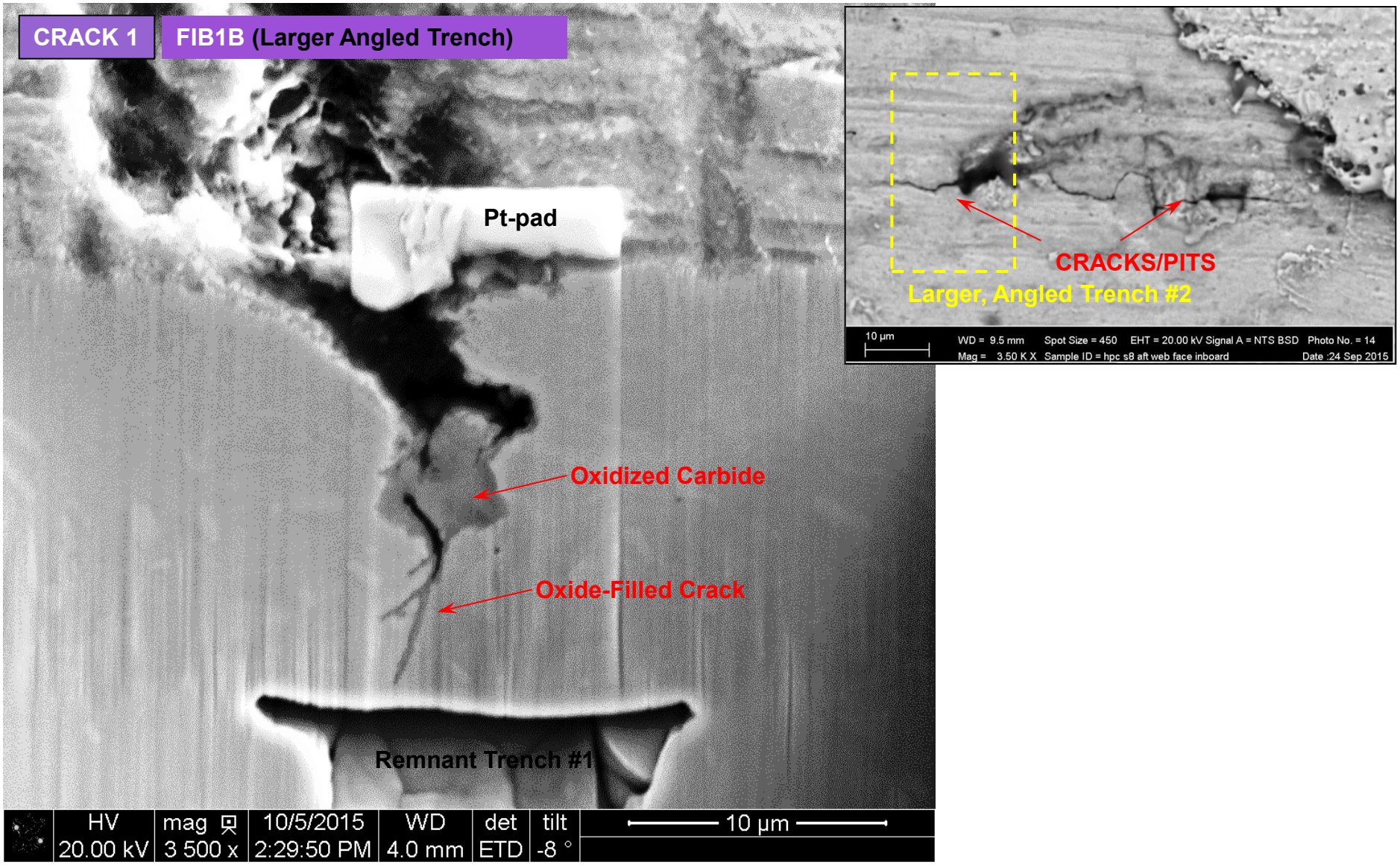

Figure 108: A second trench was generated into secondary Crack 1 that showed cracking below the surface carbide with branched features.

CRACK 1 **FIB1B (Larger Angled Trench)**

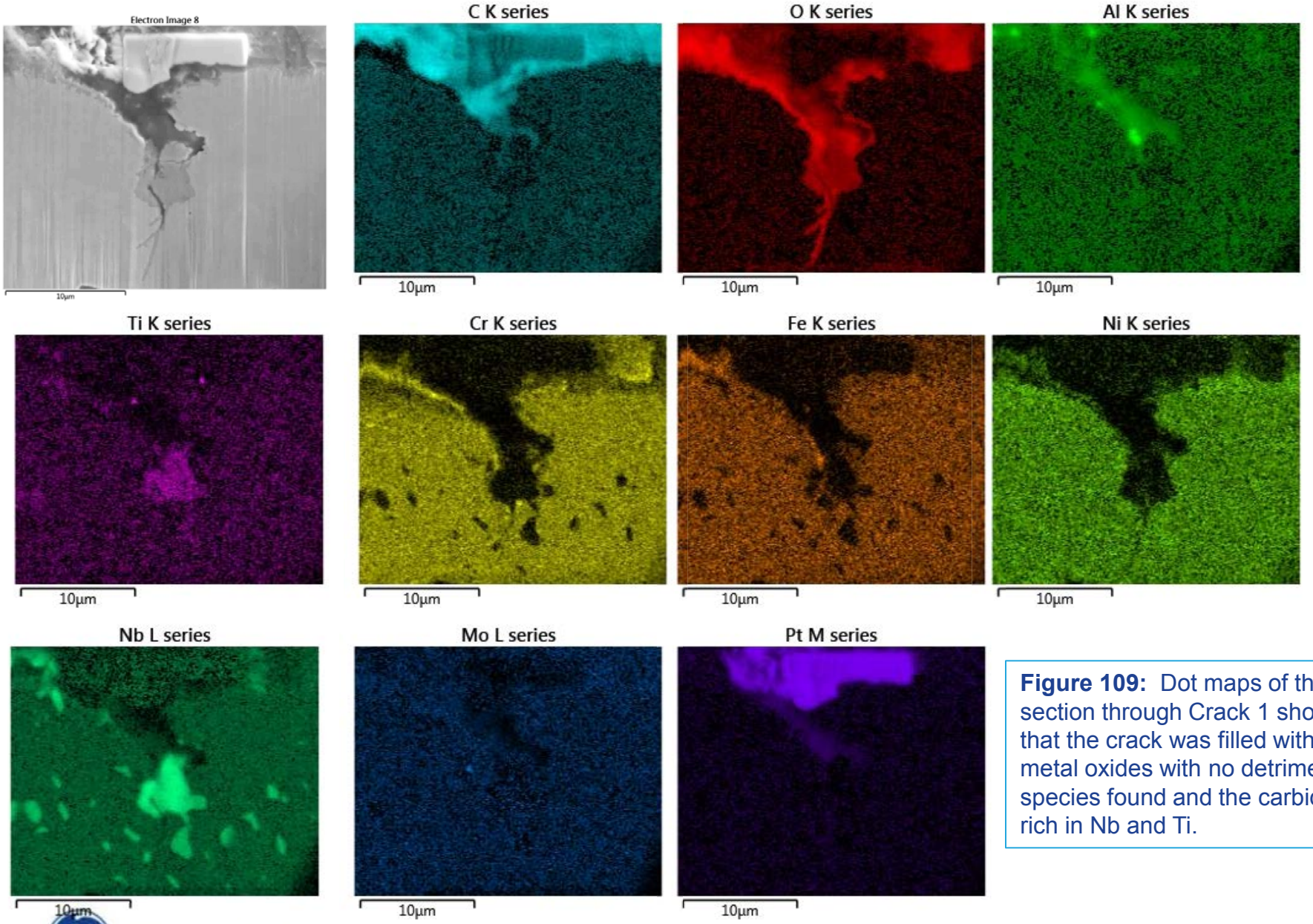

Figure 109: Dot maps of the FIB section through Crack 1 showed that the crack was filled with base metal oxides with no detrimental species found and the carbide was rich in Nb and Ti.

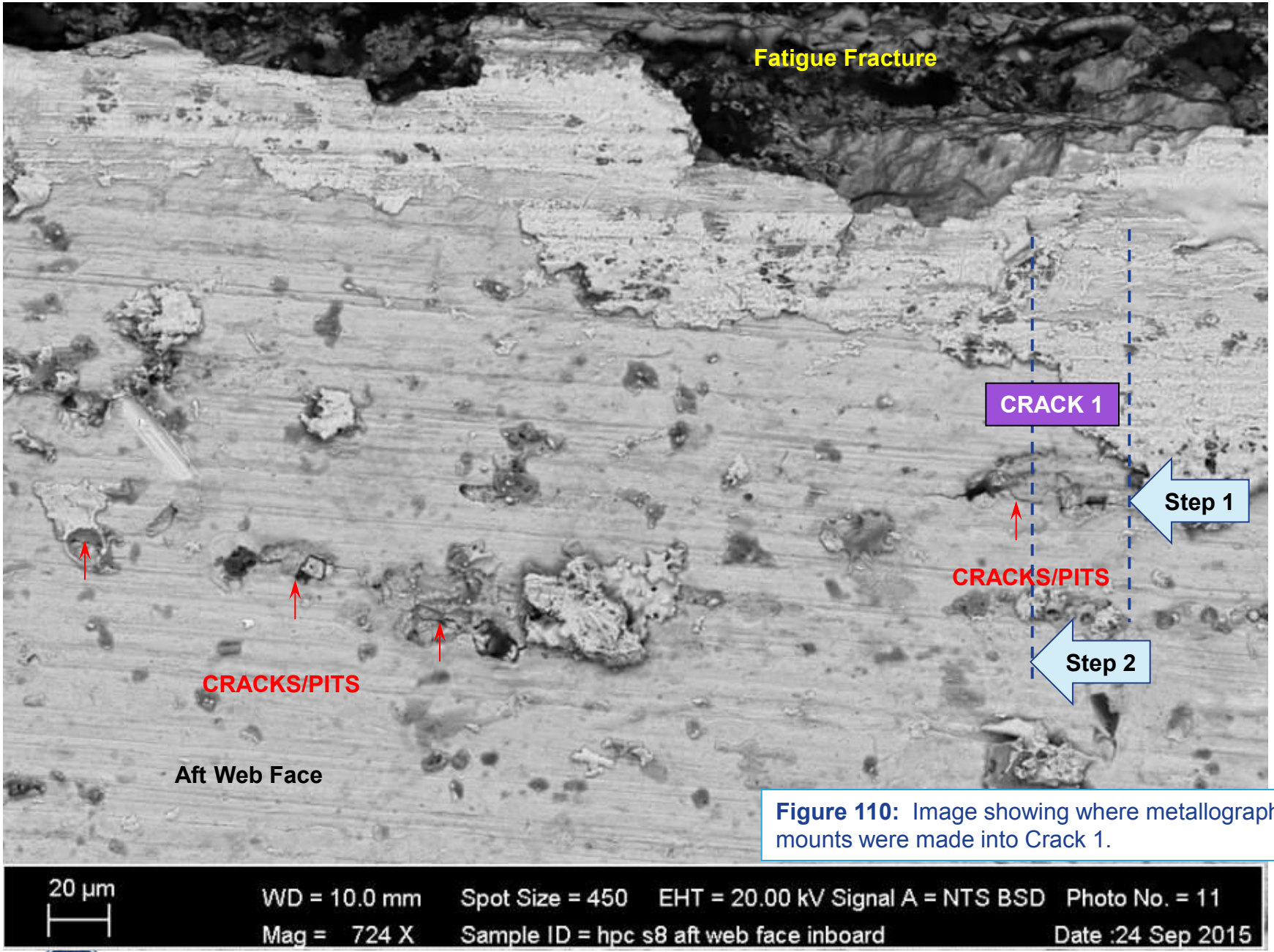

Figure 110: Image showing where metallographic mounts were made into Crack 1.

CRACK 1- Mount (Step 1)

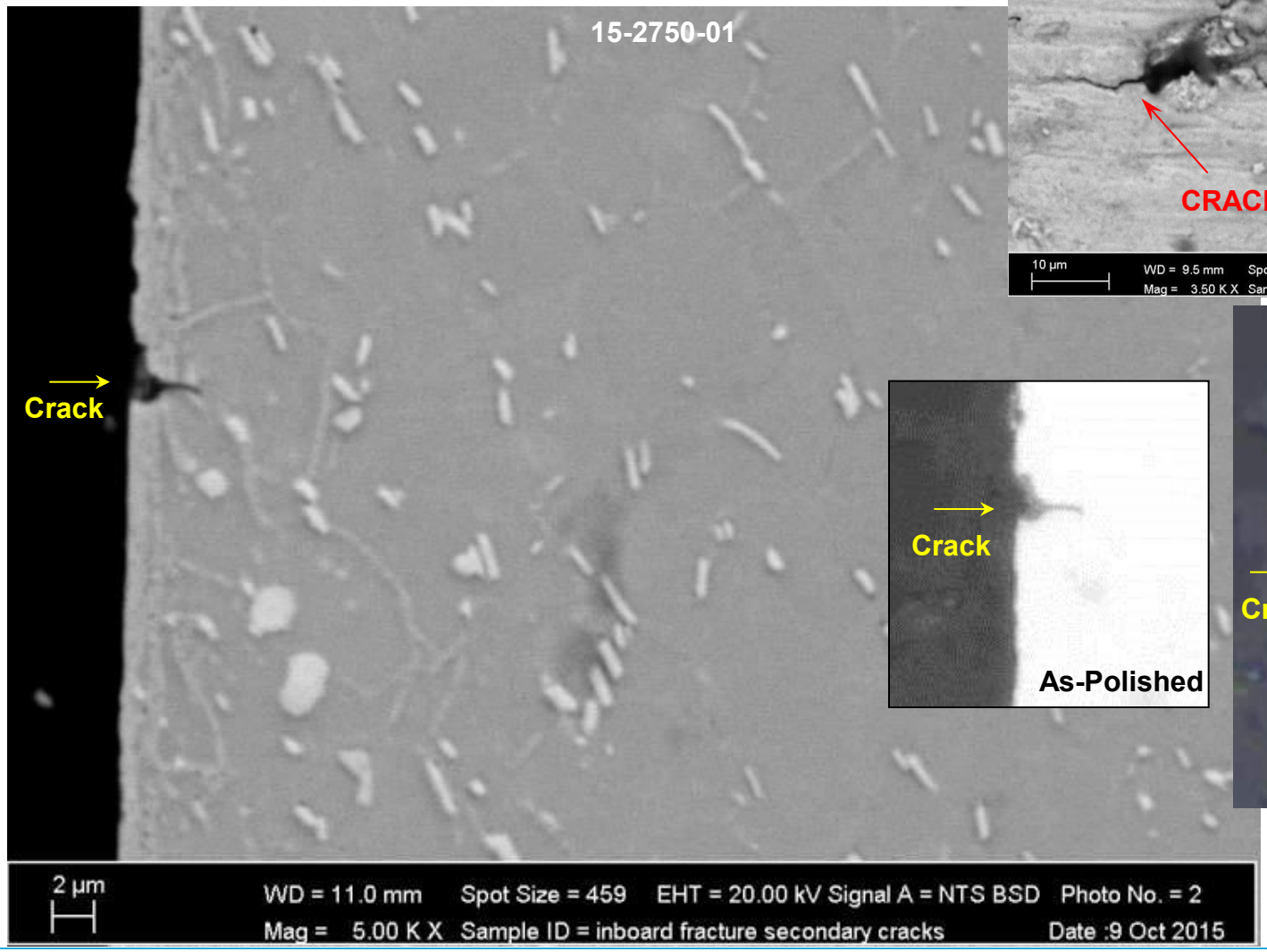

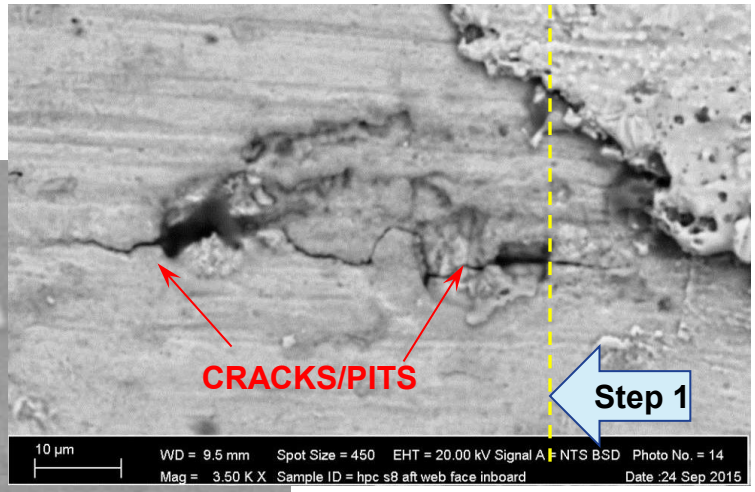

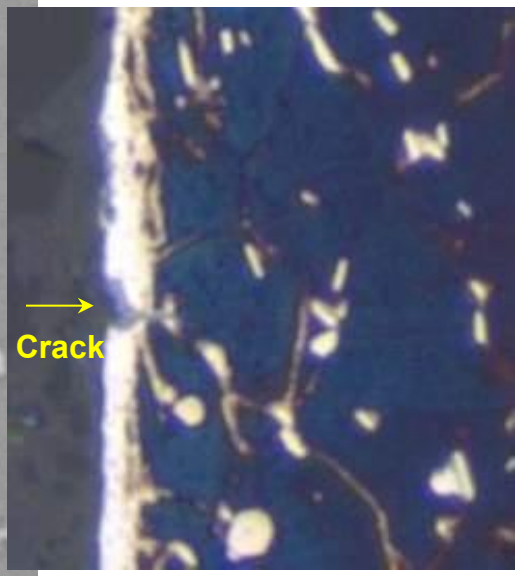

Electrolytic Phosphoric Etch

Figure 111: As-polished and etched views of the mount through Crack 1 that showed cracking normal to the surface that in the plane of polish was less than 0.1 mil deep and had more transgranular features. No microstructural anomalies/damage was noted.

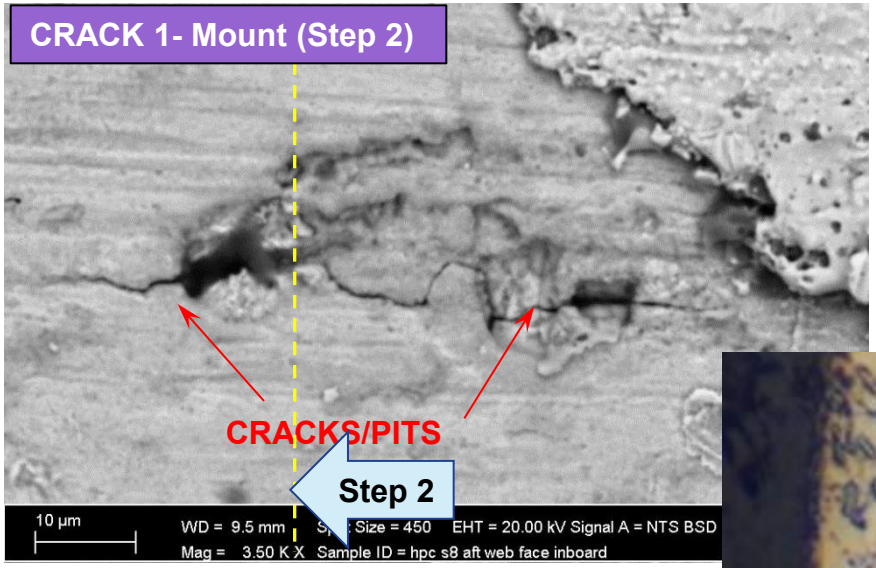

Figure 112: View of the 2nd step polish into Crack 1 that was still shallow and the local microstructure showed no damage/anomalies.

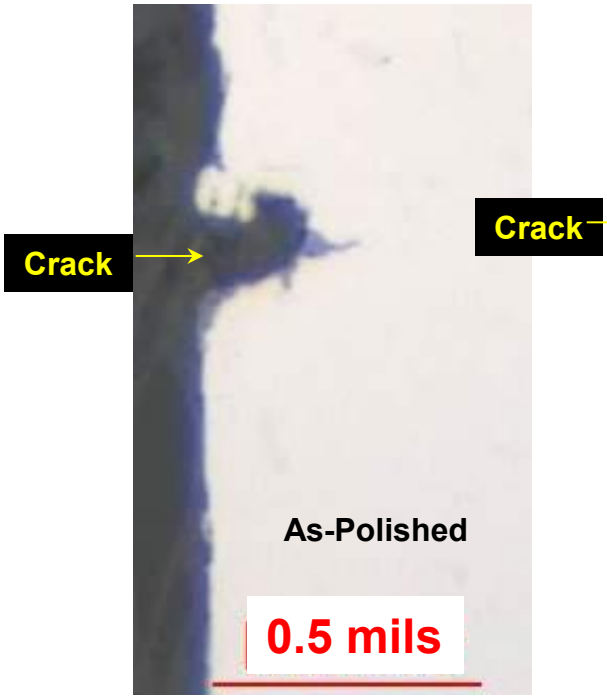

15-2750-01 **Kalling's Etch**

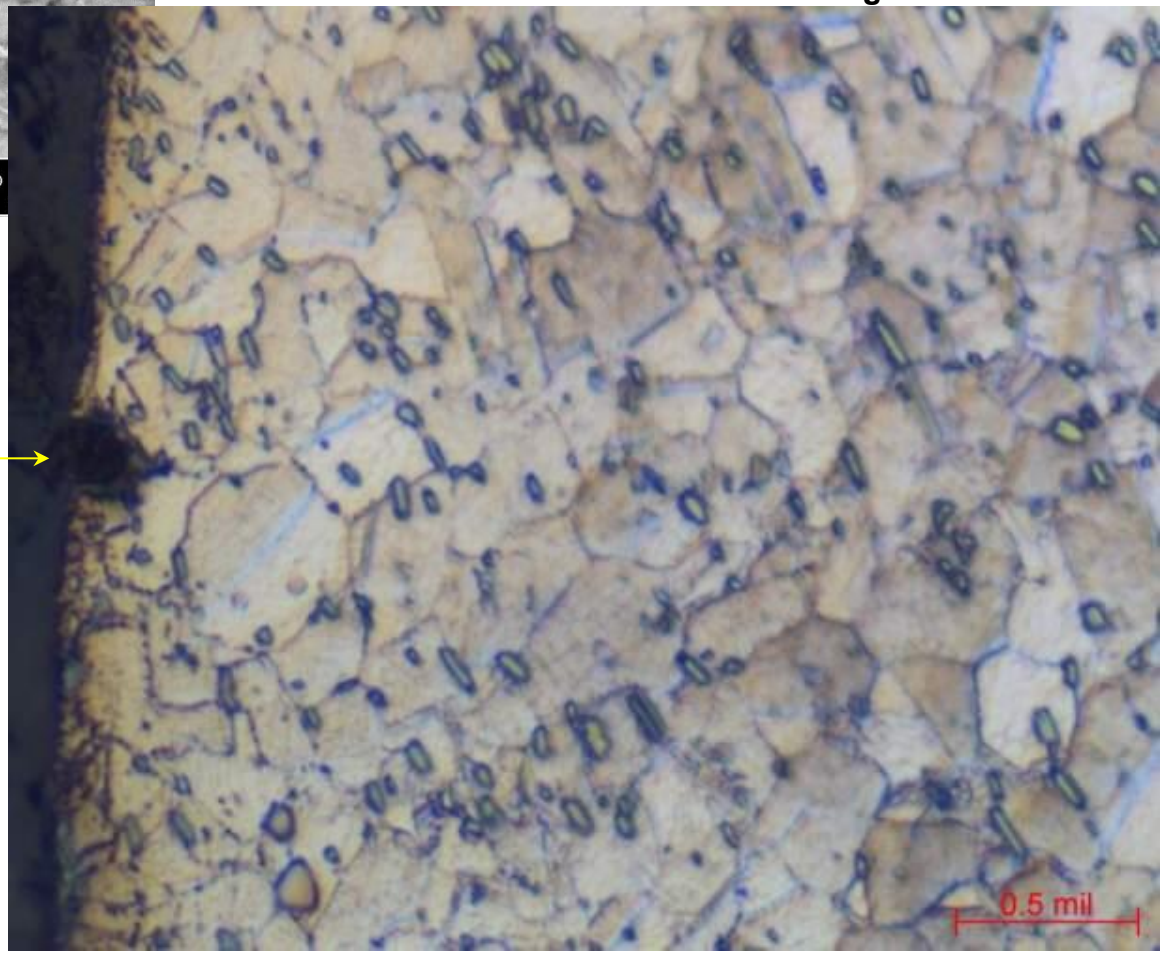

CRACK 2 **FIB 2** (Edge of Crack 2)

Figure 113: SEM views of Crack 2 showing where the 2 FIB trenches were made.

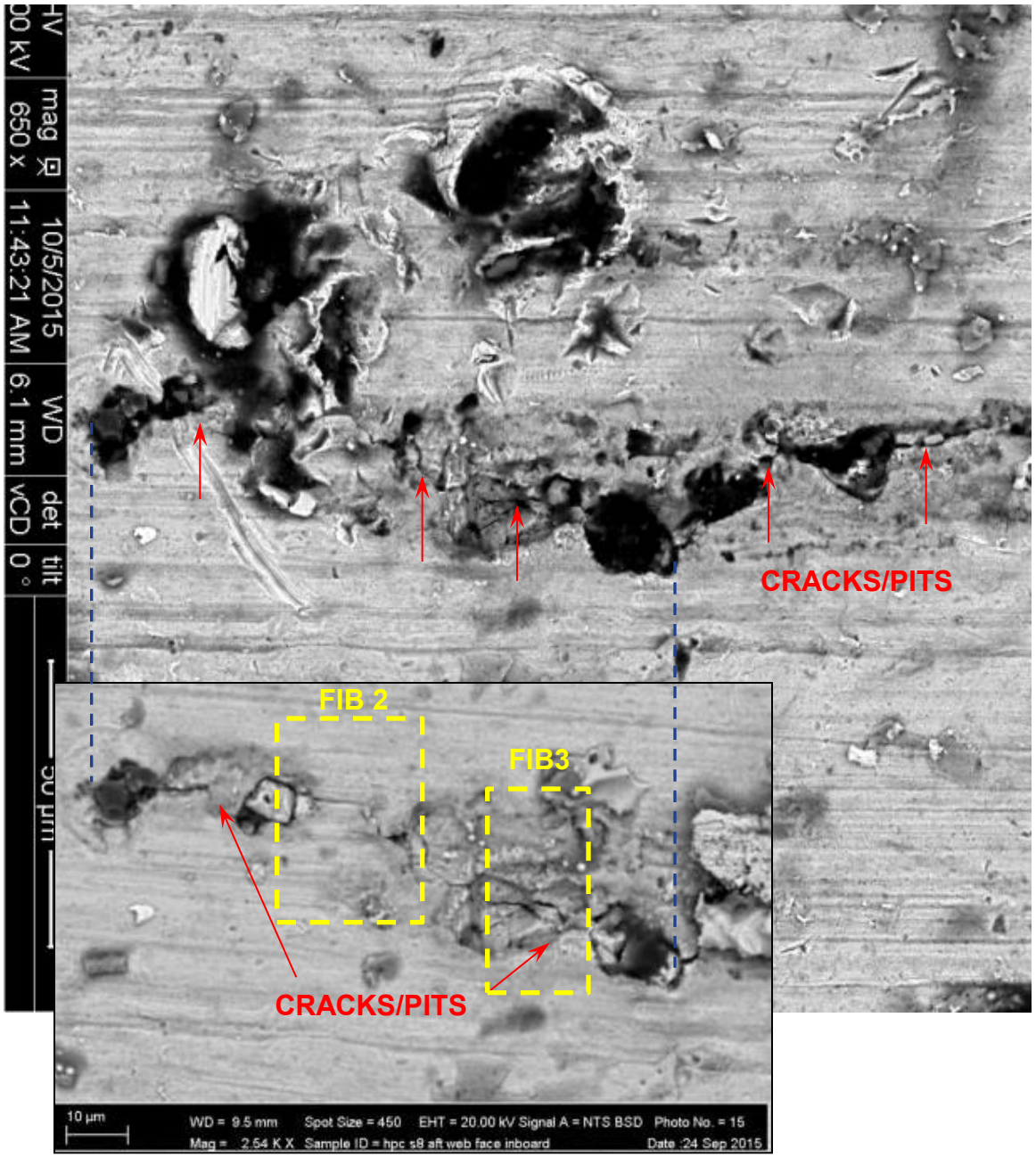

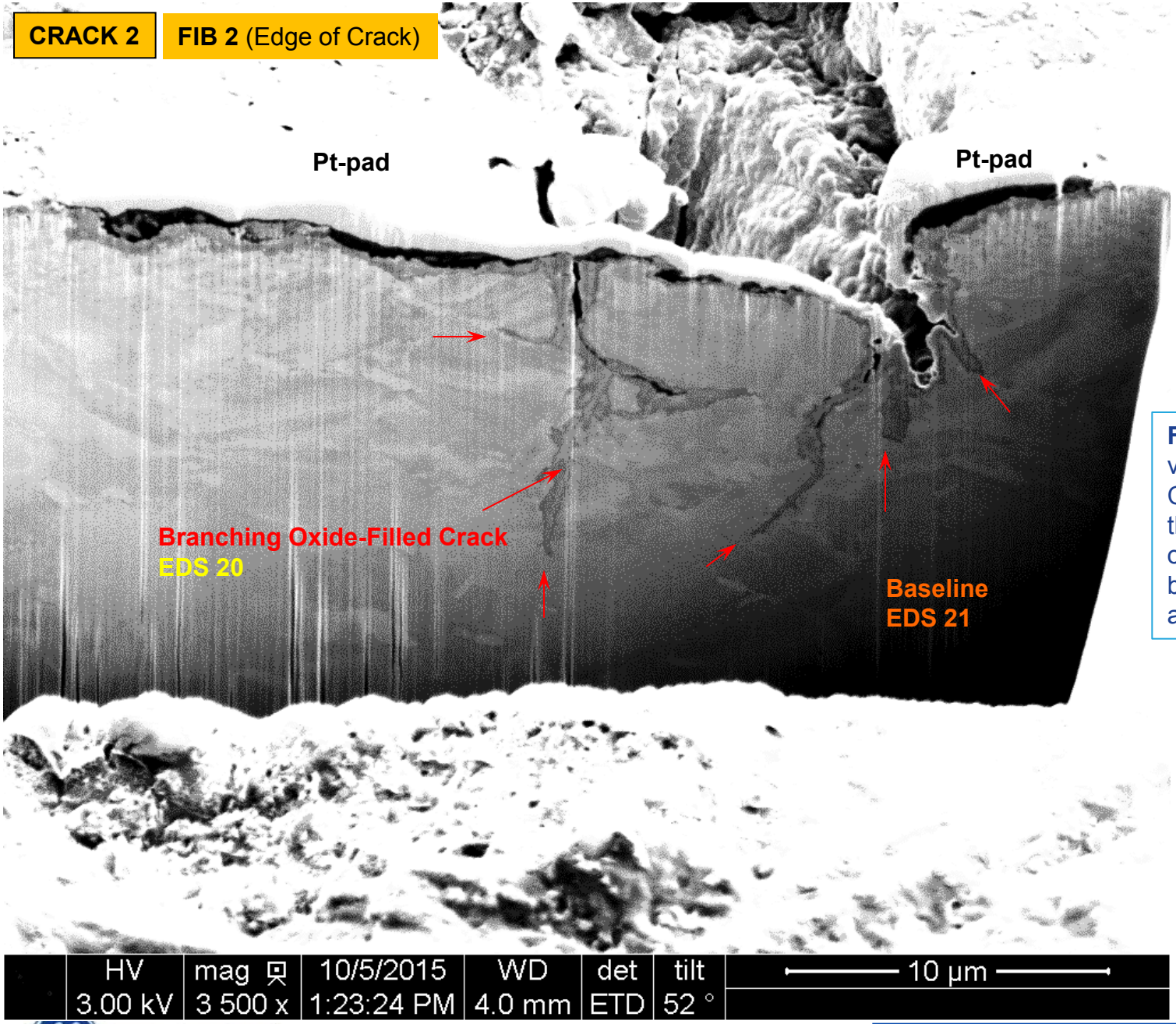

Figure 114: SEM views of FIB 2 into Crack 2 showing that the cracks were oxidized, branched/meandering and appeared blunted.

CRACK 2 **FIB 2** (Edge of Crack)

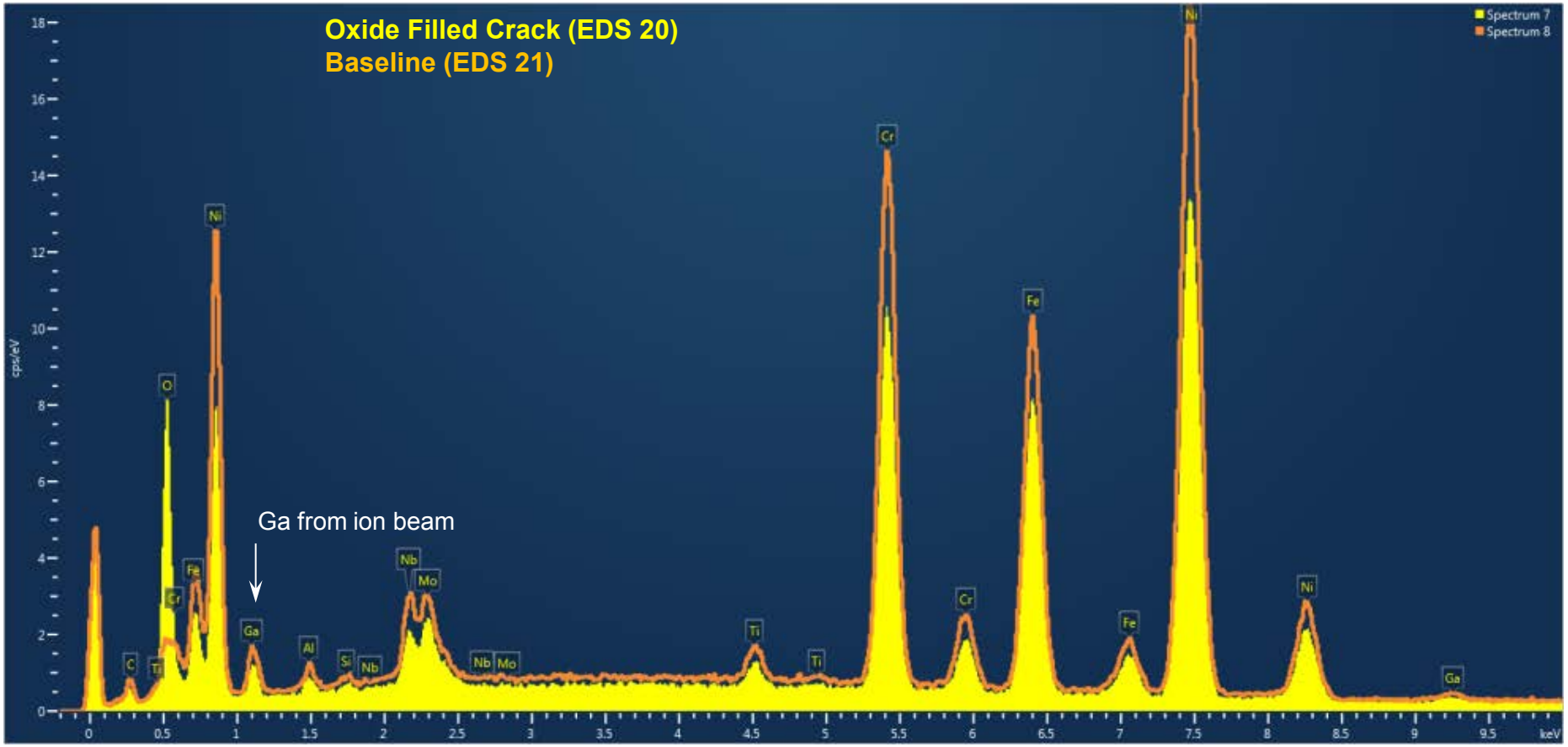

Figure 115: Superimposed EDS spectra showed that the crack only had elements consistent with oxidized base material (EDS 20), with the baseline shown in EDS 21. No detrimental species were found in the oxides.

CRACK 2 **FIB 3** (Within Crack 2)

Figure 116: SEM views of FIB 3 into Crack 2 showing that the cracks were oxidized, branched/meandering, and appeared blunted.

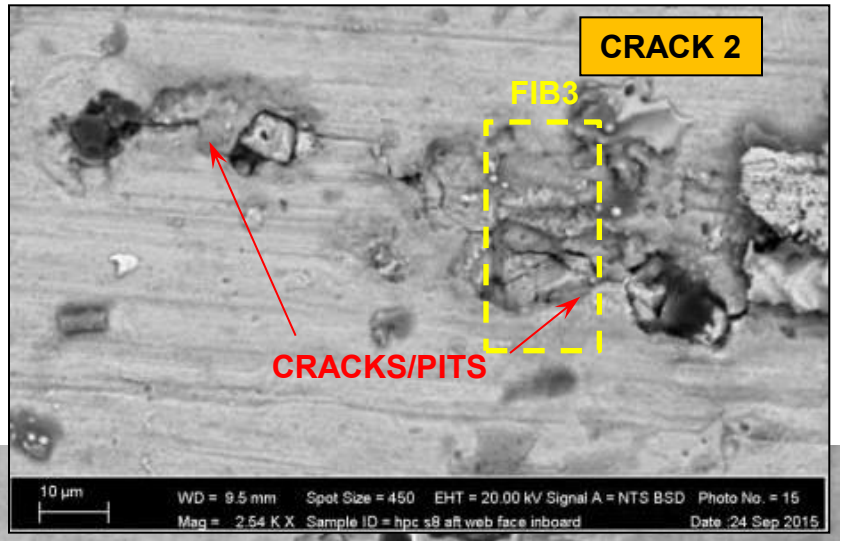

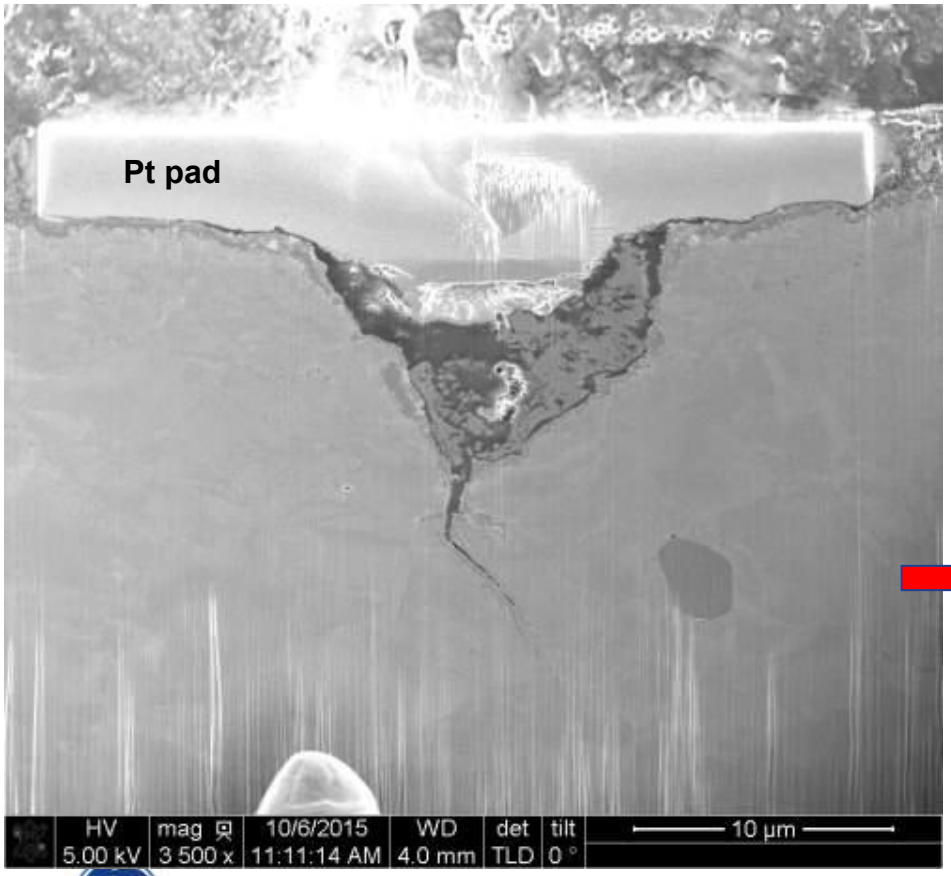

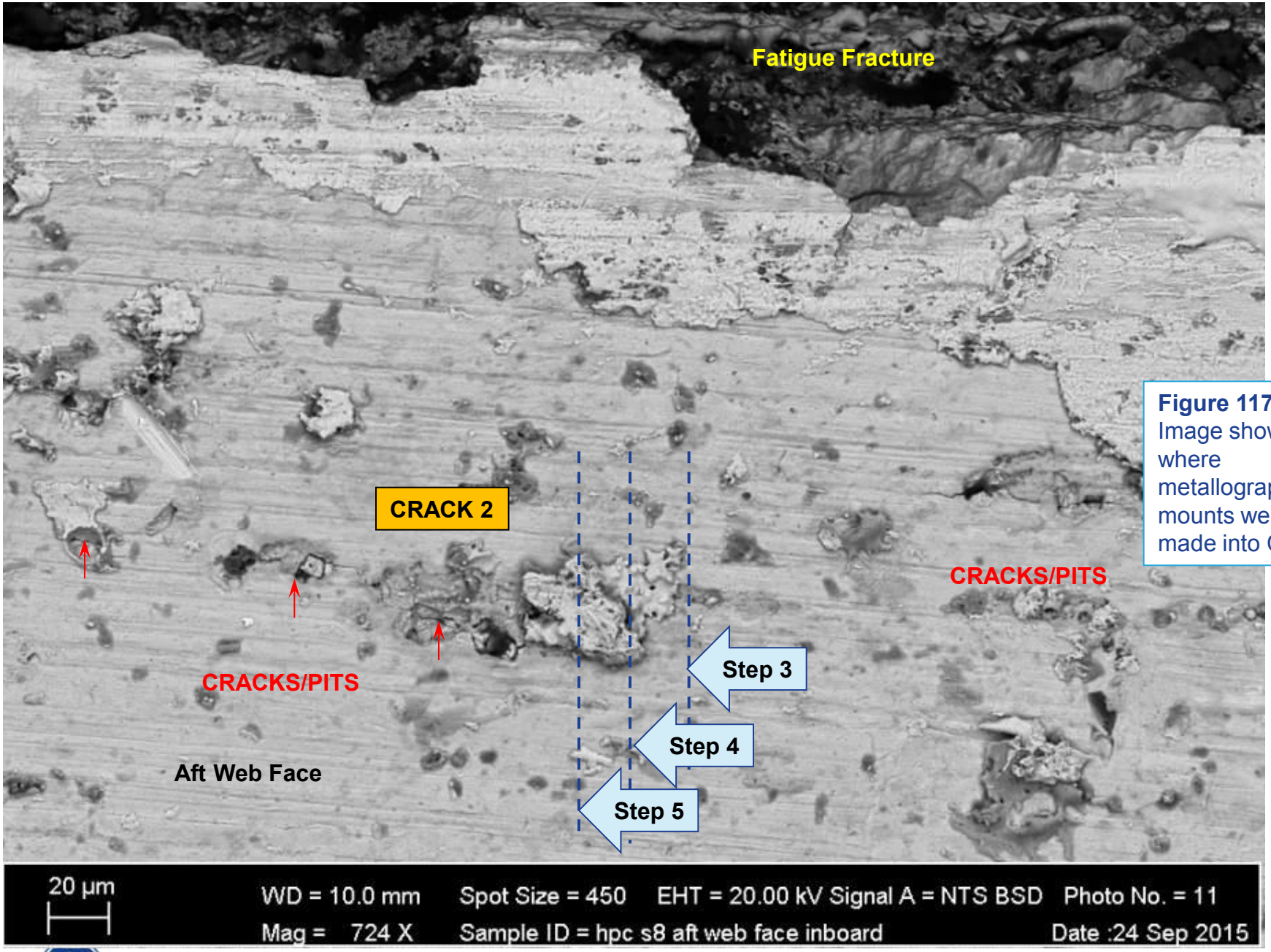

Figure 117: Image showing where metallographic mounts were made into Crack 2.

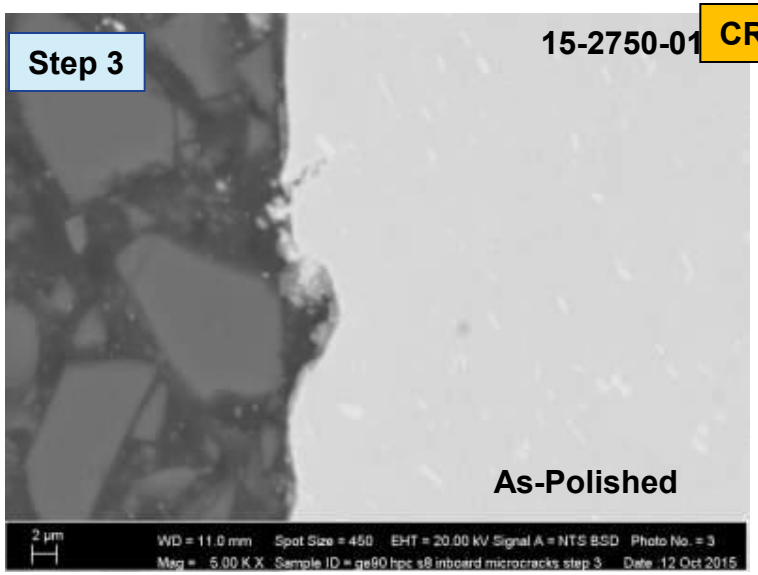

Step 4→ Not documented

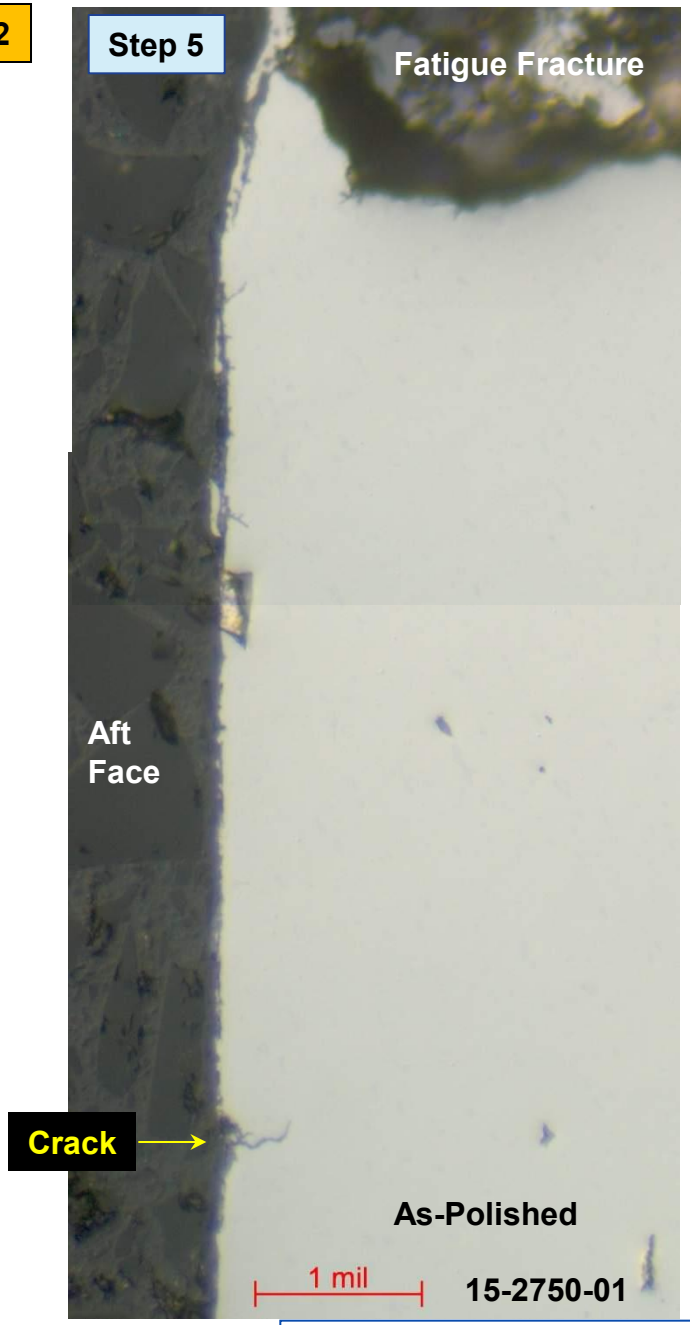

Figure 118: Three step polishes approximately 1 mil apart were made into Crack 2. At the last step (step 5 in the mount) a meandering crack approximately 0.5 mils long was observed extending from the carbide area.

CRACK 2- Mount (Step 5)

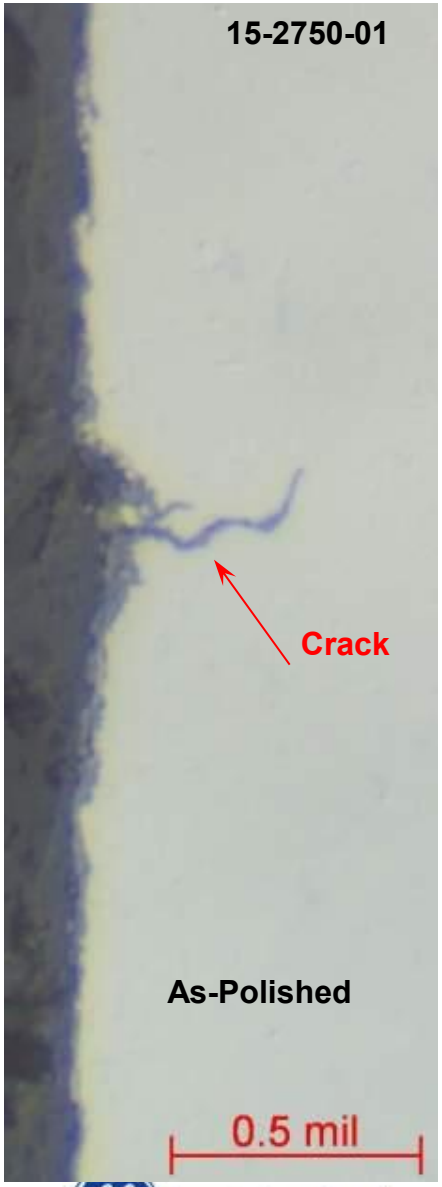

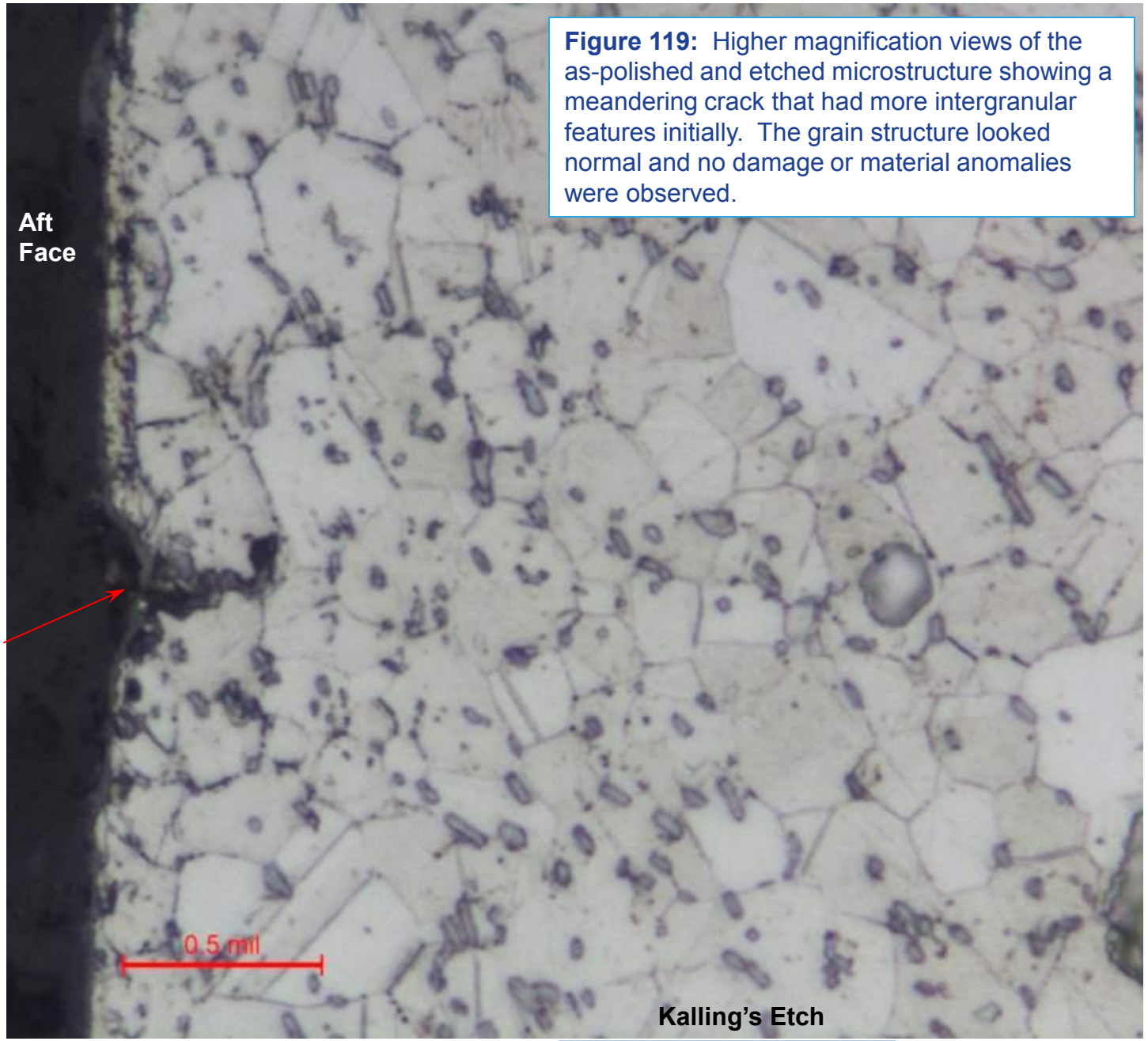

Figure 119: Higher magnification views of the as-polished and etched microstructure showing a meandering crack that had more intergranular features initially. The grain structure looked normal and no damage or material anomalies were observed.

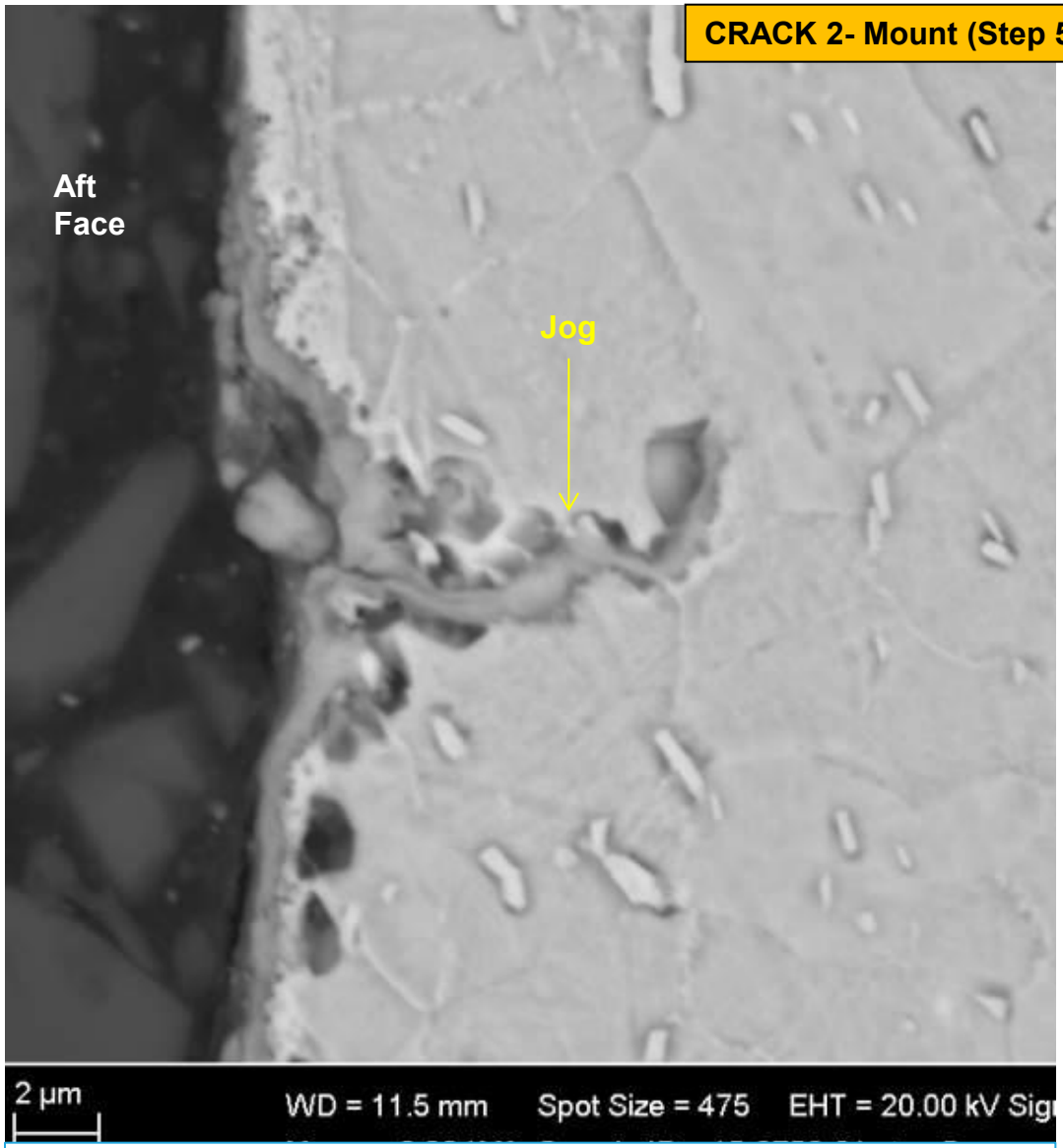

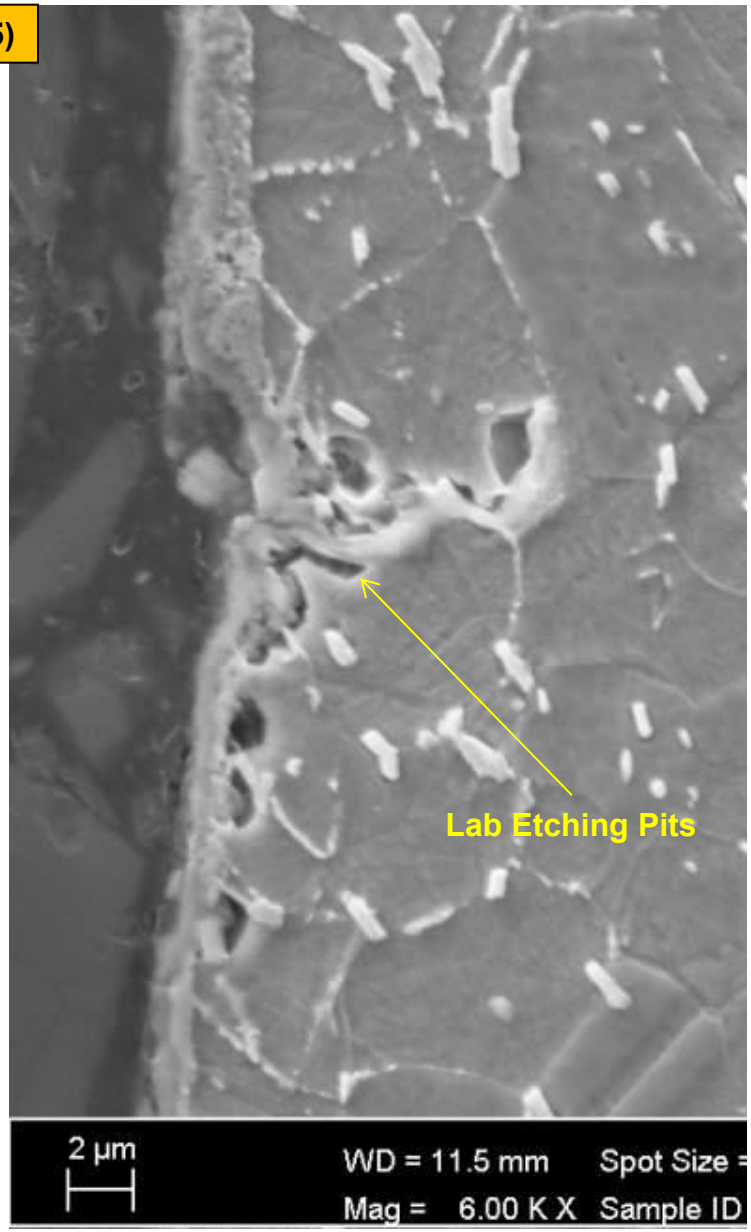

Figure 120: SEM views of the etched structure showing a meandering oxidized crack extending at the base of carbides with no material anomalies noted. The crack was more intergranular initially.

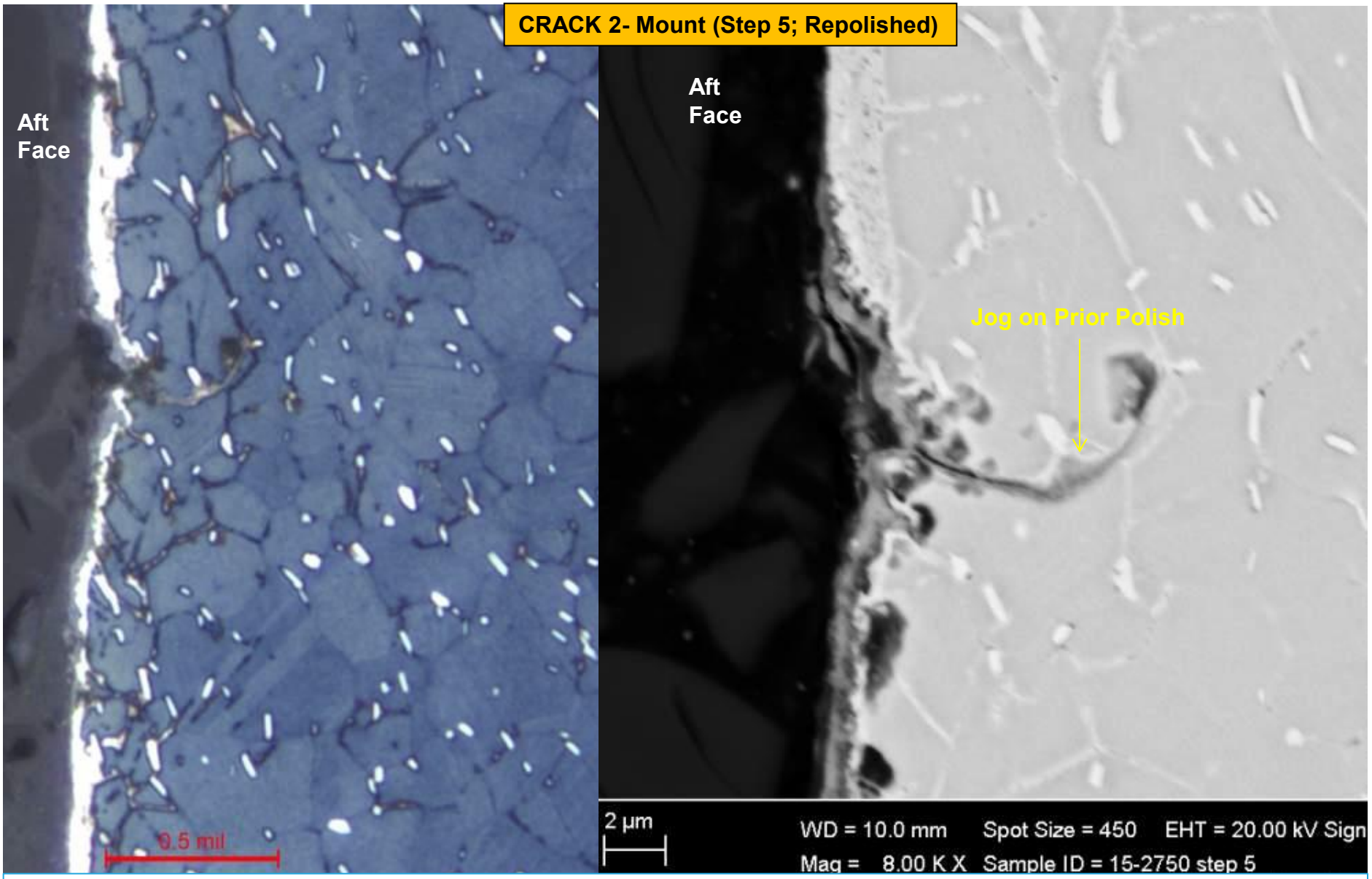

Figure 121: After re-polishing and etching the crack was found to have more intergranular features initially and then a transgranular end region.

Appendix A

Remainder of Event 8-10 spool

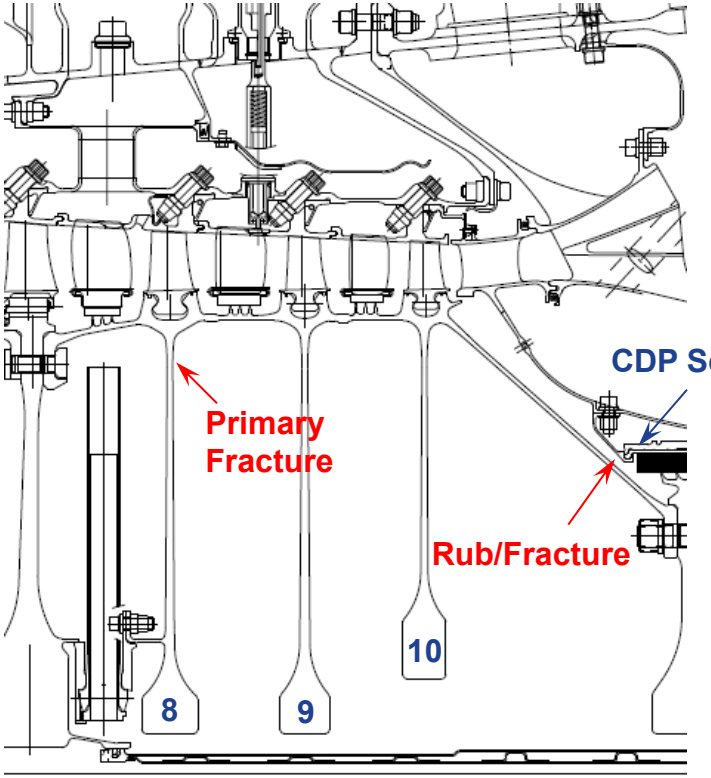

Appendix A1: Optical views of the aft end of the 8-10 spool showing the part markings and fracture locations. There was a fracture forward of the stage 9 disk, consistent with the liberation event, and the aft cone arm was fractured consistent with rubbing against the static structure/CDP seal.

Appendix A2: Representative views of the stage 9 disk forward arm fracture consistent with overstress.

Appendix B

8-10 Spool of similar vintage with no reported anomalies, S/N GWNHA139

GWNHA139- S8 Web

Forward

Aft

Appendix B1: Representative views of the stage 8 disk forward and aft web faces from spool S/N GWNHA139 showing visual differences in the peening with the forward side being more pronounced, like the event disk.

Appendix C

Residual Stress Profiles

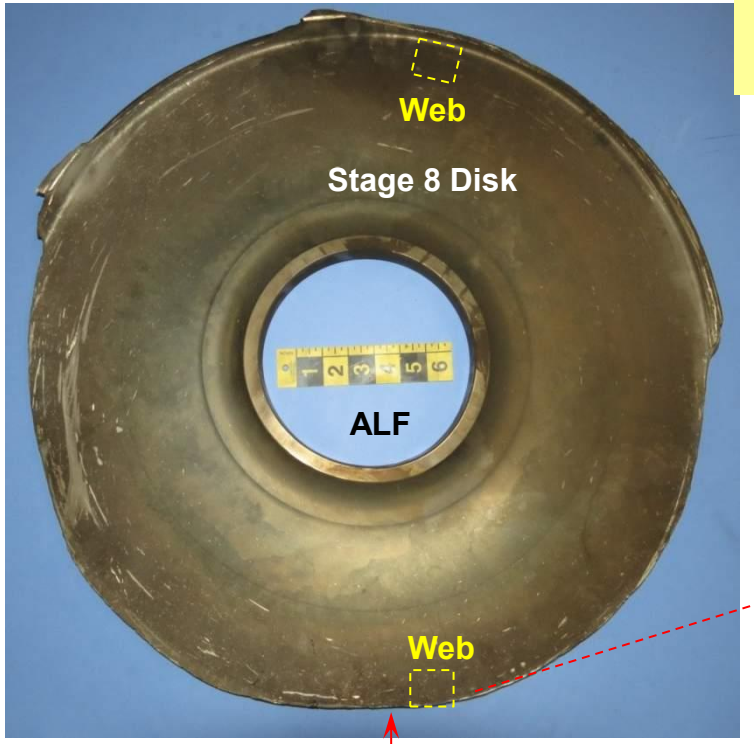

HA236
Event Disk

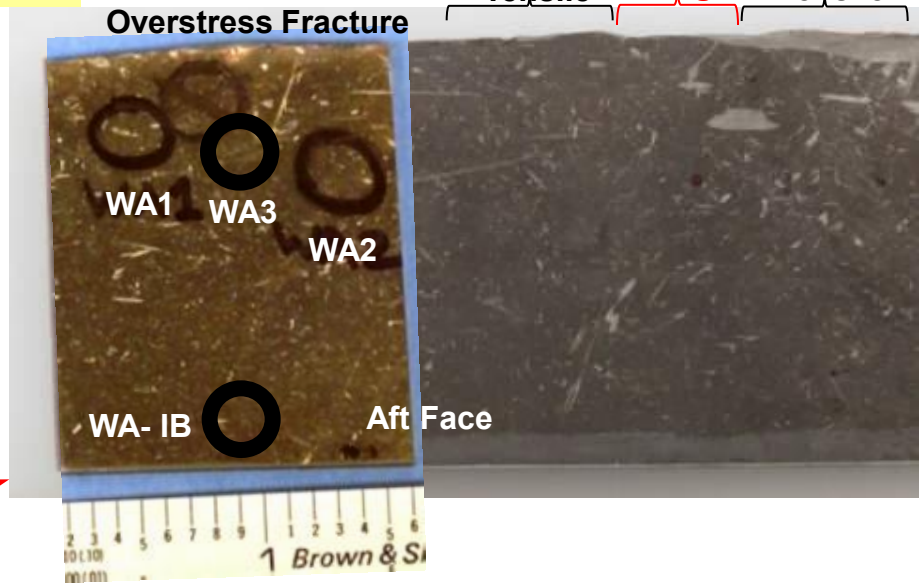

Nomenclature:
WA = web aft face
WF = web forward face
IB = inboard

HA139
Sister disk

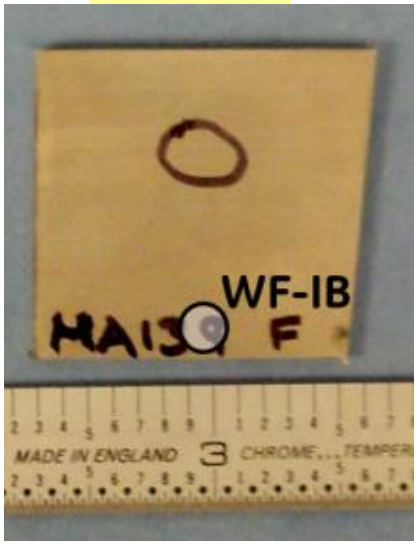

HA269
Sister disk2

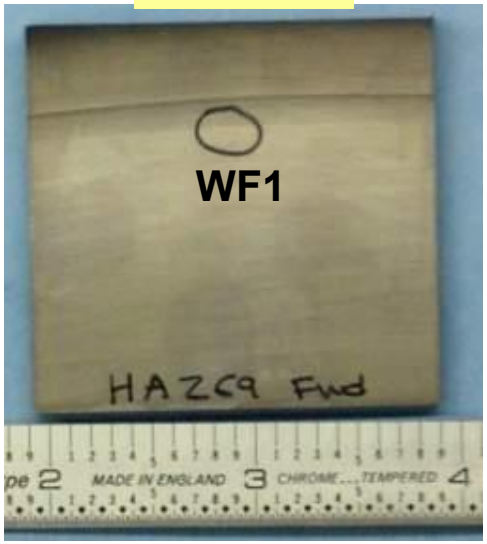

Appendix C1: Optical views showing where residual stress measurements were taken on both the aft and corresponding forward sides of the web near the fatigue region of the event disk (top images). Readings were also taken on both faces of 2 sister comparison disk webs of similar vintage (S/N GWNHA139 and GWNHA269) and on the diametrically opposite side of the fatigue region on the event disk.

Appendix C2: Residual stress results taken from the forward web of the event disk and 2 comparison disks.

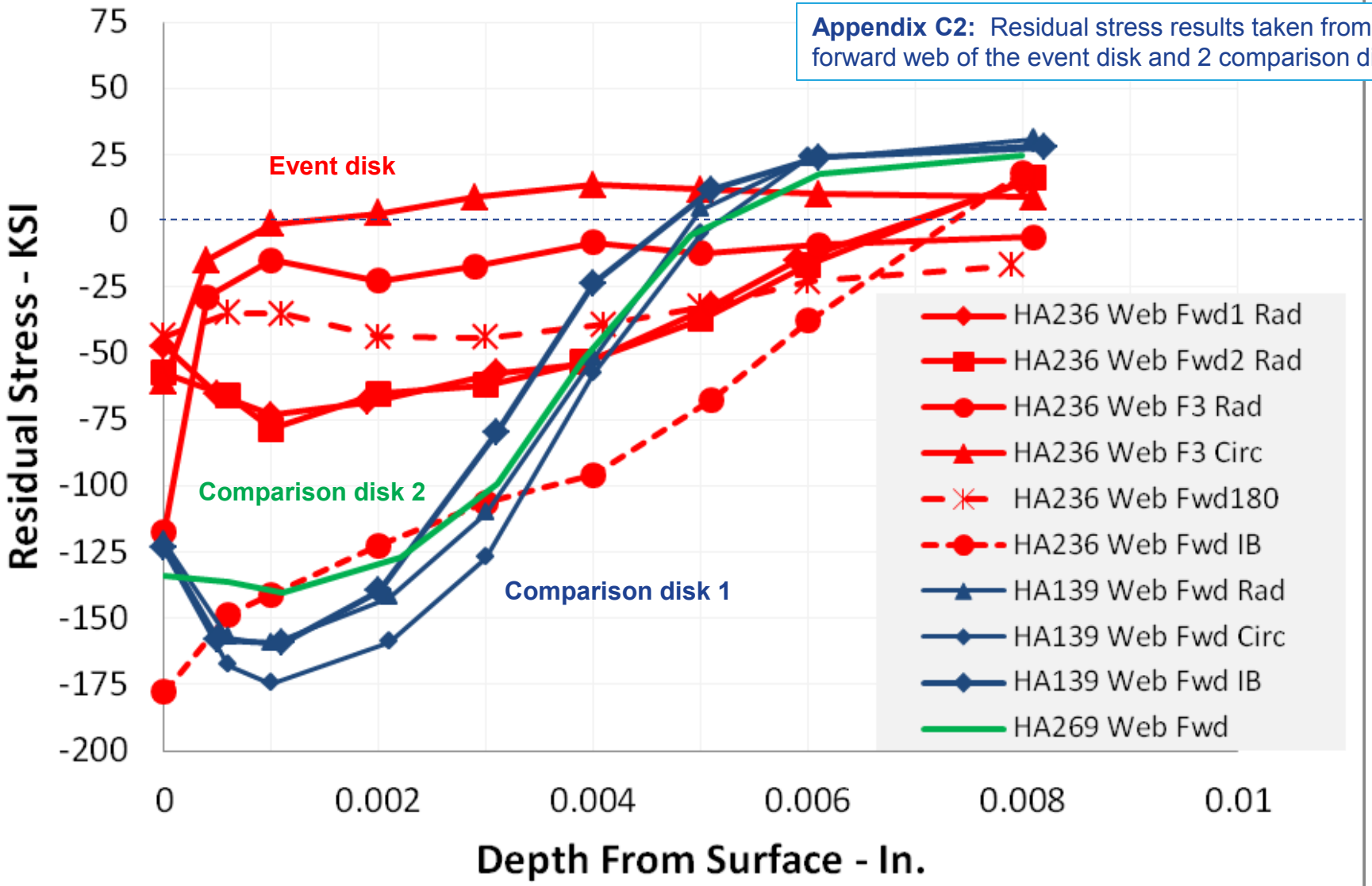

Aft Web Measurements

Appendix C3: Residual stress results taken from the aft web of the event disk and 2 comparison disks.

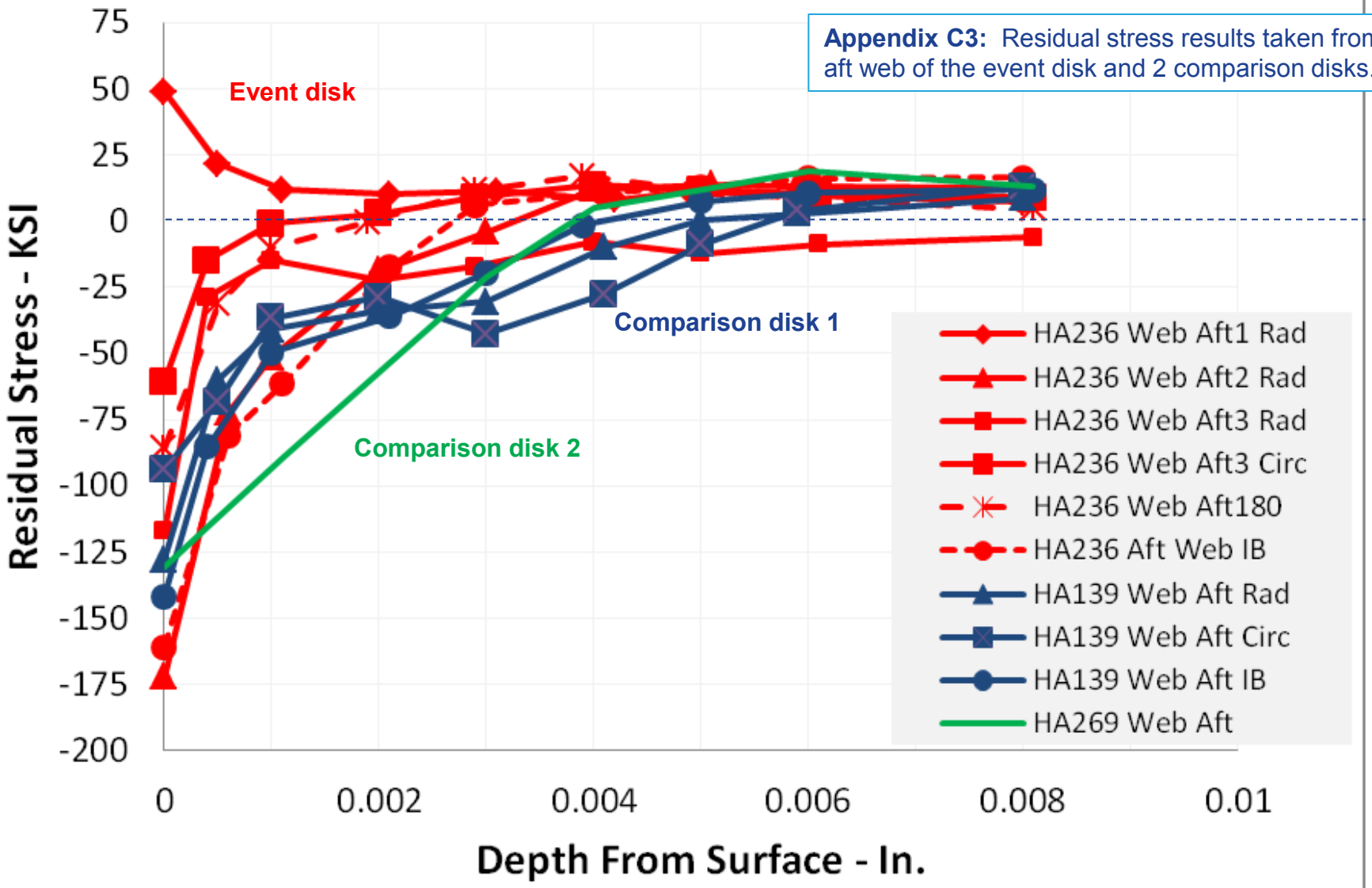

Appendix D

Event and Sister Part LCF Testing

Internal LCF Specimens

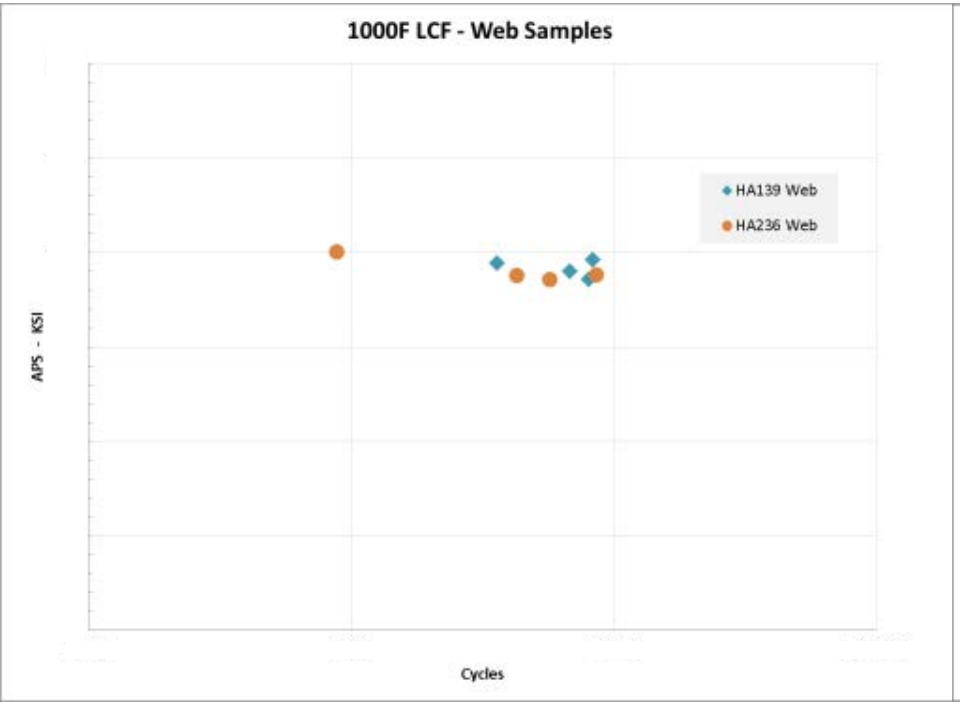

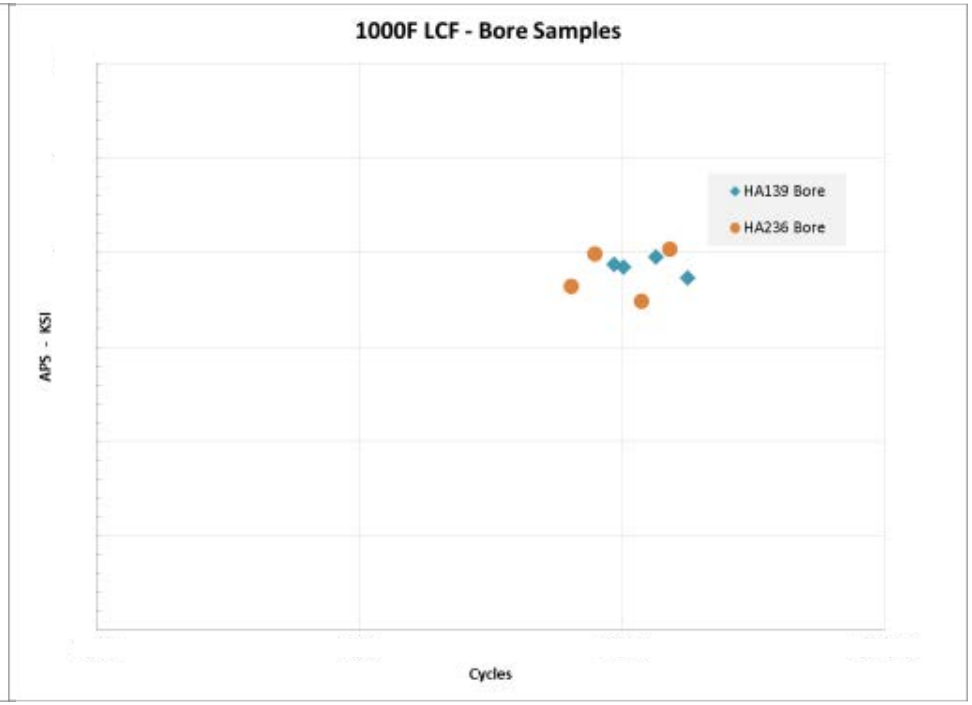

Appendix D1: Radial sheet specimens from the web and circumferential smooth bar bore specimens were taken from the event disk (GWNHA236) and comparison disk (GWNHA139). The results from the tests revealed nearly equivalent lives and all were within GE design expectations for the material.

Surface LCF Specimens

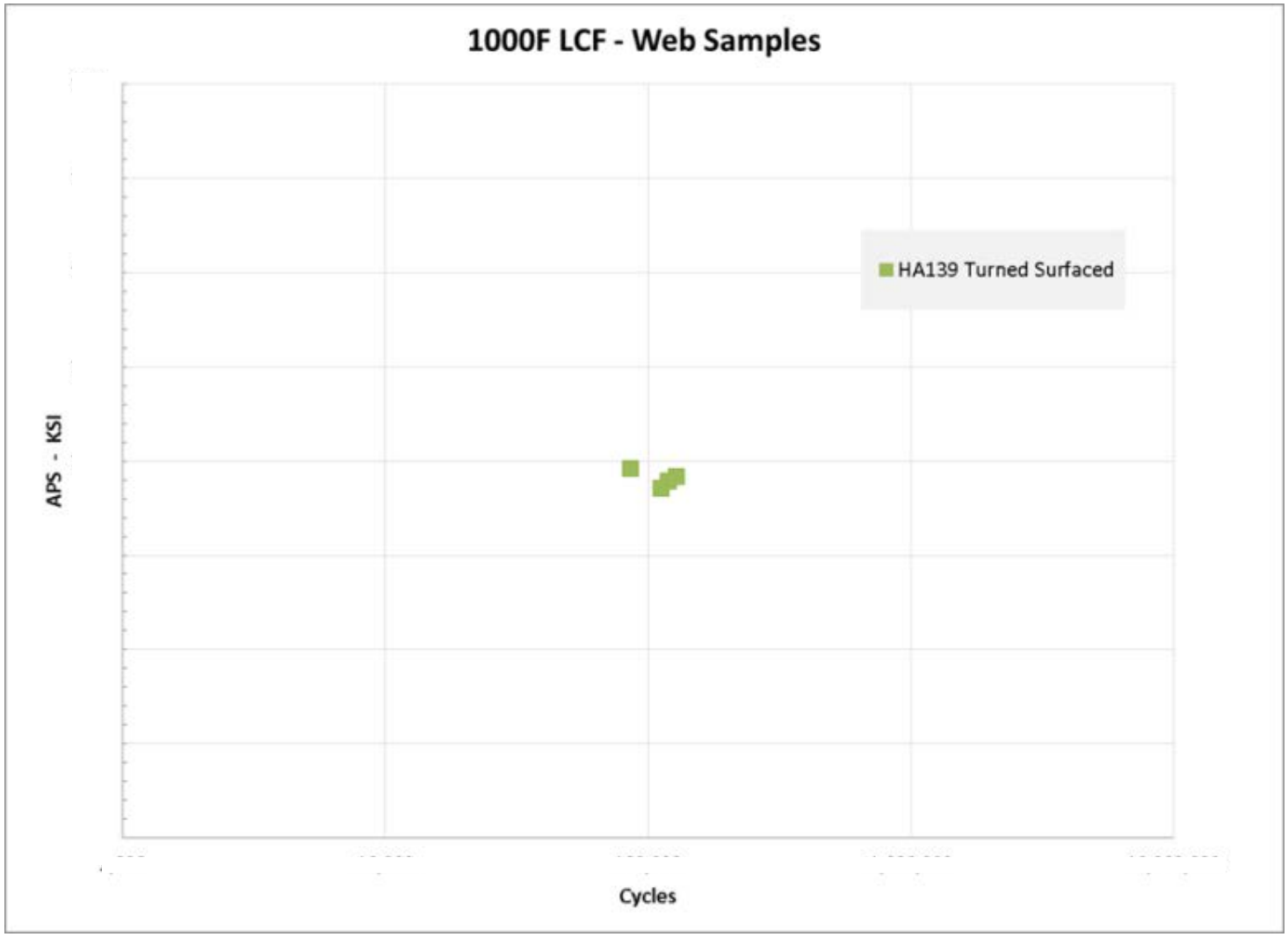

Appendix D2: Radial sheet specimens were tested from comparison disk S/N GWNHA139 with an as-manufactured aft surface with similar peening features to the event disk and the fatigue lives were at/near the average data for DA718. The event part was not tested due to event-related surface damage.

Appendix E

Characterization of Web Surfaces

GE GRC

Electron Backscatter Diffraction

How Does It Work?

An SEM is used to accelerate electrons towards a grounded, conductive sample. These electrons penetrate the sample and are scattered within the material. Some of the electrons exit and collide with the CCD screen of an EBSD camera. Electrons scattered by the periodic crystalline lattice appear as pairs of parallel light and dark lines (Kikuchi Lines). Crystallographic information (orientation, retained strain, etc.) can be derived from the pattern of these lines.

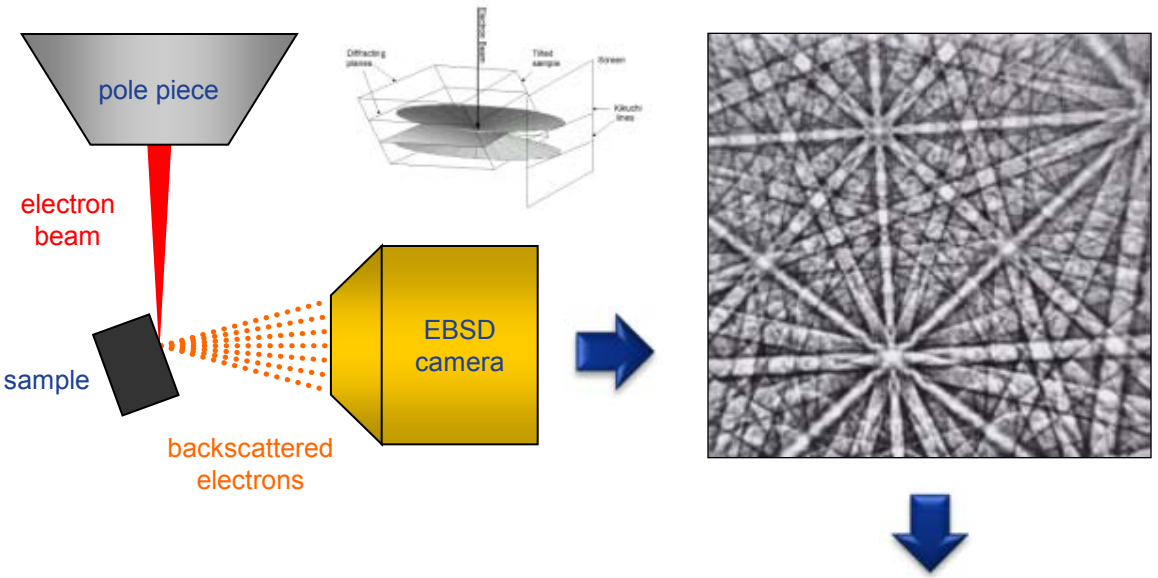

EBSD at a Glance

Generally, a FEG-SEM examining a Ni, Ti, or Fe alloy can achieve a spatial resolution of ~25nm in X, ~50nm in Y. The diffraction signal is generated in approximately the top 25nm of the sample, so it is necessary to have a flat surface with a high quality prep (i.e., vibratory polishing).

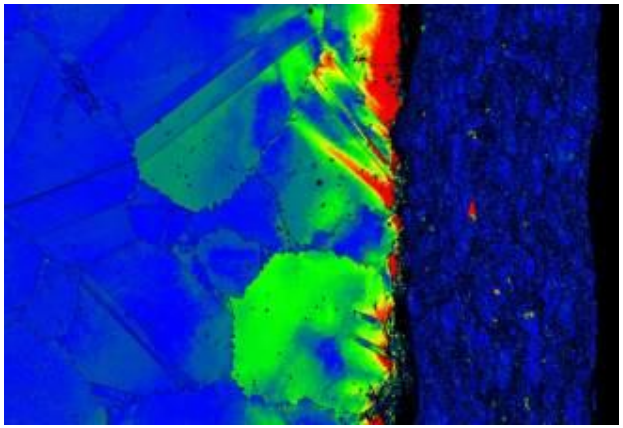

Grain Misorientation – color at every point indicates level of misorientation from its parent grain orientation. Grains with colors closer to the red end of the scale have more retained work

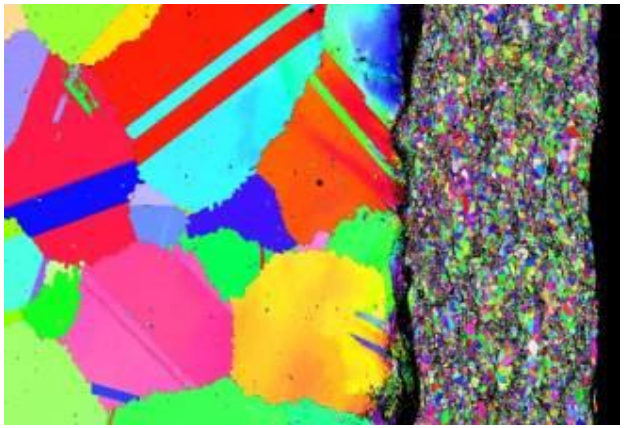

Inverse Pole Figure - colors in IPF maps identify the crystallographic orientation (e.g. red is 001) parallel with the specified sample axis

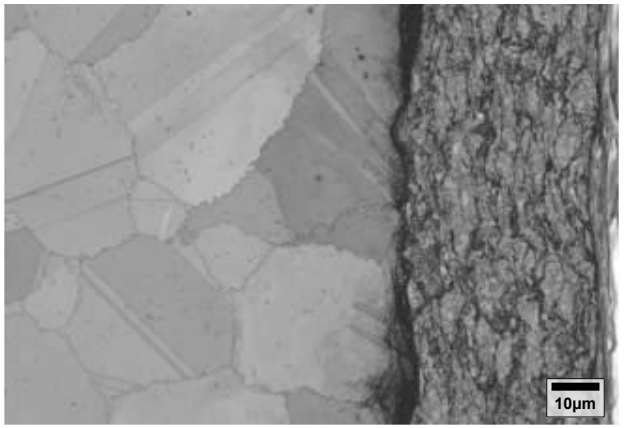

Band Contrast - indicates the contrast/quality of the diffraction pattern observed at every point of the map (black=worst, white=best).

Appendix E1: General description of EBSD.

Backscattered Electron Images

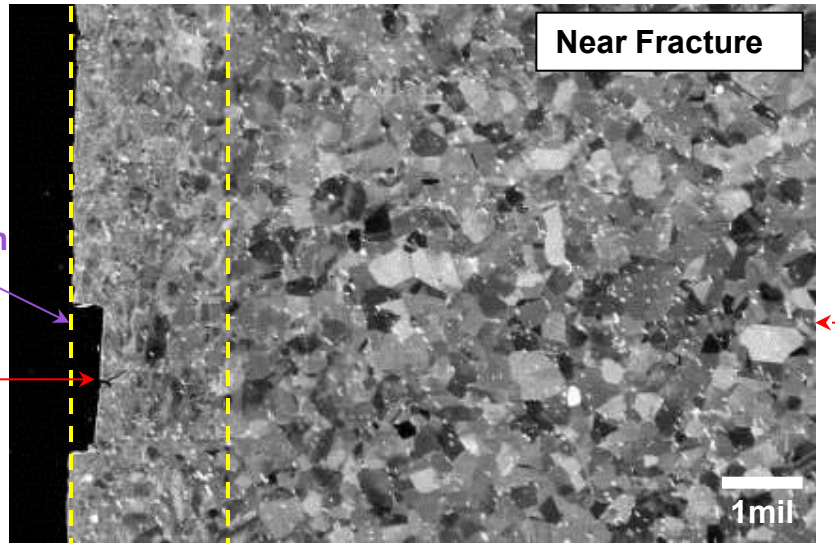

Radially Inboard Mount (EMP15-2750-01)

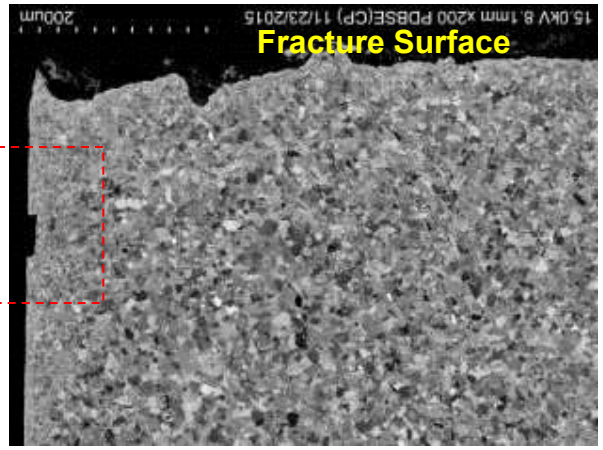

Appendix E2: High contrast backscatter images showing the difference in visual grain distortion along the forward and aft faces of the web.

~200 mils radially inboard of fracture

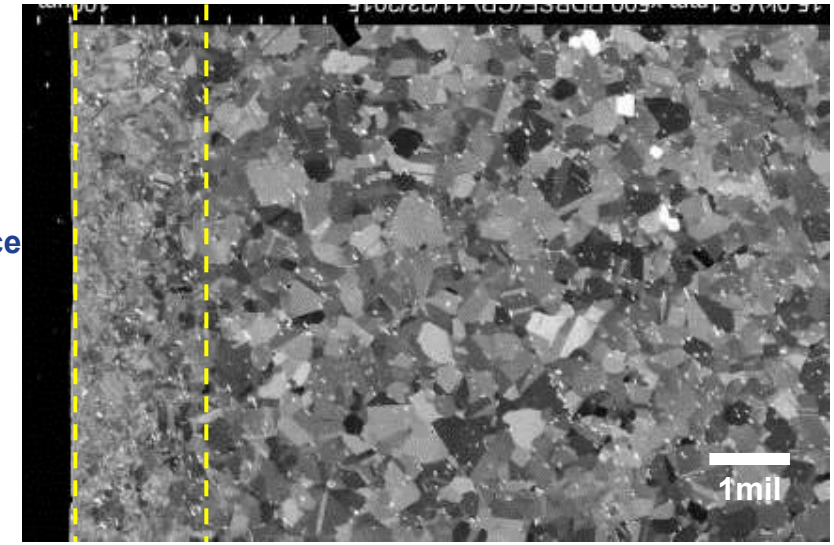

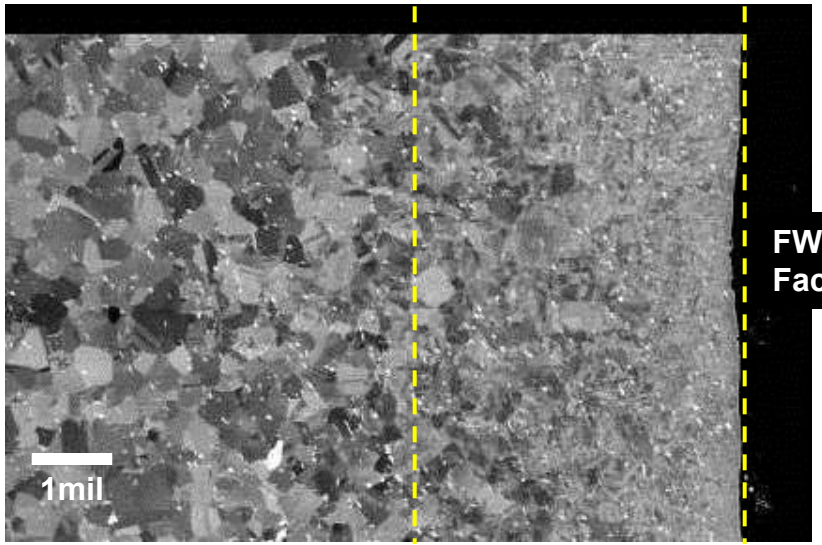

10° Grain Misorientation Maps

Radially Inboard Mount (EMP15-2750-01)

Near Fracture

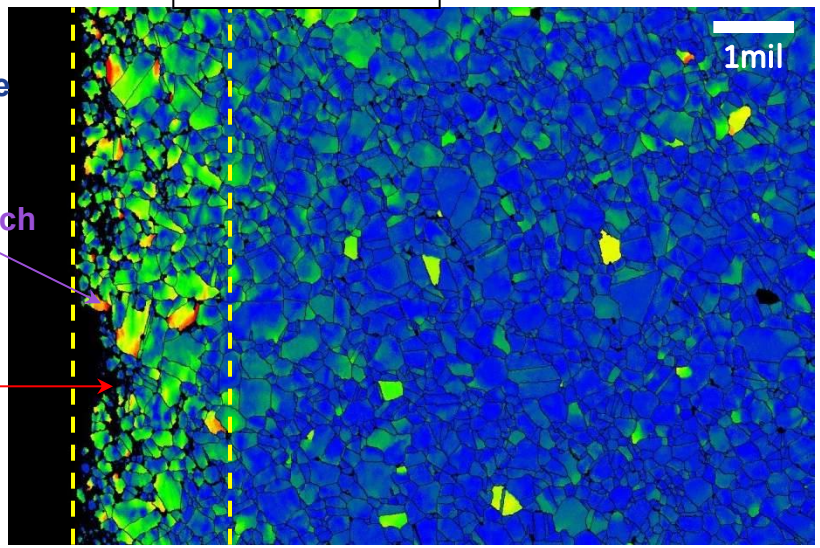

Appendix E3: Similar magnification EBSD misorientation maps showing the grain structure near/far from the fracture on the aft web face and on the forward face. The region where a secondary cracking was observed near the fracture had a uniform level of distortion very similar to further inboard radially on the part. The FIB trench was remnant from the prior examination. The forward face had more distortion (was more heavily peened).

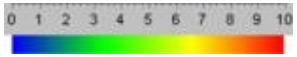

strain at edge too high to index/measure (true for all three locations)

~200 mils radially inboard of fracture

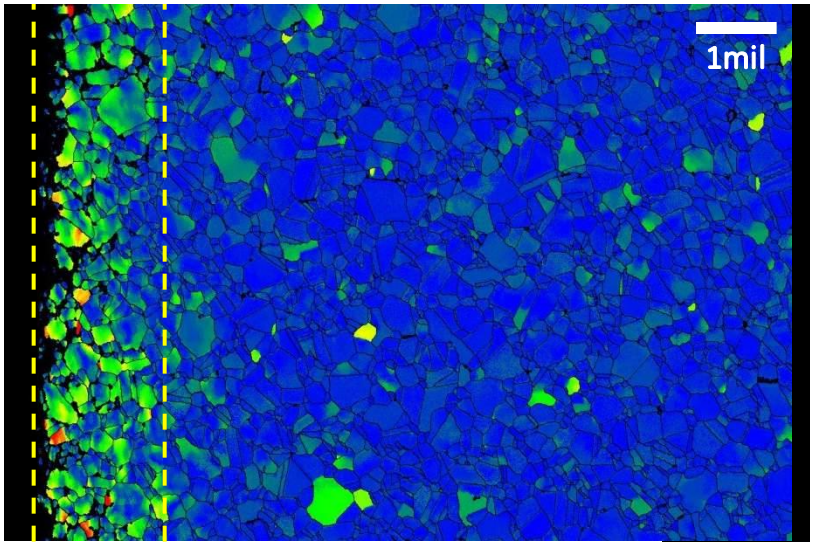

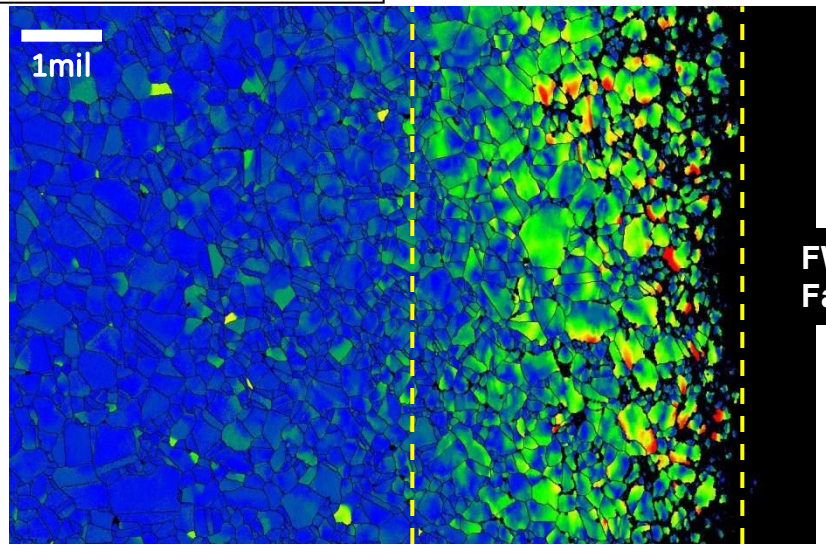

Radially Inboard Mount (EMP15-2750-01)

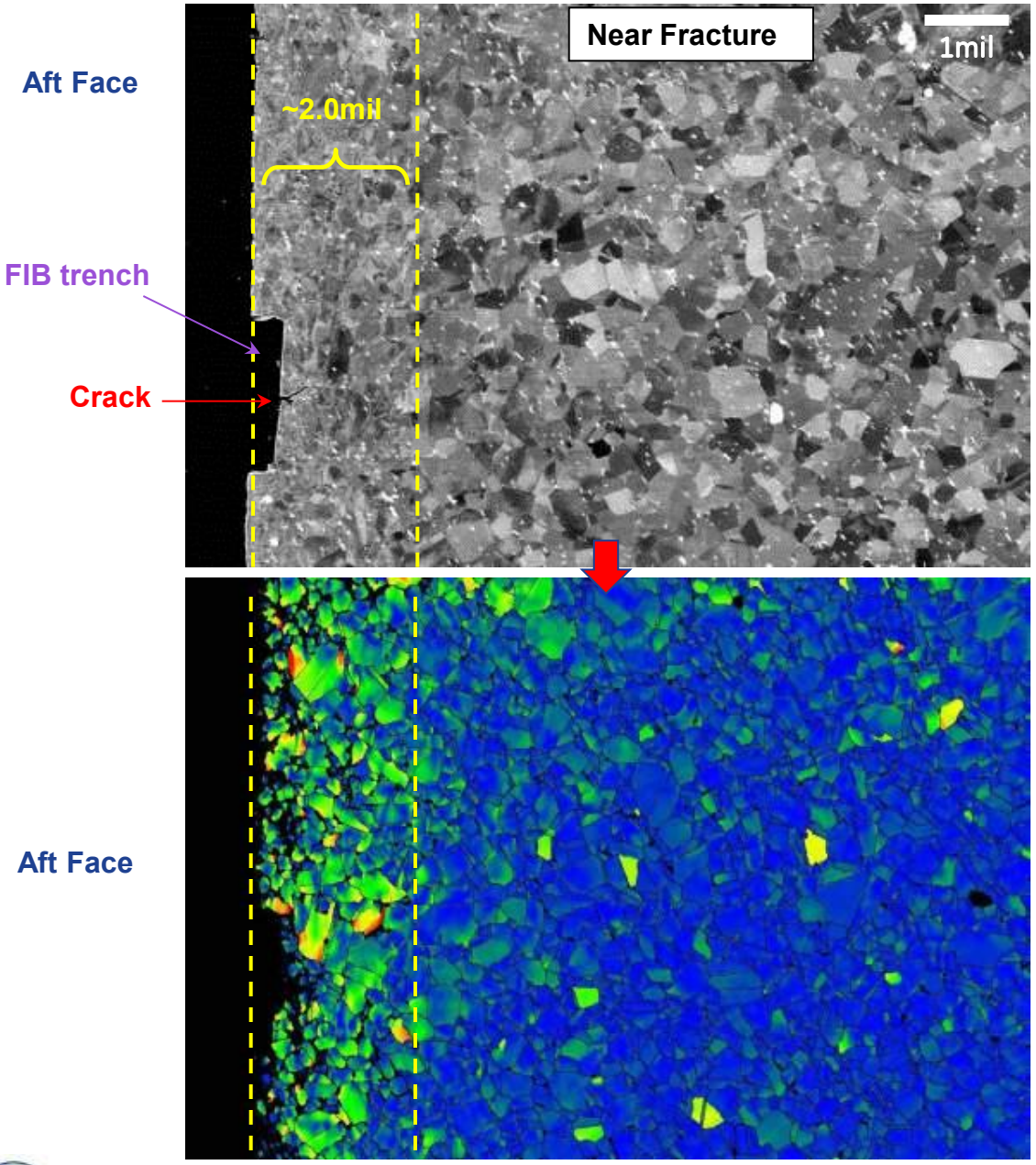

Appendix E4: Higher magnification comparison backscatter and EBSD images of the area with the small secondary crack near the main fracture.